

## $\mathcal{F}t$ values of the mirror $\beta$ transitions and the weak-magnetism-induced current in allowed nuclear $\beta$ decay

N. Severijns <sup>1,\*</sup>, L. Hayen <sup>1,2,3</sup>, V. De Leebeek <sup>1</sup>, S. Vanlangendonck <sup>1</sup>, K. Bodek<sup>4</sup>, D. Rozpedzik<sup>4</sup>, and I. S. Towner<sup>5</sup>

<sup>1</sup>*KU Leuven University, Instituut voor Kern- en Stralingsfysica, Celestijnenlaan 200D, B-3001 Leuven, Belgium*

<sup>2</sup>*Department of Physics, North Carolina State University, Raleigh, North Carolina 27695, USA*

<sup>3</sup>*Triangle Universities Nuclear Laboratory, Durham, North Carolina 27708, USA*

<sup>4</sup>*Marian Smoluchowski Institute of Physics, Jagiellonian University, 30-348 Cracow, Poland*

<sup>5</sup>*Cyclotron Institute, Texas A & M University, College Station, Texas 77843, USA*



(Received 23 September 2021; revised 28 July 2022; accepted 14 October 2022; published 23 January 2023)

The precision of correlation measurements in neutron and nuclear  $\beta$  decay has now reached the level of about 1% and better. At this level of precision, higher-order corrections such as recoil-order corrections induced by the strong interaction and radiative corrections cannot necessarily be neglected anymore. We provide here an update of the  $\mathcal{F}t$  values of the isospin  $T = 1/2$  mirror  $\beta$  decays including the neutron, of interest to determine the  $V_{ud}$  quark-mixing matrix element. We also provide an overview of current experimental and theoretical knowledge of the most important recoil term, weak magnetism, for both these mirror  $\beta$  decays and a large set of  $\beta$  decays in higher isospin multiplets. The matrix elements determining weak magnetism were calculated in the nuclear shell model and cross-checked against experimental data, showing overall good agreement. We show that the neutron and the mirror nuclei now effectively contribute to the value of  $V_{ud}$ , but we also stress the need for further work on the radiative correction  $\Delta_R^V$ . Our results provide new insight into the size of weak magnetism, extending the available information to nuclei with masses up to  $A = 75$ . This provides important guidance for planning and improved sensitivity for interpreting correlation measurements in searches for new physics or to extract  $V_{ud}$  in mirror  $\beta$  decays. It can also be of interest for further theoretical work related to the reactor neutrino problem.

DOI: [10.1103/PhysRevC.107.015502](https://doi.org/10.1103/PhysRevC.107.015502)

### I. INTRODUCTION

In the past, so-called induced or recoil terms in nuclear  $\beta$  decay have received considerable attention, both theoretically and experimentally (e.g., [1–4]). Their presence originates from QCD effects in the weak interaction of a bound quark, and folds in nuclear structure effects in heavier nuclei. Its study was motivated mainly in relation to experimental tests of the conserved vector current (CVC) hypothesis [5] (see, e.g., [6–13]) and searches for second class currents [12] (e.g., [1–4, 12, 14–29]). The most important of these induced currents, the weak magnetism term, has recently received new attention for several reasons. First, measurements of correlations between the spins and momenta of the particles involved in nuclear  $\beta$  decay, such as  $\beta$ - $\nu$  correlation and  $\beta$ -asymmetry parameter measurements [30], have now reached the level of precision where recoil terms cannot be neglected anymore (e.g., [31–36]). In such measurements, one is either searching for new physics beyond the standard model (SM), such as scalar, tensor, or right-handed weak currents [37–42], or

aiming at the determination of the  $V_{ud}$  quark-mixing matrix element in the  $\beta$  decay of mirror isotopes [43–46]. Second, weak magnetism is also important with respect to the so-called reactor antineutrino anomaly [47–54], i.e., the fact that the ratio of the observed antineutrino event rate at nuclear reactors to the predicted rate is lower than unity. Each of these respective topics is briefly commented upon below.

#### A. Searches for exotic charged weak currents

In  $\beta$  decay strong limits on the existence of charged weak scalar currents have been obtained from the corrected  $\mathcal{F}t$  values of the superallowed  $0^+ \rightarrow 0^+$  pure Fermi  $\beta$  transitions [55]. Complementary information as well as limits on tensor and right-handed weak currents are traditionally obtained from accurate measurements of correlations between the spins and momenta of the particles involved in  $\beta$  decay (reviews are given in, e.g., [37–42, 56]). The best-suited correlations are the  $\beta$ - $\nu$  angular correlation and the  $\beta$  asymmetry with respect to the polarization axis of oriented parent nuclei [30, 57, 58]. With the advent of particle traps and new detection techniques the precision of such measurements has improved significantly, and several results with a precision of about 1% or better have been reported already (see, e.g., for the  $\beta$ - $\nu$  correlation [46, 59–67], for the  $\beta$ -asymmetry parameter [32–36, 68, 69], and for other correlations [31, 70–79]). Many new experiments in search of exotic currents are ongoing or planned. An overview can be found in Table 3 in Ref. [41] (see also

\*nathal.severijns@kuleuven.be

Published by the American Physical Society under the terms of the [Creative Commons Attribution 4.0 International](https://creativecommons.org/licenses/by/4.0/) license. Further distribution of this work must maintain attribution to the author(s) and the published article's title, journal citation, and DOI.

Ref. [80]). Most of these are aiming at a precision down to the few-per-mille level. At such a precision, searches for physics beyond the standard model in  $\beta$  decay remain competitive to direct searches for new bosons in collider experiments such as those at the Large Hadron Collider (e.g., [38,42,81–83]). However, as experiments reach ever higher precision and dive below the 1% level, additional theoretical corrections arise [84]. The most important of these is the so-called recoil correction with a dominant contribution from weak magnetism, which is nuclear structure dependent. Its importance and possible limitations related to its exact knowledge were already demonstrated in the  $\beta$ -decay correlation measurements with, e.g.,  $^{37}\text{K}$  [35],  $^{60}\text{Co}$  [33],  $^{67}\text{Cu}$  [34],  $^{80}\text{Rb}$  [31], and  $^{114}\text{In}$  [32], and discussed recently in [84,85].

### B. Determining the $V_{ud}$ quark-mixing matrix element from mirror $\beta$ transitions

Apart from searches for new physics, correlation measurements in nuclear  $\beta$  decay can also be used to determine the  $V_{ud}$  quark-mixing matrix element or perform an independent test of the CVC hypothesis, i.e., by checking the constancy of the  $V_{ud}$  values for the individual transitions, as has been shown for isospin  $T = 1/2$  mirror  $\beta$  transitions [43]. Such measurements can also help us to better understand the isospin-symmetry breaking correction (noted as  $\delta_c$ ) that is required to obtain high-precision corrected  $\mathcal{F}t$  values for superallowed  $\beta$  transitions (e.g., [86,87]). Recently, very precise results were reported for the  $\beta$  asymmetry parameter in the mirror  $\beta$  decay of  $^{37}\text{K}$  [35] and  $^{19}\text{Ne}$  [69]. In addition, a double-counting instance in the extraction of  $V_{ud}$  from the mirror  $\beta$  transitions was corrected in Ref. [88]. The current value for  $V_{ud}$  from mirror  $\beta$  transitions, i.e.,  $|V_{ud}| = 0.9739(10)$  [88] (see also [42]), depends primarily on the availability of precise experimental  $\mathcal{F}t$  values [89,90] and existing experimental results, mainly for the  $\beta$ -asymmetry parameter,  $A$  [42,43].

In Refs. [84,85,91,92] prospects for a more precise determination of  $V_{ud}$  from these  $T = 1/2$  mirror  $\beta$  transitions are given. The mirror  $\beta$  decays of  $^3\text{H}$ ,  $^{17}\text{F}$ , and  $^{19}\text{Ne}$  appear to be the most sensitive in the case of  $\beta$ - $\nu$  correlation measurements, with all other mirror transitions up to  $^{41}\text{Sc}$  still having a quite good sensitivity [84,85,92]. Such measurements were recently performed with  $^{19}\text{Ne}$  and  $^{35}\text{Ar}$  [69,93,94] and new ones are planned [95–97]. For the  $\beta$ -asymmetry parameter, measurements in the mirror  $\beta$  decays of  $^{15}\text{O}$ ,  $^{19}\text{Ne}$ ,  $^{29}\text{P}$ ,  $^{33}\text{Cl}$ , and  $^{35}\text{Ar}$  would provide the best sensitivity [69,84,85,92], with a measurement of the  $\beta$ -asymmetry parameter in the decay of polarized  $^{35}\text{Ar}$  recently being attempted [98–100]. Further improvement on the  $\beta$  asymmetry parameter in the mirror  $\beta$  decay of  $^{37}\text{K}$  is anticipated as well [35]. In order to obtain sufficiently precise values for  $V_{ud}$  from such measurements a relative precision of typically 0.5% or better is needed [92], again requiring that higher-order effects are duly taken into account [84,85].

### C. Reactor neutrino anomaly

As several modern reactor neutrino experiments have come online in the search for neutrino oscillations, comparisons to

theoretical predictions have resulted in large discrepancies. Using two independent analysis methods, the ratio of experimentally detected versus theoretically predicted antineutrinos is found to be  $R = 0.943 \pm 0.023$  [47]. If genuine, this could be related to the existence of a sterile neutrino with  $\Delta m^2 \geq 1 \text{ eV}^2$  [47,101] (see also [102] for a recent review of existing limits on sterile neutrinos). Over the past few years, apart from other work, the treatment of forbidden transitions [53,54,103–106] and the evaluation of weak magnetism [50,51] has undergone some scrutiny. Recently, it was suggested [54,105] that a more proper treatment of forbidden transitions and inclusion of more pandemonium-free data in calculating the reactor antineutrino energy spectrum [106] could possibly explain the flux problem as well as the so-called spectral shoulder with respect to the theoretical spectrum. Regarding weak magnetism, all calculations of the expected antineutrino flux at reactors assume the weak magnetism contribution to depend solely on the difference between the proton and neutron magnetic moments and the  $\beta$ -particle energy. However, as will be shown explicitly later in this document, its precise value depends strongly on the isotope at hand. Using the same value for all transitions is then a substantial oversimplification, with, up to now, poorly understood consequences. As current experimental information on weak magnetism is limited to nuclei with  $A \leq 43$ , a study including also heavier masses, and especially measurements of weak magnetism for nuclei in the fission region, would be most helpful. At present several precision  $\beta$ -spectrum shape measurements to provide direct experimental information on weak magnetism are ongoing, e.g., with the isotopes  $^6\text{He}$  [107–110],  $^{20}\text{F}$  [111,112], and  $^{114}\text{In}$  [113,114], the latter effectively being in the fission isotope region. Here we present and analyze the currently existing experimental data, allowing us to determine weak magnetism for  $\beta$  transitions up to mass  $A = 75$ , and provide evidence for a nuclear structure and mass dependence of the size of the weak magnetism term.

### D. Motivation and outline of paper

Based on the above formulated arguments, a more detailed knowledge of the weak magnetism form factor in  $\beta$  decay would clearly be of great value. Previously, the weak magnetism term was evaluated for superallowed mixed Gamow-Teller/Fermi (GT/F) mirror  $\beta$  transitions between isospin  $T = 1/2$  doublets in mirror nuclei up to  $^{43}\text{Ti}$  [2,115], and for  $T = 1$  to  $T = 0$  Gamow-Teller decays in nuclei up to mass  $A = 32$  [2,49].

In this paper, the currently available experimental data leading to the weak magnetism form factor are analyzed for both the isospin  $T = 1/2$  mixed GT/F  $\beta$  transitions, including the neutron, and Gamow-Teller transitions in  $T = 1$ ,  $3/2$ , and  $2$  multiplets, based on the CVC hypothesis. For the mirror  $\beta$  transitions, the input data for the corrected  $\mathcal{F}t$  values for these transitions are reviewed and updated  $\mathcal{F}t$  values are provided. Combining these with the nuclear magnetic moments of the mirror transitions' initial and final states allows determining values for the weak magnetism form factor for these transitions up to  $^{75}\text{Sr}$ . For the Gamow-Teller transitions, the database of the Brookhaven National Laboratory National

Nuclear Data Center [116] was scanned for  $\beta$  transitions for which analog (i.e., within the same isospin multiplet)  $\gamma$  transitions are known and with sufficient information being available for both transitions in order to determine the weak magnetism form factor for the  $\beta$  transition, again using the CVC hypothesis.

In Sec. II we first review the currently available input data (the literature cutoff was February 2022) leading to the corrected  $\mathcal{F}t$  values for the mirror  $\beta$  transitions with  $A = 3\text{--}75$ , thereby updating the previously published  $\mathcal{F}t$  values for the mirror  $\beta$  transitions up to  $A = 45$  [89] and extending them further to  $A = 75$ . We combine these  $\mathcal{F}t$  values with GT/F mixing ratios from correlation measurements, thereby updating the values for the *up-down* quark-mixing matrix element,  $V_{ud}$ , from the mirror  $\beta$  decays and the neutron.

Section III focuses on the weak magnetism form factors for both the mirror  $\beta$  transitions between  $T = 1/2$  states, and the Gamow-Teller transitions in higher- $T$  multiplets. In Sec. III A, the general formalism with respect to the induced form factors is introduced with special interest in the dominant component, i.e., weak magnetism. Then, in Sec. III B, the nuclear magnetic moments of the mirror  $\beta$  transitions' mother and daughter states are reviewed and the weak magnetism term is extracted for the transitions up to  $A = 75$ , using the CVC hypothesis. Combining these with the  $\mathcal{F}t$  values allows extracting both the Gamow-Teller and orbital angular momentum matrix elements,  $M_{GT}$  and  $M_L$ , respectively. These are compared to shell model calculations in Sec. III B 3.

In Sec. III C the analysis of weak magnetism for Gamow-Teller  $\beta$  decays of states belonging to  $T = 1$ ,  $T = 3/2$ , and  $T = 2$  isospin multiplets up to mass  $A = 53$  is presented, again using the CVC hypothesis. The weak magnetism term for the respective  $\beta$  transitions is now obtained from the width of the analog  $E1$   $\gamma$  transition. Also for these transitions, the  $ft$  values are calculated in order to extract the Gamow-Teller and orbital angular momentum matrix elements, with the latter again being compared to shell model calculations (for a subset of the transitions considered).

Finally, the nuclear structure and mass dependence of the weak magnetism term and its relevance to the reactor anomaly in face of these new data are discussed.

## II. $\mathcal{F}t$ VALUES FOR MIRROR $\beta$ TRANSITIONS

In Ref. [89] the corrected  $\mathcal{F}t$  values for mirror  $\beta$  transitions in nuclei with mass  $A$  up to 45 were presented for the first time. Since then, many new experimental results for the half-lives, branching ratios, and decay energies for these transitions, as well as for mirror transitions in nuclei with higher masses, have been reported. In this update we also include the  $\beta$  decay of the neutron, being the lowest-mass mirror nucleus. First, an update of the relevant definitions and formalism will be given (Sec. II A). Thereafter, the updated data set is presented and evaluated, together with new theoretical calculations of nuclear structure and radiative corrections (Sec. II B). Finally, the current values for the  $\mathcal{F}t$  values for the mirror  $\beta$  transitions are reported (Sec. II C).

### A. Formalism

For a general  $\beta$  transition, the uncorrected partial half-life can be written as [89]

$$t = \frac{K}{G_F^2 V_{ud}^2} \frac{1}{\xi f}, \quad (1)$$

where  $G_F/(\hbar c)^3 = 1.1663787(6) \times 10^{-5} \text{ GeV}^{-2}$  [117,118] is the Fermi coupling constant,

$$K/(\hbar c)^6 = \frac{2\pi^3 \ln 2\hbar}{(m_e c^2)^5} = 8120.276236(12) \times 10^{-10} \text{ GeV}^{-4} \text{ s}, \quad (2)$$

(using the values from [118]), and

$$\xi = g_V^2 M_F^2 + g_A^2 M_{GT}^2, \quad (3)$$

with  $g_V$  and  $g_A$  the strength of the vector and axial-vector interactions (in units of  $G_F$ ) as defined in the Hamiltonian of Jackson, Treiman, and Wyld [30]. Here,  $M_{F,GT}$  is the main Fermi or Gamow-Teller matrix element, respectively. Further,  $f$  is the statistical rate function defined as the integral over the normalized spectrum shape,

$$f = \int_1^{W_0} pW(W_0 - W)^2 F(Z, W) \times C(Z, W)K(Z, W)dW, \quad (4)$$

where  $W$  is the total  $\beta$  energy in units of the electron's rest mass, i.e.,  $W = E_{\text{kin}}/m_e c^2 + 1$ , and  $W_0$  the spectral endpoint. Here  $F(Z, W)$  is the well-known Fermi function,  $C(Z, W)$  the nuclear-structure dependent shape factor, and  $K(Z, W)$  all higher-order corrections [119].

The product  $ft$  is then independent of the kinematics and produces the main matrix elements. Its experimental value for a specific  $\beta$  transition depends on three quantities: (i) the total decay transition energy,  $Q_{EC}$ , (ii) the half-life,  $t_{1/2}$ , of the decaying state, and (iii) the branching ratio, BR, of the particular transition of interest. The  $Q_{EC}$  value determines the statistical rate function,  $f$  [Eq. (4)]. The half-life and the branching ratio, together with the electron-capture fraction,  $P_{EC}$ , determine the partial half-life,  $t$ , of the transition of interest, which is defined as

$$t = t_{1/2} \left( \frac{1 + P_{EC}}{\text{BR}} \right). \quad (5)$$

The superallowed mirror  $\beta$  transitions between the analog  $T = 1/2$  states situated at both sides of the  $N = Z$  line are mixed transitions with both Fermi and Gamow-Teller components. Despite this increased complexity, they harbor a particular advantage. As the decay occurs within the same isospin multiplet—and taking the isospin limit in QCD—the Fermi matrix element is determined simply by using the Wigner-Eckart theorem. In the case of mirror  $T = 1/2$  transitions this is particularly simple and one finds  $M_F^0 = 1$ , with the superscript denoting the isospin-conserving limit. In nuclei, however, the presence of the Coulomb interaction between nucleons breaks the purported isospin symmetry, albeit at only the few percent level. Small corrections must therefore be

introduced to the single-particle matrix element

$$M_F = M_F^0(1 - \delta_C)^{1/2}, \quad (6)$$

with  $\delta_C$  a correction arising from the imperfect overlap of proton and neutron radial wave functions due to their slightly different nuclear potentials [86]. This must be provided by nuclear theory and its estimate is of particular importance in, e.g., the  $V_{ud}$  extraction in superallowed  $0^+ \rightarrow 0^+$  Fermi decays and mirror decays, as discussed below.

The weak axial-vector current, occurring in Gamow-Teller decays, is not conserved and is renormalized through QCD effects. This prevents one, in theory, from writing down an analogous isospin-invariant GT matrix element,  $M_{GT}^0$ , although this has historically been commonplace [43,89]. With previous nuclear many-body calculations, dominated by the nuclear shell model, this is at first glance merely a notational matter as  $M_{GT}$  could typically not be calculated to high enough precision for the distinction to be relevant. With the developing maturity of nuclear *ab initio* methods (see, e.g., [80,120]), however, the distinction is much more clearly defined and of interest as they enter the  $A = 10$ – $19$  mass range and beyond.

Besides strong interaction effects, additional electroweak corrections arise both at the nucleon and nucleus level. Traditionally these have been separated into a QCD-invariant, infrared-singular part (the *outer* correction,  $\delta'_R$ ) and an energy-independent renormalization of the weak coupling constants from the ultraviolet (the *inner* correction,  $\Delta_R^{V,A}$ ) [121]. Both contribute roughly at the few percent level. The latter is typically calculated for a single nucleon, i.e., in a loop calculation the nucleon interacting with both weak gauge bosons is one and the same. In a nucleus, however, this is not necessarily the case and additional nuclear-structure dependent corrections arise, noted as  $\delta_{NS}$  [122]. This once again requires nuclear theory input, and has garnered significant attention following recent progress [88,123–126].

In summary, Eq. (1) can be written as [86,89]

$$1/t = \frac{G_F^2 V_{ud}^2}{K} (1 + \delta'_R) (f_V |M_F^0|^2 (1 + \delta_{NS}^V - \delta_C^V) g_V^2 (1 + \Delta_R^V) + f_A |M_{GT}^0|^2 (1 + \delta_{NS}^A - \delta_C^A) g_A^2 (1 + \Delta_R^A)), \quad (7)$$

where  $f_V$  and  $f_A$  are the statistical rate functions for, respectively, the vector (Fermi) and axial-vector (Gamow-Teller) parts of the transitions, and we write  $M_{GT}$  similar to  $M_F$ . As denoted in Eq. (4), the  $f$  functions take into account higher-order nuclear corrections besides the main F/GT matrix elements in the shape factor,  $C(Z, W)$ . Traditionally, these corrections have been calculated in the elementary particle approach—i.e., a form factor decomposition encoding the full nuclear response—and a matrix element reduction using the impulse approximation (IA) which treats the nucleus as a sum of independent nucleons in a mean-field potential. While the results presented below are calculated in the Behrens-Bühring formalism [127], we write the results in the Holstein formalism [1] for convenience. For comparisons between them we refer the reader to Refs. [4,84,119].

We can absorb all constant corrections and define the Gamow-Teller/Fermi mixing ratio as

$$\begin{aligned} \rho &\equiv \frac{c}{a} \stackrel{\text{IA}}{=} \frac{g_A \mathcal{F}_{GT}(0)}{g_V M_F^0} \left[ \frac{1 + \Delta_R^A - \Delta_R^V}{1 + \delta_{NS}^V - \delta_C^V} \right]^{1/2} \\ &= \frac{g_A M_{GT}^0}{g_V M_F^0} \left[ \frac{(1 + \delta_{NS}^A - \delta_C^A)(1 + \Delta_R^A)}{(1 + \delta_{NS}^V - \delta_C^V)(1 + \Delta_R^V)} \right]^{1/2}, \end{aligned} \quad (8)$$

with  $a$  and  $c$ , respectively, the Fermi and Gamow-Teller form factors. The first line contains a definition analogous to Ref. [84], with  $\mathcal{F}_{GT}(0)$  the form factor evaluated at zero momentum, while the second has the more traditional notation. The benefit lies in the generality of this first line of Eq. (8), meaning experimental analysis extracts the same quantity, whether it comes from a  $\beta$  asymmetry, a  $\beta$ - $\nu$  correlation, or another correlation. Note that in the convention of Holstein [1] that we use here, the sign of  $g_A$  is positive.

From Eqs. (7) and (8) one can define the “corrected”  $\mathcal{F}t$  value for a mixed Gamow-Teller/Fermi  $\beta$  transition to be

$$\begin{aligned} \mathcal{F}t^{GT/F} &\equiv \mathcal{F}t^{\text{mirror}} \\ &\equiv f_V t (1 + \delta'_R) (1 + \delta_{NS}^V - \delta_C^V) \\ &= \frac{K}{G_F^2 V_{ud}^2 g_V^2 (1 + \Delta_R^V)} \times \frac{1}{|M_F^0|^2 [1 + \frac{f_A}{f_V} \rho^2]}. \end{aligned} \quad (9)$$

For the superallowed  $0^+ \rightarrow 0^+$  pure Fermi transitions one has  $|M_F^0|^2 = 2$  and  $M_{GT}^0 = \rho = 0$ , so that

$$\mathcal{F}t^{0^+ \rightarrow 0^+} = \frac{K}{2G_F^2 V_{ud}^2 g_V^2 (1 + \Delta_R^V)}, \quad (10)$$

which was determined to be  $3072.24(185)$  s [55]. Note that the first factor in the last line of Eq. (9) is equal to  $2\mathcal{F}t^{0^+ \rightarrow 0^+}$ .

The Gamow-Teller/Fermi mixing ratio,  $\rho$ , to a good approximation can be written as [89]

$$\rho \cong \frac{g_A M_{GT}^0}{g_V M_F^0}, \quad (11)$$

where we use the fact that the small radiative and isospin symmetry-breaking corrections do not differ much for the vector and axial-vector parts of the transition [89]. The radiative corrections  $\Delta_R^V$  and  $\Delta_R^A$  were recently shown to indeed differ only at the  $10^{-4}$  level or even less [88,128]. As the vector coupling constant  $g_V = 1$  and  $|M_F^0|^2 = 1$  for these  $T = 1/2$  mirror  $\beta$  transitions, one has

$$\rho \simeq g_A M_{GT}^0. \quad (12)$$

In the next section, a detailed survey of the data leading to the  $\mathcal{F}t$  values for the  $T = 1/2$  mirror  $\beta$  transitions is made. In addition to bringing up to date the previously published results for the mirror transitions up to  $^{45}\text{V}$  [89], we are now also incorporating existing data on the heavier  $T = 1/2$  mirror  $\beta$  transitions, leading to the  $\mathcal{F}t$  values for the transitions up to  $^{75}\text{Sr}$ .

## B. Experimental data

### 1. Data selection

We considered all measurements published up to February 2022 as well as any additional final results (available in preprint or as a Ph.D. thesis) we were aware of. Since the previous survey [89] about 65 new half-life measurements and 9 new branching ratios have been reported, for 35 different isotopes. As in our previous survey [89] the  $Q_{EC}$  values have again been taken from the most recent Atomic Mass Evaluation (AME2020) [129–131]. Since the Atomic Mass Evaluation 2003 (AME2003) [132], which was used in [89], the precision with which the  $Q_{EC}$  value is known has been (significantly) improved for 11 out of the 19 mirror  $\beta$  transitions discussed in [89]. Note that we have now also included the neutron, being the lightest of the mirror nuclei.

In the tables and throughout this work, “error bars” and “uncertainties” always refer to plus/minus one standard deviation (68% confidence level). In analyzing the tabulated data we have followed the statistical procedures used by the Particle Data Group (e.g., Ref. [133]) that were adopted also for the surveys of the superallowed  $0^+ \rightarrow 0^+$   $\beta$  decays (e.g., [87,134]) and for the previous survey of the mirror  $\beta$  transitions [89]. Thus, the one-standard-deviation error bars on weighted averages were increased by a scaling factor

$$S = [\chi^2/(N - 1)]^{1/2}, \quad (13)$$

with  $\chi^2/(N - 1)$  the reduced  $\chi^2$ . Further, data that were clearly inconsistent and results with an uncertainty that is more than a factor 10 larger than that of the most precise measurement for each quantity were rejected. Also results that deviate four or more standard deviations from the weighted average of mutually consistent results from other measurements (which are in most cases more recent and also more precise), were not considered. For the latter cases, the average values that would be obtained when the deviating results are not omitted are given as well. These all agree within error bars with the finally adopted value, but have of course larger error bars and also a larger scaling factor,  $S$ , than the adopted value.

All data that are now rejected, in addition to the ones that were already rejected in the initial survey [89], are listed in Tables III and IV. As in, e.g., Ref. [55] an alphanumeric code comprising the initial two letters of the first author’s name and the two last digits of the publication date is used to link each datum appearing in the tables to its original journal reference. The reference key linking these alphanumeric codes with the actual reference numbers is given in Table VII.

Table I shows the collected half-lives of the considered isotopes. For the neutron half-life we based ourselves on the table on page 1835 of the latest Review of Particle Physics [118], using all values with a combined statistical and systematic error within ten times that of the most precise result, and which were not included in, or replaced by, a later result (see the comments in Ref. [118]). We have also included the recent result of Ref. [135] which was published after the analysis of Ref. [118].

A breakdown of the branching ratios is collected in Table II. In comparison to the previous compilation [89] a more detailed analysis of the branching ratios was performed. It

includes all known branchings to excited states in the daughter isotopes of the mirror nuclei. Because of this, some branching ratios for the mirror  $\beta$  transitions have slightly shifted in central value or some error bars have slightly increased. Of course, the more complete analysis that was performed renders the newly adopted values more reliable.

### 2. Adopted input values for the $\mathcal{F}t^{\text{mirror}}$ values

The adopted values for the half-lives,  $t_{1/2}$  (from Table I), the branching ratios, BR (from Table II), and the decay transition energies,  $Q_{EC}$  (from [129]), are listed in Table V, together with the deduced statistical rate function,  $f_V$  [Eq. (4)], the electron-capture fraction,  $P_{EC}$ , and the resulting partial half-lives,  $t$  [Eq. (5)]. Note that the isotopes listed in Table I that are unbound to proton decay are not further considered.

The values for the statistical rate function,  $f_V$ , listed in column 5 of Table V were calculated using the same code as in the survey of the superallowed pure Fermi transitions [55]. The basic methodology for the calculation is described in the Appendix to Ref. [134]. They were evaluated with the  $Q_{EC}$  values and their uncertainties listed in column 4 of Table V. For the neutron, the value  $f_V = 1.6887(2)$  [86,140] was obtained as the sum of the first 15 entries in Table 4 of Ref. [141], i.e.,  $f_V = 1.68854(15)$  (note that the remaining entries in that table relate to the radiative correction  $\delta'_R$ ), and updated in Ref. [140] to incorporate slight nucleon mass shifts.

Finally, the  $P_{EC}$  values for the  $\beta^+$  transitions were calculated as outlined in Ref. [134] using the tables of Bambynek *et al.* [142] and Firestone [143]. No errors were assigned to these  $P_{EC}$  values as they are expected to be accurate to a few parts in 100 [134,142] such that they do not contribute perceptibly to the overall uncertainties, as was verified. All quantities listed in Table V finally allow obtaining the partial half-life,  $t$  [Eq. (5)], for each  $\beta$  transition considered. These values are listed in the last column of Table V.

### 3. Note on the mirror transitions with $A > 61$

Note that for the mirror isotopes with  $A > 61$  no detailed decay spectroscopy has been performed yet, as is indicated in Table V by a “–” for several isotopes in the column listing the branching ratios, BR. For three isotopes, i.e.,  $^{67}\text{Se}$ ,  $^{71}\text{Kr}$ , and  $^{75}\text{Sr}$ , some information is available but is, however, likely incomplete as these isotopes are for now still difficult to produce copiously at radioactive beam facilities. For the mirror  $\beta$  decays of these three isotopes we therefore list in Table V the upper limits on the branching ratios, BR, based on the currently available spectroscopic data as well as estimated values for the lower limits. Note further that for  $^{71}\text{Kr}$  the minimum value that is required to avoid a negative value for  $\rho^2$  when solving Eq. (9) is  $\text{BR} = 68.1\%$ .

## C. The $\mathcal{F}t^{\text{mirror}}$ values

Having surveyed the experimental data, we can now turn to the determination of the  $\mathcal{F}t^{\text{mirror}}$  values according to the second line of Eq. (9). To do this we must, however, still deal with the different correction terms. The values for the nucleus-dependent radiative correction  $\delta'_R$  have been calculated using

TABLE I. Half-lives,  $t_{1/2}$ , of the mirror nuclei from  ${}^3\text{H}$  to  ${}^{99}\text{Sn}$ , expressed in seconds unless specified differently under the name of the parent nucleus and in the last column [days (d), minutes (min)]. If input data contained separate statistical and systematic error bars these were added quadratically. Note that for the neutron in the literature traditionally the lifetime,  $\tau = \ln 2 \times t_{1/2}$ , is quoted. The average half-life,  $t_{1/2}$ , for the neutron adopted here corresponds to the lifetime  $\tau = 878.54(56)$  s. The scale factor  $S$  listed in the last column is defined in Eq. (13). References to data listed in this table are given in Table VII. References to data that were not used are listed in Table III together with the reason for their rejection.

Parent nucleus	Measured half-lives, $t_{1/2}$ (s)						Average half-life $t_{1/2}$ (s)	Scale $S$
	1	2	3	4	5	6		
$n$	$611.8 \pm 1.9$ [Ma93]	$608.9 \pm 0.5$ [Se05]	$610.5 \pm 1.2$ [Pi10]					
	$611.7 \pm 1.4$ [St12]	$615.3 \pm 1.6$ [Yu13]	$610.1 \pm 0.8$ [Ar15]					
	$608.8 \pm 1.3$ [Ez18]	$608.4 \pm 0.5$ [Pa18]	$611.0 \pm 0.6$ [Se18]					
	$608.41 \pm 0.23$ [Go21]						$608.96 \pm 0.39$	2.2
${}^3\text{H}$	$4419 \pm 183$ [No47]	$4551 \pm 54$ [Je50]	$4530 \pm 27$ [Jo51]					
(d)	$4479 \pm 11$ [Jo55]	$4596 \pm 66$ [Po58]	$4496 \pm 16$ [Me66]					
	$4474 \pm 11$ [Jo67]	$4501 \pm 9$ [Ru77]	$4498 \pm 11$ [Si87]					
	$4521 \pm 11$ [Ol87]	$4485 \pm 12$ [Ak88]	$4497 \pm 11$ [Bu91]					
	$4504 \pm 9$ [Un00]	$4500 \pm 8$ [Lu00]	$4479 \pm 7$ [Ak04]					
	$4497 \pm 4$ [Ma06]						$4497 \pm 4$ d <sup>a</sup>	
${}^{11}\text{C}$	$20.34 \pm 0.04$ [Ka64a]	$20.40 \pm 0.04$ [Aw69]	$20.38 \pm 0.02$ [Az75]					
(min)	$20.334 \pm 0.024$ [Wo02]	$20.3378 \pm 0.0043$ [Va18]					$20.3401 \pm 0.0053$ min	1.3
${}^{13}\text{N}$	$9.96 \pm 0.03$ [Ar58]	$9.965 \pm 0.005$ [Ja60]	$9.93 \pm 0.05$ [Ki60]					
(min)	$10.05 \pm 0.05$ [Bo65]	$9.96 \pm 0.02$ [Eb65]	$9.963 \pm 0.009$ [Ri68]					
	$9.965 \pm 0.010$ [Az77]						$9.9647 \pm 0.0039$ min	1
${}^{15}\text{O}$	$122.1 \pm 0.1$ [Ja60]	$122.23 \pm 0.23$ [Az77]	$122.308 \pm 0.049$ [Bu20]				$122.27 \pm 0.06$	1.3
${}^{17}\text{F}$	$64.50 \pm 0.25$ [Al72]	$64.31 \pm 0.09$ [Az77]	$64.347 \pm 0.035$ [Gr15a]					
	$64.402 \pm 0.042$ [Br16]						$64.366 \pm 0.026$ <sup>b</sup>	1
${}^{19}\text{Ne}$	$17.219 \pm 0.017$ [Az75]	$17.237 \pm 0.014$ <sup>c</sup> [Pi85]	$17.262 \pm 0.007$ [Tr12]					
	$17.254 \pm 0.005$ [Uj13]	$17.2832 \pm 0.0083$ [Br14]	$17.2569 \pm 0.0021$ [Fo17]				$17.2573 \pm 0.0034$ <sup>d</sup>	1.9
${}^{21}\text{Na}$	$22.422 \pm 0.010$ [Gr15]	$22.4506 \pm 0.0033$ [Fi17]	$22.4615 \pm 0.0042$ [Sh18]				$22.4527 \pm 0.0067$	2.7
${}^{23}\text{Mg}$	$11.327 \pm 0.014$ [Az75]	$11.317 \pm 0.011$ [Az77]	$11.3027 \pm 0.0033$ [Ma17]				$11.3050 \pm 0.0044$	1.4
${}^{25}\text{Al}$	$7.23 \pm 0.02$ [Ju71]	$7.177 \pm 0.023$ [Ta73]	$7.174 \pm 0.007$ [Az75]					
	$7.1657 \pm 0.0024$ [Lo17]						$7.1674 \pm 0.0044$	1.9
${}^{27}\text{Si}$	$4.109 \pm 0.004$ [Az75]	$4.1117 \pm 0.0020$ [Ma17]					$4.1112 \pm 0.0018$	1
${}^{29}\text{P}$	$4.15 \pm 0.03$ [Sc70]	$4.083 \pm 0.012$ [Az75]	$4.084 \pm 0.022$ [Wi80]					
	$4.1055 \pm 0.0044$ [Lo20]						$4.1031 \pm 0.0058$	1.4
${}^{31}\text{S}$	$2.57 \pm 0.01$ [Ja60]	$2.543 \pm 0.008$ [Az77]	$2.562 \pm 0.007$ [Wi80]					
	$2.5534 \pm 0.0018$ [Ba12]						$2.5539 \pm 0.0023$ <sup>e</sup>	1.4
${}^{33}\text{Cl}$	$2.53 \pm 0.02$ [Mu58]	$2.51 \pm 0.02$ [Ja60]	$2.47 \pm 0.02$ [Sc70]					
	$2.513 \pm 0.004$ [Ta73]	$2.507 \pm 0.008$ [Az77]	$2.5038 \pm 0.0022$ [Gr15a]				$2.5059 \pm 0.0025$	1.3
${}^{35}\text{Ar}$	$1.79 \pm 0.01$ [Ja60]	$1.770 \pm 0.006$ [Wi69]	$1.774 \pm 0.003$ [Az77]					
	$1.7754 \pm 0.0011$ [Ia06]						$1.7752 \pm 0.0010$	1
${}^{37}\text{K}$	$1.223 \pm 0.008$ [Az77]	$1.23651 \pm 0.00094$ [Sh14]	$1.23635 \pm 0.00088$ [Ku17]				$1.23634 \pm 0.00076$	1.2
${}^{39}\text{Ca}$	$0.860 \pm 0.005$ [Mi58]	$0.873 \pm 0.008$ [Li60]	$0.8604 \pm 0.0030$ [Al73]					
	$0.8594 \pm 0.0016$ [Az77]	$0.8607 \pm 0.0010$ [B110]					$0.86046 \pm 0.00080$ <sup>f</sup>	1
${}^{41}\text{Sc}$	$0.628 \pm 0.014$ [Ja60]	$0.596 \pm 0.006$ [Yo65]	$0.5963 \pm 0.0017$ [Al73]					
	$0.591 \pm 0.005$ [Ta73]						$0.5962 \pm 0.0022$	1.4
${}^{43}\text{Ti}$	$0.528 \pm 0.003$ [Ja60]	$0.56 \pm 0.02$ [Ja61]	$0.50 \pm 0.02$ [Pl62]					
	$0.49 \pm 0.01$ [Al67]	$0.54 \pm 0.01$ [Va69]	$0.509 \pm 0.005$ [Ho87]				$0.5223 \pm 0.0057$	2.4
${}^{45}\text{V}$	$0.539 \pm 0.018$ [Ho82]	$0.5472 \pm 0.0053$ [Ha87]					$0.5465 \pm 0.0051$	1
${}^{47}\text{Cr}$	$0.4600 \pm 0.0015$ [Ed77]	$0.4720 \pm 0.0063$ [Ha87]					$0.4606 \pm 0.0027$ <sup>g</sup>	1.9
${}^{49}\text{Mn}$	$0.384 \pm 0.017$ [Ha80]	$0.3817 \pm 0.0074$ [Ha87]	$0.380 \pm 0.030$ [Ku17a]				$0.3820 \pm 0.0066$	1
${}^{51}\text{Fe}$	$0.310 \pm 0.005$ [Ay84]	$0.3050 \pm 0.0043$ [Ha87]	$0.298 \pm 0.014$ [Ho89]					
	$0.301 \pm 0.004$ [Su13]	$0.308 \pm 0.005$ [Sh15]	$0.288 \pm 0.006$ [Ku17a]				$0.3031 \pm 0.0029$	1.4
${}^{53}\text{Co}$	$0.240 \pm 0.020$ [Ho89]	$0.240 \pm 0.009$ [Lo02] <sup>h</sup>	$0.230 \pm 0.017$ [Su13]					
	$0.245 \pm 0.003$ [Ku17a]						$0.2440 \pm 0.0028$	1
${}^{55}\text{Ni}$	$0.189 \pm 0.005$ [Ho77]	$0.208 \pm 0.005$ [Ay84]	$0.2121 \pm 0.0038$ [Ha87]					
	$0.204 \pm 0.003$ [Re99]	$0.196 \pm 0.005$ [Lo02] <sup>h</sup>	$0.203 \pm 0.002$ [Ku17a]				$0.2032 \pm 0.0025$	1.8
${}^{57}\text{Cu}$	$0.1994 \pm 0.0032$ [Sh89]	$0.1963 \pm 0.0007$ [Se96]	$0.195 \pm 0.004$ [Ku17a]				$0.19640 \pm 0.00067$	1

TABLE I. (Continued.)

Parent nucleus	Measured half-lives, $t_{1/2}$ (s)						Average half-life $t_{1/2}$ (s)	Scale $S$
	1		2		3			
<sup>59</sup> Zn	0.1820 ± 0.0018	[Ar84]	0.174 ± 0.002	[Ku17a]	0.1824 ± 0.0004	[Or21]	0.1821 ± 0.0011	2.9
<sup>61</sup> Ga	0.150 ± 0.030	[Wi93]	0.168 ± 0.003	[We02]	0.148 ± 0.019	[Lo02] <sup>h</sup>	0.1660 ± 0.0025	1
<sup>63</sup> Ge	0.162 ± 0.010	[Ro14]	0.163 ± 0.005	[Ku17a]				
	0.095 ± $^{0.023}_{0.020}$	[Wi93] <sup>i</sup>	0.150 ± 0.009	[Lo02] <sup>h</sup>	0.149 ± 0.004	[Ro14]	0.1485 ± 0.0051	1.5
	0.156 ± 0.011	[Ku17a]					0.1303 ± 0.0006	
<sup>65</sup> As	0.1303 ± 0.0006	[Gi20]					0.1330 ± 0.0038	1
<sup>67</sup> Se	0.107 ± 0.035	[Ba94]	0.136 ± 0.012	[Lo02] <sup>h</sup>	0.133 ± 0.004	[Ro14]	0.0988 ± 0.0003	1
<sup>69</sup> Br	<100 ns	[B195]	<24 ns	[Pf96]	<24 ns	[Ja99]	<24 ns <sup>j</sup>	
<sup>71</sup> Kr	0.100 ± 0.003	[O197]	0.0988 ± 0.0003	[Si19]			0.0988 ± 0.0003	1
<sup>73</sup> Rb	<30 ns	[Pf96]	<30 ns	[Ja99]	<81 ns	[Su17]	<30 ns <sup>j</sup>	
<sup>75</sup> Sr	0.088 ± 0.003	[Hu03]	0.0817 ± 0.0034	[Si19]			0.0852 ± 0.0031	1.4
<sup>77</sup> Y	0.057 ± $^{0.022}_{0.012}$	[Ki01] <sup>i,k</sup>					0.065 ± 0.017	
<sup>79</sup> Zr	0.056 ± 0.030	[B199]					0.056 ± 0.030	
<sup>81</sup> Nb	<80 ns	[Ja99]	<200 ns	[Ki01]	<38 ns	[Su13a]	<38 ns <sup>j</sup>	
	<40 ns	[Su17]					0.028 ± 0.019	
<sup>83</sup> Mo	0.006 ± $^{0.030}_{0.003}$	[Ki01] <sup>i</sup>						
<sup>85</sup> Tc	<100 ns	[Ja99]	<43 ns	[Ja99]	<42 ns	[Su13a]	<42 ns <sup>j</sup>	
	<43 ns	[Su17]					unknown <sup>j</sup>	
<sup>89</sup> Rh	>500 ns	[Ja99]	<120 ns	[Ce16]			0.032 ± 0.003	
<sup>91</sup> Pd	>1.5 $\mu$ s	[Ry95]	0.032 ± 0.003	[Pa18a]			228 ± 16 ns	
<sup>93</sup> Ag	228 ± 16 ns	[Ce16]					0.0316 ± 0.0028	1
<sup>95</sup> Cd	0.073 ± $^{0.053}_{0.028}$	[St11] <sup>c</sup>	0.029 ± 0.008	[Da17]	0.032 ± 0.003	[Pa18a]	0.0316 ± 0.0028	1
<sup>97</sup> In	0.026 ± $^{0.047}_{0.010}$	[St11] <sup>c</sup>	>3 $\mu$ s	[Ce16]	0.036 ± 0.006	[Pa18a]	0.0357 ± 0.0059	1
<sup>99</sup> Sn	>200 ns	[St11] <sup>c</sup>	0.024 ± 0.004	[Pa18a]			0.024 ± 0.004	

<sup>a</sup>We did not perform the analysis of the tritium half-lives ourselves, but rather used the value (and the references) from [Ma06]. An interesting effect is mentioned in [Ak04]: the half-life of molecular and atomic <sup>3</sup>H would differ by about 9 days. Due to a lack of additional information on this effect we have not included it in the present compilation. All measurements, except for [Ak04], were performed on molecular tritium.

<sup>b</sup>If the results from [Wo69] and [Al77] (see Table III) are included one has  $t_{1/2} = 64.411 \pm 0.068$  s ( $S = 2.8$ ).

<sup>c</sup>Unpublished.

<sup>d</sup>Note that  $t_{1/2} = 17.2577 \pm 0.0036$  s ( $S = 2.0$ ) when excluding the unpublished result of [Pi85], and  $t_{1/2} = 17.2561 \pm 0.0025$  s ( $S = 1.4$ ) when excluding [Br14] which differs by  $3.1\sigma$  from the weighted average. Considering only the three most precise results, i.e., [Tr12], [Uj13], and [Fo17], yields  $t_{1/2} = 17.2569 \pm 0.0019$  s ( $S = 1$ ).

<sup>e</sup>If the result from [Al74] (see Table III) is not omitted the weighted average is  $t_{1/2} = 2.5549 \pm 0.0040$  s ( $S = 2.4$ ).

<sup>f</sup>If the result from [K154] (see Table III) is not omitted the weighted average is  $t_{1/2} = 0.861 \pm 0.049$  s ( $S = 1.9$ ).

<sup>g</sup>If the result from [Bu85] (see Table III) is not omitted the weighted average is  $t_{1/2} = 0.4616 \pm 0.0051$  s ( $S = 3.6$ ).

<sup>h</sup>See also [Bl02].

<sup>i</sup>These asymmetric errors have been symmetrized for the analysis as  $\sigma_{\text{symm}}^2 = (\sigma_+^2 + \sigma_-^2)/2$ .

<sup>j</sup>Proton unbound.

<sup>k</sup>Also reported in [Fa02].

the  $Q_{EC}$  values in Table V following the same procedures as adopted for the superallowed  $0^+ \rightarrow 0^+$   $\beta$  decays [55,144]. They are listed in column 4 of Table VI.

Regarding the nuclear-structure-dependent corrections  $\delta_C^V - \delta_{NS}^V$  (column 5 in Table VI), the values previously reported in [89] were used for the mirror  $\beta$  decays from <sup>3</sup>H to <sup>45</sup>V. For the mirror decays from <sup>47</sup>Cr to <sup>75</sup>Sr estimates based on the systematic of the superallowed  $0^+ \rightarrow 0^+$   $\beta$  decays [55] and the lower-mass mirror  $\beta$  decays [89] were used, with generous error bars attached to them. In none of these cases is the uncertainty on  $\delta_C^V - \delta_{NS}^V$  the dominant contribution to the total uncertainty on the  $\mathcal{F}_t^{\text{mirror}}$  value.

Note that in their latest review Hardy and Towner [55] quote slightly different values for  $\delta_C^V - \delta_{NS}^V$  than in their earlier work [87], thereby taking into account recent results

from other authors, i.e., from Refs. [145,146] for  $\delta_C^V$  and Refs. [124,147] for  $\delta_{NS}^V$ . Except for the case of <sup>10</sup>C, the new values all differ at most about  $\pm 0.03\%$  to  $0.04\%$  from the previous values, which is equal to or significantly less than the uncertainties on the values for  $\delta_C^V - \delta_{NS}^V$  in Table VI, so that no action had to be taken for the mirror  $\beta$  transitions discussed here. Note, finally, that because the neutron is a single particle its decay does not require the application of corrections for isospin-symmetry breaking,  $\delta_C$ , or nuclear structure-dependent radiative corrections,  $\delta_{NS}$ .

The resulting  $\mathcal{F}_t^{\text{mirror}}$  values are listed in column 6 of Table VI. Since the previous survey [89] the  $\mathcal{F}_t^{\text{mirror}}$  values for all but three (i.e., <sup>13</sup>N, <sup>41</sup>Sc, and <sup>43</sup>Ti) of the 19 mirror  $\beta$  transitions with  $A = 3$  to 45 have been improved, with now a relative precision  $\leq 0.2\%$  for all transitions (previously

TABLE II. Branching ratios, BR, for the  $T = 1/2$  mirror  $\beta$  transitions up to  $A = 75$ . References to data listed here are given in Table VII. References to rejected data are listed in Table IV together with the reason for their rejection. If branching ratios in literature were quoted relative to values that are to date known more accurately because of later measurements, the published values have been updated. When weighted averages were calculated, the scale factor  $S$  in Eq. (13) is also given.

$n$	Measured branching ratios to excited states (%)								Ground state branching ratio BR (%)
	1		2		3		4		
$^3\text{H}$									100 [Si05]
$^{11}\text{C}$									100 [Ti87]
$^{13}\text{N}$									100 [Aj75]
$^{15}\text{O}$									100 [Aj70]
$^{17}\text{F}$									100 [Aj82]
$^{19}\text{Ne}$	<b>1.55 MeV</b>		<b>0.11 MeV</b>						
	0.0021(3)	[Al76]	0.012(2)	[Ad81]					
	0.0023(3)	[Ad83]	0.0099(7)	[Re19]					
	0.0017(5)	[Re19]							
	<b>0.00212(20)</b>	( $S=1$ )	<b>0.0101(7)</b>	( $S=1$ )					<b>99.9878(7)</b>
$^{21}\text{Na}$	<b>0.35 MeV</b>								
	5.1(2)	[Al74]							
	4.2(2)	[Az77]							
	4.97(16)	[Wi80]							
	4.74(4)	[Ia06]							
	<b>4.746(77)</b>	( $S=2.1$ )							<b>95.254(77)</b>
$^{23}\text{Mg}$	<b>2.39 MeV</b>		<b>0.44 MeV</b>						
	0.0064(9)	[Ma74]	9.1(5)	[Ta60]					
			8.6(3)	[Go68a]					
			9.1(4)	[Al74]					
			8.1(4)	[Ma74]					
			7.79(15)	[Az77]					
			7.805(81)	[Ma17]					
	<b>0.0064(9)</b>		<b>7.91(14)</b>	( $S=2.1$ )					<b>92.08(14)<sup>a</sup></b>
$^{25}\text{Al}$	<b>1.611 MeV</b>		<b>0.975 MeV</b>						
	0.9(2)	[Ma69]	0.036(17)	[Mo71]					
	0.7(2)	[Ba70]	0.044(7)	[Ma76]					
	0.84(7)	[Ju71]	0.040(14)	[Az77]					
	0.794(35)	[Az77]							
	0.776(28)	[Wi80]							
	<b>0.788(21)</b>	( $S=1$ )	<b>0.042(6)</b>	( $S=1$ )					<b>99.170(22)<sup>b</sup></b>
$^{27}\text{Si}$	<b>2.98 MeV</b>		<b>2.73 MeV</b>		<b>2.21 MeV</b>		<b>1.01 MeV</b>		
	0.0249(40)	[De71]	0.0155(17)	[Ma74]	0.10(2)	[Go64]	0.0024(8)	[De71]	
	0.0259(24)	[Ma74]	0.0142(10)	[Da85]	0.18(5)	[Be71]	0.0049(24)	[Ma74]	
	0.0214(14)	[Da85]			0.15(7)	[De71]	0.0050(8)	[Da85]	
					0.181(14)	[Ma74]			
					0.148(7)	[Az77]			
					0.164(28)	[Ma17]			
	<b>0.0227(14)</b>	( $S=1.2$ )	<b>0.0145(9)</b>	( $S=1$ )	<b>0.151(9)</b>	( $S=1.5$ )	<b>0.0038(9)</b>	( $S=1.7$ )	<b>99.808(9)</b>
$^{29}\text{P}$	<b>2.43 MeV</b>		<b>1.27 MeV</b>						
	0.453(16)	[Wi80]	0.8(2)	[Ro55]					
	0.4(1)	[Lo02]	1.2(2)	[Lo62]					
			1.255(22)	[Wi80]					
	<b>0.455(14)</b>	( $S=1$ )	<b>1.249(35)</b>	( $S=1.6$ )					<b>98.296(38)</b>

TABLE II. (Continued.)

	Measured branching ratios to excited states (%)							Ground state branching ratio BR (%)	
	1		2		3		4		
<sup>31</sup> S	<b>3.51 MeV</b>		<b>3.13 MeV</b>		<b>1.266 MeV</b>				
	0.011(3)	[De71]	0.032(5)	[De71]	1.1(1)	[Ta60]			
	0.0121(10)	[Wi80]	0.0326(16)	[Wi80]	0.8(4)	[De71]			
				1.25(6)	[Al74]				
				0.98(20)	[Az77]				
				1.097(33)	[Wi80]				
	<b>0.0120(9)</b>	(S=1)	<b>0.0325(15)</b>	(S=1)	<b>1.126(34)</b>	(S=1.3)		<b>98.830(34)</b>	
<sup>33</sup> Cl	<b>4.75 MeV</b>		<b>4.05 MeV</b>		<b>2.87 MeV</b>		<b>2.31 MeV</b>		
	0.00041(21)	[Wi80]	0.00047(15)	[Wi80]	0.443(58)	[Wi80]	0.0353(48)	[Wi80]	
	<b>1.97 MeV</b>		<b>0.84 MeV</b>						
	0.460(60)	[Wi80]	0.479(64)	[Wi80]				<b>98.58(11)</b>	
<sup>35</sup> Ar	<b>3.97 MeV</b>		<b>3.92 MeV</b>		<b>3.00 MeV</b>		<b>2.69 MeV</b>		
	0.00744(87)	[Wi80]	0.00790(52)	[Wi80]	0.07(2)	[De71]	0.19(3)	[De71]	
	0.00763(74)	[Ad84]	0.0104(42)	[Ad84]	0.11(3)	[Ge71]	0.16(4)	[Ge71]	
					0.0901(33)	[Wi80]	0.1606(65)	[Wi80]	
					0.0932(56)	[Ad84]	0.171(11)	[Ad84]	
					0.084(6)	[Da85]	0.160(9)	[Da85]	
		<b>0.00755(56)</b>	(S=1)	<b>0.00794(52)</b>	(S=1)	<b>0.0895(25)</b>	(S=1)	<b>0.1630(47)</b>	(S=1)
		<b>1.76 MeV</b>		<b>1.22 MeV</b>					
		0.25(7)	[Wi69]	1.04(24)	[Wi69]				
		0.234(13)	[Wi69]	1.223(46)	[Wi69]				
		0.22(3)	[De71]	1.22(20)	[Ge71]				
	0.22(5)	[Ge71]	1.228(30)	[Wi80]					
	0.272(10)	[Wi80]	1.23(7)	[Ad84]					
	0.250(16)	[Ad84]							
	0.260(11)	[Da85]							
	<b>0.2571(68)</b>	(S=1.2)	<b>1.225(9)</b>	(S=1)				<b>98.250(12)</b>	
<sup>37</sup> K	<b>3.94 MeV</b>		<b>3.60 MeV</b>		<b>3.17 MeV</b>		<b>2.80 MeV</b>		
							2.0(4)	[Ka64]	
							2.22(21)	[Az77]	
							2.07(11)	[Ha97]	
						2.20(17)	[Ku17] <sup>e</sup>		
	0.00116(13)	[Ha97]	0.0224(12)	[Ha97]	0.0027(2)	[Ha97]	<b>2.121(70)</b>	(S=1)	
	<b>2.49 MeV</b>		<b>1.61 MeV</b>		<b>1.41 MeV</b>				
	0.0029(4)	[Ha97]	0.0025(20)	[Ha97]	0.00422(75)	[Ha97]		<b>97.843(70)</b>	
<sup>39</sup> Ca	<b>0.35 MeV</b>								
	0.00226(58)	[Ad84]							
	0.00250(27)	[Ha94]							
	<b>0.00246(24)</b>	(S=1)						<b>99.9975(32)<sup>d</sup></b>	
<sup>41</sup> Sc	<b>2.96 MeV</b>		<b>2.58 MeV</b>						
	0.0139(14)	[Wi80]	0.0232(29)	[Wi80]				<b>99.9629(52)<sup>e</sup></b>	
<sup>43</sup> Ti	<b>3.63 MeV</b>		<b>3.26 MeV</b>		<b>2.76 MeV</b>		<b>2.46 MeV</b>		
	0.016(4)	[Ho87]	0.011(3)	[Ho87]	0.20(3)	[Ho87]	0.92(13)	[Ho87]	
	<b>2.34 MeV</b>		<b>2.29 MeV</b>		<b>1.96 MeV</b>		<b>1.88 MeV</b>		
	0.39(6)	[Ho87]	4.7(7)	[Ho87]	0.024(10)	[Ho87]	0.20(4)	[Ho87]	
	<b>1.41 MeV</b>		<b>0.85 MeV</b>						
	0.68(10)	[Ho87]	2.7(8)	[Ho87]				<b>90.2(11)</b>	
<sup>45</sup> V	<b>0.040 MeV</b>								
	4.3(15) <sup>f</sup>	[Ho82]						<b>95.7(15)</b>	
<sup>47</sup> Cr	<b>0.087 MeV</b>								
	3.9(12) <sup>g</sup>	[Bu85]						<b>96.1(12)</b>	
<sup>49</sup> Mn	<b>2.50 MeV</b>		<b>0.27 MeV</b>						
			6.4(26)	[Ha80]					
			5.8(26)	[Ho89]					

TABLE II. (*Continued.*)

	Measured branching ratios to excited states (%)								Ground state branching ratio BR (%)
	1		2		3		4		
	<b>2.3(9)</b>	[Ho89]	<b>6.1(18)</b>	( $S=1$ )					<b>91.6(20)</b>
<sup>51</sup> Fe	<b>3.56 MeV</b> 0.16(5)	[Ho89]	<b>3.43 MeV</b> 0.20(6)	[Ho89]	<b>2.91 MeV</b> 0.10(3)	[Ho89]	<b>2.14 MeV</b> 0.24(7)	[Ho89]	
	<b>1.82 MeV</b> 0.49(14)	[Ho89]	<b>0.237 MeV</b> 5.0(13)	[Ay84]					<b>93.8(13)</b>
<sup>53</sup> Co	<b>1.33 MeV</b> 5.6(17)	[Ho89]							<b>94.4(17)</b>
<sup>55</sup> Ni									<b>100.0(20)<sup>b</sup></b>
<sup>57</sup> Cu	<b>3.01 MeV</b> 0.35(4)	[Se96]	<b>2.44 MeV</b> 0.17(3)	[Se96]	<b>1.11 MeV</b> 8.60(60)	[Se96]	<b>0.77 MeV</b> 0.94(9)	[Se96]	<b>89.9(8)</b>
<sup>59</sup> Zn	<b>high-<math>E</math></b> 0.09(2) 0.23(8)	[Ar84] [Ho81]	<b>0.914 MeV</b> 4.8(6) 5(2)	[Ar84] [Ho81]	<b>0.491 MeV</b> 1.1(2) 1.6(8)	[Ar84] [Ho81]			
	<b>0.098(33)</b>	( $S=1.2$ )	<b>4.82(57)</b>	( $S=1$ )	<b>1.13(19)</b>	( $S=1$ )			<b>93.95(60)</b>
<sup>61</sup> Ga	<b>0.94 MeV</b> 0.68(18)	[Zu15]	<b>0.76 MeV</b> 0.86(24)	[Zu15]	<b>0.42 MeV</b> 1.3(4)	[Zu15]	<b>0.12 MeV</b> 1.2(4)	[Zu15]	
	<b>0.088 MeV</b> 1.9(6)	[Zu15]							<b>94.0(10)<sup>i</sup></b>
<sup>67</sup> Se	<b>high-<math>E</math><sup>j</sup></b> 0.5(1)	[B195]							<b>99.5(1)<sup>k</sup></b>
<sup>71</sup> Kr <sup>l</sup>	<b>≈4.25 MeV<sup>j</sup></b> 2.1(7) <sup>n</sup> ≈2	[Oi97] [Fi05] <sup>o</sup>	<b>0.407? MeV<sup>m</sup></b> ≈15	[Fi05] <sup>o</sup>	<b>0.207 MeV</b> 15.8(14) ≈15	[Oi97] [Fi05] <sup>o</sup>			<b>82.1(16)<sup>p</sup></b> to ≈68 <sup>q</sup>
	<b>2.1(7)</b>		<b>≈15</b>		<b>15.8(14)</b>				
<sup>75</sup> Sr	<b>5.50 MeV<sup>j</sup></b> 6.5(33) 5.2(9)	[B195] [Hu03]	<b>0.144 MeV</b> 5.2(11) <sup>r</sup>	[Hu03]					
	<b>5.3(9)</b>	( $S=1$ )	<b>5.2(11)</b>						<b>89.5(14)</b>

<sup>a</sup>A small correction because the 440 keV level is also fed in the decay of the 2390 keV level with a branching ratio of 0.0025(3)%, lowering the g.s. branching ratio by this amount, is negligible at the present level of precision.

<sup>b</sup>A branching ratio of 0.006(4)% to the level at 1.965 MeV is reported in [Az77] but is not retained in the ENSDF database.

<sup>c</sup>See also [Se17].

<sup>d</sup>The error is obtained from the quadratic sum of the error bars on the BR to the state at 2.52 MeV and the upper limits for the BR to states at higher excitation energies reported in [Ha94].

<sup>e</sup>Errors obtained from the quadratic sum of the errors on the BR to the states at 2.58 and 2.96 MeV and the upper limits for the BR to states at higher excitation energies reported in [Wi80].

<sup>f</sup>This includes a correction for the internal conversion coefficient  $\alpha = 0.223(10)$  for the 40 keV  $\gamma$  ray to the ground state [Bu08].

<sup>g</sup>This includes a correction for the internal conversion coefficient  $\alpha = 0.041(4)$  for the 87 keV  $\gamma$  ray to the ground state [Bu07].

<sup>h</sup>Based on the fact that the first excited state which may be populated by allowed  $\beta$  decay is near 2.5 MeV, making 100% g.s. feeding very probable [Ju08]. A 2% error bar was assumed.

<sup>i</sup>See also [We02].

<sup>j</sup> $\beta$  decay to proton-decaying level(s).

<sup>k</sup>A level assumed to be at 0.35 MeV with a supposed BR of 8% reported in [Ba94] was not observed in (HI,  $xn\gamma$ ) reactions [Ju05].

<sup>l</sup>See [Ab11] for more details.

<sup>m</sup>Level uncertain (see [Ab11]).

<sup>n</sup>The very different value of 5.2(6)% reported in [B195] might be due to the presence of an isomer at  $\approx 10$  keV [Fi05, Ab11].

<sup>o</sup>No error bars given. Results in [Fi05] are based on a re-interpretation of the data in [Oi97].

<sup>p</sup>Value for [Oi97].

<sup>q</sup>Value for [Fi05]. See also [Ab11] and Sec. II B 3. Note that a minimum value of 68.1% is required in order to avoid a negative value for  $\rho^2$  when solving Eq. (9).

<sup>r</sup>This includes a correction for the internal conversion coefficient  $\alpha = 0.15(10)$  for the 144 keV  $\gamma$  ray to the ground state [Ne13].

TABLE III. References from which results for half-lives have been rejected because the error bars are a factor 10 or more larger than that of the most precise measurement (top part) or other reasons (lower part). The correlation between the alphabetical reference code used here and the actual reference numbers is listed in Table VII.

<b>Error bar more than 10 times larger than most precise result</b>	
Parent nucleus (unit)	Half-life value [Reference]
$n$ (s)	616.3(34) [By96]
$^{11}\text{C}$ (min)	20.35(8) [Sm41]; 20.0(1) [Di51]; 20.74(10) [Ku53]; 20.26(10) [Ba55]; 20.8(2) [Pr57]; 20.11(13) [Ar58]; 20.32(12) [Be75]
$^{15}\text{O}$ (s)	123.95(50) [Pe57]; 124.1(5) [Ki59]; 122.6(10) [Ne63]
$^{19}\text{Ne}$ (s)	17.43(6) [Ea62]; 17.36(6) [Go68]; 17.7(1) [Pe57]; 17.36(6) [Wi74]
$^{21}\text{Na}$ (s)	23.0(2) [Ar58]; 22.55(10) [Al74]; 22.48(4) [Az75, Az77] <sup>a</sup>
$^{23}\text{Mg}$ (s)	11.36(4) [Al74]; 11.26(8) [Az74]; 11.41(5) [Go68]; 12.1(1) [Mi58]
$^{25}\text{Al}$ (s)	7.24(3) [Mu58]
$^{27}\text{Si}$ (s)	4.21(3) [Gr71]; 4.14(3) [Mi58]; 4.16(3) [Su62] <sup>b</sup> ; 4.19(2) [Bl68]; 4.09(2) [Ba77]
$^{31}\text{S}$ (s)	2.80(5) [Cl58]; 2.66(3) [Ha52]; 2.40(7) [Hu54]; 2.61(5) [Li60]; 2.72(2) [Mi58]; 2.58(6) [Wa60]
$^{37}\text{K}$ (s)	1.25(4) [Ka64]; 1.23(2) [Sc58]
$^{39}\text{Ca}$ (s)	0.876(12) [Cl58]; 0.865 <sup>+0.007</sup> <sub>-0.017</sub> [Ka68]
$^{43}\text{Ti}$ (s)	0.58(4) [Sc48]; 0.40(5) [Va63]
$^{47}\text{Cr}$ (s)	0.460(80) [Ku17a]
$^{53}\text{Co}$ (s)	0.267(109) [Ha87]
$^{57}\text{Cu}$ (s)	0.1994(32) [Sh84]; 0.183(17) [Lo02, Bl02]
$^{59}\text{Zn}$ (s)	0.173(14) [Lo02, Bl02]; 0.213(34) [Ro14]
$^{65}\text{As}$ (s)	0.19 <sup>+0.11</sup> <sub>-0.07</sub> [Wi93]; 0.190(11) [Mo95]; 0.126(16) [Lo02, Bl02]; 0.126(7) [Ro14]
$^{71}\text{Kr}$ (s)	0.097(9) [Ew81]; 0.100(3) [Oi97]; 0.092(9) [Ro14]; 0.083(48) [Lo02, Bl02]
$^{75}\text{Sr}$ (s)	0.080 <sup>+0.400</sup> <sub>-0.040</sub> [Ki01, Fa02]; 0.071 <sup>+0.071</sup> <sub>-0.024</sub> [Bl95]
$^{95}\text{Cd}$ (s)	0.073 <sup>+0.053</sup> <sub>-0.028</sub> [St11] <sup>b</sup>
<b>Other reasons for exclusion</b>	
Parent nucleus [Reference(s)]	Explanation
$^{17}\text{F}$ [Al77], [Wo69]	The quoted half-lives [resp. 64.80(9) s and 65.2(2) s] are significantly higher (by resp. $4.8\sigma$ and $4.2\sigma$ ) than the average of the other, more recent and also more precise results.
$^{27}\text{Si}$ [Ge76]	The quoted half-life [i.e., 4.206(8) s] was measured with a spectrometer and is significantly higher (by $12\sigma$ ) than the average of the other, mutually consistent results, as is also the case for the other half-life (for $^{24}\text{Na}$ ) that was obtained with the same apparatus.
$^{27}\text{Si}$ [Go68]	The quoted half-life [i.e., 4.17(1) s] is significantly higher (by $5.9\sigma$ ) than the average of the other, mostly more recent and also more precise and mutually consistent results.
$^{29}\text{P}$ [Ja60], [Ta73]	Both quoted half-lives [resp. 4.19(02) s and 4.149(5) s] are significantly higher (by resp. $4.3\sigma$ and $9.2\sigma$ ) than the weighted average of the other results.
$^{31}\text{S}$ [Al74]	The quoted half-life [i.e., 2.605(12) s] is significantly higher (by $4.3\sigma$ ) than the average of the other, mostly more recent and also mutually consistent results.
$^{39}\text{Ca}$ [KI54]	The larger value reported [i.e., 0.90(1) s] is most probably due to a small contamination from $^{38}\text{K}$ produced in the $^{40}\text{Ca}(\gamma, d)^{38}\text{K}$ reaction with a threshold below the maximum energy used for the $^{40}\text{Ca}(\gamma, n)^{39}\text{Ca}$ reaction.
$^{47}\text{Cr}$ [Bu85]	The quoted half-life [i.e., 0.508(10) s] is significantly higher (by $4.7\sigma$ ) than the weighted average of the two other more precise, and mutually consistent results.
$^{53}\text{Co}$ [Ko73]	The quoted half-life [i.e., 0.262(25) s] was obtained by a $\beta$ -ray measurement possibly including the positrons from $^{53m}\text{Co}$ [Ha87].
$^{53}\text{Co}$ , $^{55}\text{Ni}$ , and $^{59}\text{Cu}$ [Ru14]	The quoted half-lives of 0.2460(18) s, 0.2018(19) s, and 0.1733(33) s, respectively, were later replaced by the new values of 0.245(3) s, 0.203(2) s, and 0.174(2) s, respectively [Ku17a], following a reanalysis of the data in Ref. [Ru14] [136].
$^{63}\text{Ga}$ [Sh93]	The half-lives from [Wi93] and [Sh93] listed in [89] were obtained from the same set of data.
$^{67}\text{Se}$ and $^{71}\text{Kr}$ [Bl95]	The quoted half-lives (i.e., 0.060 <sup>+0.017</sup> <sub>-0.011</sub> s, resp. 0.064 <sup>+0.008</sup> <sub>-0.005</sub> s) were obtained with very low statistics. They are a factor of respectively about 2 and 1.5 lower than the other results and also differ by more than $5\sigma$ from the weighted average of these.

<sup>a</sup>The value  $t_{1/2} = 22.47(3)$  s [Az75] was reanalyzed. The updated value was reported in [Az77].

<sup>b</sup>Unpublished.

TABLE IV. References from which results for branching ratios have been rejected. The correlation between the alphabetical reference code used here and the actual reference numbers is listed in Table VII.

Parent nucleus [Reference(s)]	Reason for exclusion
<b>Branching ratios</b>	
<sup>19</sup> Ne [Sa93], <sup>23</sup> Mg [Da85], <sup>27</sup> Si [Go64], <sup>33</sup> Cl [Ba70] <sup>21</sup> Na [Ac07] <sup>a</sup> , [Ac10]	Error bars are a factor 10 or more larger than that of the most precise measurement.
<sup>29</sup> P [Az77]	The result from the private communication [Ac07] in [89] was recently published as [Ac10] but it is not included here as the error bar is more than 10 times larger than the most precise measurement. The error bars of the branching ratios for <sup>29</sup> P in [Az77] are more than 10 times larger than that of the most precise result (level at 1.27 MeV), or deviate by more than 12 $\sigma$ from the weighted average of the other results in the literature (level at 2.43 MeV). The branching ratio for <sup>29</sup> P to the level at 2.43 MeV in <sup>29</sup> Si reported in [Ro55] has an error bar that is 10 times larger than the one of the most precise result.
<sup>35</sup> Ar [Az77], [Ha79]	The branching ratios from [Az77] and [Ha79] were not considered, as only three, resp. one, branch(es) were observed and the reported branching ratios differ significantly from the ones reported in other experiments.
<sup>37</sup> K [Ma76]	The branching ratios from [Ma76] to levels at 2.80 and 3.60 MeV were not considered as they deviate about 4.2 $\sigma$ from the weighted average of other results in the literature.
<sup>57</sup> Cu [Sh84]	The branching ratio result from [Sh84] was not considered as only the most intensive $\beta$ branch could be observed due to interference of the $\beta$ decays of <sup>54g</sup> Co and <sup>58</sup> Cu while, in addition, the lifetime for <sup>57</sup> Cu reported in [Sh84] is significantly longer than more recent values in the literature.
<sup>61</sup> Ga [Oi99]	The results reported in [Oi99] were not considered as this experiment suffered from strong <sup>61</sup> Zn and <sup>61</sup> Cu isobaric contaminations, resulting in a limited accuracy for the measurement of the <sup>61</sup> Ga branching ratios [We02].
<sup>67</sup> Se [Ba94]	The results reported in [Ba94] were not considered as no error bars are given.
<sup>71</sup> Kr [Fi05]	The branching ratios to the different levels in the daughter isotope <sup>71</sup> Br as shown in Fig. 10 of [Fi05] are only estimated values based on the $\gamma$ spectra shown in [Oi97].

<sup>a</sup>Unpublished.

only 5) up to <sup>39</sup>Ca, as can be seen in Fig. 1, and precisions between 0.4% and 2.9% for the  $fp$ -shell mirror transitions up to <sup>61</sup>Ga. Figures 2 and 3 show the fractional uncertainties for each of the experimental and theoretical input factors to the  $\mathcal{F}t^{\text{mirror}}$  values for the  $sp$ - $sd$  shell transitions and the  $fp$  shell transitions, respectively. Note the difference in the vertical scales for both figures.

### 1. The Gamow-Teller/Fermi mixing ratio, $\rho$ , and ratio of statistical rate functions, $f_A/f_V$

From these  $\mathcal{F}t^{\text{mirror}}$  values the Gamow-Teller/Fermi mixing ratio,  $\rho$ , can now be obtained from Eq. (9). This can be used, e.g., to calculate the standard model expectation values for correlation coefficients, such as the  $\beta$ - $\nu$  correlation or the  $\beta$  asymmetry parameter, when searching for new physics (see, e.g., [85,88]). It further serves as valuable input to investigate the weak-magnetism form factor and the related matrix elements for the mirror  $\beta$  transitions, as will be discussed in Sec. III. Finally, one can also combine these experimental  $\mathcal{F}t^{\text{mirror}}$  values with values of  $\rho$  extracted from measurements of correlation coefficients, allowing one to use Eq. (9) for testing the conserved vector current hypothesis or extracting the quark-mixing matrix element  $V_{ud}$ , as will be discussed below in Secs. IIC 2 and IIC 3, respectively.

Extracting  $\rho^2$  from Eq. (9) leaves the sign of  $\rho$  undetermined, but this is determined by the sign of the Gamow-Teller matrix element,  $M_{GT}$ , which can be obtained from shell

model calculations (see Table XIX, which will be discussed in Sec. III B 4). Further, extracting  $\rho$  from Eq. (9) or using this equation in combination with experimentally determined values for  $\rho$ , in addition requires the ratio of statistical rate functions,  $f_A/f_V$ , to be known. For the neutron, Wilkinson showed the values for  $f_A$  and  $f_V$  to be equal to better than  $10^{-5}$  [141]. For the mirror  $\beta$  decays from <sup>3</sup>H to <sup>45</sup>V, the values for  $f_A/f_V$  have been calculated already [89]. However, it was recently pointed out [88,90] that a double-counting instance occurs when extracting the mixing ratio,  $\rho$ , from experimental data (such as the measurement of a correlation coefficient) and then using it in combination with Eq. (9), as these are typically based on different formalisms. Specifically, the expressions used until now for  $f_A$  and  $f_V$  were obtained in the Behrens-Bühring formalism [127], which was observed to contain parts of the Gamow-Teller-specific inner radiative correction  $\Delta_R^A$  [and missing cancellations from the full  $\mathcal{O}(\alpha)$  calculation] [88,90]. Experimental results for  $\rho$ , on the other hand, were typically obtained using (simplified) results in the Holstein formalism [1,338], which does not contain this contribution, and so return a fully renormalized mixing ratio. When combining this into Eq. (9), the electroweak renormalization was partially double-counted. The values for  $f_A/f_V$  listed in Table VI have therefore been calculated according to Refs. [88,339], resulting in values that differ from the previous ones (e.g., [89]) by up to about 2.5% for the mirror  $\beta$  transitions in the  $sd$  shell.

The effect of this shift in the values of  $f_A/f_V$  on the extraction of the mirror  $\beta$  transition-independent  $\mathcal{F}t_0$  value

TABLE V. Adopted values for the half-lives,  $t_{1/2}$  (from Table I), the branching ratios, BR (Table II), and the decay transition energies,  $Q_{EC}$  (from the 2020 Atomic Mass Evaluation [129–131] unless otherwise indicated), for the  $T = 1/2$  mirror  $\beta$  transitions with  $A \leq 83$  (i.e.,  $s$ ,  $p$ ,  $sd$ , and  $fp$  shells). Isotopes with half-lives in the range of  $\mu\text{s}$  and below are not included here. Details on the calculation of the vector statistical rate factor,  $f_V$ , and the electron-capture fraction,  $P_{EC}$ , are given in Sec. II B 2. The partial half-lives,  $t$ , are obtained from Eq. (5).

Parent nucleus	Half-life $t_{1/2}$ (s)	Branching ratio BR (%)	$Q_{EC}$ (keV)	$f_V$	$P_{EC}$ (%)	Partial half-life $t$ (s)
$n$	$608.96 \pm 0.39$	100	$782.34700 \pm 0.00044$	$1.6887 \pm 0.0002$	N/A	$608.96 \pm 0.39$
$^3\text{H}$	$(38854 \pm 35) \times 10^4$	100	$18.59202 \pm 0.00006^a$	$2.864604(26) \times 10^{-6}$	N/A	$(38854 \pm 35) \times 10^4$
$^{11}\text{C}$	$1220.41 \pm 0.32$	100	$1981.689 \pm 0.061$	$3.18289 \pm 0.00082$	0.232	$1223.24 \pm 0.32$
$^{13}\text{N}$	$597.88 \pm 0.23$	100	$2220.47 \pm 0.27$	$7.7143 \pm 0.0072$	0.196	$599.05 \pm 0.23$
$^{15}\text{O}$	$122.27 \pm 0.06$	100	$2754.18 \pm 0.49$	$35.496 \pm 0.043$	0.100	$122.392 \pm 0.060$
$^{17}\text{F}$	$64.366 \pm 0.026$	100	$2760.47 \pm 0.25$	$35.208 \pm 0.022$	0.146	$64.460 \pm 0.026$
$^{19}\text{Ne}$	$17.2573 \pm 0.0034$	$99.9878 \pm 0.0007$	$3239.50 \pm 0.16$	$98.650 \pm 0.031$	0.100	$17.2767 \pm 0.0034$
$^{21}\text{Na}$	$22.4527 \pm 0.0067$	$95.254 \pm 0.077$	$3546.919 \pm 0.018$	$170.7580 \pm 0.0054$	0.094	$23.594 \pm 0.020$
$^{23}\text{Mg}$	$11.3050 \pm 0.0044$	$92.08 \pm 0.14$	$4056.179 \pm 0.032$	$378.621 \pm 0.018$	0.073	$12.286 \pm 0.019$
$^{25}\text{Al}$	$7.1674 \pm 0.0044$	$99.170 \pm 0.022$	$4276.808 \pm 0.045$	$508.522 \pm 0.032$	0.079	$7.2331 \pm 0.0047$
$^{27}\text{Si}$	$4.1112 \pm 0.0018$	$99.808 \pm 0.009$	$4812.358 \pm 0.096$	$993.52 \pm 0.11$	0.065	$4.1218 \pm 0.0018$
$^{29}\text{P}$	$4.1031 \pm 0.0058$	$98.296 \pm 0.038$	$4942.23 \pm 0.36$	$1136.37 \pm 0.48$	0.075	$4.1774 \pm 0.0061$
$^{31}\text{S}$	$2.5539 \pm 0.0023$	$98.830 \pm 0.034$	$5398.01 \pm 0.23$	$1844.74 \pm 0.45$	0.068	$2.5859 \pm 0.0025$
$^{33}\text{Cl}$	$2.5059 \pm 0.0025$	$98.58 \pm 0.11$	$5582.52 \pm 0.39$	$2189.71 \pm 0.86$	0.075	$2.5439 \pm 0.0038$
$^{35}\text{Ar}$	$1.7752 \pm 0.0010$	$98.250 \pm 0.012$	$5966.24 \pm 0.68$	$3122.0 \pm 2.0$	0.072	$1.8081 \pm 0.0010$
$^{37}\text{K}$	$1.23634 \pm 0.00076$	$97.843 \pm 0.070$	$6147.48 \pm 0.23$	$3623.73 \pm 0.75$	0.079	$1.2646 \pm 0.0012$
$^{39}\text{Ca}$	$0.86046 \pm 0.00080$	$99.9975 \pm 0.0032$	$6524.49 \pm 0.60$	$4951.5 \pm 2.5$	0.077	$0.86114 \pm 0.00080$
$^{41}\text{Sc}$	$0.5962 \pm 0.0022$	$99.9629 \pm 0.0052$	$6495.55 \pm 0.16$	$4745.45 \pm 0.65$	0.094	$0.5970 \pm 0.0022$
$^{43}\text{Ti}$	$0.5223 \pm 0.0057$	$90.2 \pm 1.1$	$6872.6 \pm 6.0$	$6364 \pm 31$	0.092	$0.5796 \pm 0.0095$
$^{45}\text{V}$	$0.5465 \pm 0.0051$	$95.7 \pm 1.5$	$7123.82 \pm 0.21$	$7616.8 \pm 1.2$	0.096	$0.572 \pm 0.010$
$^{47}\text{Cr}$	$0.4606 \pm 0.0027$	$96.1 \pm 1.2$	$7444.0 \pm 5.2$	$9521 \pm 36$	0.097	$0.4798 \pm 0.0066$
$^{49}\text{Mn}$	$0.3820 \pm 0.0066$	$91.6 \pm 2.0$	$7712.43 \pm 0.23$	$11353.3 \pm 1.8$	0.101	$0.417 \pm 0.012$
$^{51}\text{Fe}$	$0.3031 \pm 0.0029$	$93.8 \pm 1.3$	$8054.0 \pm 1.4$	$14123 \pm 13$	0.101	$0.3235 \pm 0.0054$
$^{53}\text{Co}$	$0.2440 \pm 0.0028$	$94.4 \pm 1.7$	$8288.11 \pm 0.44$	$16222.0 \pm 4.6$	0.107	$0.2588 \pm 0.0055$
$^{55}\text{Ni}$	$0.2032 \pm 0.0025$	$100.0 \pm 2.0$	$8694.04 \pm 0.58$	$20642.3 \pm 7.4$	0.105	$0.2034 \pm 0.0048$
$^{57}\text{Cu}$	$0.19640 \pm 0.00067$	$89.9 \pm 0.8$	$8774.95 \pm 0.44$	$21374.2 \pm 5.7$	0.117	$0.2187 \pm 0.0021$
$^{59}\text{Zn}$	$0.1812 \pm 0.0011$	$93.95 \pm 0.60$	$9142.78 \pm 0.60$	$26205.3 \pm 9.2$	0.117	$0.1941 \pm 0.0017$
$^{61}\text{Ga}$	$0.1660 \pm 0.0025$	$94.0 \pm 1.0$	$9214 \pm 38$	$26914 \pm 597$	0.131	$0.1768 \pm 0.0033$
$^{63}\text{Ge}$	$0.1485 \pm 0.0051$	–	$9626 \pm 37$	$33452 \pm 688$	0.129	–
$^{65}\text{As}$	$0.1303 \pm 0.0006$	–	$9541 \pm 85$	$31458 \pm 1517$	0.151	–
$^{67}\text{Se}$	$0.1330 \pm 0.0038$	$99.5^b \pm 0.1$	$10007 \pm 67$	$39923 \pm 1435$	0.146	$0.1339 \pm 0.0038$
		$90.0^c \pm 1.5$				$0.1480 \pm 0.0049$
$^{71}\text{Kr}$	$0.0988 \pm 0.0003$	$82.1^b \pm 1.6$	$10175 \pm 129$	$42371 \pm 2916$	0.177	$0.1206 \pm 0.0024$
		$70.0^c \pm 1.5$				$0.1414 \pm 0.0031$
$^{75}\text{Sr}$	$0.0852 \pm 0.0031$	$89.5^b \pm 1.4$	$10600 \pm 220$	$51147 \pm 5841$	0.197	$0.0954 \pm 0.0038$
		$80.0^c \pm 1.5$				$0.1067 \pm 0.0044$
$^{77}\text{Y}$	$0.065 \pm 0.017$	–	$11365 \pm 203$	$71486 \pm 5734$	0.179	–
$^{79}\text{Zr}$	$0.056 \pm 0.030$	–	$11033 \pm 310$	$61468 \pm 10023$	0.217	–
$^{83}\text{Mo}$	$0.028 \pm 0.019$	–	$11273 \pm 432$	$67103 \pm 14649$	0.253	–

<sup>a</sup>From [137] which is 17, respectively 24 times more precise than the two most precise previous results, i.e., [138] resp. [139].

<sup>b</sup>Upper limit. See Sec. II B 3.

<sup>c</sup>Assumed lower limit. See Sec. II B 3.

(see Eq. (14) below and Ref. [89]) to test CVC and extract a value for the  $V_{ud}$  quark-mixing matrix element was discussed already in Ref. [88]. Removing the double-counting issue was observed to bring significantly improved internal consistency in the  $V_{ud}$  mirror data set and in addition lowered uncertainty. Further, a shift of the central value towards the much more precise value obtained from the superallowed pure Fermi transitions was observed, bringing the values obtained for both types of transitions in agreement with each other. In the next

two sections we will discuss the status of both CVC and  $V_{ud}$ , including all information from mirror nuclei and the latest results for the neutron (see also [41,42,56]).

### 2. Testing the conserved vector current hypothesis

The  $\mathcal{F}_t^{\text{mirror}}$  values can be used to provide an independent test of the conserved vector current (CVC) hypothesis [5,340] (more details on CVC are given in Sec. III A 2) as was shown

TABLE VI. Calculated quantities and corrections leading to the  $\mathcal{F}t^{\text{mirror}}$  values. The  $f_V t$  values are obtained from columns 5 and 7 in Table V. The calculation of  $f_A/f_V$  is described in Sec. II C 1, and that of  $\delta'_R$  and  $\delta_C^V - \delta_{NS}^V$  in Sec. II C.  $\mathcal{F}t^{\text{mirror}}$  values are obtained from Eq. (9) and  $\rho$  values are calculated from Eqs. (9) and (10). Uncertainties in  $f_A/f_V$  are taken as 20% of their deviation from unity (as in Ref. [89]).  $\delta(\mathcal{F}t^{\text{mirror}})$  is the relative error on  $\mathcal{F}t^{\text{mirror}}$ .

Parent nucleus	$f_V t$ (s)	$f_A/f_V$	$\delta'_R$ (%)	$\delta_C^V - \delta_{NS}^V$ (%)	$\mathcal{F}t^{\text{mirror}}$ (s)	$\delta(\mathcal{F}t^{\text{mirror}})$ %	$\rho = c$ [Eq. (12)]
$n$	$1028.25 \pm 0.66$	1.0000	1.4902(2) <sup>a</sup>	N/A	$1043.58 \pm 0.67$	0.06	+2.21086(118)
$^3\text{H}$	$1113.0 \pm 1.0$	1.0003	1.767(1)	0.16(2)	$1130.9 \pm 1.0$	0.09	-2.1053(14) <sup>b</sup>
$^{11}\text{C}$	$3893.4 \pm 1.4$	0.9992	1.660(4)	1.04(3)	$3916.9 \pm 1.9$	0.05	-0.75442(79)
$^{13}\text{N}$	$4621.3 \pm 4.7$	0.9980	1.635(6)	0.33(3)	$4681.3 \pm 4.9$	0.11	-0.5596(14)
$^{15}\text{O}$	$4344.3 \pm 5.7$	0.9964	1.555(8)	0.22(3)	$4402.3 \pm 5.9$	0.13	+0.6302(16)
$^{17}\text{F}$	$2269.5 \pm 1.7$	1.0020	1.587(10)	0.62(3)	$2291.2 \pm 1.9$	0.08	+1.2955(11)
$^{19}\text{Ne}$	$1704.34 \pm 0.63$	1.0011	1.533(12)	0.52(4)	$1721.5 \pm 1.0$	0.06	-1.60203(92)
$^{21}\text{Na}$	$4028.8 \pm 3.5$	1.0020	1.513(14)	0.41(3)	$4073.0 \pm 3.8$	0.09	+0.7125(12)
$^{23}\text{Mg}$	$4651.9 \pm 7.3$	0.9994	1.476(17)	0.40(3)	$4701.6 \pm 7.6$	0.16	-0.5541(20)
$^{25}\text{Al}$	$3678.2 \pm 2.4$	1.0019	1.475(20)	0.52(5)	$3713.0 \pm 3.2$	0.08	+0.8084(11)
$^{27}\text{Si}$	$4095.1 \pm 1.9$	1.0002	1.443(23)	0.42(4)	$4136.7 \pm 2.7$	0.07	-0.69659(93)
$^{29}\text{P}$	$4747.0 \pm 7.2$	1.0008	1.453(26)	1.07(6)	$4764.5 \pm 7.9$	0.17	+0.5380(21)
$^{31}\text{S}$	$4770.3 \pm 4.7$	0.9992	1.430(29)	0.79(4)	$4800.3 \pm 5.3$	0.11	-0.5294(15)
$^{33}\text{Cl}$	$5570.4 \pm 8.6$	0.9895	1.435(32)	0.93(6)	$5597.8 \pm 9.5$	0.17	-0.3142(32)
$^{35}\text{Ar}$	$5645.0 \pm 4.9$	0.9929	1.421(35)	0.53(5)	$5694.8 \pm 6.0$	0.11	+0.2820(23)
$^{37}\text{K}$	$4582.5 \pm 4.4$	0.9955	1.431(39)	0.79(6)	$4611.4 \pm 5.5$	0.12	-0.5779(16)
$^{39}\text{Ca}$	$4264.0 \pm 4.5$	0.9955	1.422(43)	0.95(8)	$4283.5 \pm 6.0$	0.14	+0.6606(17)
$^{41}\text{Sc}$	$2833 \pm 10$	1.0019	1.454(47)	0.86(7)	$2849 \pm 11$	0.38	+1.0743(38)
$^{43}\text{Ti}$	$3688 \pm 63$	0.9955	1.444(50)	0.63(11)	$3718 \pm 64$	1.7	-0.810(18)
$^{45}\text{V}$	$4354 \pm 79$	1.0042	1.438(53)	0.93(12)	$4375 \pm 80$	1.8	+0.635(20)
$^{47}\text{Cr}$	$4568 \pm 65$	1.0033	1.439(58)	0.8(2)	$4596 \pm 66$	1.4	-0.579(17)
$^{49}\text{Mn}$	$4739 \pm 132$	0.9991	1.438(61)	0.8(2)	$4769 \pm 133$	2.8	+0.537(34)
$^{51}\text{Fe}$	$4568 \pm 77$	0.9970	1.442(66)	0.8(2)	$4597 \pm 78$	1.7	-0.581(20)
$^{53}\text{Co}$	$4197 \pm 90$	1.0039	1.443(70)	0.8(2)	$4224 \pm 91$	2.1	+0.673(23)
$^{55}\text{Ni}$	$4199 \pm 99$	0.9965	1.433(73)	0.8(2)	$4225 \pm 100$	2.4	-0.675(25)
$^{57}\text{Cu}$	$4675 \pm 45$	0.9912	1.455(79)	1.5(3)	$4672 \pm 47$	1.0	+0.564(12)
$^{59}\text{Zn}$	$5085 \pm 45$	0.9856	1.440(81)	1.5(3)	$5081 \pm 47$	0.9	-0.461(12)
$^{61}\text{Ga}$	$4759 \pm 137$	0.9933	1.461(87)	1.5(3)	$4756 \pm 138$	2.9	+0.542(35)
$^{67}\text{Se}^c$	$5344 \pm 245$	1.0184	1.461(99)	1.7(3)	$5330 \pm 245$	4.6	-0.387(67)
$^{67}\text{Se}^d$	$5908 \pm 289$				$5893 \pm 288$	4.9	-0.20(12)
$^{71}\text{Kr}^c$	$5108 \pm 366$	0.9976	1.474(109)	1.7(3)	$5095 \pm 365$	7.2	+0.454(95)
$^{71}\text{Kr}^d$	$5991 \pm 432$				$5976 \pm 432$	7.2	+0.17(22)
$^{75}\text{Sr}^c$	$4879 \pm 590$	0.9521	1.484(118)	1.7(3)	$4867 \pm 588$	12	+0.53(15)
$^{75}\text{Sr}^d$	$5458 \pm 662$				$5445 \pm 661$	12	+0.37(20)

<sup>a</sup>From [86].

<sup>b</sup>Note that we believe that the sign in the tables of [148] (which was copied in [89]) is wrong for  $^3\text{H}$ .

<sup>c</sup>Values for upper limit of BR; see also Table V and Sec. II B 3.

<sup>d</sup>Values for lower limit of BR; see also Table V and Sec. II B 3.

already in Ref. [43]. Indeed, Eq. (9) can be written as

$$\begin{aligned}
\mathcal{F}t_0 &\equiv f_V t (1 + \delta'_R) (1 + \delta_{NS}^V - \delta_C^V) |M_F^0|^2 \left[ 1 + \frac{f_A}{f_V} \rho^2 \right] \\
&= \mathcal{F}t^{\text{mirror}} \left[ 1 + \frac{f_A}{f_V} \rho^2 \right] \\
&= \frac{K}{G_F^2 V_{ud}^2 g_V^2 (1 + \Delta_R^V)} \\
&= 2 \mathcal{F}t^{0^+ \rightarrow 0^+}.
\end{aligned} \tag{14}$$

The first line contains all transition-dependent quantities, with  $|M_F^0|^2 = 1$ . Note that for the decay of the neutron, being a single nucleon, the correction  $\delta_{NS}^V - \delta_C^V$  is identically zero,

whereas for the other mirror transitions and for the pure Fermi transitions all three corrections, i.e.,  $\delta'_R$ ,  $\delta_{NS}^V$ , and  $\delta_C^V$ , have to be considered. The third line in Eq. (14) consists only of common constants. It is thus seen that when combining the  $\mathcal{F}t^{\text{mirror}}$  values with  $\rho$  mixing ratio values obtained from independent measurements, such as from experimentally determined correlation coefficients, an identical value for  $\mathcal{F}t_0$  should be obtained for all mirror transitions.

Table VIII lists the  $\mathcal{F}t_0$  values resulting from correlation measurements in mirror  $\beta$  transitions, as well as the data leading to these. In extracting  $\rho$  from the respective correlation measurement we included weak magnetism recoil order terms as was also done in [43,69]. Only for  $^{19}\text{Ne}$  was this found to have a significant effect (i.e., about half a standard deviation).

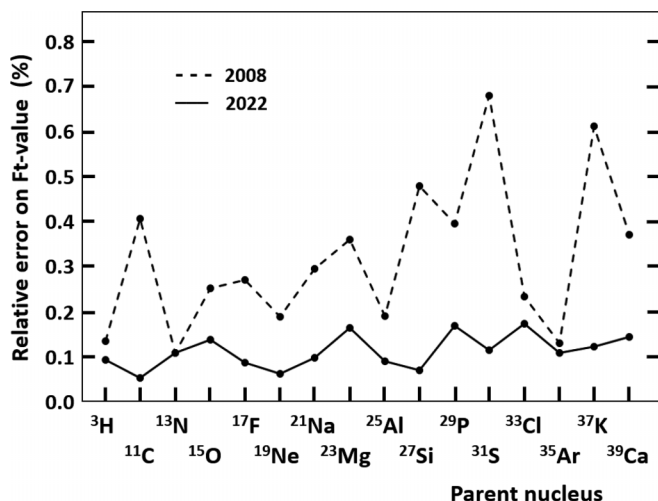


FIG. 1. Progress in the relative uncertainties of the  $\mathcal{F}_t^{\text{mirror}}$  values for the mirror  $\beta$  transitions up to  $A = 39$  from 2008 [89] (dashed) till now (solid).

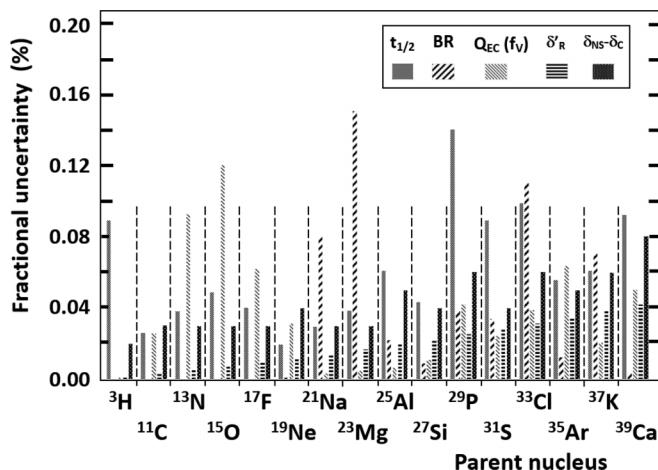


FIG. 2. Fractional contribution of the experimental and theoretical input factors to the  $\mathcal{F}_t^{\text{mirror}}$  values for the mirror  $\beta$  transitions up to  $A = 39$ .

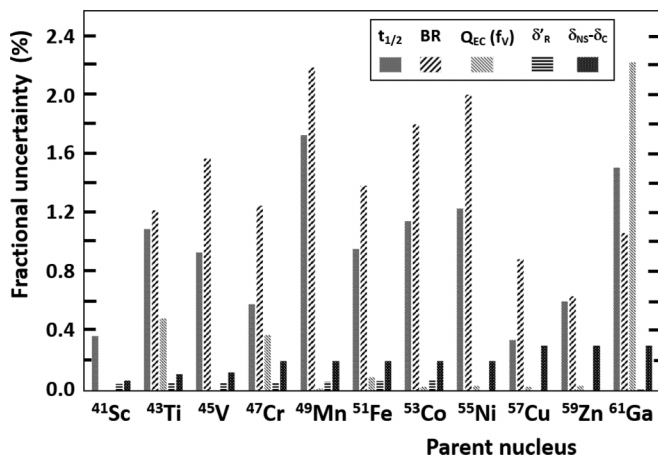


FIG. 3. Fractional contribution of the experimental and theoretical input factors to the  $\mathcal{F}_t^{\text{mirror}}$  values for the mirror  $\beta$  transitions in the mass  $A = 41-61$  range. Note the difference in vertical scale with Fig. 2.

TABLE VII. Reference key relating the reference codes used in Tables I to IV to the actual reference numbers.

Table code	Reference no.
Ab11	[149]
Ac07	[150]
Ac10	[151]
Ad81	[152]
Ad83	[153]
Ad84	[154]
Aj70	[155]
Aj75	[156]
Aj82	[157]
Ak04	[158]
Ak88	[159]
Al67	[160]
Al72	[161]
Al73	[162]
Al74	[163]
Al76	[164]
Al77	[165]
Ar15	[166]
Ar58	[167]
Ar84	[168]
Aw69	[169]
Ay84	[170]
Az74	[171]
Az75	[172]
Az77	[115]
Ba12	[173]
Ba55	[174]
Ba70	[175]
Ba77	[176]
Ba94	[177]
Be71	[178]
Be75	[179]
Bl02	[180]
Bl10	[181]
Bl68	[182]
Bl95	[183]
Bl99	[184]
Bo65	[185]
Br14	[186]
Br16	[97]
Bu07	[187]
Bu08	[188]
Bu20	[189]
Bu85	[190]
Bu91	[191]
By96	[192]
Ce16	[193]
Cl58	[194]
Da17	[195]
Da85	[196]
De71	[197]
Di51	[198]
Ea62	[199]
Eb65	[200]
Ed77	[201]
Ew81	[202]

TABLE VII. (*Continued.*)

Table code	Reference no.
Ez18	[203]
Fa02	[204]
Fi05	[205]
Fi17	[206]
Fo17	[207]
Ge71	[208]
Ge76	[209]
Gi20	[210]
Go21	[135]
Go64	[211]
Go68	[212]
Go68a	[213]
Gr15	[214]
Gr15a	[215]
Gr71	[216]
Ha52	[217]
Ha79	[218]
Ha80	[219]
Ha87	[220]
Ha94	[221]
Ha97	[222]
Ho77	[223]
Ho81	[224]
Ho82	[225]
Ho87	[226]
Ho89	[227]
Hu03	[228]
Hu54	[229]
Ia06	[230]
Ja60	[231]
Ja61	[232]
Ja99	[233]
Je50	[234]
Jo51	[235]
Jo55	[236]
Jo67	[237]
Ju05	[238]
Ju08	[239]
Ju71	[240]
Ka14	[241]
Ka64	[242]
Ka64a	[243]
Ka68	[244]
Ki01	[245]
Ki59	[246]
Ki60	[247]
Kl54	[248]
Ko73	[249]
Ku53	[250]
Ku17	[251]
Ku17a	[252]
Li60	[253]
Lo02	[254]
Lo17	[255]
Lo20	[256]
Lo62	[257]
Lu00	[258]
Ma06	[259]

TABLE VII. (*Continued.*)

Table code	Reference no.
Ma17	[260]
Ma69	[261]
Ma74	[262]
Ma76	[263]
Ma93	[264]
Me66	[265]
Mi58	[266]
Mo71	[267]
Mo95	[268]
Mu58	[269]
Ne13	[270]
Ne63	[271]
No47	[272]
Oi97	[273]
Oi99	[274]
OI87	[275]
Or21	[276]
Pa18	[277]
Pa18a	[278]
Pe57	[279]
Pf96	[280]
Pi10	[281]
Pi85	[282]
Pl62	[283]
Po58	[284]
Pr57	[285]
Re19	[286]
Re99	[287]
Ri68	[288]
Ro14	[289]
Ro55	[290]
Ru14	[291]
Ru77	[292]
Ry95	[293]
Sa93	[294]
Sc48	[295]
Sc58	[296]
Sc70	[297]
Se05	[298]
Se17	[299]
Se18	[300]
Se96	[301]
Sh14	[302]
Sh15	[303]
Sh18	[304]
Sh84	[305]
Sh89	[306]
Sh93	[307]
Si05	[308]
Si19	[309]
Si87	[310]
Sm41	[311]
St11	[312]
St12	[313]
Su13	[314]
Su13a	[315]
Su17	[316]
Su62	[317]

TABLE VII. (Continued.)

Table code	Reference no.
Ta60	[318]
Ta73	[319]
Ti87	[320]
Tr12	[321]
Uj13	[322]
Un00	[323]
Va18	[324]
Va63	[325]
Va69	[326]
Wa60	[327]
We02	[328]
Wi69	[329]
Wi74	[330]
Wi80	[331]
Wi93	[332]
Wo02	[333]
Wo69	[334]
Yo65	[335]
Yu13	[336]
Zu15	[337]

For all other cases the effect on  $\rho$  was found to be negligible, as were the effects from other recoil terms and radiative corrections (see also [84,85]). Four measurements were not included here, either because the resulting values of  $\rho$  have errors that are significantly larger than those in Table VIII (i.e.,  $A(^{17}\text{F}) = 0.960(82)$  [346],  $a(^{19}\text{Ne}) = 0.00(8)$  [347], and  $a(^{35}\text{Ar}) = 0.97(14)$  [347]), or because it was superseded by a later measurement (i.e.,  $A(^{21}\text{Na}) = 0.5243(91)$  [348], superseded by [62]).

TABLE VIII. Values for the quantity  $\mathcal{F}t_0$  [Eq. (14)] for mirror  $\beta$  transitions for which correlation measurements have already been performed. Values for  $\mathcal{F}t^{\text{mirror}}$  and  $f_A/f_V$  are taken from Table VI. Results from measurements of the beta-neutrino correlation,  $a$ , the beta-asymmetry parameter,  $A$ , or the neutrino-asymmetry parameter,  $B$ , are listed in columns 4 to 6. The corresponding values for the GT/F mixing ratio,  $\rho$ , and resulting values of  $\mathcal{F}t_0$  are listed in the last two columns. Note that when both statistical and systematic errors were given these were combined quadratically, while asymmetric error bars have been symmetrized by setting  $\sigma_{\text{symm}}^2 = (\sigma_+^2 + \sigma_-^2)/2$ . See text for further details.

Parent nucleus	$\mathcal{F}t^{\text{mirror}}$ (s)	$f_A/f_V$	$a$	$A$	$B$	$\rho$	$\mathcal{F}t_0$ (s)
$n$	1043.58(67)	1.0000				+2.2091(15) <sup>a</sup>	6136.8(80)
$^{19}\text{Ne}$	1721.5(10)	1.0011		-0.0391(14) [341]		-1.5995(45)	6131(25)
$^{19}\text{Ne}$	1721.5(10)	1.0011		-0.03871(81) [69,342]		-1.6014(26)	6141(15)
$^{21}\text{Na}$	4073.0(38)	1.0020	0.5502(60) [62]			+0.7135(72)	6151(42)
$^{29}\text{P}$	4764.5(79)	1.0008		+0.681(86) [343]		+0.594(104)	6448(589)
$^{35}\text{Ar}$	5694.8(60)	0.9929		+0.49(10) [344]		+0.322(75)	6282(272)
$^{35}\text{Ar}$	5694.8(60)	0.9929		+0.427(23) [345]		+0.277(16)	6128(51)
$^{37}\text{K}$	4611.4(55)	0.9955			-0.755(24) [74]	-0.559(27)	6046(141)
$^{37}\text{K}$	4611.4(55)	0.9955		-0.5707(19) [35]		-0.5770(59)	6140(32)

<sup>a</sup>This value is obtained as  $\rho = (C_A M_{\text{GT}})/(C_V M_F)$ , with  $M_{\text{GT}} = \sqrt{3}$  for the neutron, and using for  $\lambda \equiv C_A/C_V = +1.2754(11)$  reported in Refs. [66,118], which is the weighted average of the values obtained from measurements of  $a$ ,  $A$ , and  $B$  that were not included in later published results and which yielded a value for  $\lambda$  with an uncertainty that is within ten times that of the most precise value.

Combining the values for  $\mathcal{F}t_0$  in Table VIII, but not yet including the neutron, yields a weighted average of

$$\mathcal{F}t_0 = 6138.7(111) \text{ s (mirrors, no neutron),} \quad (15)$$

which is dominated by the two values for  $^{19}\text{Ne}$  and the result for  $^{37}\text{K}$  from Ref. [35]. The difference with the value of 6141(13) s in Ref. [88] is entirely due to the inclusion here of the earlier measurement of  $A$  with  $^{19}\text{Ne}$  [341], which is less precise but entirely consistent with the result of the more recent measurement [69,342]. Comparing the value of Eq. (15) with the one for the neutron (Table VIII), i.e.,

$$\mathcal{F}t_0 = 6136.8(80) \text{ s (neutron),} \quad (16)$$

it is seen that the higher-mass mirror nuclei approach the neutron as to precision. Combining, finally, all values in Table VIII, and thus including now also the neutron, leads to

$$\mathcal{F}t_0 = 6137.5(65) \text{ s (neutron and other mirrors),} \quad (17)$$

which is dominated by the value for the neutron and the most recent value for  $^{19}\text{Ne}$  [69,342]. This constitutes a 0.11% test of CVC from the currently available set of mirror  $\beta$  decays. Being only a factor 2 less precise than the value  $2\mathcal{F}t^{0^+ \rightarrow 0^+} = 6144.5(37) \text{ s}$  [55] [Eq. (10)] for the pure Fermi transitions, both values can be combined to yield

$$\mathcal{F}t_0 = 6142.8(32) \quad (\chi^2/\nu = 0.94) \text{ (all nuclear),} \quad (18)$$

corresponding to a  $5.2 \times 10^{-4}$  test of CVC, which is slightly better than when only the pure Fermi transitions are used [55].

### 3. The quark-mixing matrix element $V_{ud}$

Combining the  $\mathcal{F}t_0$  value for a specific mirror transition with the value of  $\rho$  that is obtained from, e.g., a measurement of a beta-correlation coefficient, provides a value for the  $V_{ud}$  quark-mixing matrix element independent of the one from the superallowed  $0^+ \rightarrow 0^+$  transitions [55]. For this, Eq. (14) can

be written as

$$|V_{ud}|^2 = \frac{K}{\mathcal{F}t_0 G_F^2 g_V^2 (1 + \Delta_R^V)}. \quad (19)$$

As can be seen, extracting  $V_{ud}^2$  requires the radiative correction  $\Delta_R^V$ . In the past few years, this correction has been addressed in detail by several authors [88,123–126,147,148,349] leading to reduced theoretical uncertainty but also a shift in the central value.

For ease of comparison with the value of  $|V_{ud}|^2$  from the superallowed  $0^+ \rightarrow 0^+$  transitions, we will use here the value of  $\Delta_R^V$  that was used in the latest review of the  $\mathcal{F}t$  values for these transitions [55], i.e.,  $\Delta_R^V = 0.024\,54(19)$  which is the weighted average of Refs. [123–125]. One then has (with the values for  $K$  and  $G_F$  as given in Sec. II A)

$$|V_{ud}|^2 = \frac{5825.90 \pm 1.08}{\mathcal{F}t_0}, \quad (20)$$

which yields for the neutron [using Eq. (16)]

$$|V_{ud}|^2 = 0.94934(125) \text{ (neutron)}, \quad (21)$$

and for all other mirror nuclei [with the  $\mathcal{F}t_0$  value of Eq. (15)]

$$|V_{ud}|^2 = 0.94904(173) \text{ (mirrors, no neutron)}. \quad (22)$$

Both values agree within one standard deviation with the value  $|V_{ud}|^2 = 0.948\,15(60)$  for the pure Fermi transitions [55]. Combining the neutron with the other mirror nuclei yields

$$|V_{ud}|^2 = 0.949\,23(102) \text{ (neutron and mirrors)}. \quad (23)$$

As this is only a factor 1.7 less precise than the value  $|V_{ud}|^2 = 0.948\,15(60)$  for the pure Fermi transitions [55], both values can be combined, leading to

$$|V_{ud}|^2 = 0.948\,41(52) \text{ (all nuclear)}, \quad (24)$$

for the entire set of pure Fermi and mirror  $\beta$  transitions, which shows a clear improvement in precision over the value for the pure Fermi transitions alone. Thus, the neutron and other mirror  $\beta$  transitions now contribute, for the first time, to improving the weighted average value for  $|V_{ud}|$ , with the neutron contributing the most. With more measurements being planned and experimental precision further improving (a nonexhaustive list of ongoing and planned measurements with the precision they aim at is given in Table 3 of [41]) the complementary approach to  $V_{ud}$  that is offered by the neutron and the mirror nuclei [42,43,56] now starts to play a visible role for testing the unitarity of the quark-mixing matrix.

*a. Note on the radiative correction  $\Delta_R^V$ .* With respect to testing the unitarity condition we briefly come back to the recent progress in calculating the  $\Delta_R^V$  radiative correction. All new calculations yielded values that are larger than the previous result from Marciano and Sirlin [350], i.e.,  $\Delta_R^V = 0.023\,61(38)$ , with the ones that are believed to be more complete also providing the largest values, i.e.  $\Delta_R^V = 0.024\,77(24)$  [88,126,349]. As is shown in Table IX, combining these two extreme values with the weighted average value  $\mathcal{F}t_0 = 6142.8(32)$  s [Eq. (18)] for all transitions in Table VIII provides values for  $|V_{ud}|^2$  that, when combined with the Particle Data Group values for  $|V_{us}| = 0.2245(8)$  and  $|V_{ub}| =$

TABLE IX. Values for  $|V_{ud}|^2$  and the unitarity test, i.e., unitarity sum  $\equiv |V_{ud}|^2 + |V_{us}|^2 + |V_{ub}|^2$  for the outermost values of the radiative correction  $\Delta_R^V$ , when using the average value  $\mathcal{F}t_0 = 6142.8(32)$  s from all nuclear decays [Eq. (18)] and  $|V_{us}| = 0.2245(8)$  and  $|V_{ub}| = 0.00382(24)$  from Ref. [118].

Quantity	$\Delta_R^V = 0.02361(38)$ 2006 [350]	$\Delta_R^V = 0.02477(24)$ 2020/2021 [88,126,349]
$ V_{ud} ^2$	0.94927(61)	0.94820(54)
Unitarity sum	0.99968(71)	0.99861(65)
Deviation	$0.5\sigma$	$2.1\sigma$

$0.003\,82(24)$  [118], lead either to good agreement with unitarity (i.e., for the 2006 value of  $\Delta_R^V$ ), or to a  $2.1\sigma$  deviation from it (for the 2020/2021 value). The latter becomes  $2.3\sigma$  when using the slightly larger value  $\mathcal{F}t_0 = 6144.5(37)$  s [Eq. (10)] for the pure Fermi transitions.

Note that the value of  $|V_{us}| = 0.2245(8)$  presently adopted by the Particle Data Group [118] is in fact the weighted average of two values conflicting at the  $3\sigma$  level, i.e.,  $|V_{us}| = 0.2231(7)$  from  $K_{l3}$  decays and  $|V_{us}| = 0.2252(5)$  from  $K_{\mu 2}$  decay data. When using the latter and larger of these two values in combination with the larger value  $\Delta_R^V = 0.024\,77(24)$  [88,126,349], the unitarity sum amounts to  $0.998\,93(59)$ , deviating  $1.8\sigma$  from unity. All this clearly shows the paramount importance of the value of  $\Delta_R^V$  for the unitarity test and calls for further theoretical investigation.

### III. WEAK MAGNETISM

The second part of this work focuses on the weak-magnetism correction to the  $\beta$  spectrum shape (and corresponding  $\mathcal{F}t$  values) and to  $\beta$ -correlation measurements. Its importance has been hinted at throughout the previous sections, and cannot be understated as experimental precision reaches the subpercent level. Its correct evaluation is an important factor in the extraction of new physics as well as in the extraction of  $V_{ud}$  from precise  $\beta$ -correlation measurements, such that a thorough discussion of its origin and properties is worthwhile as the field continues and grows.

We give here a fairly in-depth presentation of the theoretical origin and state, followed by a discussion of experimental behavior in mirror and other isospin multiplet  $\beta$  decays. In both cases we compare against results of the nuclear shell model, assisted by simple single-particle results to aid in its interpretation. Based on these results, we discuss the ability of nuclear theory to correctly predict this quantity and the prospects in experimentally unexplored territories.

#### A. Theoretical foundations

Throughout the years the effects of weak magnetism have been studied by various groups of authors, using different formalisms (e.g., Refs. [1,2,4,127]). Its precise evaluation comes with several subtleties and a number of caveats. It is of interest then, to lay out the theoretical foundations underlying the evaluation. To ease the interpretation for the reader, we will present all final results in the formalism by Holstein [1,338],

although some intermediate results have been derived from other works.

We will first discuss the generalization of the Hamiltonian to include induced currents and the electromagnetic interaction. We follow with the treatment of the conserved vector current (CVC) hypothesis and how it connects these two components. Finally, we discuss the evaluation of the matrix elements that appear when comparing to theoretical results.

### 1. Generalized Hamiltonian

*a. Generalized nuclear  $\beta$  decay Hamiltonian.* In the original Fermi approach, the  $\beta$  decay Hamiltonian is constructed as a simple current-current interaction, analogous to the electromagnetic interaction:

$$H_\beta(x) = \frac{G_F \cos \theta_C}{\sqrt{2}} [H_\mu(x)L^\mu(x) + \text{H.c.}], \quad (25)$$

where  $G_F$  is the Fermi coupling constant obtained from muon decay,  $\theta_C$  is the Cabibbo angle, and  $H_\mu(x)$  and  $L^\mu(x)$  are the hadron and lepton currents, respectively. The standard model (SM) expression for the latter is defined as

$$L^\mu = \bar{u}_e \gamma^\mu (1 - \gamma^5) v_\nu, \quad (26)$$

with  $u, v$  the lepton wave functions and  $\gamma_i$  the Dirac  $\gamma$  matrices, which couple only to left-handed particles. In the absence of any other forces, all relevant particle states are simple plane waves. The nuclear medium is, however, hardly a place devoid of additional forces. This is mainly due to the strong interaction, which renormalizes the weak vertex. Further, the presence of an electrostatic potential (i.e., QED) forces a slew of changes compared to the simple plane wave picture. Since  $\beta$  decay occurs only at low momentum transfer, however, most of the SM intricacies are not kinematically visible and instead serve to renormalize the coupling constants. The renormalization of the weak vertex due to QCD effects results in two changes. The first is a modification of the axial vector operator,  $\langle n | \bar{u} \gamma^\mu \gamma^5 d | p \rangle$ , which can, e.g., be calculated using first principles on the lattice [351,352], but is most precisely determined experimentally (see, e.g., the recent FLAG Review 2021 [353]). The vector part,  $\langle n | \bar{u} \gamma^\mu d | p \rangle$ , is protected through the CVC hypothesis discussed in the following section and remains unchanged, even to higher order [354]. While in the standard model the simple  $V$ - $A$  behavior is a direct consequence of the electroweak interaction, the nuclear medium allows for some modification. Additional operators which still adhere to the required  $V$ - $A$  behavior can be constructed through a combination with the nuclear momentum transfer  $q = p_i - p_f$ . In preparation we write the hadronic current of Eq. (25) more generally:

$$H_\mu(x) = \langle f | V_\mu(x) + A_\mu(x) | i \rangle. \quad (27)$$

The approach spearheaded by Holstein [1,338] and contemporaries [127,355] consists of treating the nucleus as an elementary particle, and says nothing about its constituents or internal turmoil. This allows one to encode all behavior through form factors that depend only on  $q^2$  as mentioned

above. For the simple neutron this becomes

$$V_\mu(x) = \left[ g_V \gamma_\mu - \frac{g_M - g_V}{2M} \sigma_{\mu\nu} q^\nu + i \frac{g_S}{2M} q_\mu \right] \tau^+, \quad (28)$$

$$A_\mu(x) = \left[ g_A \gamma_5 \gamma_\mu - \frac{g_T}{2M} \sigma_{\mu\nu} \gamma_5 q^\nu + \frac{g_P}{2M} \gamma_5 q_\mu \right] \tau^+, \quad (29)$$

where all  $g_i$  form factors are a dimensionless function of  $q^2$ , and  $\tau^+$  is the isospin ladder operator. The appearance of factors  $\mathcal{O}(q/M)$  traditionally lends them the name of recoil-order corrections or recoil terms. In order of appearance, these are called the vector (Fermi), weak magnetism, induced scalar, axial vector (Gamow-Teller), induced tensor, and induced pseudoscalar terms.

The presence of the electromagnetic field now has two additional consequences for nuclear  $\beta$  decay. The first entails a renormalization of the decay vertex, as we have done before with the strong interaction in Eqs. (28) and (29). Up to  $\mathcal{O}(\alpha)$ , with  $\alpha$  the fine-structure constant, these simply renormalize the leading order terms [i.e.,  $\Delta_R^{V,A}$  as in Eqs. (7) and (8)] and do not introduce additional structure. The experimental definition of the GT/F mixing ratio (and  $g_A$  in the case of the neutron) simply absorbs the difference of vector and axial vector inner radiative corrections, in addition to the other small corrections in Eq. (8). The second consequence concerns the operators in Eqs. (28) and (29), specifically those coupling to the momentum  $q_\mu$ . In the traditional quantum mechanics calculation, turning on the electromagnetic field requires the standard substitution  $\partial_\mu \rightarrow \partial_\mu - ieA_\mu$ , where  $A_\mu = (i\phi, \mathbf{A})$  is the electromagnetic four-vector. It is in part this effect which in the traditional  $\beta$  decay calculations [127] causes a contribution to what is now understood to be part of the inner radiative correction [88]. We will come back to this below.

We have, up to now, only discussed the generalization to a system with spin 1/2, leading to Eqs. (28) and (29). For general allowed  $\beta$  transitions where  $\Delta J = 0, 1$ , several additional terms appear. Using the notation of Holstein [338], the form factors are then written as  $a$  (vector),  $b$  (weak magnetism),  $c$  (axial vector),  $d$  (induced tensor),  $e$  (induced scalar),  $h$  (induced pseudoscalar),  $f, g, j_2$ , and  $j_3$ . Full formulas can be found in several publications (e.g., [1,3]). Once again, all form factors are a function of  $q^2$ . Typically, however, only the dominant form factors are expanded as

$$a(q^2) \approx a_1 + a_2 q^2, \quad (30a)$$

$$c(q^2) \approx c_1 + c_2 q^2, \quad (30b)$$

while all others are approximated as their value for  $q^2 = 0$ . This is possible because the momentum transfer in  $\beta$  decay is sufficiently small such that  $qR \ll 1$ , where  $R$  is the nuclear radius (see also the last paragraph in Sec. III A 3 a and Ref. [85]).

*b. Nuclear electromagnetic interaction.* The influence of the electromagnetic field on the weak vertex was summarized in the previous section. As a charged particle, the nucleus also directly couples to the electromagnetic field via

$$\mathcal{L}(x) = ie \mathcal{J}_\mu A^\mu(x), \quad (31)$$

where  $\mathcal{J}_\mu$  contains both nucleon,  $J_\mu$ , and electron,  $l_\mu$ , parts. As before, we can treat the interaction of the latter in the

elementary particle approach and write

$$\langle f|J_\mu(0)|i\rangle = i\langle f|F_1\gamma_\mu + F_2\sigma_{\mu\nu}q^\nu|i\rangle, \quad (32)$$

where again all  $F_i$  are a function of  $q^2$ . The first of these represents the charge, while the second corresponds to the magnetic dipole interaction. These can be split into an isoscalar and isovector part, writing  $F_i = F_i^{(S)} + F_i^{(V)}\tau_3$ . The absence of higher order isospin operators in the electromagnetic interaction has obvious consequences for selection rules between nuclear levels [356,357], and allows one to write down the mass formula within isospin multiplets [358],

$$M(A, T, T_3) = a(A, T) - b(A, T)T_3 + c(A, T)T_3^2, \quad (33)$$

to only second order in  $T_3$ , where  $A$  is the mass number,  $T$  the isospin, and  $T_3 = \frac{1}{2}(Z - N)$ . The parameters  $a$ ,  $b$ , and  $c$ , which are not to be confused with the form factors defined above, can be found in several textbooks [358,359] and in a recent evaluation of the relevant experimental data [360], and depend mainly on the different isomoments of the Coulomb displacement energy and the difference in proton and neutron mass.

## 2. Conserved vector current

Several years before the Weinberg-Salam model of electroweak interactions was proposed, a more intimate connection between electromagnetic and weak interactions was put forward by Feynman and Gell-Mann [5] and Sudarshan and Marshak [340]. Called the conserved vector current hypothesis, the name only covers the “weak” part of the conjecture, namely that

$$\partial^\mu V_\mu = 0, \quad (34)$$

analogous to the classical continuity equation. Equation (34) strictly only holds in the absence of electromagnetism, as the inclusion of the latter requires the substitution  $\partial^\mu \rightarrow \partial^\mu - ieA^\mu$  as before. Application of the weak CVC principle forces  $g_V(q^2 = 0) = 1$  and  $g_S(q^2 = 0) = 0$ , and allows one to express the Fermi matrix element as [127]

$$\begin{aligned} &\langle J_f M_f T_f T_{3f} | V_0(0) | J_i M_i T_i T_{3i} \rangle \\ &= \sqrt{(T_i \pm T_{3i})(T_i \mp T_{3i} + 1)} \delta_{J_i J_f} \delta_{M_i M_f}. \end{aligned} \quad (35)$$

Evaluating this for  $0^+ \rightarrow 0^+$  superallowed decays, one finds  $\sqrt{2}$ , and this is implicitly present in the factor 2 in Eq. (9) [127]. For the  $\beta$  transitions between the isospin  $T = 1/2$  mirror nuclei, one finds  $\sqrt{1}$ . The “strong” CVC principle states that the vector current from  $\beta$  decay forms an isospin triplet with the electromagnetic current [361],

$$V_\mu = \mp[\tau^\pm, J_\mu^{\text{em}}], \quad (36)$$

where  $\tau^\pm$  is the isospin ladder operator. Clearly the “weak” principle directly follows from Eq. (36), and further allows one to relate *weak* interaction matrix elements to their *electromagnetic* analogs. This further implies that Eqs. (28) and (32) can be directly compared. We consider here two cases.

The first deals with  $\beta$  decays within the same isospin multiplet (so with  $\Delta T = 0$ )

$$\langle T T_{3i} \pm 1 | V_\mu^\pm | T T_{3i} \rangle, \quad (37)$$

for which we then find<sup>1</sup>

$$b = \pm aA \sqrt{\frac{J+1}{J}} (\mu_f - \mu_i), \quad (38)$$

where the upper/lower sign is for  $\beta^-/\beta^+$  decay, respectively,  $A$  is the mass number, and  $\mu_{i,f}$  are the nuclear dipole moments of the mother and daughter nuclear states, respectively. Evaluating this for the neutron we find

$$\frac{1}{\sqrt{3}} b = g_M = \mu_p - \mu_n = 4.706, \quad (39)$$

where we used  $a(0) = 1$  for the neutron. The natural extensions of neutron decay from an isospin point of view are the mirror  $\beta$  transitions, where  $T = 1/2$ ,  $T_3 = \pm 1/2$  for initial and final states. When experimental nuclear moment data are available, Eq. (38) allows for an unambiguous determination of the weak magnetism contribution. For the higher multiplets, with  $T = 1$  and higher, analog decays are typically energetically forbidden or connect unbound states due to the behavior of Eq. (33), so that Eq. (38) can no longer be used.

The second case is that of a decay where  $\Delta T = 1$ ,  $\Delta T_3 = \pm 1$ . The strong CVC conjecture then allows one to relate the weak magnetism form factor to the *isovector* part of the decay width of the corresponding analog  $M1$   $\gamma$  transition,  $\Gamma_{M1}^{\text{iso}}$ . In this case, one finds [361]

$$b^2 = \eta \frac{\Gamma_{M1}^{\text{iso}} 6M^2}{\alpha E_\gamma^3}, \quad (40)$$

with  $\alpha$  the fine structure constant and  $M$  the average mass of the mother and daughter nucleus (we used  $M = Au$  with  $A$  the mass number and  $u$  the unified atomic mass unit). The factor  $\eta$  is unity when the final state is the same for  $\beta$  and  $\gamma$  analog transitions, while it is  $\eta = (2J_i + 1)/(2J_f + 1)$  when initial and final states of the  $\gamma$  transition (resp.  $J_i$  and  $J_f$ ) are reversed relative to the  $\beta$  decay, to compensate for the degeneracy in the  $\gamma$  transition phase space. Note that CVC only relates the square of  $b$ , such that a sign ambiguity remains.

It is of interest to note that for  $\beta$  transitions between members of a common isotopic multiplet (like the mirror  $\beta$  transitions) CVC requires the form factors  $e = f = 0$ , while the  $d$  form factor can only be nonzero if second-class currents exist [1,338]. In addition, as many of the transitions that are considered here involve low-spin states, the triangle inequality satisfied by Clebsh-Gordan coefficients requires the vanishing of one or more form factors, i.e., one has for  $J$  to  $J'$  transitions

$$J = 1, J' = 0: \quad a = e = f = g = j_2 = j_3 = 0,$$

$$J = 0, J' = 1: \quad a = e = f = g = j_2 = j_3 = 0,$$

$$J = J' = 1: \quad j_3 = 0,$$

$$J = 1/2, J' = 1/2: \quad f = g = j_2 = j_3 = 0,$$

<sup>1</sup>The CVC hypothesis relates only the *isovector* part of the electromagnetic interaction to the corresponding weak vector decay, while the magnetic moment has both an isoscalar and isovector part. When taking the difference within an isospin multiplet, the isoscalar component obviously drops out.

TABLE X. Summary of the  $a, b, c$ , etc. form factors and their relation to the nuclear matrix elements defined in Table XI. Here, the impulse approximation is given to first order only, and the relativistic matrix elements are neglected, as is also done in [1]. Further,  $M = 1/2(M_i + M_f)$ , with  $M_i$  and  $M_f$  being the masses of the initial and final states of the decay, is the nuclear mass, and  $\Delta = M_i - M_f$  is the nuclear energy release. It is important to note is that the induced tensor form factor,  $d$ , contains both a first-class ( $d_I$ ) and second-class ( $d_{II}$ ) contributions [1]. The former can be shown to disappear for decays between analog states (e.g., the mirror  $\beta$  transitions) [1], while no second-class currents have been observed till now (see, e.g., [12,24,26,29,365]).

Form factor	Formula for impulse approximation	Remark
$a$	$a \cong g_V M_F$	$g_V = 1$ (CVC)
$b$	$b \cong A(g_M M_{GT} + g_V M_L)$	$g_M = 4.706$ (CVC)
$c_1$	$c_1 \cong g_A M_{GT}$	$g_A \rightarrow g_{A,eff} = +1^a$ [366], but $g_A = +1.2754(11)$ [56,66] for $n$ and $+1.27$ for ${}^3\text{He}$
$c_2$	$c_2 \cong g_A/6[M_{\sigma r^2} + \sqrt{1/10}M_{1y}]$	$c_2/c_1 = a_2/a_1 = R^2/10$ [367] ( $R$ = nuclear radius)
$d$	$d = d_I + d_{II} \cong A(g_A M_{\sigma L} \pm g_{II} M_{GT})$	$g_{II} \sim g_T \cong 0^b$
$f$	$f \cong \sqrt{2/3}M\Delta g_V M_Q/(\hbar c)^2$	$M = 1/2(M_i + M_f)$ = nuclear mass
$g$	$g \cong (-4/3)M^2 g_V M_Q/(\hbar c)^2$	$\Delta = M_i - M_f$ = nuclear energy release
$h$	$h \cong (-2/\sqrt{10})M^2 g_A M_{1y}/(\hbar c)^2 - A^2 g_P M_{GT}$	$g_P = -181.03^c$
$j_k$	$j_k \cong (-2/3)M^2 g_A M_{ky}/(\hbar c)^2$	

<sup>a</sup>Note that we follow the positive sign convention for  $g_A$  of Ref. [1].

<sup>b</sup>We assume the absence of second-class currents.

<sup>c</sup>See also Ref. [368].

$$\begin{aligned}
 J = 1/2, J' = 3/2: \quad a = e = j_3 = 0, \\
 J = 3/2, J' = 1/2: \quad a = e = j_3 = 0.
 \end{aligned}
 \tag{41}$$

Finally, the effect of the higher-order form factors  $a_2, c_2$  and the induced pseudoscalar form factor  $h$ , that were not yet mentioned here, but which appear in the  $\beta$ -spectrum shape (cf. Eq. (B7) in Ref. [1]) and so determine the  $ft$  value of a transition, are all reduced by a factor  $M^2$  ( $M$  being the average mass of the initial and final nuclei) with respect to the  $a, c, b$ , and  $d$  form factors. They can therefore be neglected at the level of precision of the  $ft$  values we are dealing with in this paper, which is of the order of per mille to several percent.

### 3. Form factor evaluation

The weak magnetism correction shows up in a specific combination in the Gamow-Teller  $\beta$  spectrum, i.e., as

$$\delta_{WM} = \frac{b}{Ac_1}, \tag{42}$$

where  $c_1$  is the first component of the Gamow-Teller form factor as defined in Eq. (30b). Considering we have generalized the nuclear current using the elementary particle approach, and related the form factors to electromagnetic observables for specific cases, one could consider the work to be done and leave the determination of these form factors to experiment. Often, however, application of CVC is impossible and one would like input from nuclear models. We consider here the impulse approximation and discuss the quenching of the axial vector coupling constant.

*a. Impulse approximation.* The easiest way through which the form factors can be connected to nuclear models (i.e., nuclear matrix elements) is by using the impulse approximation, where we consider the nuclear current a sum of independent single-particle nucleon currents. In doing this, one neglects meson exchange, off-shell mass effects and other many-body

effects. This is typically a reasonable assumption for allowed transitions. Indeed, discrepancies resulting from using the impulse approximation as compared to the elementary particle treatment have been discussed in the light of CVC and PCAC, and were found to be in good agreement for allowed transitions [355,362].

The usual approach is performed by generalizing Eqs. (28) and (29) to a system of  $A$  nucleons, and performing a Foldy-Wouthuysen transformation to yield the nonrelativistic limit [363]. Comparing terms with that of the elementary particle approach, one can write the corresponding reduction of the form factors to proper nuclear matrix elements. A summary of the relevant form factors is given in Table X, with the required nuclear matrix elements being listed in Table XI. For clarity, these are only given to first order. The correction term of Eq. (42) then becomes

$$\frac{b}{Ac_1} = \frac{1}{g_A} \left( g_M + g_V \frac{M_L}{M_{GT}} \right), \tag{43}$$

TABLE XI. Definitions of the reduced nuclear matrix elements relevant for the Holstein form factors in Table X (from Refs. [1,3]).

Matrix element	Operator form
$M_F$	$\langle \psi_f \  \Sigma \tau_i^\pm \  \psi_i \rangle$
$M_{GT}$	$\langle \psi_f \  \Sigma \tau_i^\pm \vec{\sigma}_i \  \psi_i \rangle$
$M_L$	$\langle \psi_f \  \Sigma \tau_i^\pm \vec{l}_i \  \psi_i \rangle$
$M_{\sigma r^2}$	$\langle \psi_f \  \Sigma \tau_i^\pm \vec{\sigma}_i r_i^2 \  \psi_i \rangle$
$M_{\sigma L}$	$\langle \psi_f \  \Sigma \tau_i^\pm i \vec{\sigma}_i \times \vec{l}_i \  \psi_i \rangle$
$M_Q$	$(4\pi/5)^{1/2} \langle \psi_f \  \Sigma \tau_i^\pm r_i^2 Y_2(r_i) \  \psi_i \rangle$
$M_{ky}$	$(16\pi/5)^{1/2} \langle \psi_f \  \Sigma \tau_i^\pm \sigma_i^z C_{12k}^{m'k} Y_2^{n'}(r_i) \sigma_{in} \  \psi_i \rangle$

and is seen to consist of a universal weak-magnetism part, determined by the form factor  $g_M$ , and a transition-dependent part, determined by the ratio  $M_L/M_{GT}$ . To compare experimental values for  $b/Ac_1$  we are thus left with the evaluation of these two matrix elements.

It is interesting to note that recently [364] the universal weak magnetism form factor,  $g_M$ , could for the first time be extracted from a fit to the experimental data for the  $\mathcal{F}_T$  values for the  $0^+ \rightarrow 0^+$  transitions (which fixed  $g_V$ ), the neutron's lifetime (fixing  $g_A$ ), and the correlation measurements in neutron decay (which then fixed  $g_M$ ). The fit [364] yielded  $g_M/g_V = 3.7(11)$  (noted as  $C_M^+/C_V^+$  in Ref. [364]) consistent with the CVC prediction  $g_M = 4.7$  (see Table X).

Apart from this universal weak magnetism contribution, the ratio  $b/Ac_1$  thus measures the relative strength of  $M_L$  and  $M_{GT}$ . For a pure-spin transition, with  $M_L \ll M_{GT}$  and  $g_A = 1.00$  (see Sec. III A 3 c), one obtains  $b/Ac_1 = 4.7$ . As  $g_V = 1$ , values of  $b/Ac_1$  smaller than 2.7 or larger than 6.7 indicate the orbital matrix element,  $M_L$ , to be at least twice as large as  $M_{GT}$ , indicating a clear dominance of the orbital contribution. Finally, at the level of precision we will be dealing with in the evaluation of  $b/Ac_1$  later in this paper, we can neglect the  $q^2$  dependence of the  $c$  form factor in Eq. (30b) and so replace  $c_1$  by  $c$ , i.e., the total Gamow-Teller form factor as it is present in the  $\mathcal{F}_T^{\text{mirror}}$  value [Eqs. (8) and (9)]. Thus, the form factor ratio will be denoted further as  $b/ac$ .

*b. Long-wavelength and other approximations.* One can understand Eq. (40) more intuitively by writing down the  $M1$  matrix element in the long-wavelength approximation, in which case it becomes proportional to

$$\langle f | \sum_i^A \mathbf{l}_i \left( \frac{1 + \tau_3^{(i)}}{2} \right) + \frac{\boldsymbol{\sigma}^{(i)}}{2} (\mu_V^+ + \mu_V^- \tau_3^{(i)}) | i \rangle, \quad (44)$$

where  $\mu_V^\pm = (\mu_p \pm \mu_n)$ , with  $\mu_p$  and  $\mu_n$  the proton and neutron magnetic moments. Using the experimental values for these, it is clear that the isovector contribution is much more dominant than its isoscalar counterpart, leading to several quasiselection rules [369–371].

The use of the Eqs. (43) and (44) depends on several approximations, with increasing importance:

- (1) *Long wavelength:* The expression for the  $M1$  operator was derived for  $kR \ll 1$ , with  $k$  the wave number of the emitted  $\gamma$  ray. This is most certainly valid for the low energies coming from nuclear transitions, and is relevant only for energies upwards of 200 MeV.
- (2) *Nuclear currents:* The orbital (convection) part of the nuclear current that interacts with the vector potential is typically constructed using  $\mathbf{v} = \mathbf{p}/M$ , whereas more precisely it should be  $\mathbf{v} = i[H, \mathbf{r}]/\hbar$  where  $H$  is the full Hamiltonian, including spin-orbit terms and exchange terms.
- (3) *Deformation:* The comparison of weak magnetism and the  $M1$  matrix elements assumes the isobaric analog states are identical in all quantum numbers except for  $T_3$ . When introducing deformation, however, this picture can quickly turn around, as often the analog

state sits at high excitation energies and differing deformation. Furthermore, states can be parts of different rotational or vibrational bands, resulting in additional quenching of transition amplitudes.

- (4) *Isospin purity:* Typically we consider transitions for which  $\Delta T = \pm 1$ , meaning the isovector part is automatically the only contributing factor. This, however, assumes perfect isospin symmetry which is violated in practice so that isoscalar contributions can sneak in.

Nevertheless, due to the smallness of the violation and the numerical weight of the isovector moment, this is typically negligible [358]. However, in cases where the Gamow-Teller matrix element is strongly suppressed, the dominant contribution can arise from the angular momentum part in Eq. (44) instead. The biggest culprit for isospin mixing is the isovector part of the Coulomb interaction, resulting in an isospin impurity proportional to  $\sum_j [(f|V_C|j)/(E_f - E_j)]^2$  [358]. Due to a variety of mechanisms, the isospin purity remains rather low even for higher  $Z$  nuclei, though individual variation can change significantly [358,372].

- (5) *Meson exchange:* An important distinction between Eqs. (40) and (44) is the treatment of meson exchange currents. The strong CVC principle [Eq. (36)] relates weak interaction and electromagnetic *form factors*, including all meson exchange effects, induced currents, etc. While Eq. (40) is always correct since it directly follows from the strong CVC principle [Eq. (36)], the evaluation through Eq. (44) is not and requires a remedy. In usual nuclear physics fashion this can be performed by introducing effective charges to both the proton and neutron [373]. Recently much work was performed using *ab initio* methods [374].

It is clear that many subtleties can underlie the proper evaluation of weak magnetism. Often, though, all of these approximations are sufficiently well behaved. In case of discrepancies, a breakdown of one or more of these approximations can be investigated.

*c. Evaluation of  $g_A$ .* In the neutron system, the value of  $g_A/g_V$  is experimentally found to be 1.2754(11) [66] (see also [118]). In more complex systems, however, typically lower (quenched) values of  $g_A$  are required to reach agreement with experimental data when employing shell model or mean field theories [375–377]. The reason for this quenching lies in a failure to take into account the required degrees of freedom inside the nuclear medium, meaning truncated valence spaces, three-body interactions, and nucleon-nucleon correlations. The quenching is then an attempt at a parametrization of theoretical deficiencies of commonly used theories. It speaks for itself then that no quenching is unique, and is inherently coupled to the details of the underlying theory with its effective interactions and basis states. Intensive research was performed in the second half of the twentieth century [378–380], and has recently become very actual again due to its relevance in neutrinoless double  $\beta$  decay searches [381–384]. Some explanation is required then, as we

consider here both shell model and deformed single-particle results.

Two effects are at play here. The first is traditionally called core polarization [385,386]. One usually considers as starting point a single-particle Hamiltonian as  $H_0 = T + U$ , where  $U$  is an average single-particle potential. The true solutions of the system, however, are solutions of the true Hamiltonian,  $H = H_0 + \mathcal{V}$ , where  $\mathcal{V} = V - U$  is additional influence from the true nucleon-nucleon potential. Further, solutions are constructed using single-particle orbitals generated from only a subspace of finite dimension. The correction required using this approach is typically called *core polarization*, and represents the lack of multiparticle correlations in the individual wave functions. This includes residual interactions between valence particles, core deformation,  $\Delta(1236)$ -isobar excitations, and relativistic effects [380].

The second effect is that of meson exchange [366,387,388]. Typically, the proper nucleon-nucleon interaction can be reduced in an effective manner to correspond to the exchange of several mesons, principally the pion and heavier  $\rho$  and  $\omega$  excitations. Combined with possible  $\Delta$  isobars, this leads to an impressive number of required calculations. A modern example can be found in Ref. [389].

The choice for a quenching factor then depends on how well these effects are present in the models we employ [384]. In the case of the shell model, one often uses  $g_A = 1.0$  (e.g., [366,389]) to counter model-space truncations and meson exchange effects. The evaluation of the single-particle results is slightly less straightforward. For low mass nuclei and transitions close to closed shells, meson exchange will be the dominating factor. Going to higher masses and more exotic transitions, deformation effects will start to play a role. This can be mitigated using a deformed potential (see Appendix A). In mid-shell nuclei proton-neutron residual interactions can become nontrivial and give dominant contributions. It is clear and hardly unexpected that there is no easy solution. As a way of making do, one often uses the  $g_A$  quenching factors extracted from early shell model calculations, i.e., those not containing extensive core polarization and meson exchange corrections, i.e.,  $g_A = 1.1$  for the  $sd$  shell [390],  $g_A = 1.0$  for the  $pf$  shell and onwards [391] (see [384] for a comprehensive overview and discussion of the renormalization of  $g_A$ ).

As here experimental results for the  $b$  and  $c$  form factors and the Gamow-Teller and orbital current matrix elements, respectively  $M_{GT}$  and  $M_L$ , will be compared to shell model calculations that used  $g_A = 1$  (besides  $g_V = 1$ ,  $g_M = 4.706$ ,  $g_P = -181.03$ , and  $g_S = g_T = 0$ ), we will also use  $g_A = 1$  in dealing with the experimental quantities. Only for the decay of the neutron and tritium ( $A = 3$ ), where there is very little core polarization, do we use the free-nucleon value. We thus use  $g_A = +1.2754(11)$  [66] for the neutron (which was obtained from correlation measurements that are independent of the neutron  $\mathcal{F}t^{\text{mirror}}$  value) and  $g_A = +1.27$  for tritium.

### B. Weak magnetism for the mirror $\beta$ transitions

For the superallowed  $\beta$  transitions between  $T = 1/2$  isospin doublets in mirror nuclei ( ${}^A_{Z+1}X_N \rightarrow {}^A_ZX'_{N+1}$ ) the vec-

tor form factor,  $a$ , is unity [Eq. (35) and Table X], while the weak-magnetism form factor,  $b$ , and the axial-vector form factor,  $c$ , can be determined experimentally using the CVC hypothesis [Eq. (38)] and the experimental  $ft$  value [Eq. (9)], respectively. Form factors  $d$ ,  $e$ ,  $f$ , and  $j_2$  are set to zero as it was shown that the first-class contributions to these form factors that arise in the impulse approximation either vanish for transitions between states of a common isospin multiplet or contribute negligibly compared to the  $a$ ,  $b$ , and  $c$  form factors [1]. Here we update the work of Ref. [2], extending the range of mirror transitions for which experimental data on the weak magnetism term are available up to mass  $A = 75$ .

#### 1. Magnetic moments of the $T = 1/2$ mirror nuclei

The experimental data required to calculate the weak-magnetism form factor,  $b$ , from experimental data, i.e., the nuclear magnetic moments of the mother and the daughter isotopes [Eq. (38)], are reviewed here.

Table XII lists the available experimental values for the magnetic moments of the mirror nuclei up to  $A = 75$ , as published in the recent survey of Refs. [392,393] and updated up to February 2022 via the database of the Brookhaven National Nuclear Data Center [116]. The publications containing the respective input data are again indicated with an alphanumeric code, with the reference key linking these codes with the actual reference numbers listed in Table XV.

The same data-selection procedure that was used for the data leading to the  $\mathcal{F}t$  values is used here for the analysis of the magnetic moments. Thus, data with an uncertainty that is a factor 10 or more larger than that of the most precise measurement, as well as values with other problems, have again been rejected. These are listed and commented in Table XIII. The finally adopted values for the magnetic moments that were used in the further analysis are listed in column 4 of Table XII. When two or more input values are available and the error bars are of similar size, the weighted average is used with the uncertainty being increased by a factor  $S = \sqrt{\chi^2/\nu}$  [Eq. (13)] if  $\chi^2/\nu > 1$ . This scale factor is then listed in column 5. When two, often very precise measurements differ by many standard deviations with no clear argument in favor of either one, the unweighted average is used as the adopted value. This is then indicated in the table.

For the heavier mirror nuclei, i.e., in the  $fp$  shell, experimental magnetic moment values are often not available. For these, the magnetic moments were calculated from the strong linear correlations between the mirror pair magnetic moments and their  $\mathcal{F}t$  values, that was obtained in Ref. [394]. There, ground state gyromagnetic ratios for the odd-proton and odd-neutron partners of the mirror nuclei,  $\gamma_{p/n} = \mu_{p/n}/J$ , could be related [394,395] to their superallowed  $\beta$ -transition strengths,  $\gamma_\beta$ , defined as

$$|\gamma_\beta| = \frac{1}{2} \sqrt{\left( \frac{6170}{\mathcal{F}t^{\text{mirror}}} - 1 \right) \frac{1}{J(J+1)}}, \quad (45)$$

via

$$(\gamma_p + \Delta\gamma_p) = g_p + \frac{G_p - g_p}{R} \gamma_\beta \quad (46)$$

TABLE XII. Magnetic moments of the  $T = 1/2$  mirror nuclei. In column 2 the experimental values available in the literature [116,392,393] are listed, with adopted values listed in column 4. When an average was calculated the scale factor,  $S$  [Eq. (13)], is also given. The columns in the right-hand section of the table relate to the values calculated from the linear relations [394] between the mirror pair magnetic moments and the corrected  $\mathcal{F}T^{\text{mirror}}$  value for the  $\beta$  transition linking them. The  $\gamma_\beta$  values were obtained from Eq. (45) using the corrected  $\mathcal{F}T^{\text{mirror}}$  values of Table VI. The values for the quantities  $\Delta\gamma_p$  and  $\Delta\gamma_n$  are from Tables I and V in Ref. [394]. The calculated values for the magnetic moments were then obtained from Eqs. (46) to (51) [394], using the values listed for  $\gamma_\beta$ ,  $\Delta\gamma_p$ , and  $\Delta\gamma_n$ . Calculated magnetic moment values for isotopes for which no experimental moment value is available yet, are shown in italics. The last column, finally, lists the difference between the adopted and calculated values for the magnetic moments. Note that when the sign for a magnetic moment value in column 2 is given, this has been explicitly measured. When the sign has not been determined experimentally, it was obtained from the linear relation between the  $g$  factors of the  $T = 1/2$  mirror nuclei ground states deduced in Ref. [399], unless otherwise noted. The correlations between the alphabetical reference codes used here and the actual reference numbers are listed in Table XV.

Parent nucleus	Measured magnetic moment(s)		Adopted value ( $\mu_N$ )	Scale $S$	$\gamma_\beta$	$\Delta\gamma_{(p,n)}$	Calculated value ( $\mu_N$ )	expt. – calc.  ( $\mu_N$ )
	$(\mu_N)$							
$n$	–1.91304273(45)	[Ti21]	–1.91304273(45)		+1.27963(49)	– <sup>a</sup>	–2.373(33)	0.460
$p$	+2.79284734462(82)	[U117]	+2.79284734462(82)		+1.27963(49)	– <sup>a</sup>	+3.246(46)	0.453
$^3\text{H}$	+2.9789624656(59) <sup>b</sup>	[Ti21]	+2.9789624656(59)		+1.21872(66)	– <sup>a</sup>	+3.116(44)	0.137
$^3\text{He}$	–2.127625307(25)	[Ti21,Ne12]	–2.127625307(25)		+1.21872(66)	– <sup>a</sup>	–2.260(32)	0.133
$^{11}\text{C}$	–0.964(1)	[Wo70]	–0.964(10)		+0.19583(13)	–0.1864	–0.824(28)	0.140
$^{11}\text{B}$	+2.6886489(10)	[Mi39,Ep75]	+2.6886489(10)		+0.19583(13)	+0.1804	+2.541(36)	0.148
$^{13}\text{N}$	0.3222(4)	[Be64]	–0.3222(4)		–0.32558(71)	+0.2646	–0.306(15)	0.016
$^{13}\text{C}$	+0.7024118(14)	[Ro54]	+0.7024118(14)		–0.32558(71)	–0.2586	+0.726(11)	0.024
$^{15}\text{O}$	0.7189(8)	[Co63]	+0.71950(12)	1	–0.36585(86)	0.0000	+0.671(12)	0.048
	0.71951(12)	[Ta93]						
$^{15}\text{N}$	–0.28318884(5)	[Ba62]	–0.28318884(5)		–0.36585(86)	0.0000	–0.259(16)	0.024
$^{17}\text{F}$	+4.7223(12)	[Su66]	+4.72136(29)	1	+0.21993(14)	0.0000	+4.942(63)	0.221
	+4.7213(3)	[Mi93]						
$^{17}\text{O}$	–1.89379(9)	[Al51a]	–1.89379(9)		+0.21993(14)	0.0000	–2.062(49)	0.168
$^{19}\text{Ne}$	–1.88542(8)	[Ma82]	–1.88542(8)		+0.92810(37)	+0.4032	–1.924(25)	0.039
$^{19}\text{F}$	+2.628868(8)	[Li52,Ba64]	+2.628868(8)		+0.92810(37)	–0.3972	+2.695(34)	0.067
$^{21}\text{Na}$	+2.38630(10)	[Am65]	+2.38630(10)		+0.18527(25)	+0.1657	+2.495(36)	0.109
$^{21}\text{Ne}$	–0.661797(5)	[La57]	–0.661797(5)		+0.18527(25)	–0.1881	–0.763(28)	0.101
$^{23}\text{Mg}$	0.5364(3)	[Fu93]	–0.5365(2)	1	+0.14430(49)	–0.2377	–0.461(26)	0.076
	–0.5366(3)	[Yo17]						
$^{23}\text{Na}$	+2.2176556(6)	[Wa54,Fu76]	+2.21759(7)	unw <sup>c</sup>	+0.14430(49)	+0.2137	+2.162(34)	0.056
	+2.217522(2)	[Be74]						
$^{25}\text{Al}$	3.6455(12)	[Mi76a]	+3.6455(12)		+0.13750(15)	+0.1459	+3.700(56)	0.054
$^{25}\text{Mg}$	–0.85545(8)	[Al51b]	–0.85545(8)		+0.13750(15)	–0.1678	–0.880(44)	0.024
$^{27}\text{Si}$	(–)0.8652(4)	[Ma98]	–0.86533(24)	1	+0.11851(12)	–0.1692	–0.701(43)	0.165
	0.8654(3)	[Ma99]						
$^{27}\text{Al}$	+3.6415069(7)	[Ep68]	+3.6415069(7)		+0.11851(12)	+0.1459	+3.497(54)	0.144
$^{29}\text{P}$	1.2349(3)	[Su71]	+1.23475(21)	1	+0.3136(11)	+0.0109	+1.182(15)	0.052
	1.2346(3)	[Zh09]						
$^{29}\text{Si}$	–0.55529(3)	[We53]	–0.55529(3)		+0.3136(11)	–0.0595	–0.556(11)	0.001
$^{31}\text{S}$	0.48793(8)	[Mi76b]	–0.48793(8)		+0.30840(77)	–0.3044	–0.424(11)	0.064
$^{31}\text{P}$	+1.13160(3)	[Wa54]	+1.13160(3)		+0.30840(77)	+0.2472	+1.053(15)	0.078
$^{33}\text{Cl}$	+0.7523(16)	[Ro86]	+0.7548(5)	1.6	–0.08255(76)	+0.1440	+0.817(32)	0.062
	+0.7549(3)	[Ma04]						
$^{33}\text{S}$	+0.6438212(14)	[Dh51,Lu73]	+0.6438212(14)		–0.08255(76)	–0.1193	+0.621(25)	0.023
$^{35}\text{Ar}$	+0.6322(2)	[Ma02]	+0.6322(2)		–0.07459(51)	–0.1424	+0.611(25)	0.021
$^{35}\text{Cl}$	+0.8218743(4)	[Bl72]	+0.8218743(4)		–0.07459(51)	+0.1681	+0.831(31)	0.009
$^{37}\text{K}$	+0.20321(6)	[Vo71]	+0.20321(6)		–0.15011(35)	+0.2426	+0.237(34)	0.034
$^{37}\text{Ar}$	+1.145(5)	[Pi88]	+1.145(5)		–0.15011(35)	–0.2027	+1.121(27)	0.024
$^{39}\text{Ca}$	1.02168(12)	[Mi76c]	+1.02168(12)		–0.17135(39)	0.0000	+0.934(27)	0.087
$^{39}\text{K}$	+0.39150731(12)	[Sa74a,b]	+0.391487(21)	unw <sup>c</sup>	–0.17135(39)	0.0000	+0.465(35)	0.074
	+0.3914662(3)	[Be74]						
$^{41}\text{Sc}$	+5.431(2)	[Mi90]	+5.431(2)		+0.13602(49)	0.0000	+5.668(78)	0.237
$^{41}\text{Ca}$	–1.594781(9)	[Br62]	–1.594781(9)		+0.13602(49)	0.0000	–1.800(61)	0.205
$^{43}\text{Ti}$	0.85(2)	[Ma93]	–0.85(2)		+0.1023(22)	–0.1992	–0.666(65)	0.184
$^{43}\text{Sc}$	+4.62(4)	[Co66a]	+4.533(22)	2.2	+0.1023(22)	+0.1723	+4.562(81)	0.029
	+4.528(10)	[Av11]						

TABLE XII. (Continued.)

Parent nucleus	Measured magnetic moment(s) ( $\mu_N$ )		Adopted value ( $\mu_N$ )	Scale $S$	$\gamma_\beta$	$\Delta_{\gamma(p,n)}$	Calculated value ( $\mu_N$ )	expt. – calc.  ( $\mu_N$ )
<sup>45</sup> V					+0.0807(25)	+0.1753	+ 4.230(82)	
<sup>45</sup> Ti	0.095(2)	[Co66b]	(+)0.095(2) <sup>d</sup>		+0.0807(25)	–0.2139	–0.335(66)	0.430
<sup>47</sup> Cr					+0.1511(43)	–0.1360	–0.651(36)	
<sup>47</sup> V					+0.1511(43)	+0.1050	+2.368(43)	
<sup>49</sup> Mn					+0.0916(57)	+0.1222	+3.270(80)	
<sup>49</sup> Cr	0.476(3)	[Jo70]	(–)0.476(3) <sup>d</sup>		+0.0916(57)	–0.1595	–0.476(67)	0.000
<sup>51</sup> Fe					+0.0989(33)	–0.1073	–0.674(52)	
<sup>51</sup> Mn	3.5683(13)	[Jo71]	+3.5691(26)	2.1	+0.0989(33)	+0.0785	+3.457(63)	0.111
	+3.577(4)	[Ba15]						
<sup>53</sup> Co					+0.0855(29)	+0.1053	+4.546(85)	
<sup>53</sup> Fe	–0.65(1)	[Mi17]	–0.65(1)		+0.0855(29)	–0.1431	–0.645(69)	0.005
<sup>55</sup> Ni	(–)0.976(26) <sup>e</sup>	[Be09]	(–)0.976(26)		+0.0855(32)	–0.0708	–0.898(71)	0.078
<sup>55</sup> Co	+4.822(3)	[Ca73]	+4.822(3)		+0.0855(32)	+0.0397	+4.776(87)	0.046
<sup>57</sup> Cu	+2.582(7)	[Co10]	+2.582(7)		+0.1462(30)	+0.0607	+2.403(39)	0.179
<sup>57</sup> Ni	–0.7975(4)	[Oh96]	–0.7975(14)		+0.1462(30)	–0.1061	–0.669(31)	0.129
<sup>59</sup> Zn					+0.1263(57)	–0.14(5)	–0.51(8)	
<sup>59</sup> Cu	+1.891(9)	[Go04]	+1.8919(29)	3.2	+0.1263(57)	+0.11(5)	+2.20(8)	0.390
	+1.910(4)	[Co10]						
	+1.8910(9)	[Vi11]						
<sup>61</sup> Ga					+0.1408(89)	+0.11(5)	+2.29(9)	
<sup>61</sup> Zn					+0.1408(89)	–0.14(5)	–0.59(8)	
<sup>63</sup> Ga	+1.469(5)	[Pr12]	+1.469(5)		+ <sup>f</sup>			
<sup>67</sup> Se					–0.067(12)	–0.14(5)	+0.94(13)	
<sup>67</sup> As					–0.067(12)	+0.11(5)	+1.61(14)	
<sup>71</sup> Kr					–0.078(17)	–0.14(5)	+1.04(14)	
<sup>71</sup> Br					–0.078(17)	+0.11(5)	+1.50(15)	
<sup>75</sup> Sr					–0.134(40)	–0.14(5)	+0.93(17)	
<sup>75</sup> Rb					–0.134(40)	+0.11(5)	+0.54(19)	
<sup>77</sup> Sr	–0.348(4)	[Li92]	–0.348(4)		– <sup>f</sup>			

<sup>a</sup>No value is available from [394].

<sup>b</sup>See also [Ne11,U117,Pu15].

<sup>c</sup>Because the two (very precise) measurements differ by many standard deviations, the unweighted average is used.

<sup>d</sup>The sign was obtained from shell model calculations [399].

<sup>e</sup>The sign was obtained from shell model calculations [400].

<sup>f</sup>The magnetic moment values for <sup>63</sup>Ga and <sup>77</sup>Sr cannot be calculated with Eqs. (46) to (51) because the corrected  $\mathcal{F}t^{\text{mirror}}$  values for the beta transitions between these isotopes and their mirror partners (<sup>63</sup>Ge and <sup>77</sup>Y, respectively), providing  $|\gamma_\beta|$  [Eq. (45)], are not yet known.

and

$$(\gamma_n + \Delta\gamma_n) = g_n + \frac{G_n - g_n}{R} \gamma_\beta. \quad (47)$$

The sign of  $\gamma_\beta$  is negative for isotopes with  $j = l - 1/2$  (with  $j$  and  $l$  being, respectively, the spin and orbital angular momentum of the subshell of the odd nucleon), i.e., for the  $p_{1/2}$  shell (the mirror nuclei with  $A = 13$  and  $15$ ), the  $d_{3/2}$  shell ( $A = 33$  to  $39$ ), and the  $f_{5/2}$  shell ( $A = 65$  to  $77$ ). For all other mirror nuclei one has  $j = l + 1/2$  and a positive sign for  $\gamma_\beta$ .

The quantities  $\Delta\gamma_p$  and  $\Delta\gamma_n$  are small quantities representing the contributions to the total spin and total angular momentum of the mirror pair generated by the even type of nucleon in these odd-even nuclei. They were obtained from  $0\hbar\omega$  shell model calculations based on the Hamiltonians from Refs. [396–398] and are given in Ref. [394]. As one is dealing here with nucleons in nuclei, the free-nucleon values of the  $g$  factors, i.e.,  $g_p = 1.0$ ,  $g_n = 0$ ,  $G_p = 5.586$ , and  $G_n = -3.826$ ,

as well as the ratio of the axial-vector to vector coupling constant  $R = |C_A/C_V| \simeq 1.27$ , were replaced by effective values denoted by  $\tilde{g}$ ,  $\tilde{G}$ , and  $\tilde{R}$ . The linear relations of Eqs. (46) and (47) were used to determine values for  $\tilde{g}$ , and  $(\tilde{G} - \tilde{g})/\tilde{R}$  for protons and neutrons from least-square fits to  $(\gamma_{p,n} + \Delta\gamma_{p,n})$  and  $\gamma_\beta$ , thereby using the experimental magnetic dipole moments and  $\beta$ -decay half-lives for the mirror nuclei with  $A = 11$  to  $43$ , yielding (“Fit (B)” in Ref. [394])

$$\tilde{g}_p = 1.040 \pm 0.020, \quad (48)$$

$$\tilde{g}_n = -0.011 \pm 0.016, \quad (49)$$

$$(\tilde{G}_p - \tilde{g}_p)/\tilde{R} = 4.26 \pm 0.07, \quad (50)$$

$$(\tilde{G}_n - \tilde{g}_n)/\tilde{R} = -3.70 \pm 0.05. \quad (51)$$

Using the  $\mathcal{F}t^{\text{mirror}}$  values listed in Table VI and Eqs. (45) to (47) then yields the calculated magnetic moment values listed in column 8 of Table XII for all mirror isotopes. For the mirror

TABLE XIII. References from which magnetic moment results have been rejected. The correlation between the alphabetical reference code used here and the actual reference numbers is listed in Table XV.

Nucleus	Value	[Ref.]	Reason for rejection
<sup>27</sup> Si	-0.8554(4)	[Hu84]	No correction for diamagnetism was applied. Result is strongly deviating from the two other more recent and mutually consistent results reported in [Ma98] and [Ma99].
<sup>19</sup> Ne	-1.8846(8)	[Ge05]	Uncertainty is a factor 10 or more larger than that of the most precise measurement.
<sup>35</sup> Ar	+0.633(2)	[Ca65]	
<sup>35</sup> Ar	+0.633(7)	[Kl96]	
<sup>37</sup> Ar	+0.95(20)	[Ro65]	
<sup>39</sup> K	+0.39147(3)	[Du93]	
<sup>41</sup> Ca	-1.61(2)	[An82]	
	-1.5942(7)	[Ar83]	
<sup>57</sup> Ni	0.88(6)	[Ro75]	
<sup>59</sup> Cu	+1.84(3)	[St08]	
<sup>57</sup> Cu	2.00(5)	[Mi06]	Result is much less precise and differs by more than 10 standard deviations from the newer value from [Co10] which agrees well with $\mu \simeq 2.5\mu_N$ as is calculated in the shell model [301,401,402].

isotopes in the  $fp$  shell with  $A = 59$  to  $75$ , no  $\Delta\gamma_{p,n}$  values were available. We therefore used the average values of these quantities for the isotopes with  $A = 45$  to  $57$  in the  $fp$  shell listed in Table V of Ref. [394] with a one-standard-deviation error to cover the full range of individual values listed there, i.e.,  $\Delta\gamma_p = +0.11(5)$  and  $\Delta\gamma_n = -0.14(5)$ . The errors due to the uncertainties on these estimated values have been added in quadrature to the other contributions to the error bars on the calculated magnetic moment values.

Good correspondence with the known experimental values is obtained, as shown from the fact that for the 45 cases for which experimental values are available the difference between the experimental and calculated values, listed in the last column of Table XII, is less than  $0.1\mu_N$  for 27 nuclei, between  $0.1\mu_N$  and  $0.2\mu_N$  for another 13 nuclei, and larger than  $0.2\mu_N$  for 5 nuclei (i.e., <sup>17</sup>F, <sup>41</sup>Sc, <sup>41</sup>Ca, <sup>45</sup>Ti, and <sup>59</sup>Cu; the neutron, the proton, <sup>3</sup>H, and <sup>3</sup>He were not included in this count, as no values for the correction  $\Delta\gamma_{(p,n)}$  are available). Reasonably good confidence can thus also be given to the values calculated for those mirror nuclei for which experimental magnetic moment values are not available yet. For the heaviest isotopes, i.e., with mass  $A = 61$  to  $75$ , this is shown in Table XIV by comparing the calculated moment values with those of neighboring nuclei with the odd proton or neutron occupying the same shell model orbital.

## 2. Experimental weak magnetism form factors $b$ and $b/Ac$

With the isovector magnetic moment for most of the  $T = 1/2$  mirror pairs up to  $A = 75$  determined, we can deduce the weak magnetism  $b$  form factors using Eq. (38) and combine these with the  $c$  form factors deduced from the corrected  $\mathcal{F}_T^{\text{mirror}}$  values (Table VI) using Eq. (9), to obtain the normalized  $b/Ac$  form factors ( $A$  being the mass number). Results are listed in Table XVI and shown in Fig. 4. As can be seen, large absolute values for  $\mu_f - \mu_i$ , and so for  $b$ , are observed for mirror pairs in subshells with  $j = l + 1/2$ , i.e., in the  $s_{1/2}$

( $A = 1-3$ ),  $p_{3/2}$  ( $A = 11$ ),  $d_{5/2}$  ( $A = 17-27$ ),  $s_{1/2}$  ( $A = 29-31$ ),  $f_{7/2}$  ( $A = 41-55$ ), and  $2p_{3/2}$  ( $A = 57-61$ ) subshells. Small values for  $\mu_f - \mu_i$  are observed for mirror pairs in subshells with  $j = l - 1/2$ , i.e., the  $p_{1/2}$  ( $A = 13-15$ ),  $d_{3/2}$  ( $A = 33-39$ ), and  $f_{5/2}$  ( $A = 67-75$ ) subshells. This is fully in line with the values for the difference of the odd-proton and odd-neutron Schmidt values,  $\mu_p^{\text{Sch}} - \mu_n^{\text{Sch}}$ , for the different subshells with spin  $j$ , which is large for  $j = l + 1/2$  (i.e., between 4.7 and 7.7 for the subshells involved here) and relatively small for  $j = l - 1/2$  (i.e., ranging between  $-1.0$  and  $+0.2$ ) (see Table XVII). As a consequence, the values for  $b$  share the same systematic, as is clear from Fig. 4 which shows large

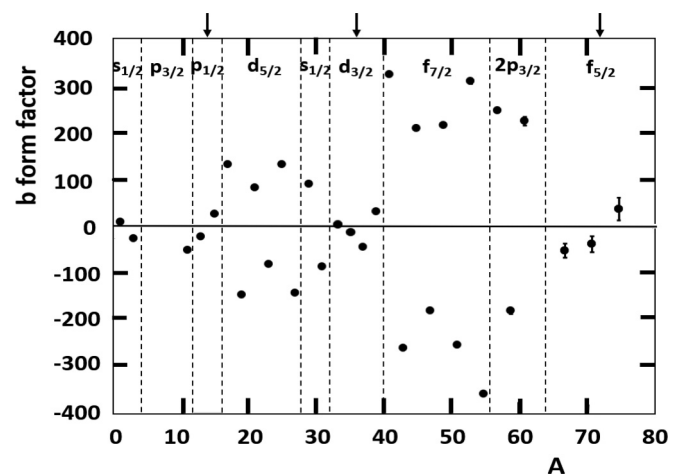


FIG. 4. Weak-magnetism form factor  $b$  for the  $T = 1/2$  mirror  $\beta$  transitions from the experimental/calculated magnetic moments in column 8 of Table XII and Eq. (38). The dashed vertical lines separate the shell model subshells, the labels of which are indicated. The arrows at the top of the figure indicate subshells with  $j = l - 1/2$ . If not explicitly shown, error bars are smaller than the size of the symbol.

TABLE XIV. Magnetic moments for the mirror nuclei with  $A = 61, 67, 71$ , and  $75$ , calculated with Eqs. (45)–(47) for the two possible signs of  $\gamma_\beta$  (see Table XII). The preferred values for the magnetic moments, listed in column 6 and corresponding to  $\text{sgn}(\gamma_\beta) = +$  for the  $j = l + 1/2$   $p_{3/2}$  subshell and  $\text{sgn}(\gamma_\beta) = -$  for the  $j = l - 1/2$   $f_{5/2}$  subshell, agree with the systematic of the magnetic moments for neighboring nuclei with the odd proton or odd neutron occupying the same shell model orbital, listed in the last column. Note that when the sign for a magnetic moment value in the last column is given, the sign has been explicitly measured. The correlation between the alphabetical reference code used here and the actual reference numbers is listed in Table XV.

Isot.	$J^\pi$	Sub-shell	Magn. mom. ( $\mu_N$ ) for $\text{sgn}(\gamma_\beta) = -$	Magn. mom. ( $\mu_N$ ) for $\text{sgn}(\gamma_\beta) = +$	Preferred value ( $\mu_N$ )	Reason, based on magnetic moments of neighboring nuclei with similar single particle configuration
<sup>61</sup> Ga	3/2 <sup>-</sup>	$p_{3/2}$	+2.29(19)	+0.33(7)	+2.29(19)	Similar to the value $\mu \approx +1.5$ to $+2.6$ for the 3/2 <sup>-</sup> ground states of <sup>63–77</sup> Ga [Ch10] and <sup>57–73</sup> Cu [Vi10]
<sup>61</sup> Zn	3/2 <sup>-</sup>		-0.59(8)	+0.97(8)	-0.59(8)	Similar to the values $\mu = -0.28164(5)$ and $\mu = -0.8(2)$ for the 3/2 <sup>-</sup> g.s. of <sup>63</sup> Zn [La69], resp. the lowest-lying 3/2 <sup>-</sup> state of <sup>65</sup> Zn [We75]
<sup>67</sup> Se	5/2 <sup>-</sup>	$f_{5/2}$	-0.30(13)	+0.94(13)	+0.94(13)	Similar to the values $\mu = 0.735(7)$ [OI70], $\mu = +1.018(10)$ [Mo68], $\mu = +1.124(10)$ [Bl68] and $\mu = +1.12(3)$ [Za84] for the lowest lying 5/2 <sup>-</sup> states in respectively <sup>69</sup> Ge, <sup>71</sup> Ge, <sup>79</sup> Kr, and <sup>77</sup> Se (see also text)
<sup>67</sup> As	5/2 <sup>-</sup>		+3.04(14)	+1.61(14)	+1.61(14)	Similar to the values $\mu = +1.6229(16)$ [Go05], $\mu = +1.674(2)$ [He76a,b], $\mu = +1.63(10)$ [Bo63], $\mu = 1.0(3)$ [Sp94] and $\mu = 1.6(5)$ [Ja96] for the lowest 5/2 <sup>-</sup> states in respectively <sup>69</sup> As, <sup>71</sup> As, <sup>73</sup> As, <sup>79</sup> Br, and <sup>81</sup> Br (see also text)
<sup>71</sup> Kr	5/2 <sup>-</sup>		-0.40(14)	+1.04(14)	+1.04(14)	Similar to the values $\mu = 0.735(7)$ [OI70], $\mu = +1.018(10)$ [Mo68], $\mu = +1.124(10)$ [Bl68] and $\mu = +1.12(3)$ [Za84] for the lowest lying 5/2 <sup>-</sup> states in respectively <sup>69</sup> Ge, <sup>71</sup> Ge, <sup>79</sup> Kr, and <sup>77</sup> Se
<sup>71</sup> Br	5/2 <sup>-</sup>		+3.15(15)	+1.50(15)	+1.50(15)	Similar to the values $\mu = +1.6229(16)$ [Go05], $\mu = +1.674(2)$ [He76a,b], $\mu = +1.63(10)$ [Bo63], $\mu = 1.0(3)$ [Sp94] and $\mu = 1.6(5)$ [Ja96] for the lowest 5/2 <sup>-</sup> states in respectively <sup>69</sup> As, <sup>71</sup> As, <sup>73</sup> As, <sup>79</sup> Br, and <sup>81</sup> Br (see <sup>75</sup> Rb and text)
<sup>75</sup> Sr	3/2 <sup>-</sup>		-0.55(17)	+0.93(17)	+0.93(17) <sup>a</sup>	Similar to the value $\mu = +0.6544680(16)$ for the 3/2 <sup>-</sup> g.s. state of <sup>77</sup> Rb [Du86, Th81] (see also text)
<sup>75</sup> Rb	3/2 <sup>-</sup>		+2.25(19)	+0.54(19)	+0.54(19) <sup>a</sup>	

<sup>a</sup>The calculated moments for  $\text{sgn}(\gamma_\beta) = +$  are preferred because of the agreement for <sup>75</sup>Rb with the experimental value  $\mu = +0.6544680(16)$  for the 3/2<sup>-</sup> g.s. state of the neighboring <sup>77</sup>Rb [Du86, Th81], and because the 3/2<sup>-</sup> g.s. states of <sup>79</sup>Sr [Bu90] and <sup>81</sup>Rb [Th81] with, respectively,  $\mu = -0.474(4)$  and  $\mu = +2.0595(14)$ , are farther away in mass and also situated above the  $N = 40$  subshell closure.

values for  $b$  in the  $s_{1/2}$ ,  $p_{3/2}$ ,  $d_{5/2}$ ,  $f_{7/2}$ , and  $2p_{3/2}$  subshells (with  $j = l + 1/2$ ), and significantly smaller values in the  $p_{1/2}$ ,  $d_{3/2}$ , and  $f_{5/2}$  subshells (with  $j = l - 1/2$  and indicated by arrows).

Figure 5 shows the evolution of the Gamow-Teller form factor,  $|c|$ , (the sign of  $c$  is straightforwardly obtained from shell model calculations) as a function of the mass number. While a clear local increase is visible when crossing the doubly magic nuclei at  $A = 16$ , respectively  $A = 40$ , a general overall, slow decrease can be observed. This can be understood intuitively as the Fermi surfaces of proton and neutron become increasingly distanced for higher masses.

This trend persists in the ratio  $b/Ac$  as is seen in Fig. 6, where again a distinction is made between  $j = l \pm 1/2$  transitions. Despite significant variation in the absolute value of  $b$  (Fig. 4 and Table XVI), subshell behavior of  $b/Ac$  is reasonably uniform, as is also clear from the last two columns in Table XVI. The already large values in the  $d_{5/2}$  and  $f_{7/2}$  subshells are further accentuated by the decrease of the  $|c|$

values throughout these subshells (Fig. 5). The behavior of  $b/Ac$  versus  $A$  for the mirror decays is thus understood in terms of the single particle Schmidt values for the magnetic moments and the slight decrease of the size of the Gamow-Teller form factor  $c$  with increasing  $A$ .

### 3. Theoretical form factor comparison

While some substructure is clearly visible in the experimental results of Fig. 6, a variation of a full order of magnitude is observed. In the face of ever-increasing experimental precision, it is paramount that theory can meet this challenge. Here we will compare experimental results to theoretical predictions, using both single-particle estimates and the nuclear shell model.

*a. Single-particle calculations.* As noted in the previous sections, significant variation occurs in the values for  $b/Ac$  for different spin-orbit orbitals. This can be understood intuitively from a single-particle view of the transition. Using Eq. (43)

TABLE XV. Reference key relating the reference codes used in Tables XII to XIV to the actual reference numbers.

Table code	Reference no.
A151a	[403]
A151b	[404]
Am65	[405]
An82	[406]
Ar83	[407]
Av11	[408]
Ba15	[409]
Ba62	[410]
Ba64	[411]
Be09	[400]
Be64	[412]
Be74	[413]
Bl68	[414]
Bl72	[415]
Bo63	[416]
Br62	[417]
Bu90	[418]
Ca65	[419]
Ca73	[420]
Ch10	[421]
Co10	[422]
Co63	[423]
Co66a	[424]
Co66b	[425]
Dh51	[426]
Du86	[427]
Du93	[428]
Ep68	[429]
Ep75	[430]
Fu76	[431]
Fu93	[432]
Ge05	[433]
Go04	[401]
Go05	[434]
He76a	[435]
He76b	[436]
Hu84	[437]
Ja96	[438]
Jo70	[439]
Jo71	[440]
K196	[441]
La57	[442]
La69	[443]
Li52	[444]
Li92	[445]
Lu73	[446]
Ma02	[447]
Ma04	[448]
Ma82	[449]
Ma93	[450]
Ma98	[451]
Ma99	[452]
Mi06	[453]
Mi17	[454]
Mi39	[455]
Mi76a	[456]

TABLE XV. (*Continued.*)

Table code	Reference no.
Mi76b	[457]
Mi76c	[458]
Mi90	[459]
Mi93	[460]
Mo16	[461]
Mo68	[462]
Ne11	[463]
Ne12	[464]
Ne77	[465]
Oh96	[466]
Ol70	[467]
Pi88	[468]
Pr12	[469]
Pu15	[470]
Ro54	[471]
Ro65	[472]
Ro75	[473]
Ro86	[474]
Sa74a	[475]
Sa74b	[476]
Sp94	[477]
St08	[478]
Su66	[479]
Su71	[480]
Ta93	[481]
Ti21	[482]
Th81	[483]
Ul17	[484]
Vi10	[485]
Vi11	[486]
Vo71	[487]
Wa54	[488]
We53	[489]
We75	[490]
Wo70	[491]
Yo17	[492]
Za84	[493]
Zh09	[494]

this means we are interested in the ratio of matrix elements  $R = M_L/M_{GT}$ . Using simple harmonic oscillator wave functions, this ratio is

$$\begin{aligned} \frac{M_L}{M_{GT}} &= \frac{\langle n_f l_f j_f | l | n_i l_i j_i \rangle}{\langle n_f l_f j_f | \sigma | n_i l_i j_i \rangle} \\ &= (-1)^{j_i - j_f} \frac{\begin{Bmatrix} 1/2 & l & j_i \\ 1 & j_f & l \end{Bmatrix}}{\begin{Bmatrix} l & 1/2 & j_i \\ 1 & j_f & 1/2 \end{Bmatrix}} \frac{\sqrt{l(l+1)(2l+1)}}{\sqrt{6}}. \end{aligned} \quad (52)$$

Using the four possibilities for transitions with  $j_{i,f} = l \pm 1/2$ , this results in

$$\begin{aligned} R^{--} &= -(l+1), & R^{-+} &= -1/2 \\ R^{+-} &= -1/2, & R^{++} &= l. \end{aligned} \quad (53)$$

TABLE XVI. Input data and CVC results for the  $b$  form factors [calculated from Eq. (38) with  $a = 1$ ] and  $b/Ac$  ratios [Eq. (43)] for the mirror  $\beta$  transitions up to  $A = 39$ . The + or - sign following the subshell label in column 4 indicates whether the subshell has  $j = l + 1/2$  or  $j = l - 1/2$ , respectively.  $\mu_f - \mu_i$  is the difference of the magnetic moments of the daughter and mother isotopes, where the values adopted in Table XII were used. Values for the Gamow-Teller form factor  $c$  are from Table VI.

$\beta$ transition	$A$	$J$	Subshell	$\mu_f - \mu_i$ [ $\mu_N$ ]	$b^a$	$c$	$(b/Ac)^{\text{exp}}$	$(b/Ac)^{\text{exp}}$ Subshell average <sup>b</sup>
$n \rightarrow p$	1	1/2	$s_{1/2}, +$	+4.70589007(45)	+8.15084070(78)	+2.21086(118)	3.6867(20)	3.86(24)
$H \rightarrow He$	3	1/2		-5.106587773(26)	-26.53460843(13)	-2.1053(14)	4.2012(28)	3.94(36)
$C \rightarrow B$	11	3/2	$p_{3/2}, +$	+3.6526(10)	-51.871(14)	-0.75442(79)	6.2506(68)	6.2506(68)
$N \rightarrow C$	13	1/2	$p_{1/2}, -$	+1.02461(40)	-23.0708(90)	-0.5596(14)	3.1712(80)	2.94(21)
$O \rightarrow N$	15	1/2		-1.00269(12)	26.0506(31)	0.6302(16)	2.7557(70)	2.96(29)
$F \rightarrow O$	17	5/2	$d_{5/2}, +$	-6.61515(30)	133.0616(61)	1.2955(11)	6.0416(51)	5.37(34)
$Ne \rightarrow F$	19	1/2		+4.51429(8)	-148.5605(26)	-1.60203(92)	4.8807(27)	6.18(95)
$Na \rightarrow Ne$	21	3/2		-3.04810(10)	82.6366(27)	0.7125(12)	5.5233(93)	
$Mg \rightarrow Na$	23	3/2		+2.75409(21)	-81.7768(63)	-0.5541(20)	6.416(23)	
$Al \rightarrow Mg$	25	5/2		-4.5010(12)	133.140(36)	0.8084(11)	6.5875(91)	
$Si \rightarrow Al$	27	5/2		+4.50684(24)	-143.9792(77)	-0.69659(93)	7.655(10)	
$P \rightarrow Si$	29	1/2	$s_{1/2}, +$	-1.79004(21)	89.913(11)	0.5380(21)	5.763(23)	5.44(21)
$S \rightarrow P$	31	1/2		+1.61953(9)	-86.9584(46)	-0.5294(15)	5.299(15)	5.53(33)
$Cl \rightarrow S$	33	3/2	$d_{3/2}, -$	-0.11098(50)	4.728(21)	-0.3142(32)	-0.4561(51)	0.61(53)
$Ar \rightarrow Cl$	35	3/2		+0.18967(20)	-8.5704(90)	0.2820(23)	-0.8684(71)	0.5(14)
$K \rightarrow Ar$	37	3/2		+0.9418(50)	-44.99(24)	-0.5779(16)	2.104(13)	
$Ca \rightarrow K$	39	3/2		-0.63019(12)	31.7295(61)	0.6606(17)	1.2316(32)	
$Sc \rightarrow Ca$	41	7/2	$f_{7/2}, +$	-7.0258(20)	326.626(93)	1.0743(38)	7.415(26)	7.438(87)
$Ti \rightarrow Sc$	43	7/2		+5.383(30)	-262.5(14)	-0.810(18)	7.54(17)	8.05(97)
$V \rightarrow Ti$	45	7/2		-4.135(82) <sup>c</sup>	211.0(42)	0.635(20)	7.39(27)	
$Cr \rightarrow V$	47	3/2		+3.012(57) <sup>c</sup>	-182.8(34)	-0.579(17)	6.71(23)	
$Mn \rightarrow Cr$	49	5/2		-3.746(80) <sup>c</sup>	217.2(46)	0.537(34)	8.25(55)	
$Fe \rightarrow Mn$	51	5/2		+4.243(52) <sup>c</sup>	-256.0(31)	-0.581(20)	8.64(32)	
$Co \rightarrow Fe$	53	7/2		-5.196(86) <sup>c</sup>	312.3(51)	0.673(23)	8.75(33)	
$Ni \rightarrow Co$	55	7/2		+5.798(26)	-361.6(16)	-0.675(25)	9.74(36)	
$Cu \rightarrow Ni$	57	3/2	$p_{3/2}, +$	-3.3795(71)	248.69(53)	0.564(12)	7.74(17)	7.42(33)
$Zn \rightarrow Cu$	59	3/2		+2.402(80) <sup>c</sup>	-182.9(61)	-0.461(12)	6.73(28)	7.10(55)
$Ga \rightarrow Zn$	61	3/2		-2.87(12) <sup>c</sup>	226.0(95)	0.542(35)	6.84(53)	
$Se \rightarrow As$	67	5/2	$f_{5/2}, -$	+0.67(19) <sup>c</sup>	-53(15)	-0.387(67)	2.05(68) <sup>d</sup>	0.42(99) <sup>d</sup>
$Kr \rightarrow Br$	71	5/2		+0.46(21) <sup>c</sup>	-39(17)	0.454(95)	3.9(26) <sup>e</sup>	1.6(11) <sup>e</sup>
$Sr \rightarrow Rb$	75	3/2		-0.38(25) <sup>c</sup>	37(25)	0.53(15)	-1.20(59) <sup>d</sup>	
						0.17(22)	-3.2(44) <sup>e</sup>	
						0.37(19)	0.93(67) <sup>d</sup>	
							1.3(11) <sup>e</sup>	

<sup>a</sup>For  $A = 45-53$  and  $A > 57$ , at least one of the mirror pair magnetic moments was not measured experimentally but calculated based on the experimental  $\mathcal{F}t$  value and the procedure outlined in Sec. III B 1 [394].

<sup>b</sup>As values and error bars sometimes vary significantly, unweighted averages are given as well, in italics.

<sup>c</sup>Based on at least one value calculated according to the procedure outlined in Sec. III B 1. See also Table XII.

<sup>d</sup>Value for upper limit of BR; see also Table V and Sec. II B 3.

<sup>e</sup>Value for lower limit of BR; see also Table V and Sec. II B 3.

In the case of mirror decays, the sign in  $j_{i,f} = l \pm 1/2$  is the same for initial and final states. As such, the expected behavior of  $b/Ac$  is opposite for spin-orbit partners. This split can clearly be seen in the data previously presented. Despite this insight, there is still significant variation in the experimental values within the same subshell (see Table XVI and Fig. 6). Additional insight can be gleaned by incorporating deformation into the single particle potential. As discussed in Appendix A, we move on to an axially deformed Woods-Saxon potential. Thanks to mean-field results [495] we have theoretical deformations available for all participating nuclei.

Wave functions are computed numerically [339] and projected on a spherical harmonic oscillator basis, for which we can use the analytical results of Eq. (53). Performing the calculation, we find the results shown in Fig. 7.

As was noted, the general trends are replicated by the simple spherical harmonic oscillator results of Eq. (53). When taking into account nuclear deformation through the single-particle potential of Eq. (A10), deviations are introduced at an individual level. It is remarkable to note that the agreement with experimental data now becomes excellent for all transitions considered (Fig. 7). Of particular interest is the

TABLE XVII. Differences,  $\mu_p^{\text{Sch}} - \mu_n^{\text{Sch}}$ , of the Schmidt values for magnetic moments of odd-proton and odd-neutron nuclei with spin  $j = 1/2$  to  $j = 7/2$ , for  $j = l + 1/2$  and  $j = l - 1/2$ , and for both  $g_S^{\text{free}}$  and  $0.6 \times g_S^{\text{free}}$ . Large values are obtained for  $j = l + 1/2$  and much smaller values for  $j = l - 1/2$ .

$j$	$\mu_p^{\text{Sch}} - \mu_n^{\text{Sch}}$			
	$j = l + 1/2$		$j = l - 1/2$	
	$g_S^{\text{free}}$	$0.6 \times g_S^{\text{free}}$	$g_S^{\text{free}}$	$0.6 \times g_S^{\text{free}}$
1/2	4.71	2.82	-0.90	-0.27
3/2	5.71	3.82	-1.02	+0.11
5/2	6.71	4.82	-0.50	+0.84
7/2	7.71	5.82	+0.23	+1.69

agreement with cases of large deviations from traditional estimates for  $A = 33$  and  $A = 35$ . In contrast to most of the other nuclei, both initial and final states are oblate deformed, resulting in large cancellation effects. The case of  $^{33}\text{Cl}$  has been discussed in more detail in Ref. [339], including the dependence on the input deformation parameters (see also Sec. III B 4).

TABLE XVIII. Comparison of experimental and theoretical values for the ratio  $(b/Ac)$  for the mirror  $\beta$  transitions up to  $^{45}\text{V}$ . Values for  $(b/Ac)^{\text{exp}}$  are obtained from the experimental  $\mathcal{F}t$  values (for  $c$ ; see Table VI) and the magnetic moments of the mirror nuclei pairs (for  $b$ ; see Table XVI). Theoretical values for  $A = 3$  to 45 were calculated using the shell model, with  $g_A = 1.27$  for  $^3\text{H}$  decay and  $g_A = 1$  for all other decays. The theoretical value for  $(b/Ac)^{\text{theo}}$  for the neutron is obtained from Eq. (43) with  $M_L \equiv 0$  and the FLAG'21 average  $g_A = 1.246(28)$  [353] (from lattice calculations). Except for the case of the neutron, the uncertainties on the ratios in the last column take only the uncertainty on the experimental values in account. See Sec. III B 3 b for more details.

$\beta$ decay	$A$	$(b/Ac)^{\text{exp}}$	$(b/Ac)^{\text{theo}}$	$\frac{(b/Ac)^{\text{exp}}}{(b/Ac)^{\text{theo}}}$
$n \rightarrow p$	1	3.6867(20)	3.777(85)	0.976(22)
$\text{H} \rightarrow \text{He}$	3	4.2012(28)	3.706	1.134(1)
$\text{C} \rightarrow \text{B}$	11	6.2506(68)	5.759	1.085(1)
$\text{N} \rightarrow \text{C}$	13	3.1712(80)	3.479	0.912(2)
$\text{O} \rightarrow \text{N}$	15	2.7557(70)	2.753	1.001(3)
$\text{F} \rightarrow \text{O}$	17	6.0416(51)	6.682	0.904(1)
$\text{Ne} \rightarrow \text{F}$	19	4.8807(27)	5.134	0.951(1)
$\text{Na} \rightarrow \text{Ne}$	21	5.5233(93)	6.005	0.920(2)
$\text{Mg} \rightarrow \text{Na}$	23	6.416(23)	6.004	1.069(4)
$\text{Al} \rightarrow \text{Mg}$	25	6.5875(91)	6.858	0.961(1)
$\text{Si} \rightarrow \text{Al}$	27	7.655(10)	7.320	1.046(1)
$\text{P} \rightarrow \text{Si}$	29	5.763(23)	5.790	0.995(4)
$\text{S} \rightarrow \text{P}$	31	5.299(15)	5.030	1.053(3)
$\text{Cl} \rightarrow \text{S}$	33	-0.4561(51)	-0.206	2.219(25)
$\text{Ar} \rightarrow \text{Cl}$	35	-0.8684(71)	0.154	-5.633(46)
$\text{K} \rightarrow \text{Ar}$	37	2.104(13)	2.437	0.863(5)
$\text{Ca} \rightarrow \text{K}$	39	1.2316(32)	1.863	0.661(2)
$\text{Sc} \rightarrow \text{Ca}$	41	7.415(26)	7.669	0.967(3)
$\text{Ti} \rightarrow \text{Sc}$	43	7.54(17)	6.520	1.156(26)
$\text{V} \rightarrow \text{Ti}$	45	7.39(27)	8.121	0.910(34)

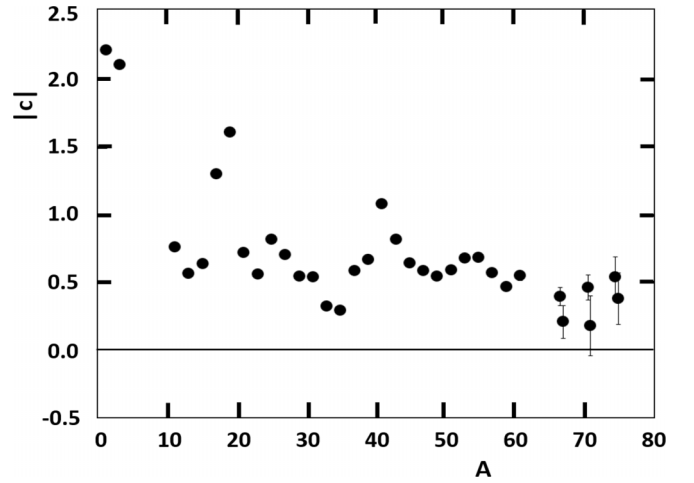


FIG. 5. Absolute value of the Gamow-Teller form factor,  $c$ , as a function of the mass number for the mirror  $\beta$  transitions. A slight general downward trend with increasing mass is apparent, with clear shell closure effects around the doubly magic  $A = 16$  and  $A = 40$  nuclei. For  $^{67}\text{Se}$ ,  $^{71}\text{Kr}$ , and  $^{75}\text{Sr}$  the values corresponding to the upper and lower limits of the BR values (see Tables V and VI) are shown. If not explicitly shown, error bars are smaller than the size of the symbol.

A final feature to note is the convergence to the simple harmonic oscillator results as subshells are filled. This can be understood using well-known Nilsson orbitals [496]. In the case of prolate deformation, projections with low spin relative to the symmetry axis are pushed down in energy and vice versa for high spin projections. When a subshell is filled, valence nucleons reside in low spin projections. Due to the proximity of other low spin states, significant mixing

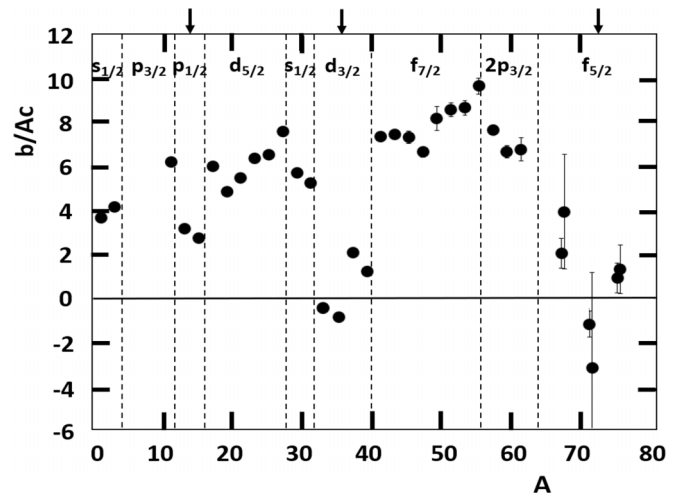


FIG. 6. Experimental values of  $b/Ac$  for the  $T = 1/2$  mirror  $\beta$  transitions listed in Table XVI. For  $^{67}\text{Se}$ ,  $^{71}\text{Kr}$ , and  $^{75}\text{Sr}$  the values corresponding to the upper and lower limits of the BR values are shown (see also Tables V, VI, and XVI, and text). The different shell model subshells are indicated. The arrows at the top of the figure indicate subshells with  $j = l - 1/2$ . If not explicitly shown, error bars are smaller than the size of the symbol.

TABLE XIX. Comparison of experimental and theoretical values for the  $M_{GT}$  and  $M_L$  matrix elements (in fm units) for the mirror  $\beta$  transitions up to  $^{45}\text{V}$ . Theoretical values were calculated using the shell model (see Sec. III B 3 b for details). Values for  $M_{GT}^{\text{exp}}$  are obtained from the Gamow-Teller form factors,  $c$ , listed in Table VI. Values for  $M_L^{\text{exp}}$  were calculated from Eq. (43) using the  $(b/Ac)^{\text{exp}}$  values listed in Table XVIII. As to  $g_A$ , we used for the neutron the value  $g_A = 1.2754(11)$  which was obtained from correlation measurements in neutron decay [56,66] and is independent of the  $\mathcal{F}_t^{\text{mirror}}$  value, while for  $A = 3$  the value  $g_A = 1.27$  was used, and  $g_A = 1.00$  for all other cases (see Sec. III A 3 c).

$\beta$ decay	A	Shell	$M_{GT}^{\text{exp}}$	$M_{GT}^{\text{theo}}$	$\frac{M_{GT}^{\text{exp}}}{M_{GT}^{\text{theo}}}$	$M_{GT}^{\text{exp-theo}}$	$M_L^{\text{exp}}$	$M_L^{\text{theo}}$	$\frac{M_L^{\text{exp}}}{M_L^{\text{theo}}}$	$M_L^{\text{exp-theo}}$	$\frac{M_L^{\text{theo}}}{M_{GT}^{\text{theo}}}$	$\frac{M_L^{\text{exp}}}{M_{GT}^{\text{exp}}}$
$n \rightarrow p$	1	$s_{1/2}$	+1.7335(18)	+1.732	1.001(1)	+0.002(2)	-0.0069(51)	+0.000	-	-0.007(5)	+0.000	-0.004
$\text{H} \rightarrow \text{He}$	3		-1.6577(11)	-1.706	0.972(1)	+0.048(1)	-1.0438(58)	+0.000	-	-1.044(6)	+0.000	+0.630
$\text{C} \rightarrow \text{B}$	11	$p_{3/2}$	-0.75442(79)	-0.789	0.956(1)	+0.035(1)	-1.1653(52)	-0.831	1.402(6)	-0.334(5)	+1.053	+1.545
$\text{N} \rightarrow \text{C}$	13	$p_{1/2}$	-0.5596(14)	-0.568	0.985(2)	+0.008(1)	+0.8589(50)	+0.697	1.232(7)	+0.162(5)	-1.227	-1.535
$\text{O} \rightarrow \text{N}$	15		+0.6302(16)	+0.576	1.094(3)	+0.054(2)	-1.2291(64)	-1.125	1.093(5)	-0.104(5)	-1.953	-1.950
$\text{F} \rightarrow \text{O}$	17	$d_{5/2}$	+1.2955(11)	+1.182	1.096(1)	+0.114(1)	+1.7303(62)	+2.336	0.741(3)	-0.606(6)	+1.976	+1.336
$\text{Ne} \rightarrow \text{F}$	19		-1.60203(92)	-1.676	0.956(1)	+0.074(1)	-0.2799(43)	-0.717	0.390(6)	+0.437(4)	+0.428	+0.175
$\text{Na} \rightarrow \text{Ne}$	21		+0.7125(12)	+0.726	0.981(2)	-0.014(1)	+0.5823(67)	+0.943	0.617(7)	-0.361(7)	+1.299	+0.817
$\text{Mg} \rightarrow \text{Na}$	23		-0.5541(20)	-0.588	0.942(3)	+0.034(2)	-0.948(13)	-0.763	1.242(17)	-0.185(13)	+1.298	+1.710
$\text{Al} \rightarrow \text{Mg}$	25		+0.8084(11)	+0.781	1.035(1)	+0.027(1)	+1.5211(76)	+1.681	0.905(5)	-0.160(8)	+2.152	+1.881
$\text{Si} \rightarrow \text{Al}$	27		-0.69659(93)	-0.769	0.906(1)	+0.072(1)	-2.0542(75)	-2.010	1.022(4)	-0.044(7)	+2.614	+2.949
$\text{P} \rightarrow \text{Si}$	29	$s_{1/2}$	+0.5380(21)	+0.513	1.049(4)	+0.025(2)	+0.569(13)	+0.556	1.023(23)	+0.013(13)	+1.084	+1.057
$\text{S} \rightarrow \text{P}$	31		-0.5294(15)	-0.490	1.080(3)	-0.039(2)	-0.3138(80)	-0.159	1.974(50)	-0.155(8)	+0.324	+0.593
$\text{Cl} \rightarrow \text{S}$	33	$d_{3/2}$	-0.3142(32)	-0.328	0.958(10)	+0.014(3)	+1.622(16)	+1.611	1.007(10)	+0.011(16)	-4.912	-5.162
$\text{Ar} \rightarrow \text{Cl}$	35		+0.2820(23)	+0.328	0.860(7)	-0.046(2)	-1.572(13)	-1.493	1.053(9)	-0.079(13)	-4.552	-5.574
$\text{K} \rightarrow \text{Ar}$	37		-0.5779(16)	-0.624	0.926(3)	+0.046(2)	+1.5037(80)	+1.416	1.062(6)	+0.088(8)	-2.269	-2.602
$\text{Ca} \rightarrow \text{K}$	39		+0.6606(17)	+0.764	0.865(2)	-0.103(2)	-2.2952(60)	-2.172	1.057(3)	-0.123(6)	-2.843	-3.474
$\text{Sc} \rightarrow \text{Ca}$	41	$f_{7/2}$	+1.0743(38)	+1.116	0.963(3)	-0.042(4)	+2.910(30)	+3.307	0.880(9)	-0.397(30)	+2.963	+2.709
$\text{Ti} \rightarrow \text{Sc}$	43		-0.810(18)	-0.989	0.819(18)	+0.179(17)	-2.29(14)	-1.794	1.279(77)	-0.50(14)	+1.814	+2.833
$\text{V} \rightarrow \text{Ti}$	45		+0.635(20)	+0.619	1.025(33)	+0.016(20)	+1.70(19)	+2.114	0.804(88)	-0.41(19)	+3.415	+2.684

occurs and the wave function of Eq. (A11) becomes nontrivial. All possible combinations in Eq. (53) occur, and lower (higher) values occur for  $j = l + 1/2$  ( $j = l - 1/2$ ) orbitals. As the subshell is filled, nearby equally high spin states be-

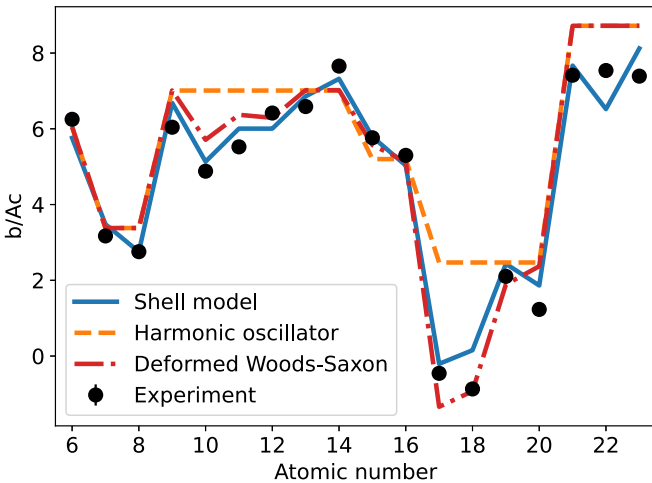


FIG. 7. Comparison of different methods of calculating the weak-magnetism contribution  $b/Ac$  with experimental data using CVC, for the mirror  $\beta$  transitions with  $Z = 6$  ( $^{11}\text{C}$ ) to  $Z = 23$  ( $^{45}\text{V}$ ). The simple spherical harmonic oscillator results are summarized in Eq. (53). Clearly, single-particle results using the deformed Woods-Saxon potential give excellent agreement throughout, including the outliers  $^{33}\text{Cl}$  and  $^{35}\text{Ar}$  at atomic numbers 17 and 18.

come sparse and the resultant mixing is strongly reduced. The results then converge to the spherical harmonic oscillator estimates.

*b. Nuclear shell model.* For the mirror nuclei up to mass  $A = 45$  the  $b$  and  $c$  form factors, which depend in the impulse approximation on the nuclear matrix elements  $M_{GT}$  and  $M_L$ , were also calculated in the nuclear shell model. To do so, effective interactions for the different (sub)shell regions we are dealing with here had to be selected. Such effective interactions were typically obtained by fitting energy data of nuclear levels in a specific region of the nuclear chart. The experimental data were usually obtained from one-nucleon or two-nucleon transfer reactions. The wave functions constructed from these interactions can then be used to calculate values for observable quantities other than the energies, such as magnetic dipole moments and probabilities for  $M1$  gamma transitions and beta decay. Comparison of such quantities with experiment provides an important check on the validity of the effective interactions and in some cases even allows one to improve the interactions via free (i.e., to be fitted) parameters.

For the calculations performed here we are dealing with light nuclei whose principal configurations involve several valence nucleons away from major shell closures. The choice of an effective interaction is then rather easily made. Indeed, there are well established interactions available in the literature that give excellent fits to experimental spectra. Thus we use for  $p$ -shell nuclei the Cohen-Kurath [396] interaction, i.e., (8-16)POT; for  $s, d$ -shell nuclei the universal  $s, d$  interaction USD of Wildenthal [497]; and for  $p, f$ -shell nuclei the

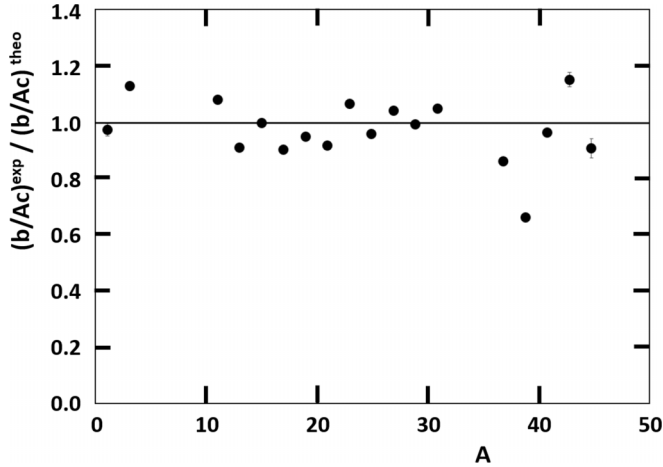


FIG. 8. Ratio of experimental values and nuclear shell model calculated values for the  $b/Ac$  form factor ratio for the  $T = 1/2$  mirror beta transitions up to  $A = 45$  (see Table XVIII). The values for  $A = 33$  and  $35$  have been omitted (see text). In nearly all cases, error bars (based only on the experimental  $b/Ac$  values) are smaller than the size of the symbols.

Kuo-Brown  $G$  matrix [498] as modified by Poves and Zuker [499] and denoted KB3. Close to major shell closures the choice of a model space and effective interaction is more problematic. Our approach is to construct a hybrid interaction comprising the Millener-Kurath [500] interaction for the cross-shell matrix elements, and the (8-16)POT, USD, or KB3 interactions for the in-shell matrix elements. The calculations further used  $g_A = g_V = 1$ ,  $g_M = 4.706$ ,  $g_P = -181.03$ , and  $g_S = g_T = 0$ . Note that we are dealing here with light nuclei, therefore, the recent advances in *ab initio* shell-structure calculations (see, e.g., Refs. [501–505]) offer interesting prospects as well.

Results thus obtained for the form factor ratio  $b/Ac$  up to  $A = 45$  are listed in column 4 of Table XVIII. For higher masses the required truncation of the shell model space, due to calculation power limitations, was too important to yield reliable values. The ratio of the values for  $b/Ac$  extracted from experiment (column 3 in Table XVIII) and these shell model calculated values are listed in the last column of Table XVIII and displayed in Fig. 8. The average for the ratios  $(b/Ac)^{\text{exp}}/(b/Ac)^{\text{theo}}$  for the mass range up to  $A = 45$ , omitting the values for  $A = 33$  and  $35$ , which both deviate significantly from unity, is  $0.96(11)$ . The cases of  $A = 33$  and  $35$  will be discussed in more detail in the next paragraph.

#### 4. Impulse approximation: Access to $M_{GT}$ and $M_L$ and comparison with shell model calculations

Using the impulse approximation, the ratio  $b/Ac$  was written in Eq. (43) in terms of the Gamow-Teller and orbital current matrix elements,  $M_{GT}$  and  $M_L$ , respectively. The first is directly obtained from the Gamow-Teller form factor,  $c \cong g_A M_{GT}$ , that was extracted from the experimental  $\mathcal{F}t$  values (cf. Table VI). Using then this value for  $M_{GT}$ , Eq. (43) allows extracting  $M_L$ . Note that we use here the sign convention of Holstein [1,338], which uses a positive value for  $g_A$ , so that  $M_{GT}^{\text{exp}}$  and  $c$  have the same sign. The resulting values for  $M_{GT}^{\text{exp}}$

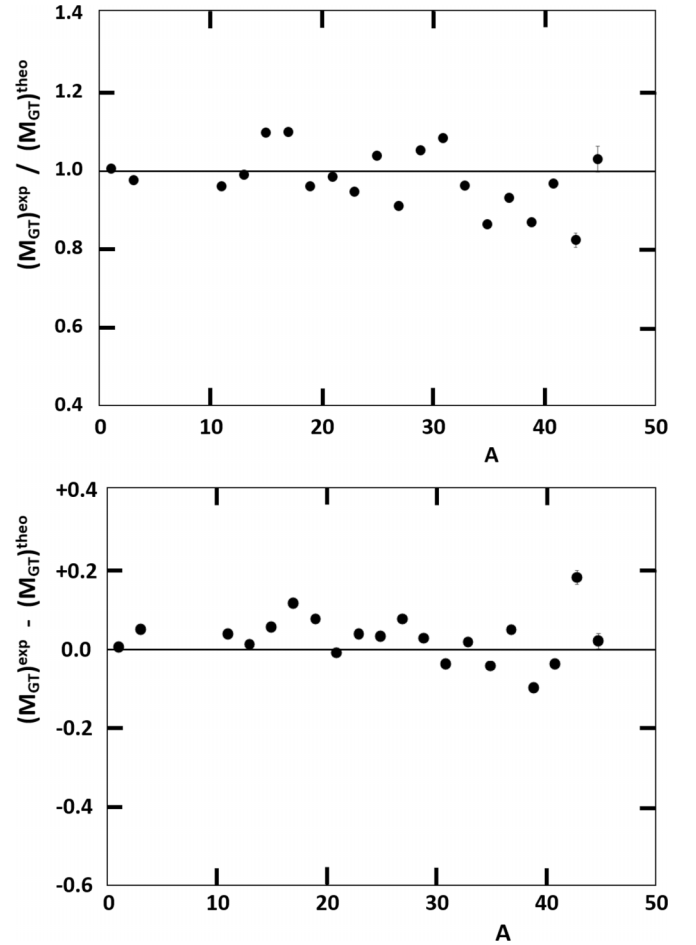


FIG. 9. Ratios (top) and differences (bottom) of experimental and nuclear shell model (Sec. III B 3 b) calculated values of the  $M_{GT}$  matrix elements for the  $T = 1/2$  mirror  $\beta$  transitions with masses  $A = 3$  to  $45$  as listed in Table XIX. Note that to extract  $M_{GT}^{\text{exp}}$  from the Gamow-Teller form factor,  $c$ , the value  $g_A = 1.2754(11)$  [56,66] was used for the neutron,  $g_A = 1.27$  for  $A = 3$ , and  $g_A = 1$  for all other cases (see Sec. III A 3 c). Error bars (based only on the experimental  $M_{GT}$  values) are smaller than the size of the symbols if not shown.

and  $M_L^{\text{exp}}$  [using  $g_A = +1.2754(11)$  [56,66] for the neutron (which was obtained from correlation measurements that are independent of the neutron  $\mathcal{F}t^{\text{mirror}}$  value),  $g_A = +1.27$  for  $A = 3$  and  $g_A = +1.00$  for all other cases (Sec. III A 3 c)] are listed in columns 4 and 8 of Table XIX. The corresponding shell model calculated values are listed in columns 5 and 9.

The ratio and the difference of the experimental and shell model calculated values for  $M_{GT}$  are shown in Fig. 9 (see also Table XIX). It is seen that the shell model is very capable in calculating  $M_{GT}$ , with the ratio differing 10% to 20% from unity and the difference being typically limited to about 0.1. Taking an unweighted average, we find the ratio of experimental to theoretical values to be  $M_{GT}^{\text{exp}}/M_{GT}^{\text{theo}} = 0.97(8)$ .

As a further check for the quality of the shell model calculations, Fig. 10 shows the ratio and the difference of the experimental and theoretical values for the orbital current matrix element,  $M_L$ , for the mirror transitions up to mass 45 (listed also in Table XIX). Again, reasonably good agreement

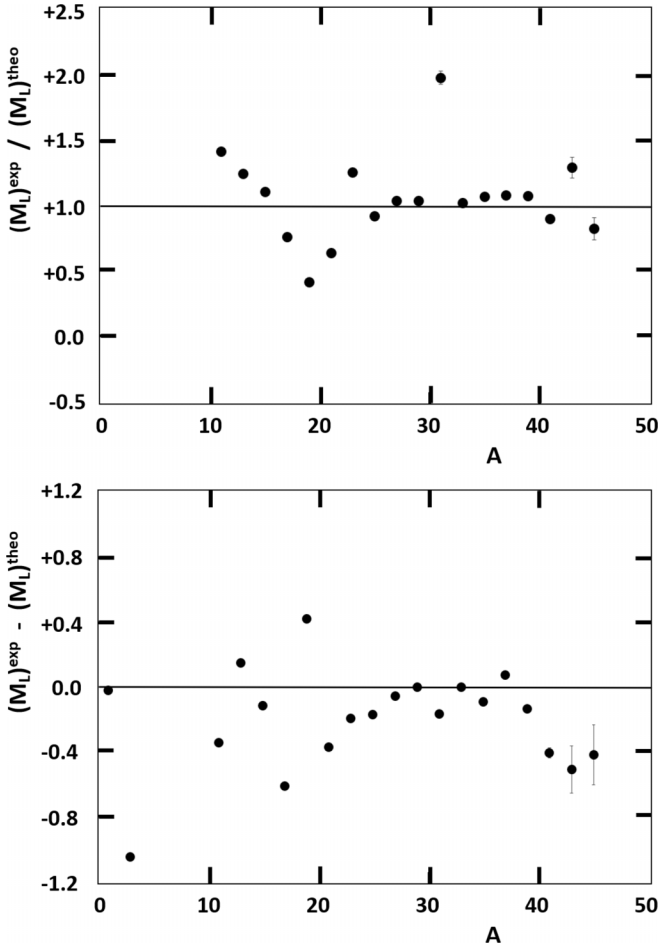


FIG. 10. Ratios (top) and differences (bottom) of experimental and nuclear shell model (Sec. III B 3 b) calculated values of the  $M_L$  matrix elements for the  $T = 1/2$  mirror  $\beta$  transitions with masses  $A = 3$  to 45 as listed in Table XIX. Note that to get  $M_L^{\text{exp}}$  from Eq. (43) the value  $g_A = 1.2754(11)$  [56,66] was used for the neutron,  $g_A = 1.27$  for  $A = 3$ , and  $g_A = 1.00$  for all other cases (see Sec. III A 3 c). The ratios for  $A = 1$  and 3 are not shown as  $M_L^{\text{theo}} = 0$  in this case. If not explicitly shown, error bars (based on the experimental  $M_L$  values only) are smaller than the size of the symbols. Note the different scales for the vertical axes with respect to Fig. 9.

between theory and experiment is observed. A tendency of the shell model calculation to slightly overestimate the value of  $M_L$  is seen. The average value of  $M_L^{\text{exp}}/M_L^{\text{theo}} = 0.99(35)$  for  $A = 11\text{--}29$  and  $33\text{--}45$  is close to unity, however. The masses 1, 3, and 31 are left out when constructing this average because their shell model calculations give  $M_L = 0$  for  $A = 1$  and 3, and  $M_L = -0.159$  for  $A = 31$ , all being close to zero due to the dominant  $s$ -state configuration in their wave function. Not omitting the case of  $A = 31$  slightly modifies the ratio to  $1.04(34)$ . It is unclear why the experimentally deduced  $M_L$  values of  $-1.044(6)$  for  ${}^3\text{He}$  and  $-0.314(8)$  for  ${}^{31}\text{S}$ , are so large. Contributions from meson exchange which are incorrectly estimated in the quenching of  $g_A$  could partially explain this discrepancy.

The last two columns of Table XIX list the theoretical and experimental values for the ratio  $M_L/M_{\text{GT}}$ , respectively. As

TABLE XX. Extreme single-particle values of  $b/Ac$  for the mirror  $\beta$  decays of  ${}^{33}\text{Cl}$  and  ${}^{35}\text{Ar}$  calculated with three different possibilities for the nuclear potential, i.e., spherical harmonic oscillator (SHO), spherical Woods-Saxon (WS), and deformed Woods-Saxon (DWS), and within the nuclear shell model (NSM) using the universal  $s, d$  interaction USD of Wildenthal [497]. The experimental values are listed in the last column.

Decay	SHO	WS	DWS	NSM	Expt.
${}^{33}\text{Cl}$	2.46	2.46	-1.13	-0.21	-0.456(5)
${}^{35}\text{Ar}$	2.46	2.46	-0.94	+0.15	-0.868(7)

can be seen, reasonable agreement between the experimental and theoretical ratios is obtained. Note further that for about half of the transitions (most of which with  $A > 23$ ) the absolute value of  $M_L/M_{\text{GT}}$  is larger than 2, indicating a strong dominance of the orbital current.

As can be seen from Table XVI and Fig. 6, most  $(b/Ac)^{\text{exp}}$  values are positive, except for the mirror  $\beta$  decays of  ${}^{33}\text{Cl}$ ,  ${}^{35}\text{Ar}$ , and  ${}^{71}\text{Kr}$ , for which slightly negative values are found. This is what one could expect from Eq. (43), in the sign convention of Holstein [1,338]. Indeed, since the first term in Eq. (43) is equal to  $g_M/g_A = 4.706$  (for  $g_A = +1$ ), a negative value for  $b/Ac$  can only occur if  $M_L$  and  $M_{\text{GT}}$  have opposite signs and  $|M_L| > 4.706|M_{\text{GT}}|$  in absolute value. As can be seen from the last two columns in Table XIX, the ratio  $M_L/M_{\text{GT}}$  is found (both from experiment and theory) to be positive in subshells with  $j = l + 1/2$  (i.e., the  $s_{1/2}$ ,  $p_{3/2}$ ,  $d_{5/2}$ , and  $f_{7/2}$  subshells), leading to large values for  $b/Ac$  [Eq. (43)], and negative in subshells with  $j = l - 1/2$  (the  $p_{1/2}$  and  $d_{3/2}$  subshells, i.e., the masses  $A = 13\text{--}15$ , and  $A = 33\text{--}39$ ), resulting in much smaller values for  $b/Ac$ , as can be seen in Table XVI. This is in line with the CVC-based relation (38) and the values for  $j = l \pm 1/2$  states in Table XVII (see also Sec. III B 2), combined with small values for  $c = M_{\text{GT}}$ . For the cases of  ${}^{33}\text{Cl}$ ,  ${}^{35}\text{Ar}$ , and  ${}^{71}\text{Kr}$ , the values of  $M_{\text{GT}}$  are indeed the smallest among all mirror  $\beta$  transitions, as is reflected by their large  $\mathcal{F}_t$  values (Table VI). For all three cases the ratios  $(M_L/M_{\text{GT}})^{\text{exp}} = (b/Ac)^{\text{exp}} - 4.7$  [see Eq. (43)], equal about  $-5$ , thereby overcompensating the value of 4.7 of the first term in Eq. (43) and causing  $b/Ac$  to be small and negative (cf. the last but one column in Table XVI). This, together with the fact that  ${}^{33}\text{Cl}$ ,  ${}^{35}\text{Ar}$ , and  ${}^{71}\text{Kr}$  and their respective daughter isotopes are rare cases of oblate deformation (with deformation parameters  $\beta_2 \approx -0.23$  for  ${}^{33}\text{Cl}$  and  ${}^{35}\text{Ar}$ , and  $\beta_2 \approx -0.36$  for  ${}^{71}\text{Kr}$  [495]), then poses a challenge to theoretical calculations. However, with  $M_L/M_{\text{GT}}$  being a ratio of matrix elements of the same order in spherical tensor formulation, such that complex many-body couplings drop out when neglecting core polarization and meson exchange, one is left with a ratio of single-particle matrix elements such that one can expect the extreme single-particle approach to capture most of the required dynamic [339]. The challenge then remains to pick a suitable single-particle state based on an underlying potential. The case of  ${}^{71}\text{Kr}$  obviously is too complex for this. For  ${}^{33}\text{Cl}$  and  ${}^{35}\text{Ar}$  Table XX compares the values for  $b/Ac$  obtained in Ref. [339] using the spherical harmonic oscillator, the spherical Woods-Saxon potential, and

TABLE XXI. Form factors calculated in the shell model for the  $T = 1/2$  mirror  $\beta$  transitions up to mass  $A = 45$ . Details on the calculations and the interactions used can be found in Sec. III B 3 b. Note that  $g_A = 1.27$  was used for  ${}^3\text{H}$  and  $g_A = 1$  for all other decays. Further, the first-class part of the  $d$  form factor, i.e.,  $d_I \approx Ag_A M_{\sigma L}$  (see Table X), is zero as these are transitions within an isospin multiplet, rendering  $d = 0$  in the absence of second-class currents (i.e.,  $d_{II} = 0$ ), as is assumed here.<sup>a</sup> Note also that the form factor  $j_2$  was calculated to be smaller than  $8 \times 10^{-2}$  in absolute value, and so is negligible for all transitions listed here. Note that for  $c$  in the form factor ratios the value  $c = c_1$  was used (see Sec. III A 3 a).

$\beta$ decay	Shell model interaction	$c_1$	$c_2$ (fm <sup>2</sup> )	$b/Ac$	$f/Ac$	$g/A^2c$	$j_1/A^2c$	$j_3/A^2c$	$h/A^2c$
${}^3\text{H}$	MSDI3	-2.167	-1.233	3.705	0.0	0.0	0.0	0.0	+142.5
${}^{11}\text{C}$	CK816POT	-0.789	-1.092	5.761	0.064	-66.83	-70.39	+185.4	+114.2
${}^{13}\text{N}$	CK816POT	-0.568	-1.133	3.480	0.0	0.0	-232.3	0.0	-39.38
${}^{15}\text{O}$	MK	+0.576	+1.267	2.755	0.0	0.0	-277.0	0.0	-81.79
${}^{17}\text{F}$	MK	+1.182	+2.319	6.684	-0.188	+127.9	-57.38	+172.1	+126.5
${}^{19}\text{Ne}$	USD	-1.676	-3.044	5.134	0.0	0.0	-1.311	0.0	+180.2
${}^{21}\text{Na}$	USD	+0.726	+1.397	6.008	0.098	-49.66	-19.12	-206.8	+163.0
${}^{23}\text{Mg}$	USD	-0.588	-1.219	6.004	-0.059	+25.49	-49.19	-244.3	+134.4
${}^{25}\text{Al}$	USD	+0.781	+1.767	6.858	-0.161	+65.56	-91.98	+41.8	+93.83
${}^{27}\text{Si}$	USD	-0.769	-1.871	7.321	0.419	-149.3	-130.2	+130.2	+57.44
${}^{29}\text{P}$	USD	+0.513	+1.293	5.794	0.0	0.0	-143.9	0.0	+44.73
${}^{31}\text{S}$	USD	-0.490	-1.260	5.030	0.0	0.0	-149.3	0.0	+39.29
${}^{33}\text{Cl}$	USD	-0.328	-1.133	-0.212	0.898	-271.3	-393.9	+166.3	-191.8
${}^{35}\text{Ar}$	USD	+0.328	+1.143	0.148	-0.092	+25.88	-390.7	+161.0	-190.6
${}^{37}\text{K}$	USD	-0.624	-1.873	2.434	0.147	-40.03	-244.7	+49.6	-50.92
${}^{39}\text{Ca}$	MK	+0.764	+2.336	1.859	-0.856	+217.7	-247.0	+67.3	-53.35
${}^{41}\text{Sc}$	MK	+1.116	+3.591	7.667	-0.848	+217.5	-109.3	+253.7	+77.29
${}^{43}\text{Ti}$	KB3	-0.989	-3.095	6.523	0.437	-105.5	-71.64	+141.1	+113.2
${}^{45}\text{V}$	KB3	+0.619	+2.218	8.120	-0.689	+159.6	-149.2	+308.7	+392.5

<sup>a</sup>A measurement with  ${}^{19}\text{Ne}$  [341] yielded a nonvanishing value  $d = 250(100)$ , corresponding to  $d/Ac = -8.2(33)$ , but a recent reanalysis [69] of the data from this experiment corrected this to  $d = 140({}_{-29}^{+43})_{\text{sys}}(130)_{\text{stat}} = 140(135)$ , corresponding to  $d/Ac = -4.6(45)$ .

the deformed Woods-Saxon model, with the here-performed shell model calculations and with experimental results. As can be seen, only the deformed Woods-Saxon potential (column 4 in Table XX) can reproduce the experimental values within a factor of about 2 and with the correct sign.

The good agreement with single-particle estimates in a deformed potential—particularly  ${}^{33}\text{Cl}$  and  ${}^{35}\text{Ar}$ , which turned out to be difficult for the shell model—stresses the importance of an appropriate basis choice. While the shell model reaches for most cases similar accuracy, it of course comes as a result of many higher-order particle-hole excitations to effectively reproduce nuclear deformation. Additionally, results are obtained using different effective interactions with tuned parameters, effective charges, and renormalization of coupling constants. When the transition permits it, results of similar accuracy can be obtained for the mirror nuclei in a much more simple fashion in the extreme single-particle approximation. Even so, while reassuring, the possibilities for a just application of single-particle results are slim and limited by transitions dominated by single-particle states. Inspection of  $g$  factors can be a useful tool here, so that single-particle results are an interesting cross-check when applicable.

### 5. Discussion

Good agreement between theoretical and experimental values for the Gamow-Teller matrix elements  $M_{\text{GT}}$ , the orbital

current matrix elements  $M_L$ , and the form factor ratio  $b/Ac$  for the mirror  $\beta$  transitions considered here is obtained. Differences reveal no significant trend in  $A$  or in the shell model states occupied, except for a small downward slope towards higher  $A$  values related to the required truncation of the shell model space. The observed deviation in  $b/Ac$  for the cases of  ${}^{33}\text{Cl}$  and  ${}^{35}\text{Ar}$  is understood in terms of the smallness of these  $b/Ac$  values, due to the large ratio of  $M_L/M_{\text{GT}}$  in the  $d_{3/2}$  subshell ( $j = l - 1/2$ ), and the large oblate deformation of these isotopes.

The good correspondence between experimental and theoretical values for the  $M_L$  matrix elements, with the exception of the case of  ${}^{31}\text{S}$  with a strong  $s$ -state configuration in the wave function, gives confidence in the reliability of the shell model calculations performed and thus perhaps also in the calculations of the matrix elements determining yet other, although usually less important, form factors (e.g., the induced pseudoscalar form factor,  $h$  [1]). We therefore list in Table XXI the full set of form factors from the shell model calculations discussed above (Sec. III B 3 b). These can be used in the analysis of experiments determining the  $\beta$ - $\nu$  correlation or the  $\beta$  asymmetry parameter for the mirror  $\beta$  transitions, that are being planned at different laboratories (e.g., [35,44,97]). Additional information on the effect of recoil terms, radiative corrections, and specific experimental conditions on such measurements are also discussed in Refs. [84,85].

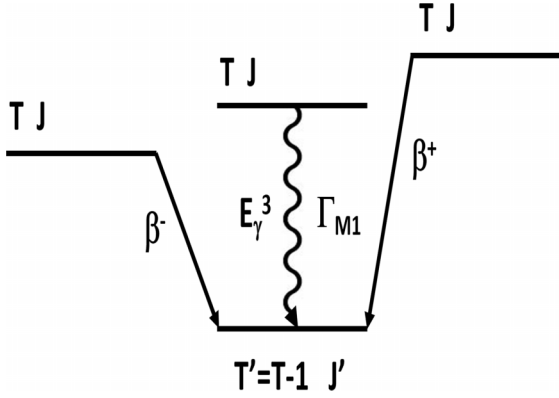


FIG. 11. Generic scheme showing the  $\beta$  and  $\gamma$  decays from the isobaric analog states in a  $T = 1$  triplet to a common  $T' = 0$  daughter state. The weak magnetism form factor of the  $\beta$  transitions can be obtained from the energy,  $E_\gamma$ , and the  $M1$ -decay width,  $\Gamma_{M1}$ , of the corresponding isovector  $\gamma$  transition from the isobaric  $T = 1$  analog state.

### C. Isospin $T = 1, 3/2$ , and $2$ multiplet decays

We have also investigated weak magnetism for  $\beta$  decays from states in isospin  $T = 1$ ,  $T = 3/2$ , and  $T = 2$  isobar multiplets for which experimental input data required to calculate the  $b$  and  $c$  form factors are available. Weak-magnetism studies for  $\beta$  decays of isobaric  $T = 1$  triplet states have been performed before [2,49]. Here we update and significantly extend these works, yielding results for as many as 68 (previously only 14 [2,49])  $\beta$  transitions from isospin multiplet states and the corresponding analog  $\gamma$  transitions.

a. *Weak-magnetism form factor*; b. Figure 11 displays the generic decay scheme for the  $\beta$  and  $\gamma$  decays of isobaric analog states in a  $T = 1$  triplet to a common  $T' = 0$  final state. For the  $\Delta T = 1$ ,  $\Delta T = \pm 1$  transitions considered here the weak-magnetism form factor for the  $\beta$  transitions is now given by Eq. (40). The decay width,  $\Gamma$ , of the  $\gamma$ -decaying analog state in this equation is related to the half-life  $t_{1/2}$  (in seconds) of the state by

$$\Gamma = \frac{\hbar \ln 2}{t_{1/2}} = \frac{4.56238 \times 10^{-16}}{t_{1/2}} \text{ eV}. \quad (54)$$

When several  $\gamma$  rays are deexciting the analog state the partial decay width for each transition is obtained by multiplying  $\Gamma$  with the transition's fractional intensity.

In the tables, sometimes the  $B(M1)$  transition strength for the specific  $\gamma$  ray is listed. To then obtain the  $\Gamma_{M1}$  width, we first calculate the transition strength of the  $\gamma$  transition,  $T_\gamma$ , in terms of the  $B(M1)$  matrix element. For a magnetic transition ( $M$ ) of multipolarity  $L$  one has [143]

$$T_{\gamma,ML} = 8\pi \frac{L+1}{L} \frac{1}{[(2L+1)!!]^2} \frac{1}{\hbar} \left( \frac{E_\gamma}{\hbar c} \right)^{2L+1} \times B(ML) [\text{W.u.}] B_W(ML), \quad (55)$$

where  $B(ML)$  is in Weisskopf units, and  $B_W(ML)$  is the Weisskopf unit, i.e., the single-particle estimate for the  $B(ML)$  matrix element based on the shell model [506]. For an  $M1$

transition this reduces to

$$T_{\gamma,M1} = 1.1043 \times 10^{15} E_\gamma^3 \times B(M1) [\text{W.u.}] B_W(M1). \quad (56)$$

To calculate the Weisskopf unit for the  $B(M1)$  matrix element, i.e.,  $B_W(M1)$ , we note that [143]

$$B(ML) = 10 \left( \frac{\hbar}{m_p c R} \right)^2 B(EL), \quad (57)$$

with  $m_p$  the proton mass,  $R = 1.20 A^{1/3}$  fm the nuclear radius, and

$$B(EL) = \frac{e^2}{4\pi} \left( \frac{3R^L}{3+L} \right)^2, \quad (58)$$

where  $e$  is the electron charge. One then finds:

$$B_W(M1) = 1.7905 \left( \frac{\hbar e}{2m_p c} \right)^2 = 2.851 \times 10^{-2} \text{ MeV fm}^{-3}. \quad (59)$$

Combining now Eqs. (56) and (59), one finally gets for the  $\Gamma_{M1}$  width for a  $\gamma$  transition:

$$\Gamma_{M1} = T_{\gamma,M1} \hbar = 20.723 \times 10^{-3} E_\gamma^3 B(M1) \text{ eV}. \quad (60)$$

with  $E_\gamma$  in MeV and  $B(M1)$  in Weisskopf units.

b. *Gamow-Teller form factor*, c. Using Eqs. (8), and (10), the partial half-life,  $t$ , for a general mixed Gamow-Teller/Fermi (GT/F) transition in Eq. (7) can be rewritten as

$$t = \frac{2 \mathcal{F} t^{0^+ \rightarrow 0^+} (1 + \Delta_R^V)}{(1 + \delta_R^s) [f_V a^2 + f_A c^2]}. \quad (61)$$

All  $\beta$  transitions considered here are either  $J^\pi \rightarrow J^\pi$  or  $J^\pi \rightarrow J^\pi \pm 1$ ,  $\Delta T = 1$  transitions. The latter are of pure Gamow-Teller type while in the former isospin-symmetry breaking due to the electromagnetic interaction may induce a small isospin-forbidden Fermi component into the otherwise pure Gamow-Teller decay. The Fermi matrix element in the form factor  $a = g_V M_F$  can then be written as  $M_F = \alpha \sqrt{2T}$  with  $\alpha$  the amplitude of the admixture of the analog state to the final state of the  $\beta$  decay into the initial state [372]. An extensive survey of isospin-forbidden  $J^\pi \rightarrow J^\pi$  Fermi transitions [372] has shown  $\alpha$  to be of the order of  $10^{-3}$  and lower (see also [34,507,508]). At the level of precision we are dealing with here (which is determined by the uncertainty on the values of  $\Gamma_{M1}$  or  $B_{M1}$  used to extract the weak magnetism form factor,  $b$ ), the term  $a^2$  in Eq. (61) can be neglected with respect to  $c^2$ . One then has, for all transitions considered here,

$$f_{At} \equiv ft = \frac{2 \mathcal{F} t^{0^+ \rightarrow 0^+} (1 + \Delta_R^V)}{(1 + \delta_R^s) c^2}. \quad (62)$$

As was discussed in Sec. II C 3 a, the inner radiative correction,  $\Delta_R^V$ , was recently the subject of new and more complete calculations [88,125,126,349]. We use here the value  $\Delta_R^V = 0.02473(27)$  of Ref. [88], which is in agreement with the values of Refs. [349] and [126] (all three calculations being also slightly more encompassing than Ref. [125]) and has a slightly more conservative approach in determining the uncertainty.

TABLE XXII. Input data to determine the  $\log ft$  values [Eq. (62)], and values for the radiative correction  $\delta'_R$  (last column) for the  $\beta$  transitions from the  $A = 6$  to  $A = 26$ ,  $T = 1$  triplet states (see Figs. 17–19 in Appendix B) for which  $|b/Ac|^{\text{exp}}$  can be obtained from the  $\Gamma_{M1}$  transition strength of the corresponding analog  $\gamma$  transitions.  $Q_{\beta^-/\text{EC}}$  values were obtained from the ground-state to ground-state  $Q$  values from the 2020 Atomic Mass Evaluation [131] corrected for the energy of the final state,  $E_{\text{level}}(J_f)$ , as listed in the Brookhaven National Nuclear Data Base [116], from which also most values for the half-life,  $t_{1/2}$  (see text), and all branching ratios, BR, were obtained. Values for the phase space factor  $f_A$  were calculated with the beta spectrum generator code described in Ref. [339] (see text for more details). Details on the calculation of the electron-capture fraction,  $P_{\text{EC}}$ , are given in Sec. IIB 2. The partial half-lives,  $t$ , are obtained from Eq. (5). Element labels  $X$  in the first column without superscripts denote nuclear ground states. Superscripts “1” to “4” indicate excited states (see Figs. 17–19 in Appendix B). For the energies of the  $^{24m}\text{Al}$  and  $^{24m}\text{Na}$  isomers the values 472.2074(8) keV and 425.8(1) keV were used, respectively [116].

Transition	$A$	$J_i \xrightarrow{\beta} J_f$	$E_{\text{level}}(J_f)$ (keV)	$Q_{\beta^-/\text{EC}}$ (keV)	$f_A$	$t_{1/2}$ (s)	BR (%)	$P_{\text{EC}}$ (%)	$t$ (s)	$\delta'_R$ (%)
He $\xrightarrow{\beta^-}$ Li	6	$0^+ \rightarrow 1^+$	0	3505.215(53)	997.795(68)	0.8067(1)	100		0.8067(10)	1.203
C $\xrightarrow{\beta^+}$ B <sup>1</sup>	10	$0^+ \rightarrow 1^+$	718.380(11)	2929.682(70)	56.6306(90)	19.3016(24)	98.53(2)	0.0285	19.583(13)	1.454
B $\xrightarrow{\beta^-}$ C	12	$1^+ \rightarrow 0^+$	0	13369.4(13)	557180(260)	0.02020(2)	98.216(28)		0.020567(21)	0.740
N $\xrightarrow{\beta^+}$ C		$1^+ \rightarrow 0^+$	0	17338.1(10)	1128063(335)	0.011000(16)	96.17(5)	0.0000817	0.011438(18)	0.700
B $\xrightarrow{\beta^-}$ C <sup>1</sup>	12	$1^+ \rightarrow 2^+$	4439.82(21)	8929.6(13)	81196(57)	0.02020(2)	1.182(19)		1.709(28)	0.911
N $\xrightarrow{\beta^+}$ C <sup>1</sup>		$1^+ \rightarrow 2^+$	4439.82(21)	12898.3(60)	243533(591)	0.011000(16)	1.898(32)	0.000209	0.5796(98)	0.814
B $\xrightarrow{\beta^-}$ C <sup>2</sup>	12	$1^+ \rightarrow 0^+$	7654.07(19)	5715.3(13)	10016(11)	0.02020(2)	0.54(2)		3.74(14)	1.093
N $\xrightarrow{\beta^+}$ C <sup>2</sup>		$1^+ \rightarrow 0^+$	7654.07(19)	9684.0(60)	53912(177)	0.011000(16)	1.41(3)	0.000533	0.780(17)	0.934
N $\xrightarrow{\beta^+}$ C <sup>3</sup>	12	$1^+ \rightarrow 1^+$	12710(6)	4628.1(61)	925.5(99)	0.011000(16)	0.120(3)	0.00708	9.17(23)	1.265
O $\xrightarrow{\beta^+}$ N <sup>1</sup>	14	$0^+ \rightarrow 1^+$	3948.10(20)	1196.26(20)	0.003800(24)	70.619(11)	0.054(2)	176	360(13) $\times 10^3$	2.000
C $\xrightarrow{\beta^-}$ N	14	$0^+ \rightarrow 1^+$	0	156.476(4)	0.00933138(82)	5700(30) y	100		179.88(95) $\times 10^9$	2.033
O $\xrightarrow{\beta^+}$ N		$0^+ \rightarrow 1^+$	0	5144.364(25)	1760.522(49)	70.619(11)	0.61(1)	0.00701	11576(190)	1.268
N $\xrightarrow{\beta^-}$ O <sup>1</sup>	16	$2^- \rightarrow 3^-$	6129.89(4)	4291.0(13)	2847.3(39)	7.13(2)	66.2(6)		10.77(10)	1.267
N $\xrightarrow{\beta^-}$ O <sup>2</sup>	16	$2^- \rightarrow 1^-$	7116.85(14)	3304.1(23)	876.9(27)	7.13(2)	4.8(4)		149(12)	1.371
N $\xrightarrow{\beta^-}$ O <sup>3</sup>	16	$2^- \rightarrow 2^-$	8871.9(5)	1549.0(24)	33.94(22)	7.13(2)	1.06(7)		673(44)	1.643
Ne $\xrightarrow{\beta^+}$ F	18	$0^+ \rightarrow 1^+$	0	4444.50(59)	689.42(54)	1.66422(47)	92.11(21)	0.0270	1.8157(96)	1.368
F $\xrightarrow{\beta^+}$ O		$1^+ \rightarrow 0^+$	0	1655.93(46)	0.5564(16)	6586.2(30)	100	3.33	6805.6(31)	1.851
Ne $\xrightarrow{\beta^+}$ F <sup>1</sup>	18	$0^+ \rightarrow 1^+$	1700.81(18)	2743.69(62)	33.411(54)	1.66422(47)	0.188(6)	0.212	891(29)	1.611
F $\xrightarrow{\beta^-}$ Ne <sup>1</sup>	20	$2^+ \rightarrow 2^+$	1633.674(15)	5390.795(34)	8626.32(27)	11.096(36) <sup>a</sup>	99.9913(8)		11.097(36)	1.213
Na $\xrightarrow{\beta^+}$ Ne <sup>1</sup>		$2^+ \rightarrow 2^+$	1633.674(15)	12258.7(11)	175906(83)	0.4479(23)	79.3(11)	0.00109	0.5648(84)	0.929
Na $\xrightarrow{\beta^+}$ Ne <sup>2</sup>	20	$2^+ \rightarrow 2^+$	7421.9(12)	6470.5(16)	5675.1(97)	0.4479(23)	16.4(13)	0.00943	2.73(22)	1.208
Na $\xrightarrow{\beta^+}$ Ne <sup>3</sup>	20	$2^+ \rightarrow 2^+$	7833.4(15)	6059.0(19)	3933.2(87)	0.4479(23)	0.67(6)	0.0119	66.9(60)	1.238
Mg $\xrightarrow{\beta^+}$ Na <sup>1</sup>	22	$0^+ \rightarrow 1^+$	583.05(10)	4198.36(18)	473.65(14)	3.87445(69)	41.33(20)	0.0626	9.383(45)	1.449
Na $\xrightarrow{\beta^+}$ Ne <sup>1</sup>	22	$3^+ \rightarrow 2^+$	1274.537(7)	1568.78(15)	0.29144(32)	82108(69) $\times 10^3$	99.944(14)	10.8	91016(78) $\times 10^3$	1.950
Na $\xrightarrow{\beta^-}$ Mg <sup>2</sup>	24	$4^+ \rightarrow 4^+$	4122.889(12)	1392.79(24)	24.726(17)	53989(43)	99.855(5)		54067(43)	1.815
Al $\xrightarrow{\beta^+}$ Mg <sup>2</sup>		$4^+ \rightarrow 4^+$	4122.889(12)	9761.88(23)	50529.1(63)	2.053(4)	7.7(10)	0.00413	26.7(35)	1.054
Al $\xrightarrow{\beta^+}$ Mg <sup>3</sup>	24	$4^+ \rightarrow 3^+$	5235.12(4)	8649.65(23)	26246.4(38)	2.053(4)	1.40(13)	0.00624	147(14)	1.105
Al $\xrightarrow{\beta^+}$ Mg <sup>4</sup>	24	$4^+ \rightarrow 4^+$	6010.84(4)	7873.93(23)	15951.0(26)	2.053(4)	1.2(1)	0.00851	171(14)	1.157
Al $\xrightarrow{\beta^+}$ Mg <sup>5</sup>	24	$4^+ \rightarrow 4^+$	8439.36(4)	5445.41(23)	2081.61(50)	2.053(4)	50.0(20)	0.0312	4.11(16)	1.340
$^m\text{Na}$ $\xrightarrow{\beta^-}$ Mg	24	$1^+ \rightarrow 0^+$	0	5987.884(21)	21350.49(33)	0.02020(7)	0.05(1)		40.4(81)	1.177
$^m\text{Al}$ $\xrightarrow{\beta^+}$ Mg		$1^+ \rightarrow 0^+$	0	14310.6(25)	466680(410)	0.1313(25)	10(3)	0.000961	1.31(39)	0.941
$^m\text{Al}$ $\xrightarrow{\beta^+}$ Mg <sup>1</sup>	24	$1^+ \rightarrow 2^+$	1368.672(5)	12941.83(23)	279859(25)	0.1313(25)	4.4(5)	0.00131	2.98(34)	0.968
Si $\xrightarrow{\beta^+}$ Al <sup>1</sup>	26	$0^+ \rightarrow 1^+$	1057.739(12)	4011.397(86)	348.764(45)	2.2453(7)	21.9(4)	0.128	10.27(19)	1.529
Si $\xrightarrow{\beta^+}$ Al <sup>2</sup>	26	$0^+ \rightarrow 1^+$	1850.62(3)	3218.52(9)	87.844(17)	2.2453(7)	2.73(7)	0.328	82.5(21)	1.646
Si $\xrightarrow{\beta^+}$ Al <sup>3</sup>	26	$0^+ \rightarrow 1^+$	2071.64(4)	2997.50(9)	55.087(12)	2.2453(7)	0.290(11)	0.454	778(30)	1.685
Si $\xrightarrow{\beta^+}$ Al <sup>4</sup>	26	$0^+ \rightarrow 1^+$	2740.03(3)	2329.11(9)	9.4555(29)	2.2453(7)	0.0618(25)	1.60	3691(149)	1.826

<sup>a</sup>Weighted average of the values listed in Table V of [112].

TABLE XXIII. Input data to determine the  $\log ft$  values [Eq. (62)], and values for the radiative correction  $\delta'_R$  (last column) for the  $\beta$  transitions from the  $A = 28$  to  $A = 42$ ,  $T = 1$  multiplet states (bloc 1; see Figs. 19–21 in Appendix B), the  $A = 9$  to  $A = 53$ ,  $T = 3/2$  multiplet states (bloc 2; Figs. 22–23 in Appendix B), and the  $A = 32$ ,  $T = 2$  multiplet state (bottom line; Fig. 21 in Appendix B) for which  $|b/Ac|^{\text{EXP}}$  can be obtained from the  $\Gamma_{M1}$  transition strength of the corresponding analog  $\gamma$  transitions.  $Q_{\beta^-/\text{EC}}$  values were obtained from the ground-state to ground-state  $Q$  values from the 2020 Atomic Mass Evaluation [131] corrected for the energy of the final state,  $E_{\text{level}}(J_f)$ , as listed in the Brookhaven National Nuclear Data Base [116], from which also most values for the half-life,  $t_{1/2}$  (see text), and all branching ratios, BR, were obtained. Values for the phase space factor  $f_A$  were calculated with the  $\beta$  spectrum generator code described in Ref. [339] which is based on the recent high-precision analytical description of the allowed  $\beta$  spectrum shape [119]. Details on the calculation of the electron-capture fraction,  $P_{\text{EC}}$ , are given in Sec. II B 2. The partial half-lives,  $t$ , are obtained from Eq. (5). Element labels  $X$  in the fits column without superscripts denote nuclear ground states. Superscripts “1” to “4” indicate excited states. For the  $^{53}\text{Ni} \rightarrow ^{53}\text{Co}$  transition the half-life is from Ref. [509] and the branching ratio from Ref. [510].

Transition	$A$	$J_i \xrightarrow{\beta} J_f$	$E_{\text{level}}(J_f)$ (keV)	$Q_{\beta^-/\text{EC}}$ (keV)	$f_A$	$t_{1/2}$ (s)	BR (%)	$P_{\text{EC}}$ (%)	$t$ (s)	$\delta'_R$ (%)
$\text{Al} \xrightarrow{\beta^-} \text{Si}^1$	28	$3^+ \rightarrow 2^+$	1779.030(11)	2663.048(48)	396.2(35)	134.70(12)	99.99(1)		134.71(12)	1.640
$\text{P} \xrightarrow{\beta^+} \text{Si}^1$		$3^+ \rightarrow 2^+$	1779.030(11)	12566.1(11)	180803(1554)	0.2703(5)	69.1(7)	0.00302	0.3912(40)	0.944
$\text{P} \xrightarrow{\beta^+} \text{Si}^2$	28	$3^+ \rightarrow 3^+$	6276.20(7)	8065.9(11)	17215(331)	0.2730(5)	7.6(4)	0.0129	3.56(19)	1.177
$\text{S} \xrightarrow{\beta^+} \text{P}$	30	$0^+ \rightarrow 1^+$	0	6141.60(20)	3804(104)	1.17977(77)	21.3(5)	0.0415	5.53(13)	1.344
$\text{P} \xrightarrow{\beta^+} \text{Si}$		$1^+ \rightarrow 0^+$	0	4232.106(61)	459(12)	149.88(24)	99.939(3)	0.132	150.17(24)	1.522
$\text{Cl} \xrightarrow{\beta^+} \text{S}^1$	32	$1^+ \rightarrow 2^+$	2230.57(15)	10450.26(58)	67076(20)	0.298(1)	60(4)	0.00855	0.497(33)	1.086
$\text{Cl} \xrightarrow{\beta^+} \text{S}^2$	32	$1^+ \rightarrow 0^+$	3778.4(10)	8902.4(11)	28917(26)	0.298(1)	2.6(8)	0.0144	11.5(35)	1.178
$\text{Ar} \xrightarrow{\beta^+} \text{Cl}^1$	34	$0^+ \rightarrow 1^+$	461.00(4)	5600.793(75)	2189(84)	0.84644(35)	0.91(10)	0.0874	93(10)	1.439
$\text{Ar} \xrightarrow{\beta^+} \text{Cl}^2$	34	$0^+ \rightarrow 1^+$	665.56(4)	5396.233(75)	1774(15)	0.84644(35)	2.49(11)	0.103	33.9(15)	1.460
$\text{Ar} \xrightarrow{\beta^+} \text{Cl}^3$	34	$0^+ \rightarrow 1^+$	2589.5(14)	3482.3(14)	132.3(13)	0.84644(35)	0.86(5)	0.585	98.7(57)	1.711
$\text{Ar} \xrightarrow{\beta^+} \text{Cl}^4$	34	$0^+ \rightarrow 1^+$	3129.2(10)	2932.5(10)	43.59(60)	0.84644(35)	1.30(7)	1.23	65.7(35)	1.812
$\text{K} \xrightarrow{\beta^+} \text{Ar}^1$	36	$1^+ \rightarrow 2^+$	1970.38(5)	10883.98(33)	79044(77)	0.342(2)	44(4)	0.0114	0.777(71)	1.084
$\text{K} \xrightarrow{\beta^+} \text{Ar}^2$	36	$1^+ \rightarrow 0^+$	4440.11(19)	8374.25(38)	19589(137)	0.342(2)	8.4(10)	0.0263	4.07(49)	1.234
$\text{Ca} \xrightarrow{\beta^+} \text{K}^1$	38	$0^+ \rightarrow 1^+$	458.53(16)	6283.73(17)	4019(134)	0.44370(25)	2.84(6)	0.0856	15.64(33)	1.421
$\text{Ca} \xrightarrow{\beta^+} \text{K}^2$	38	$0^+ \rightarrow 1^+$	1697.65(25)	5044.61(26)	1166.0(92)	0.44370(25)	19.48(13)	0.195	2.282(15)	1.549
$\text{Ti} \xrightarrow{\beta^+} \text{Sc}^1$	42	$0^+ \rightarrow 1^+$	611.051(6)	6405.60(22)	4318(152)	0.20833(80)	55.9(36)	0.114	0.374(24)	1.452
$\text{Li} \xrightarrow{\beta^-} \text{Be}$	9	$3/2^- \rightarrow 3/2^-$	0	13606.45(20)	582680(41)	0.1783(4)	49.2(9)		0.3624(67)	0.676
$\text{Li} \xrightarrow{\beta^-} \text{Be}^1$	9	$3/2^- \rightarrow 5/2^-$	2429.4(13)	11177.1(13)	227139(179)	0.1783(4)	29.7(30)		0.600(61)	0.759
$\text{C} \xrightarrow{\beta^+} \text{B}$	9	$3/2^- \rightarrow 3/2^-$	0	16494.5(23)	895467(644)	0.1265(9)	54.1(15)	0.0000571	0.2338(67)	0.735
$\text{C} \xrightarrow{\beta^+} \text{B}^1$	9	$3/2^- \rightarrow 5/2^-$	2345(11)	14150(11)	405910(2317)	0.1265(9)	30.4(58)	0.0000927	0.416(79)	0.796
$\text{C} \xrightarrow{\beta^+} \text{B}^2$	9	$3/2^- \rightarrow 1/2^-$	2780(16)	13715(16)	344584(2957)	0.1265(9)	5.8(6)	0.000103	2.18(23)	0.802
$\text{B} \xrightarrow{\beta^-} \text{C}$	13	$3/2^- \rightarrow 1/2^-$	0	13436.9(10)	569259(203)	0.01736(16)	92.1(18)		0.01885(41)	0.744
$\text{B} \xrightarrow{\beta^-} \text{C}^1$	13	$3/2^- \rightarrow 3/2^-$	3684.507(19)	9752.4(10)	123890(60)	0.01736(16)	7.6(8)		0.228(24)	0.863
$\text{O} \xrightarrow{\beta^+} \text{N}$	13	$3/2^- \rightarrow 1/2^-$	0	17770.0(95)	1253437(3444)	0.00858(5)	89.2(22)	0.000118	0.00962(24)	0.693
$\text{O} \xrightarrow{\beta^+} \text{N}^1$	13	$3/2^- \rightarrow 3/2^-$	3502(2)	14268(10)	406858(1509)	0.00858(5)	9.8(20)	0.000234	0.088(18)	0.809
$\text{C} \xrightarrow{\beta^-} \text{N}^1$	15	$1/2^+ \rightarrow 1/2^+$	5298.822(14)	4472.89(80)	3325.0(27)	2.449(5)	63.2(8)		3.875(50)	1.213
$\text{O} \xrightarrow{\beta^-} \text{F}^1$	19	$5/2^+ \rightarrow 3/2^+$	1554.038(9)	3266.3(26)	863.9(31)	26.88(5)	54.4(12)		49.4(11)	1.399
$\text{O} \xrightarrow{\beta^-} \text{F}^2$	19	$5/2^+ \rightarrow 7/2^+$	4377.700(42)	442.6(26)	0.2684(58)	26.88(5)	0.0984(30)		27317(834)	1.991
$\text{Ne} \xrightarrow{\beta^-} \text{Na}$	23	$5/2^+ \rightarrow 3/2^+$	0	4375.80(10)	3431.23(36)	37.24(12)	66.9(13)		55.7(11)	1.331
$\text{Ne} \xrightarrow{\beta^-} \text{Na}^1$	23	$5/2^+ \rightarrow 5/2^+$	439.990(9)	3935.82(10)	2115.26(24)	37.24(12)	32.0(13)		116.4(47)	1.379
$\text{Ni} \xrightarrow{\beta^+} \text{Co}^1$	53	$7/2^- \rightarrow 9/2^-$	1327.0(9)	11702(25)	101177(1135)	0.0552(7)	17(8)	0.0389	0.32(15)	1.201
$\text{Si} \xrightarrow{\beta^-} \text{P}$	32	$0^+ \rightarrow 1^+$	0	227.19(30)	0.03376(86)	$4828(600) \times 10^6$	100	4.09	$5.03(62) \times 10^3$	2.329

The values for  $\delta_R$  are listed in the last column of Tables XXII and XXIII.

Note that Eq. (62) only holds for “normal” allowed  $\beta$  transitions. For strongly hindered transitions, with large  $\log ft$  values (i.e., typically larger than about 6.7) the  $\beta$  spectrum is unlikely to have an allowed shape, and the connection between  $\log ft$  and  $c$  is in principle lost because the electromagnetic interaction is very much amplified in this case [2]. For similar reasons Huber [49] recently suggested that a detailed study of the breakdown of the impulse approximation in nuclei with large  $\log ft$  transitions would be useful.

*c. Approach for  $T = 1, 3/2$ , and 2 multiplet decays.* Combining the weak magnetism form factor,  $b$ , obtained from the energy and decay width of the analog  $M1$   $\gamma$  transition via Eq. (40), and the Gamow-Teller form factor,  $c$ , obtained from the  $\beta$  decay  $ft$  value via Eq. (62), the  $b/Ac$  value for the  $\beta$  transitions in  $T \geq 1$  isospin multiplets can be obtained. The new analysis presented here significantly extends the available data set. Thereafter, experimental values for the  $M_L$  matrix elements will again be deduced from these experimental  $b/Ac$  ratios and Eq. (43). Finally, the experimental results can again be compared to shell model calculations that have been performed for several  $\beta$  transitions from the  $T = 1$  multiplets, as will be discussed below.

### 1. Experimental values for Gamow-Teller and weak magnetism form factors

Searching the Brookhaven National Nuclear Data Base files [116], input data have been found for 52 pairs of  $\beta$  and  $\gamma$  transitions from analog states in isospin  $T = 1$  isobaric triplets with masses ranging from  $A = 6$  to 42, for 15 pairs of transitions from analog states in  $T = 3/2$  quartets with  $A = 9$  to 23 and  $A = 53$ , and for a single pair of transitions from analog states in a  $T = 2$  multiplet with  $A = 32$ .

Detailed information and input data related to the  $\beta$  and  $\gamma$  transitions considered here, as well as the results obtained in the analysis, are listed in the Tables XXII to XXVII that are discussed below. To clearly indicate which transitions are considered here, Figs. 17–21 in Appendix B show the partial decay scheme for all pairs of analog  $\beta$  and  $\gamma$  transitions from states in the  $T = 1$  triplets and the  $T = 2$  multiplet with  $A = 32$ , indicating the  $\log ft$  value for the  $\beta$  transitions and the energy and the  $\Gamma_{M1}$  or  $B(M1)$  value [Eq. (60)] for the  $\gamma$  transitions. Figures 22 and 23 in Appendix B provide the same information for the pairs of analog  $\beta$  and  $\gamma$  transitions from states in the  $T = 3/2$  multiplets with mass  $A = 9$  to 53.

*a. Experimental data and resulting  $b/Ac$  values.* Tables XXII and XXIII provide, for each  $\beta$  transition considered here, the input data leading to the  $ft$  value, as well as the transition-dependent radiative correction,  $\delta'_R$ , required to extract the Gamow-Teller form factor,  $c$ , via Eq. (62). The  $\beta$  transitions are identified by the information in columns 1 to 3. Columns 4 and 5 then list, respectively, the energy of the final state of the  $\beta$  transition,  $E_{\text{level}}(J_f)$ , and the  $\beta$  decay transition energy,  $Q_{\beta^-}$  or  $Q_{\text{EC}}$  (obtained by combining  $E_{\text{level}}(J_f)$  with the ground-state to ground-state  $Q$  values listed in Ref. [131]). The resulting  $f_A$  value is listed in column 6 and was calculated from Eq. (4) using the  $\beta$  spectrum generator code described

in Ref. [339]. The latter is based on the recent high-precision analytical description of the allowed  $\beta$  spectrum shape [119].

Columns 7 to 10 list the half-life,  $t_{1/2}$ , of the  $\beta$ -decaying states, the branching ratio, BR, and (if relevant) the electron-capture fraction,  $P_{\text{EC}}$ , of the respective  $\beta$  transitions, and the partial half-life,  $t$ , resulting from these input values [Eq. (5)]. Most half-lives and all branching ratio values were obtained from the Brookhaven National Nuclear Data Base [116]. For isotopes with a superallowed pure Fermi transition, i.e.,  $^{10}\text{C}$ ,  $^{14}\text{O}$ ,  $^{18}\text{Ne}$ ,  $^{22}\text{Mg}$ ,  $^{26}\text{Si}$ ,  $^{30}\text{S}$ ,  $^{34}\text{Ar}$ ,  $^{38}\text{Ca}$ , and  $^{42}\text{Ti}$ , the half-lives were taken from the detailed analysis presented in Ref. [55]. For  $^{20}\text{F}$ , with varying values being reported in the literature, the weighted average of the values listed in Table V of Ref. [112] was used with the error bar increased by a factor  $\sqrt{(\chi^2/\nu)}$ . The electron-capture fraction,  $P_{\text{EC}}$ , was calculated using the same procedure as described in Sec. IIB 2 for the mirror  $\beta$  transitions.

For all 68 pairs of analog  $\beta$  and  $\gamma$  transitions considered, the  $\log ft$  values are given in column 4 in Tables XXIV to XXVII. These values result from the values for  $f_A$  and  $t$  listed in Tables XXII and XXIII. The  $\beta$  transitions are again identified by the information in columns 1 to 3. Columns 5 to 8 list for the analog  $\gamma$  transitions the energies of the initial state, the transition energies,  $E_\gamma$ , the  $M1$  decay widths,  $\Gamma_{M1}$ , and the resulting weak magnetism values,  $b_\gamma/\sqrt{\eta}$  [Eq. (40)], respectively. Combining the latter with the Gamow-Teller form factors,  $|c|^{\text{exp}}$ , obtained from the  $\log ft$  values using Eq. (62) and listed in column 9, the  $|b/Ac|^{\text{exp}}$  values listed in column 10 are obtained for the different  $\beta$  transitions.

*b. Note on the sign of  $b/Ac$ .* From Eqs. (40) and (62) it follows that the signs of  $b$  and  $c$  cannot be determined experimentally. However, as the ratio  $b/Ac$  was found to be positive (in the convention of Holstein [1,338], where the sign of  $g_A$  is taken to be positive) for nearly all mirror  $\beta$  transitions (see Table XVI and Sec. III B 4), it was chosen to be positive for the transitions considered here as well. Shell model calculations for a subset of the transitions considered here indeed showed the ratio  $b/Ac$  to be positive when using  $g_A = +1$  (see Sec. III C 2 c, and Table XXVIII). As it turns out, only one value out of 68 is found to be close to zero [i.e.,  $b/Ac = 0.189(42)$  for the transition  $^{36}\text{K} \rightarrow ^{36}\text{Ar}^1$  (Table XXVI)] and could thus possibly have a negative sign as was observed for the transitions of  $^{33}\text{Cl}$ ,  $^{35}\text{Ar}$ , and  $^{71}\text{Kr}$  [Table XVI and Sec. III B 4].

In the mass  $A = 14$  triplet the  $\beta$  decays from the ground states of  $^{14}\text{C}$  and  $^{14}\text{O}$  to the ground state of  $^{14}\text{N}$  yield values for  $b/Ac$  that are very large [i.e.,  $|b/Ac|^{\text{exp}} = 324(7)$  and  $35.6(8)$ , respectively] compared to all other decays listed in Tables XXIV to XXVII. These are clear cases of strongly hindered transitions [with  $\log ft$  values of 9.225(2) and 7.309(7)] for which the  $\beta$  spectrum is unlikely to have an allowed shape and the connection between  $\log ft$  and  $c$  [Eq. (62)] is lost (see also [2]). When nevertheless trying to use Eq. (62) for such cases very small values for  $c$  are obtained, often leading to large values for the ratio  $b/Ac$ . However, other hindered transitions, i.e.,  $^{22}\text{Na}$  [with  $\log ft = 7.4227(6)$ ; Table XXV] and  $^{32}\text{Si}$  [ $\log ft = 8.230(55)$ ; Table XXVII], do not lead to similarly large  $b/Ac$  values, but rather yield values that are in line with the nonhindered transitions. The reason for this is not clear.

TABLE XXIV. Data for the  $\beta$  transitions between  $A = 6$  to 18,  $T = 1$  triplet states and their corresponding analog  $\gamma$  transitions (see Figs. 17 and 18 in Appendix B), leading to the form factor ratio  $|b/Ac|^{\text{exp}}$ .  $\log ft$  values [Eq. (62)] are from Table XXII. Level energies and  $E_\gamma$  and  $\Gamma_{M1}$  values are from Ref. [116]. Element labels  $X$  in column 1 without superscripts denote nuclear ground states, while superscripts “1” to “3” indicate excited states, and “IA” indicates the analog state to the  $\beta$  decaying state(s) (see Figs. 17 and 18 in Appendix B). Values for “ $|b_\gamma|^{\text{exp}}/\sqrt{\eta}$ ” were obtained from Eq. (40). For analog  $\gamma$  and  $\beta$  transitions with the same spin sequence,  $\eta = 1$ . For opposite spin sequence  $\eta = (2J_i + 1)/(2J_f + 1)$  with  $J_{i,f}$  the initial and final spins of the  $\gamma$  transition. The  $|b/Ac|^{\text{exp}}$  values for  $\beta$  transitions with  $\eta \neq 0$  are flagged with a dagger in the last but one column. Note that the sign of  $M_L$  is relative to the sign of  $M_{GT}$  since  $M_L$  is extracted using the absolute value of the  $c$  form factor.

$T = 1$ decays	$A$	$J_i(T_i) \rightarrow J_f(T_f)$	$\log ft$	Level of $\gamma$ (keV)	$E_\gamma$ (keV)	$\Gamma_{M1}$ (eV)	$ b_\gamma ^{\text{exp}}/\sqrt{\eta}$	$ c ^{\text{exp}}$	$ b/Ac ^{\text{exp}}$	$M_L^{\text{exp}}$
He $\beta^- \rightarrow$ Li	6	$0^+(1) \rightarrow 1^+(0)$	2.905753(61)					2.7802(19)	4.088(42)	-1.72(12)
Li <sup>IA</sup> $\gamma \rightarrow$ Li		$0^+(1) \rightarrow 1^+(0)$		3562.88(10)	3561.75(10)	8.19(17)	68.2(7)			
C $\beta^+ \rightarrow$ B <sup>1</sup>	10	$0^+(1) \rightarrow 1^+(0)$	3.04520(13)					2.3649(19)	3.34(72)	-3.2(17)
B <sup>IA</sup> $\gamma \rightarrow$ B <sup>1</sup>		$0^+(1) \rightarrow 1^+(0)$		1740.05(4)	1021.646(14)	0.094(40)	79(17)			
B $\beta^- \rightarrow$ C	12	$1^+(1) \rightarrow 0^+(0)$	4.05917(49)					0.73852(55)	3.825(45)	-0.650(33)
N $\beta^+ \rightarrow$ C		$1^+(1) \rightarrow 0^+(0)$	4.11069(68)					0.69613(64)	4.058(48)	-0.451(33)
C <sup>IA</sup> $\gamma \rightarrow$ C		$1^+(1) \rightarrow 0^+(0)$		15110(3)	15100(3)	38.5(8)	33.9(4)			
B $\beta^- \rightarrow$ C <sup>1</sup>	12	$1^+(1) \rightarrow 2^+(0)$	5.1423(70)					0.2121(17)	3.54(24)	-0.248(50)
N $\beta^+ \rightarrow$ C <sup>1</sup>		$1^+(1) \rightarrow 2^+(0)$	5.1497(74)					0.2104(18)	3.57(24)	-0.240(50)
C <sup>IA</sup> $\gamma \rightarrow$ C <sup>1</sup>		$1^+(1) \rightarrow 2^+(0)$		15110(3)	10666(3)	0.96(13)	9.0(6)			
B $\beta^- \rightarrow$ C <sup>2</sup>	12	$1^+(1) \rightarrow 0^+(0)$	4.574(16)					0.4077(76)	3.35(23)	-0.552(96)
N $\beta^+ \rightarrow$ C <sup>2</sup>		$1^+(1) \rightarrow 0^+(0)$	4.6239(94)					0.3851(42)	3.55(24)	-0.446(93)
C <sup>IA</sup> $\gamma \rightarrow$ C <sup>2</sup>		$1^+(1) \rightarrow 0^+(0)$		15110(3)	7453(3)	1.09(14)	16.4(11)			
N $\beta^+ \rightarrow$ C <sup>3</sup>	12	$1^+(1) \rightarrow 1^+(0)$	3.929(12)					0.856(12)	6.44(93)	1.49(80)
C <sup>IA</sup> $\gamma \rightarrow$ C <sup>3</sup>		$1^+(1) \rightarrow 1^+(0)$		15110(3)	2400(7)	0.59(17)	66.2(95)			
O $\beta^+ \rightarrow$ N <sup>1</sup>	14	$0^+(1) \rightarrow 1^+(0)$	3.137(16)					2.123(40)	3.15(70) <sup>†</sup>	-3.3(15)
N <sup>1A</sup> $\gamma \rightarrow$ N <sup>IA</sup>		$1^+(0) \rightarrow 0^+(1)$		3948.10(20)	1635.2(2)	0.091(40)	54(12)			
C $\beta^- \rightarrow$ N	14	$0^+(1) \rightarrow 1^+(0)$	9.2249(23)					0.0019174(54)	324.1(71)	0.612(14)
O $\beta^+ \rightarrow$ N		$0^+(1) \rightarrow 1^+(0)$	7.3093(71)					0.01747(14)	35.58(83)	0.539(15)
N <sup>IA</sup> $\gamma \rightarrow$ N		$0^+(1) \rightarrow 1^+(0)$		2312.798(11)	2312.593(11)	0.0067(3)	8.70(19)			
N $\beta^- \rightarrow$ O <sup>1</sup>	16	$2^-(1) \rightarrow 3^-(0)$	4.4867(42)					0.4503(22)	4.46(25)	-0.11(11)
O <sup>IA</sup> $\gamma \rightarrow$ O <sup>1</sup>		$2^-(1) \rightarrow 3^-(0)$		12968.6(4)	6837.1(4)	1.8(2)	32.1(18)			
N $\beta^- \rightarrow$ O <sup>2</sup>	16	$2^-(1) \rightarrow 1^-(0)$	5.115(36)					0.2184(91)	3.95(41)	-0.165(89)
O <sup>IA</sup> $\gamma \rightarrow$ O <sup>2</sup>		$2^-(1) \rightarrow 1^-(0)$		12968.6(4)	5850.7(5)	0.21(4)	13.8(13)			
N $\beta^- \rightarrow$ O <sup>3</sup>	16	$2^-(1) \rightarrow 2^-(0)$	4.359(29)					0.521(17)	7.57(56)	1.49(30)
O <sup>IA</sup> $\gamma \rightarrow$ O <sup>3</sup>		$2^-(1) \rightarrow 2^-(0)$		12968.6(4)	4096.1(7)	1.5(2)	63.1(42)			
Ne $\beta^+ \rightarrow$ F	18	$0^+(1) \rightarrow 1^+(0)$	3.0955(11)					2.2328(32)	5.72(55)	2.3(12)
F $\beta^+ \rightarrow$ O		$1^+(0) \rightarrow 0^+(1)$	3.5783(13)					1.2778(22)	5.77(55) <sup>†</sup>	1.36(71)
F <sup>IA</sup> $\gamma \rightarrow$ F		$0^+(1) \rightarrow 1^+(0)$		1041.55(8)	1041.55(8)	0.26(5)	230(22)			
Ne $\beta^+ \rightarrow$ F <sup>1</sup>	18	$0^+(1) \rightarrow 1^+(0)$	4.472(14)					0.4572(73)	4.13(10) <sup>†</sup>	-0.262(44)
F <sup>1A</sup> $\gamma \rightarrow$ F <sup>IA</sup>		$1^+(0) \rightarrow 0^+(1)$		1700.81(18)	659.25(20)	0.000478(16)	19.64(33)			

*c. Discussion.* The  $|b/Ac|^{\text{exp}}$  values for the  $\beta$  transitions from the  $T = 1$  triplet states listed in Tables XXIV to XXVI and the  $T = 3/2$  states listed in Table XXVII, except for the strongly hindered transitions in the  $A = 14$  triplet, are shown

graphically in Fig. 12. As can be seen, for almost all  $\beta$  transitions the  $|b/Ac|$  values range between 0 and 10, except for the transitions from the  $A = 24$  triplet formed by the isomeric states  $^{24m}\text{Na}$  and  $^{24m}\text{Al}$  and the excited state at 9967 keV

TABLE XXV. Data for the  $\beta$  transitions between  $A = 20$  to  $26$ ,  $T = 1$  triplet states and their corresponding analog  $\gamma$  transitions (see Figs. 18 and 19 in Appendix B), leading to the form factor ratio  $|b/Ac|^{\text{exp}}$ .  $\log ft$  values [Eq. (62)] are from Table XXII. Level energies and  $E_\gamma$  and  $\Gamma_{M1}$  values are from Ref. [116]. The  $\Gamma_{M1}$  value for the transition from  $^{22}\text{Na} \rightarrow ^{22}\text{Ne}^1$  is from [511,512]. Element labels  $X$  in column 1 without superscripts denote nuclear ground states, while superscripts “1” to “4” indicate excited states, and “IA” indicates the analog state to the  $\beta$  decaying state(s) (see Figs. 18 and 19 in Appendix B). Values for “ $|b_\gamma|^{\text{exp}}/\sqrt{\eta}$ ” were obtained from Eq. (40). For analog  $\gamma$  and  $\beta$  transitions with the same spin sequence,  $\eta = 1$ . For opposite spin sequence  $\eta = (2J_i + 1)/(2J_f + 1)$  with  $J_{i,f}$  the initial and final spins of the  $\gamma$  transition. The  $|b/Ac|^{\text{exp}}$  values for  $\beta$  transitions with  $\eta \neq 0$  are flagged with a dagger in the last but one column. Note that the sign of  $M_L$  is relative to the sign of  $M_{\text{GT}}$  since  $M_L$  is extracted using the absolute value of the  $c$  form factor.

$T = 1$ decays	$A$	$J_i(T_i) \rightarrow J_f(T_f)$	$\log ft$	Level of $\gamma$ (keV)	$E_\gamma$ (keV)	$\Gamma_{M1}$ (eV)	$ b_\gamma ^{\text{exp}}/\sqrt{\eta}$	$ c ^{\text{exp}}$	$ b/Ac ^{\text{exp}}$	$M_L^{\text{exp}}$
F $\xrightarrow{\beta^-}$ Ne <sup>1</sup>	20	2 <sup>+</sup> (1) $\rightarrow$ 2 <sup>+</sup> (0)	4.9810(14)					0.25493(45)	8.26(41)	0.91(11)
Na $\xrightarrow{\beta^+}$ Ne <sup>1</sup>		2 <sup>+</sup> (1) $\rightarrow$ 2 <sup>+</sup> (0)	4.9972(64)					0.2506(19)	8.40(42)	0.93(11)
Ne <sup>IA</sup> $\xrightarrow{\gamma}$ Ne <sup>1</sup>		2 <sup>+</sup> (1) $\rightarrow$ 2 <sup>+</sup> (0)		10273.2(19)	8638(3)	4.0(4)	42.1(21)			
Na $\xrightarrow{\beta^+}$ Ne <sup>2</sup>	20	2 <sup>+</sup> (1) $\rightarrow$ 2 <sup>+</sup> (0)	4.190(35)					0.634(25)	4.88(37)	0.11(23)
Ne <sup>IA</sup> $\xrightarrow{\gamma}$ Ne <sup>2</sup>		2 <sup>+</sup> (1) $\rightarrow$ 2 <sup>+</sup> (0)		10273.2(19)	2852(4)	0.31(4)	61.8(40)			
Na $\xrightarrow{\beta^+}$ Ne <sup>3</sup>	20	2 <sup>+</sup> (1) $\rightarrow$ 2 <sup>+</sup> (0)	5.420(39)					0.1538(69)	4.03(58)	-0.104(90)
Ne <sup>IA</sup> $\xrightarrow{\gamma}$ Ne <sup>3</sup>		2 <sup>+</sup> (1) $\rightarrow$ 2 <sup>+</sup> (0)		10273.2(19)	2440.4(33)	0.0078(21)	12.4(17)			
Mg $\xrightarrow{\beta^+}$ Na <sup>1</sup>	22	0 <sup>+</sup> (1) $\rightarrow$ 1 <sup>+</sup> (0)	3.6477(21)					1.1819(30)	5.419(93)	0.84(11)
Na <sup>IA(Mg)</sup> $\xrightarrow{\gamma}$ Na <sup>1</sup>		0 <sup>+</sup> (1) $\rightarrow$ 1 <sup>+</sup> (0)		657.00(14)	73.9(1)	0.0000232(8)	140.9(24)			
Na $\xrightarrow{\beta^+}$ Ne <sup>1</sup>	22	3 <sup>+</sup> (0) $\rightarrow$ 2 <sup>+</sup> (1)	7.42366(60)					0.015259(19)	7.5(12) <sup>†</sup>	0.043(19)
Na <sup>IA(Ne)</sup> $\xrightarrow{\gamma}$ Na		2 <sup>+</sup> (1) $\rightarrow$ 3 <sup>+</sup> (0)		1951.8(3)	1951.8(3)	0.000269(88)	2.99(49)			
Na $\xrightarrow{\beta^-}$ Mg <sup>2</sup>	24	4 <sup>+</sup> (1) $\rightarrow$ 4 <sup>+</sup> (0)	6.12609(46)					0.068014(74)	4.8(12)	0.005(83)
Al $\xrightarrow{\beta^+}$ Mg <sup>2</sup>		4 <sup>+</sup> (1) $\rightarrow$ 4 <sup>+</sup> (0)	6.129(57)					0.0680(44)	4.8(13)	0.005(86)
Mg <sup>IA1</sup> $\xrightarrow{\gamma}$ Mg <sup>2</sup>		4 <sup>+</sup> (1) $\rightarrow$ 4 <sup>+</sup> (0)		9516.28(4)	5392.68(9)	0.023(12)	7.8(20)			
Al $\xrightarrow{\beta^+}$ Mg <sup>3</sup>	24	4 <sup>+</sup> (1) $\rightarrow$ 3 <sup>+</sup> (0)	6.585(40)					0.0402(19)	2.16(56)	-0.102(23)
Mg <sup>IA1</sup> $\xrightarrow{\gamma}$ Mg <sup>3</sup>		4 <sup>+</sup> (1) $\rightarrow$ 3 <sup>+</sup> (0)		9516.28(4)	4280.62(13)	0.00083(42)	2.09(53)			
Al $\xrightarrow{\beta^+}$ Mg <sup>4</sup>	24	4 <sup>+</sup> (1) $\rightarrow$ 4 <sup>+</sup> (0)	6.436(36)					0.0478(20)	4.28(11)	-0.021(51)
Mg <sup>IA1</sup> $\xrightarrow{\gamma}$ Mg <sup>4</sup>		4 <sup>+</sup> (1) $\rightarrow$ 4 <sup>+</sup> (0)		9516.28(4)	3505.61(9)	0.0025(12)	4.9(12)			
Al $\xrightarrow{\beta^+}$ Mg <sup>5</sup>	24	4 <sup>+</sup> (1) $\rightarrow$ 4 <sup>+</sup> (0)	3.932(17)					0.852(17)	3.86(93)	-0.72(79)
Mg <sup>IA1</sup> $\xrightarrow{\gamma}$ Mg <sup>5</sup>		4 <sup>+</sup> (1) $\rightarrow$ 4 <sup>+</sup> (0)		9516.28(4)	1076.86(4)	0.019(9)	79(19)			
Na(m) $\xrightarrow{\beta^-}$ Mg	24	1 <sup>+</sup> (1) $\rightarrow$ 0 <sup>+</sup> (0)	5.936(88)					0.0849(85)	20.7(30)	1.36(29)
Al(m) $\xrightarrow{\beta^+}$ Mg		1 <sup>+</sup> (1) $\rightarrow$ 0 <sup>+</sup> (0)	5.79(13)					0.101(15)	17.5(32)	1.29(38)
Mg <sup>IA2</sup> $\xrightarrow{\gamma}$ Mg		1 <sup>+</sup> (1) $\rightarrow$ 0 <sup>+</sup> (0)		9967.19(22)	9963.0(15)	4.3(9)	42.3(44)			
Al(m) $\xrightarrow{\beta^+}$ Mg <sup>1</sup>	24	1 <sup>+</sup> (1) $\rightarrow$ 2 <sup>+</sup> (0)	5.921(50)					0.0860(50)	15.8(21)	0.96(19)
Mg <sup>IA2</sup> $\xrightarrow{\gamma}$ Mg <sup>1</sup>		1 <sup>+</sup> (1) $\rightarrow$ 2 <sup>+</sup> (0)		9967.19(22)	8595.1(15)	1.65(39)	32.7(39)			
Si $\xrightarrow{\beta^+}$ Al <sup>1</sup>	26	0 <sup>+</sup> (1) $\rightarrow$ 1 <sup>+</sup> (0)	3.5539(79)					1.316(12)	6.18(61) <sup>†</sup>	1.93(80)
Al <sup>1</sup> $\xrightarrow{\gamma}$ Al <sup>IA</sup>		1 <sup>+</sup> (0) $\rightarrow$ 0 <sup>+</sup> (1)		1057.739(12)	829.3(4)	0.0177(35)	122(12)			
Si $\xrightarrow{\beta^+}$ Al <sup>2</sup>	26	0 <sup>+</sup> (1) $\rightarrow$ 1 <sup>+</sup> (0)	3.861(11)					0.924(12)	2.88(13) <sup>†</sup>	-1.69(13)
Al <sup>2</sup> $\xrightarrow{\gamma}$ Al <sup>IA</sup>		1 <sup>+</sup> (0) $\rightarrow$ 0 <sup>+</sup> (1)		1850.62(3)	1622(7)	0.0141(13)	39.9(18)			
Si $\xrightarrow{\beta^+}$ Al <sup>3</sup>	26	0 <sup>+</sup> (1) $\rightarrow$ 1 <sup>+</sup> (0)	4.632(16)					0.3802(72)	1.63(16) <sup>†</sup>	-1.170(66)
Al <sup>3</sup> $\xrightarrow{\gamma}$ Al <sup>IA</sup>		1 <sup>+</sup> (0) $\rightarrow$ 0 <sup>+</sup> (1)		2071.64(4)	1842.8(7)	0.00112(22)	9.29(91)			
Si $\xrightarrow{\beta^+}$ Al <sup>4</sup>	26	0 <sup>+</sup> (1) $\rightarrow$ 1 <sup>+</sup> (0)	4.543(18)					0.4209(85)	3.31(20) <sup>†</sup>	-0.588(86)
Al <sup>4</sup> $\xrightarrow{\gamma}$ Al <sup>IA</sup>		1 <sup>+</sup> (0) $\rightarrow$ 0 <sup>+</sup> (1)		2740.03(3)	2511.59(10)	0.0144(16)	20.9(12)			

TABLE XXVI. Data for the  $\beta$  transitions between  $A = 28$  to  $42$ ,  $T = 1$  triplet states and their corresponding analog  $\gamma$  transitions (see Figs. 19–21 in Appendix B), leading to the form factor ratio  $|b/Ac|^{\text{exp}}$ .  $\log ft$  values [Eq. (62)] are from Table XXIII. Level energies and  $E_\gamma$  and  $\Gamma_{M1}$  values are from Ref. [116]. Element labels  $X$  in column 1 without superscripts denote nuclear ground states, while superscripts “1” to “4” indicate excited states, and “IA” indicates the analog state to the  $\beta$  decaying state(s) (see Figs. 19–21 in Appendix B). Values for “ $|b_\gamma|^{\text{exp}}/\sqrt{\eta}$ ” were obtained from Eq. (40). For analog  $\gamma$  and  $\beta$  transitions with the same spin sequence,  $\eta = 1$ . For opposite spin sequence  $\eta = (2J_i + 1)/(2J_f + 1)$  with  $J_{i,f}$  the initial and final spins of the  $\gamma$  transition. The  $|b/Ac|^{\text{exp}}$  values for  $\beta$  transitions with  $\eta \neq 0$  are flagged with a dagger in the last but one column. Note that the sign of  $M_L$  is relative to the sign of  $M_{GT}$  since  $M_L$  is extracted using the absolute value of the  $c$  form factor.

$T = 1$ decays	$A$	$J_i(T_i) \rightarrow J_f(T_f)$	$\log ft$	Level of $\gamma$ (keV)	$E_\gamma$ (keV)	$\Gamma_{M1}$ (eV)	$ b_\gamma ^{\text{exp}}/\sqrt{\eta}$	$ c ^{\text{exp}}$	$ b/Ac ^{\text{exp}}$	$M_L^{\text{exp}}$
Al $\xrightarrow{\beta^-}$ Si <sup>1</sup>	28	3 <sup>+</sup> (1) $\rightarrow$ 2 <sup>+</sup> (0)	4.7273(38)					0.3407(15)	1.74(38)	−1.01(13)
P $\xrightarrow{\beta^+}$ Si <sup>1</sup>		3 <sup>+</sup> (1) $\rightarrow$ 2 <sup>+</sup> (0)	4.8496(58)					0.2970(20)	2.00(43)	−0.80(13)
Si <sup>IA</sup> $\xrightarrow{\gamma}$ Si <sup>1</sup>		3 <sup>+</sup> (1) $\rightarrow$ 2 <sup>+</sup> (0)		9315.92(10)	7535.7(4)	0.21(9)	16.6(36)			
P $\xrightarrow{\beta^+}$ Si <sup>2</sup>	28	3 <sup>+</sup> (1) $\rightarrow$ 3 <sup>+</sup> (0)	4.787(24)					0.3188(89)	4.47(85)	−0.08(27)
Si <sup>IA</sup> $\xrightarrow{\gamma}$ Si <sup>2</sup>		3 <sup>+</sup> (1) $\rightarrow$ 3 <sup>+</sup> (0)		9315.92(10)	3039.16(17)	0.08(3)	39.9(75)			
S $\xrightarrow{\beta^+}$ P	30	0 <sup>+</sup> (1) $\rightarrow$ 1 <sup>+</sup> (0)	4.324(16)					0.5429(98)	6.08(34)	0.75(18)
P $\xrightarrow{\beta^+}$ Si		1 <sup>+</sup> (0) $\rightarrow$ 0 <sup>+</sup> (1)	4.839(12)					0.2998(41)	6.36(34) <sup>†</sup>	0.50(10)
P <sup>IA</sup> $\xrightarrow{\gamma}$ P		0 <sup>+</sup> (1) $\rightarrow$ 1 <sup>+</sup> (0)		677.01(3)	677.01(3)	0.00475(50)	99.1(52)			
Cl $\xrightarrow{\beta^+}$ S <sup>1</sup>	32	1 <sup>+</sup> (1) $\rightarrow$ 2 <sup>+</sup> (0)	4.523(29)					0.432(14)	3.08(52)	−0.70(23)
S <sup>IA</sup> $\xrightarrow{\gamma}$ S <sup>1</sup>		1 <sup>+</sup> (1) $\rightarrow$ 2 <sup>+</sup> (0)		7001.4(4)	4770.5(3)	0.27(9)	42.6(71)			
Cl $\xrightarrow{\beta^+}$ S <sup>2</sup>	32	1 <sup>+</sup> (1) $\rightarrow$ 0 <sup>+</sup> (0)	5.52(14)					0.137(21)	5.5(19)	0.11(25)
S <sup>IA</sup> $\xrightarrow{\gamma}$ S <sup>2</sup>		1 <sup>+</sup> (1) $\rightarrow$ 0 <sup>+</sup> (0)		7001.4(4)	3223.4(10)	0.027(16)	24.3(72)			
Ar $\xrightarrow{\beta^+}$ Cl <sup>1</sup>	34	0 <sup>+</sup> (1) $\rightarrow$ 1 <sup>+</sup> (0)	5.309(51)					0.175(10)	7.91(58) <sup>†</sup>	0.56(11)
Cl <sup>1</sup> $\xrightarrow{\gamma}$ Cl <sup>IA</sup>		1 <sup>+</sup> (0) $\rightarrow$ 0 <sup>+</sup> (1)		461.00(4)	461.00(4)	0.000087(8)	27.1(12)			
Ar $\xrightarrow{\beta^+}$ Cl <sup>2</sup>	34	0 <sup>+</sup> (1) $\rightarrow$ 1 <sup>+</sup> (0)	4.781(20)					0.3206(72)	1.72(11) <sup>†</sup>	−0.957(41)
Cl <sup>2</sup> $\xrightarrow{\gamma}$ Cl <sup>IA</sup>		1 <sup>+</sup> (0) $\rightarrow$ 0 <sup>+</sup> (1)		665.56(4)	665.55(5)	0.000042(5)	10.84(65)			
Ar $\xrightarrow{\beta^+}$ Cl <sup>3</sup>	34	0 <sup>+</sup> (1) $\rightarrow$ 1 <sup>+</sup> (0)	4.117(26)					0.688(20)	1.89(26) <sup>†</sup>	−1.94(19)
Cl <sup>3</sup> $\xrightarrow{\gamma}$ Cl <sup>IA</sup>		1 <sup>+</sup> (0) $\rightarrow$ 0 <sup>+</sup> (1)		2580.4(2)	2579.4(14)	0.0135(36)	25.5(34)			
Ar $\xrightarrow{\beta^+}$ Cl <sup>4</sup>	34	0 <sup>+</sup> (1) $\rightarrow$ 1 <sup>+</sup> (0)	3.458(24)					1.467(41)	2.78(94) <sup>†</sup>	−2.8(14)
Cl <sup>4</sup> $\xrightarrow{\gamma}$ Cl <sup>IA</sup>		1 <sup>+</sup> (0) $\rightarrow$ 0 <sup>+</sup> (1)		3129.13(12)	3129(10)	0.24(16)	80(27)			
K $\xrightarrow{\beta^+}$ Ar <sup>1</sup>	36	1 <sup>+</sup> (1) $\rightarrow$ 2 <sup>+</sup> (0)	4.778(40)					0.318(15)	0.189(42)	−1.438(67)
Ar <sup>IA</sup> $\xrightarrow{\gamma}$ Ar <sup>1</sup>		1 <sup>+</sup> (1) $\rightarrow$ 2 <sup>+</sup> (0)		6612.12(20)	4641.0(5)	0.00051(22)	2.17(47)			
K $\xrightarrow{\beta^+}$ Ar <sup>2</sup>	36	1 <sup>+</sup> (1) $\rightarrow$ 0 <sup>+</sup> (0)	4.902(52)					0.279(17)	1.37(31)	−0.93(10)
Ar <sup>IA</sup> $\xrightarrow{\gamma}$ Ar <sup>2</sup>		1 <sup>+</sup> (1) $\rightarrow$ 0 <sup>+</sup> (0)		6612.12(20)	2170.29(20)	0.0021(9)	13.8(30)			
Ca $\xrightarrow{\beta^+}$ K <sup>1</sup>	38	0 <sup>+</sup> (1) $\rightarrow$ 1 <sup>+</sup> (0)	4.798(17)					0.3143(62)	6.26(32) <sup>†</sup>	0.49(10)
K <sup>1</sup> $\xrightarrow{\gamma}$ K <sup>IA</sup>		1 <sup>+</sup> (0) $\rightarrow$ 0 <sup>+</sup> (1)		458.4(4)	327.9(2)	0.000064(6)	43.2(20)			
Ca $\xrightarrow{\beta^+}$ K <sup>2</sup>	38	0 <sup>+</sup> (1) $\rightarrow$ 1 <sup>+</sup> (0)	3.4251(45)					1.5262(80)	1.49(15) <sup>†</sup>	−4.91(23)
K <sup>2</sup> $\xrightarrow{\gamma}$ K <sup>IA</sup>		1 <sup>+</sup> (0) $\rightarrow$ 0 <sup>+</sup> (1)		1697.84(12)	1567.39(12)	0.0093(19)	49.9(51)			
Ti $\xrightarrow{\beta^+}$ Sc <sup>1</sup>	42	0 <sup>+</sup> (1) $\rightarrow$ 1 <sup>+</sup> (0)	3.207(32)					1.963(72)	6.2(14) <sup>†</sup>	3.0(27)
Sc <sup>1</sup> $\xrightarrow{\gamma}$ Sc <sup>IA</sup>		1 <sup>+</sup> (0) $\rightarrow$ 0 <sup>+</sup> (1)		611.051(6)	611.046(6)	0.016(7)	297(65)			

in <sup>24</sup>Mg (Fig. 19 in Appendix B). Even though all three  $\beta$  transitions in this triplet have low  $\log ft$  values [i.e., between 5.79(13) and 5.936(88)], they show large  $|b/Ac|$  values ranging from 15.8(21) to 20.7(30). Other  $\beta$  transitions with similar or even larger  $\log ft$  values, such as the  $\beta$  transitions from <sup>9</sup>C

( $T = 3/2$ ) or from the ground states of <sup>24</sup>Na and <sup>24</sup>Al ( $T = 1$ ) [with  $\log ft$  values from 5.876(45) to 6.585(40)], and even the strongly hindered transitions from <sup>22</sup>Na [ $\log ft = 7.4237(6)$ ] and <sup>32</sup>Si [ $\log ft = 8.230(55)$ ], all show values for  $|b/Ac|$  ranging from 2.2(6) to 7.3(11). The large values for the  $A = 24$

TABLE XXVII. Data for the  $\beta$  transitions between  $A = 9$  to  $53$ ,  $T = 3/2$  quartet states and their corresponding analog  $\gamma$  transitions (see Figs. 22 and 23 in Appendix B), leading to the form factor ratio  $|b/Ac|^{\text{exp}}$ . At the bottom of the table the single  $\beta$  transition from a  $T = 2$  quintet state and its analog  $\gamma$  transition are included as well (Fig. 21 in Appendix B).  $\log ft$  values [Eq. (62)] are from Table XXIII. Level energies and  $E_\gamma$  and  $\Gamma_{M1}$  values are from Ref. [116]. The data for the transition  $^{53}\text{Ni} \rightarrow ^{53}\text{Co}^1$  are from [510]. The  $\Gamma_{M1}$  value for this case is from theory [510], with a 20% error being assumed [513]. Element labels  $X$  in column 1 without superscripts denote nuclear ground states, while superscripts “1” to “2” indicate excited states, and “IA” indicates the analog state to the  $\beta$  decaying state(s) (see Figs. 21–23 in Appendix B). Values for  $|b_\gamma|^{\text{exp}}$  were obtained from Eq. (40), with the factor  $\eta$  being unity for all  $\beta$  transitions listed here. Note that the sign of  $M_L$  is relative to the sign of  $M_{\text{GT}}$  since  $M_L$  is extracted using the absolute value of the  $c$  form factor.

$T = 3/2$										
decays	A	$J_i(T_i) \rightarrow J_f(T_f)$	$\log ft$	Level of $\gamma$ (keV)	$E_\gamma$ (keV)	$\Gamma_{M1}$ (eV)	$ b_\gamma ^{\text{exp}}$	$ c ^{\text{exp}}$	$ b/Ac ^{\text{exp}}$	$M_L^{\text{exp}}$
$\text{Li} \xrightarrow{\beta^-} \text{Be}$	9	$3/2^-(3/2) \rightarrow 3/2^-(1/2)$	5.3246(80)					0.1721(16)	7.31(23)	0.448(40)
$\text{Be}^{\text{IA}} \xrightarrow{\gamma} \text{Be}$		$3/2^-(3/2) \rightarrow 3/2^-(1/2)$		14392.2(18)	14380.0(18)	6.6(4)	11.32(34)			
$\text{Li} \xrightarrow{\beta^-} \text{Be}^1$	9	$3/2^-(3/2) \rightarrow 5/2^-(1/2)$	5.135(44)					0.214(11)	8.26(42)	0.760(98)
$\text{Be}^{\text{IA}} \xrightarrow{\gamma} \text{Be}^1$		$3/2^-(3/2) \rightarrow 5/2^-(1/2)$		14392.2(18)	11954.3(22)	7.48(7)	15.907(75)			
$\text{C} \xrightarrow{\beta^+} \text{B}$	9	$3/2^-(3/2) \rightarrow 3/2^-(1/2)$	5.320(12)					0.1728(25)	7.42(25)	0.469(44)
$\text{B}^{\text{IA}} \xrightarrow{\gamma} \text{B}$		$3/2^-(3/2) \rightarrow 3/2^-(1/2)$		14655.0(25)	14642.2(25)	6.97(42)	11.54(35)			
$\text{C} \xrightarrow{\beta^+} \text{B}^1$	9	$3/2^-(3/2) \rightarrow 5/2^-(1/2)$	5.228(84)					0.192(18)	8.7(10)	0.77(21)
$\text{B}^{\text{IA}} \xrightarrow{\gamma} \text{B}^1$		$3/2^-(3/2) \rightarrow 5/2^-(1/2)$		14655.0(25)	12301(11)	7.3(11)	15.1(11)			
$\text{C} \xrightarrow{\beta^+} \text{B}^2$	9	$3/2^-(3/2) \rightarrow 1/2^-(1/2)$	5.876(45)					0.0912(47)	7.8(24)	0.28(21)
$\text{B}^{\text{IA}} \xrightarrow{\gamma} \text{B}^2$		$3/2^-(3/2) \rightarrow 1/2^-(1/2)$		14655.0(25)	11870(160)	1.17(70)	6.4(19)			
$\text{B} \xrightarrow{\beta^-} \text{C}$	13	$3/2^-(3/2) \rightarrow 1/2^-(1/2)$	4.0294(94)					0.7632(83)	2.804(94)	-1.452(73)
$\text{C}^{\text{IA}} \xrightarrow{\gamma} \text{C}$		$3/2^-(3/2) \rightarrow 1/2^-(1/2)$		15108.2(12)	15098.8(12)	22.1(14)	27.82(88)			
$\text{B} \xrightarrow{\beta^-} \text{C}^1$	13	$3/2^-(3/2) \rightarrow 3/2^-(1/2)$	4.452(46)					0.470(25)	6.24(55)	0.72(26)
$\text{C}^{\text{IA}} \xrightarrow{\gamma} \text{C}^1$		$3/2^-(3/2) \rightarrow 3/2^-(1/2)$		15108.2(12)	11418.2(12)	17.9(25)	38.1(27)			
$\text{O} \xrightarrow{\beta^+} \text{N}$	13	$3/2^-(3/2) \rightarrow 1/2^-(1/2)$	4.081(11)					0.7202(92)	3.11(10)	-1.149(73)
$\text{N}^{\text{IA}} \xrightarrow{\gamma} \text{N}$		$3/2^-(3/2) \rightarrow 1/2^-(1/2)$		15064.6(4)	15055.2(4)	24.0(14)	29.12(85)			
$\text{O} \xrightarrow{\beta^+} \text{N}^1$	13	$3/2^-(3/2) \rightarrow 3/2^-(1/2)$	4.552(90)					0.419(43)	7.11(78)	1.01(34)
$\text{N}^{\text{IA}} \xrightarrow{\gamma} \text{N}^1$		$3/2^-(3/2) \rightarrow 3/2^-(1/2)$		15064.6(4)	11557(2)	19.2(16)	38.7(16)			
$\text{C} \xrightarrow{\beta^-} \text{N}^1$	15	$1/2^+(3/2) \rightarrow 1/2^+(1/2)$	4.1101(56)					0.6949(45)	3.06(38)	-1.14(27)
$\text{N}^{\text{IA}} \xrightarrow{\gamma} \text{N}^1$		$1/2^+(3/2) \rightarrow 1/2^+(1/2)$		11615(4)	6316(4)	1.6(4)	31.9(40)			
$\text{O} \xrightarrow{\beta^-} \text{F}^1$	19	$5/2^+(3/2) \rightarrow 3/2^+(1/2)$	4.6303(97)					0.3814(43)	7.26(79)	0.97(30)
$\text{F}^{\text{IA}} \xrightarrow{\gamma} \text{F}^1$		$5/2^+(3/2) \rightarrow 3/2^+(1/2)$		7539.6(9)	5986(9)	2.3(5)	52.6(57)			
$\text{O} \xrightarrow{\beta^-} \text{F}^2$	19	$5/2^+(3/2) \rightarrow 7/2^+(1/2)$	3.865(16)					0.918(17)	6.31(64)	1.47(59)
$\text{F}^{\text{IA}} \xrightarrow{\gamma} \text{F}^2$		$5/2^+(3/2) \rightarrow 7/2^+(1/2)$		7539.6(9)	3161.9(9)	1.5(3)	110(11)			
$\text{Ne} \xrightarrow{\beta^-} \text{Na}$	23	$5/2^+(3/2) \rightarrow 3/2^+(1/2)$	5.2810(86)					0.1804(18)	9.38(37)	0.842(68)
$\text{Na}^{\text{IA}} \xrightarrow{\gamma} \text{Na}$		$5/2^+(3/2) \rightarrow 3/2^+(1/2)$		7891.19(25)	7889.7(3)	1.97(15)	38.9(15)			
$\text{Ne} \xrightarrow{\beta^-} \text{Na}^1$	23	$5/2^+(3/2) \rightarrow 5/2^+(1/2)$	5.391(18)					0.1588(32)	8.16(42)	0.548(67)
$\text{Na}^{\text{IA}} \xrightarrow{\gamma} \text{Na}^1$		$5/2^+(3/2) \rightarrow 5/2^+(1/2)$		7891.19(25)	7449.9(3)	0.97(9)	29.8(14)			
$\text{Ni} \xrightarrow{\beta^+} \text{Co}^1$	53	$7/2^-(3/2) \rightarrow 9/2^-(1/2)$	4.52(22)					0.44(10)	2.26(57)	-1.06(35)
$\text{Co}^{\text{IA}} \xrightarrow{\gamma} \text{Co}^1$		$7/2^-(3/2) \rightarrow 9/2^-(1/2)$		4325(2)	2995	0.11(2)	52.2(47)			
$T = 2$ decay	A	$J_i(T_i) \rightarrow J_f(T_f)$	$\log ft$	Level of $\gamma$ (keV)	$E_\gamma$ (keV)	$\Gamma_{M1}$ (eV)	$ b _\gamma^{\text{exp}}$	$ c ^{\text{exp}}$	$ b/Ac ^{\text{exp}}$	$M_L^{\text{exp}}$
$\text{Si} \xrightarrow{\beta^+} \text{P}$	32	$0^+(2) \rightarrow 1^+(1)$	8.230(55)					0.00602(38)	5.76(39)	0.0063(24)
$\text{P}^{\text{IA}} \xrightarrow{\gamma} \text{P}$		$0^+(2) \rightarrow 1^+(1)$		5072.44(6)	5072.00(6)	0.00022(1)	1.110(25)			

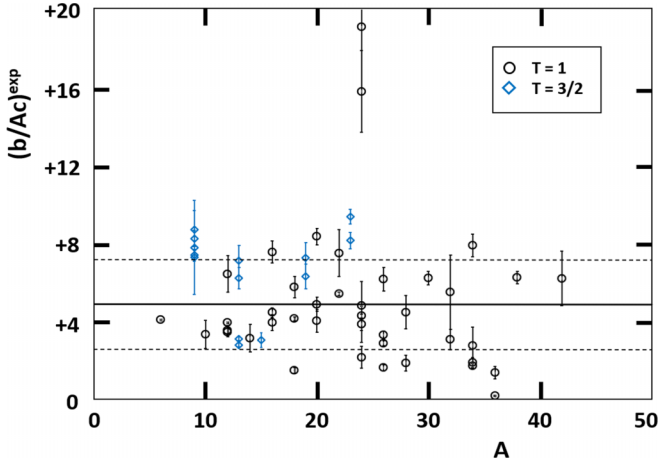


FIG. 12. Experimental  $b/Ac$  values for the  $\beta$  transitions from  $T = 1$  and  $T = 3/2$  states (Tables XXIV to XXVII). The bold and dashed horizontal lines indicate the unweighted average value of  $4.8 \pm 2.3$ , not including the two strongly deviating values at  $A = 24$  (see also Table XXX).

triplet of the isomeric states  $^{24m}\text{Na}$  and  $^{24m}\text{Al}$  and the excited state at 9967 keV in  $^{24}\text{Mg}$  are, however, not so much due to the small value for the Gamow-Teller form factor,  $c$ , but mainly to the large values of the M1  $\gamma$ -decay width,  $\Gamma_{M1}$ , of the analog  $\gamma$  transitions, i.e.,  $\Gamma_{M1} = 4.3(9)$  eV and  $1.65(39)$  eV (Table XXV). Note that the value of  $|b/Ac| = 17.5(32)$  for the transition from  $^{24m}\text{Al}$  to the ground state of  $^{24}\text{Mg}$  was addressed in shell model calculations (to be discussed in the next section, Sec. III C 2), with the theoretical result being in agreement with experiment within error bars.

Figure 12 does not show evidence of the single-particle-related structure that was noticed for the  $\beta$  transitions of the  $T = 1/2$  mirror nuclei (Fig. 6). This is not surprising as for most of the  $T = 1$ ,  $3/2$ , and  $2$  transitions the final states are in fact excited states that usually have a more complicated structure. Nevertheless, some low values of  $b/Ac$  are clearly present in the  $p_{1/2}$  (around  $A = 13$  to  $15$ ) and  $d_{3/2}$  (region from  $A = 33$  to  $40$ ) subshells with  $j = l - 1/2$  (see Sec. III B 2). A more extensive discussion will be given in Sec. III D 1 b.

For the transitions from the  $T = 1$  triplet states the unweighted average (an unweighted average is used because individual error bars differ a lot) is  $(b/Ac)^{\text{exp}} = 4.2 \pm 2.0$  (the error bar indicating one standard deviation) when not including the large values for  $^{24m}\text{Na}$  and  $^{24m}\text{Al}$ , and  $4.9 \pm 3.5$  when including them. For the transitions from the  $T = 3/2$  states an unweighted average value  $(b/Ac)^{\text{exp}} = 6.3 \pm 2.4$  is found.

## 2. Nuclear matrix elements $M_{GT}$ and $M_L$

*a. Experimental values for  $M_{GT}$  and  $M_L$ .* Using the experimental values for the  $b$  and  $c$  form factors in Tables XXIV to XXVII, and assuming the ratio  $b/Ac$  to be positive (Sec. III C 1 b), the matrix element  $M_L$  can be derived using Eq. (43). To do this we use the absolute values of the  $c$  form factor. Therefore, the sign obtained for  $M_L$  is relative to that of  $M_{GT}$  [Eq. (43)]. The resulting values for  $M_L$  are listed in the last columns of Tables XXIV to XXVII.

*b. Shell model values for  $M_{GT}$  and  $M_L$ .* For a number of  $\beta$  transitions in the  $T = 1$  multiplets, shell model calculations of the matrix elements relevant for the different form factors were again performed. These transitions correspond to the ones considered in an early version of this paper dating from before one of the authors retired and before the data set was significantly extended by a thorough inspection of the Nuclear Data Base [116]. For each case, several calculations were performed with different effective shell model interactions (Table XXVIII). As for the mirror  $\beta$  transitions, Sec. III B 3 b, well-established effective interactions that are available in the literature and give excellent fits to experimental spectra were again chosen for this. Thus, in the  $p$ -shell ( $p_{3/2}$  and  $p_{1/2}$  orbits), three interactions of Cohen-Kurath (i.e., CK6162BME, CK8162BME, and CK816POT, and labeled as such in Table XXVIII) [396] and a more recent one from Brown-Warburton (PWBT) [514] were used. In the  $sd$  shell ( $d_{5/2}$ ,  $s_{1/2}$ , and  $d_{3/2}$  orbits), we used three versions of the universal  $sd$ -shell interaction, i.e., USD [497] and two more recent ones, USD-A and USD-B [397]. For  $A = 16$  and possibly  $A = 18$  a cross-shell interaction is needed. Here, the Millener-Kurath (MK) interaction [500] that was designed to give 1p-1h matrix elements (relative to a closed-shell  $^{16}\text{O}$ ) and including the  $p_{3/2}$ ,  $p_{1/2}$ ,  $d_{5/2}$ ,  $s_{1/2}$ , and  $d_{3/2}$  orbits was used, together with USD for  $sd$ -shell interactions and a Cohen-Kurath interaction for  $p$ -shell interactions. That left the 2p-2h interaction to be determined. This was computed from the Millener-Kurath potential, adjusting its strength so the excited  $0^+$  state in  $A = 18$  (4p-2h configuration) came at about the right energy. The accuracy of this interaction for  $A = 16$  and  $A = 18$  might therefore be inferior to the others. Note also here that, as we are dealing with light nuclei, the recent advances in *ab initio* shell-structure calculations (see, e.g., Refs. [501–505]) offer interesting prospects as well.

*c. Comparison of theoretical and experimental matrix elements.* Results from the shell model calculations of the  $M_{GT}$  and  $M_L$  matrix elements and the corresponding values for the  $b$  form factor and the  $b/Ac$  ratio [the latter being obtained from Eq. (43)] for the fourteen  $\beta$  transitions considered are listed in Table XXVIII.

Comparing the theoretically calculated and experimentally obtained values for the Gamow-Teller matrix element, the Cohen-Kurath interaction seems to perform best for  $A = 6$  (indicated by the boldface font in the fifth column), with there not being a preferred choice for  $A = 10$ , and with the PWBT interaction yielding results closest to experiment for  $A = 12$ . As can be seen by comparing the last two columns in Table XXVIII, for all these cases the theoretically predicted value for  $b/Ac$  (listed in the last column) is significantly larger (i.e., well outside the experimental error bars) than the experimental one (next-to-last column). This is due to the systematically too low theoretical values for  $M_L^{\text{theo}}$ , as is clear from a comparison of columns 6 and 7. The reason for this is not clear.

For  $A = 16$  and  $18$ , the MK interaction seems to perform quite well, reproducing the value for  $|b/Ac|^{\text{exp}}$  always within about one standard deviation. For  $A = 18$  the USD interaction is further found to provide similar results to the MK interaction. For  $A = 20$  and  $24$  the USD-A interaction

TABLE XXVIII. Comparison of the experimental values for the Gamow-Teller matrix element,  $M_{GT}$  (the  $c$  form factor), the orbital current matrix element,  $M_L$ , the form factor  $|b|$ , and the ratio  $|b/Ac|$ , with theoretical values calculated in the shell model using the interactions mentioned in the text (Sec. III C 2 b), for 14  $\beta$  transitions from  $T = 1$  triplet states in Tables XXIV to XXVII. The theoretically calculated values of  $M_{GT}^{\text{theo}}$  in column 5 that agree best with the experimental results,  $|M_{GT}|^{\text{exp}}$ , listed in column 4 are indicated in boldface. For the transition from  $^{10}\text{C}$  to  $^{10}\text{B}$  no preference can be given. Values for  $b^{\text{theo}}$  were obtained from the calculated matrix elements with the equation for  $b$  in Table X. Values for  $(b/Ac)^{\text{theo}}$  were calculated with Eq. (43). The value  $g_A = +1$  was used throughout. Note that for the experimental values  $M_{GT}^{\text{exp}}$ ,  $b^{\text{exp}}$ , and  $(b/Ac)^{\text{exp}}$ , only absolute values can be given as the  $f_{At}$  value gives access to  $c^2$  only [Eq. (62)]. Note also that for the shell model calculated values for  $M_{GT}^{\text{theo}}$  and  $M_L^{\text{theo}}$  only the relative sign is important. Further, also the sign of  $M_L^{\text{exp}}$  is only known relative to that of  $M_{GT}^{\text{exp}}$  as the ratio  $M_L^{\text{exp}}/M_{GT}^{\text{exp}}$  is extracted from Eq. (43) using the absolute value of  $M_{GT}$  since Eq. (62) gives access to  $c^2 = (g_A M_{GT})^2$  only. If theory agrees with experiment one thus expects for  $M_L^{\text{exp}}$  a positive (negative) sign when  $M_{GT}^{\text{theo}}$  and  $M_L^{\text{theo}}$  have the same (opposite) sign, respectively. This is the case for all transitions in the table except for the one of  $^6\text{He}$ . The reason for this is unclear but might be related to the fact that the values for  $M_L^{\text{theo}}$  are systematically too low for the transitions with mass  $A = 6$  to 12 (see also Sec. III C 2 c).

$\beta$ decay	$J_i \rightarrow J_f$	Shell model interaction	$ M_{GT} ^{\text{exp}}$	$M_{GT}^{\text{theo}}$	$M_L^{\text{exp}}$	$M_L^{\text{theo}}$	$ b ^{\text{exp}}$	$b^{\text{theo}}$	$ b/Ac ^{\text{exp}}$	$b/Ac^{\text{theo}}$
$^6\text{He} \xrightarrow{\beta^-} ^6\text{Li}$	$0^+ \rightarrow 1^+$	CK6162BME	2.7802(20)	<b>-2.348</b>	-1.72(12)	-0.17	68.2(7)	-67.3	4.088(42)	<b>4.78</b>
		PWBT		-1.819		-0.003		-51.4		4.71
$^{10}\text{C} \xrightarrow{\beta^+} ^{10}\text{B}^1$	$0^+ \rightarrow 1^+$	CK6162BME	2.3649(19)	2.210	-3.2(17)	-0.138	79(17)	102.6	3.34(72)	4.64
		CK8162BME		2.141		-0.288		97.9		4.57
		CK816POT		2.213		-0.241		101.7		4.60
		PWBT		2.208		0.238		106.3		4.81
$^{12}\text{B} \xrightarrow{\beta^-} ^{12}\text{C}$	$1^+ \rightarrow 0^+$	CK6162BME	0.73852(55)	-0.558	-0.650(33)	0.012	33.9(4)	-31.4	3.825(45)	4.89
		CK8162BME		0.573		-0.050		31.8		4.62
		CK816POT		-0.554		0.065		-30.5		4.59
		PWBT		<b>0.699</b>		-0.123		38.0		<b>4.53</b>
$^{12}\text{N} \xrightarrow{\beta^+} ^{12}\text{C}$	$1^+ \rightarrow 0^+$	CK6162BME	0.69613(64)	0.558	-0.451(33)	-0.012	33.9(4)	31.4	4.058(48)	4.68
		CK8162BME		-0.573		0.050		-31.8		4.62
		CK816POT		0.554		-0.065		30.5		4.59
		PWBT		<b>-0.699</b>		0.123		-38.0		<b>4.53</b>
$^{16}\text{N} \xrightarrow{\beta^-} ^{16}\text{O}^1$	$2^- \rightarrow 3^-$	MK	0.4503(22)	<b>-0.338</b>	-0.11(11)	0.155	32.1(18)	-23.0	4.46(25)	<b>4.25</b>
$^{16}\text{N} \xrightarrow{\beta^-} ^{16}\text{O}^2$	$2^- \rightarrow 1^-$	MK	0.2184(91)	<b>-0.079</b>	-0.165(89)	0.041	13.8(13)	-5.3	3.95(41)	<b>4.19</b>
$^{16}\text{N} \xrightarrow{\beta^-} ^{16}\text{O}^3$	$2^- \rightarrow 2^-$	MK	0.521(17)	<b>-0.595</b>	1.49(30)	-1.181	63.1(42)	-63.7	7.57(56)	<b>6.69</b>
$^{18}\text{Ne} \xrightarrow{\beta^+} ^{18}\text{F}$	$0^+ \rightarrow 1^+$	MK	2.2328(32)	<b>-2.252</b>	2.3(12)	-1.060	230(22)	-209.8	5.72(55)	<b>5.18</b>
		USD		-2.250		-1.128		-210.9		5.21
$^{18}\text{F} \xrightarrow{\beta^+} ^{18}\text{O}$	$1^+ \rightarrow 0^+$	MK	1.2778(22)	<b>-1.300</b>	1.36(71)	-0.612	133(13)	-121.2	5.77(55)	<b>5.18</b>
		USD		-1.299		-0.651		-121.8		5.21
$^{20}\text{F} \xrightarrow{\beta^-} ^{20}\text{Ne}^1$	$2^+ \rightarrow 2^+$	USD	0.25493(45)	0.246	0.91(11)	0.851	42.1(21)	40.2	8.26(41)	8.17
		USD-A		<b>-0.251</b>		-0.827		-40.2		<b>8.00</b>
		USD-B		-0.244		-0.868		-40.3		8.26
$^{20}\text{Na} \xrightarrow{\beta^+} ^{20}\text{Ne}^1$	$2^+ \rightarrow 2^+$	USD	0.2506(19)	-0.246	0.93(11)	-0.851	42.1(21)	-40.2	8.40(22)	8.17
		USD-A		<b>0.251</b>		0.827		40.2		<b>8.00</b>
		USD-B		0.244		0.868		40.3		8.26
$^{24m}\text{Al} \xrightarrow{\beta^+} ^{24}\text{Mg}$	$1^+ \rightarrow 0^+$	USD	0.101(15)	0.139	1.29(38)	1.020	42.3(44)	40.2	17.5(32)	12.04
		USD-A		<b>-0.100</b>		-0.873		-32.2		<b>13.44</b>
		USD-B		0.199		1.009		46.7		9.78
$^{30}\text{S} \xrightarrow{\beta^+} ^{30}\text{P}$	$0^+ \rightarrow 1^+$	USD	0.5429(98)	<b>0.532</b>	0.75(18)	0.593	99.1(52)	92.9	6.08(34)	<b>5.82</b>
		USD-A		-0.354		-0.637		-69.0		6.51
		USD-B		-0.473		-0.606		-84.9		5.99
$^{30}\text{P} \xrightarrow{\beta^+} ^{30}\text{Si}$	$1^+ \rightarrow 0^+$	USD	0.2998(41)	<b>0.307</b>	0.50(10)	0.342	57.2(30)	53.6	6.36(34)	<b>5.82</b>
		USD-A		-0.204		-0.368		-39.9		6.51
		USD-B		-0.273		-0.350		-49.0		5.99

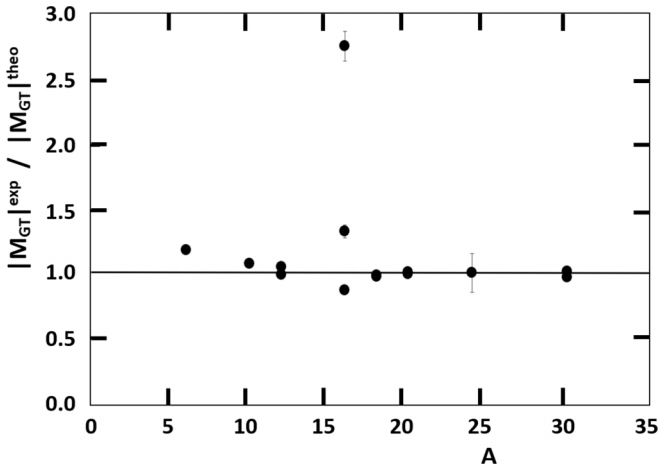


FIG. 13. Ratio of the absolute values of theoretically calculated and experimental Gamow-Teller matrix elements for the triplet  $\beta$  transitions in Table XXVIII. If not explicitly shown, error bars (based on the experimental  $M_{GT}$  values only) are smaller than the size of the symbols.

seems to reproduce the experimental Gamow-Teller matrix elements slightly better than the USD and USD-B interactions, whereas for  $A = 30$  the USD interaction gives the best agreement. Note that even the case of  $^{24m}\text{Al}$ —the large value of  $|b/Ac|^{\text{exp}} = 17.5(32)$  of which is due to the combination of a very small Gamow-Teller matrix element and a relatively large  $M1$   $\gamma$ -decay width,  $\Gamma_{M1}$ —is reproduced quite well.

Figure 13 shows the theoretical and calculated Gamow-Teller matrix elements to agree within about 20% (see also columns 4 and 5 in Table XXVIII). The unweighted average of their ratio yields  $|M_{GT}^{\text{exp}}/|M_{GT}^{\text{theo}} = 1.16(47)$  [and 1.04(11) when omitting the  $^{16}\text{N}(2^-) \rightarrow ^{16}\text{O}(1^-)$  transition for which the calculated Gamow-Teller matrix element is about a factor of 3 lower than the experimental one]. This average value being in agreement with unity indicates that also for these  $\beta$  decays from  $T = 1$  states, with in general a more complex nuclear structure than the  $T = 1/2$  mirror nuclei, the shell model reproduces the Gamow-Teller matrix elements rather well. However, as was mentioned already in this paragraph, the  $M_L$  matrix elements calculated for the transitions with  $A = 6$  to 12 turn out to be systematically too low, while for the higher masses they do agree with experiment within about one standard deviation (see columns 6 and 7 in Table XXVIII).

The unweighted average of the ratio of experimental and theoretical  $|b/Ac|$  values for all 14 transitions [obtained from the last two columns in Table XXVIII and using the  $(b/Ac)^{\text{theo}}$  values corresponding to the  $M_{GT}^{\text{theo}}$  values listed in boldface in column 5] is found to be  $|b/Ac|^{\text{exp}}/|b/Ac|^{\text{theo}} = 1.01(15)$ , again showing good overall agreement (within typically about 20%) between the shell model calculations and experiment (Fig. 14). Finally, the weak-magnetism form factor,  $b/Ac$ , which depends on both the spin matrix element,  $M_{GT}$ , and the orbital current matrix element,  $M_L$  [see Eq. (43)], is found to be dominated by the spin terms in these isovector transitions, except for the case of  $^{24m}\text{Al}$  which was discussed already in Sec. III C 1 c.

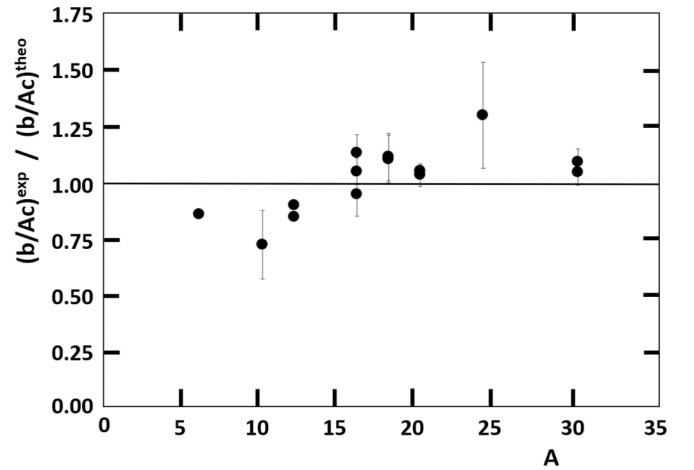


FIG. 14. Ratio of theoretically calculated and experimental  $b/Ac$  values for the triplet  $\beta$  transitions in Table XXVIII. If not explicitly shown, error bars (based on the experimental  $b/Ac$  values only) are smaller than the size of the symbols.

## D. General discussion of the weak magnetism results

### 1. Relation to nuclear structure

*a.  $\beta$  transitions from the  $T = 1/2$  mirror nuclei.* For the  $T = 1/2$  mirror  $\beta$  transitions for which CVC relates the weak magnetism form factor  $b$  to the difference between the mirror pair magnetic moments, a clear subshell behavior related to the single-particle Schmidt values of the magnetic moments is observed, despite significant variation in the absolute values of  $b$ . This behavior is further accentuated in the values of  $b/Ac$ , in part due to the slight decrease of the size of the Gamow-Teller form factor,  $c$ , with increasing mass (Fig. 6 and Sec. III B 2).

For the mirror nuclei up to mass  $A = 45$  the  $b$  and  $c$  form factors, which are related to the  $M_{GT}$  and  $M_L$  matrix elements, were also calculated in the nuclear shell model (Secs. III B 3 b and III B 4). For this, well-established interactions that give excellent fits to experimental spectra were used. Calculations were limited to mass  $A = 45$  as for higher masses the truncation of the shell model space required, due to calculation power limitations, was too important to yield reliable results. Good agreement between the experimental and theoretically calculated values for the form factor ratio  $b/Ac$  was obtained (Fig. 8). Further, the shell model calculated values for the  $M_{GT}$  and  $M_L$  matrix elements also show good correspondence with the experimental values extracted from the experimental  $b/Ac$  ratio when using the impulse approximation (Figs. 9 and 10). This is also the case for the special cases of  $^{35}\text{Cl}$  and  $^{35}\text{Ar}$  with large oblate deformation, although the shell model was not able to reproduce the sign of  $b/Ac$  for  $^{35}\text{Ar}$ . However, an extreme single-particle calculation in a deformed basis correctly reproduced the sign as well as the magnitude of  $b/Ac$  for both cases within a factor of about 2.

*b.  $\beta$  transitions from  $T = 1$  and  $T = 3/2$  states.* The  $b/Ac$  values for the  $\beta$  transitions from  $T = 1$  and  $T = 3/2$  states (Fig. 12) do not exhibit the clear single-particle related systematic that is obeyed by the  $T = 1/2$  mirror transitions. Of course, many of the  $T = 1$  and  $T = 3/2$  transitions involve excited states with often strongly mixed configurations,

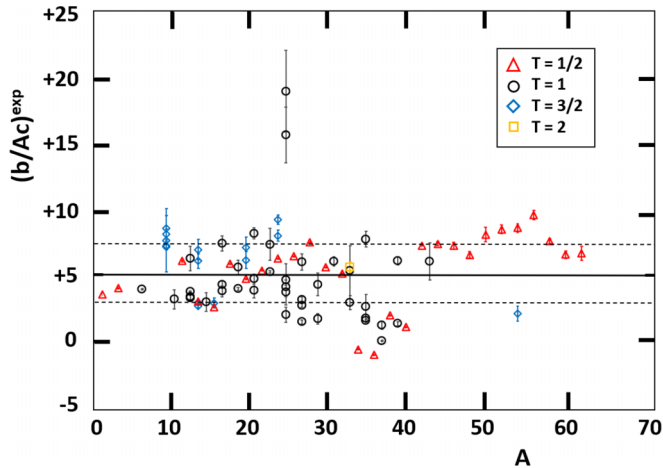


FIG. 15. Experimental  $b/Ac$  values for all 85  $\beta$  transitions from isotopes with  $A = 3$  to 61 considered here (Tables VI and XXIV to XXVII). The bold and dashed horizontal lines indicate the unweighted average value of  $5.1 \pm 2.4$ , not including the two strongly deviating values at  $A = 24$  (see also Table XXX).

implying the involvement of many shell model orbitals, each with a fractional occupation. One may nevertheless hope that the transitions to ground states and transitions to high-lying first-excited  $2^+$  states, which in general all exhibit a rather “simple” nuclear structure, do show some simple shell-structure related systematic as well. Table XXIX therefore lists all  $T = 1/2, 1,$  and  $3/2$  transitions to ground states or high-lying first-excited  $2^+$  states. As can be seen (although statistics is rather limited) the  $T = 1$  and  $T = 3/2$  transitions in this table indeed turn out to follow the trend of  $b/Ac$  being typically large for the subshells with  $j = l + 1/2$  and smaller for  $j = l - 1/2$ . The (unweighted) averages of  $(b/Ac)^{\text{exp}}$  for all transitions in a given subshell turn out not to differ significantly from the values calculated for only the mirror  $\beta$  transitions. Note, however, that many transitions from the higher isospin multiplets discussed here cannot be included in this comparison as they involve odd-odd nuclei with the odd proton in a  $j = l + 1/2$  orbital and the odd neutron in a  $j = l - 1/2$  orbital, or vice versa.

## 2. Averages and their role for $\beta$ decay experiments and the reactor neutrino anomaly

*a.  $\beta$  decay experiments.* In Fig. 15 the experimental values for  $b/Ac$  for all  $\beta$  transitions up to mass  $A = 61$  considered here are shown on a single plot. For the  $\beta$  transitions from  $T = 1, 3/2,$  and  $2$  states the sign of  $b/Ac$  is assumed positive (see Sec. III C). As can be seen, all values are in the same range, with a maximum of about  $+10.0$  and a minimum value of about  $-1.0$ . The transitions from  $^{14}\text{O}$  and  $^{14}\text{C}$  are again excluded, while, for the nine cases where both the  $\beta^-$  and  $\beta^+$  transition in a  $T = 1$  triplet yield a value for  $b/Ac$ , only the average of both values is used. The unweighted average of the 28  $T = 1/2$  transitions with mass  $A = 1$  to 61, showing a clear subshell dependence related to their single-particle structure (Table VI and Fig. 6), is  $(b/Ac)^{\text{exp}} = 5.6 \pm 2.7$ . This is in good agreement with the overall unweighted average of

the 57 transitions from  $T = 1, 3/2,$  and  $2$  states (Fig. 12), i.e.,  $(b/Ac)^{\text{exp}} = 4.8 \pm 2.3$ , or  $(b/Ac)^{\text{exp}} = 5.3 \pm 3.2$  when not omitting the very large values for  $^{24m}\text{Na}$  and  $^{24m}\text{Al}$  (see Table XXV and Fig. 15). The average for the entire set of 85  $\beta$  transitions discussed here is  $b/Ac = 5.1 \pm 2.4$  (and  $5.4 \pm 3.1$  when not omitting the very large values for  $^{24m}\text{Na}$  and  $^{24m}\text{Al}$ ). In all cases the one-standard-deviation error is rather large due to the spread in the individual values.

An overview of all averages and spreads of the weak magnetism term,  $b/Ac$ , and the matching matrix elements,  $M_{\text{GT}}$  and  $M_L$ , mentioned in this text is given in Table XXX.

The weak-magnetism form factor provides in most cases the major recoil correction to the  $\beta$ -spectrum shape and  $\beta$ -correlation coefficients for allowed transitions with “normal” strength (i.e., nonretarded transitions with  $\log ft$  values less than about 6.7). This is true for both analog transitions, such as the  $\beta$  transitions within the  $T = 1/2$  isospin doublets discussed here, and non-analog transitions (i.e., between states that are not members of a common isotopic multiplet), such as the ones from states with isospin  $T = 1, 3/2,$  and  $2$ . The above analysis of weak-magnetism form factors for the  $T = 1/2$  mirror  $\beta$  transitions allows taking this form factor explicitly into account in the analysis of experimental data, as was done in the determination of the  $\beta\nu$  correlation with  $^{21}\text{Na}$  [62] and of the  $\beta$ -asymmetry parameter for  $^{37}\text{K}$  [35]. In this way higher precision and sensitivity can be reached when searching for new physics or when determining the  $V_{\text{ud}}$  quark mixing matrix element in experiments in  $\beta$ -decay correlation measurements with the mirror nuclei.

The observation that for nonanalog allowed  $\beta$  transitions the  $b/Ac$  value is approximately nucleus independent, within certain limits, enables estimating its effect on  $\beta$  decay correlation results for allowed transitions for which no experimental nor theoretical data leading to  $b/Ac$  are readily available. This was done already in the analysis of, e.g., the  $\beta$ -asymmetry parameters in the decay of  $^{114}\text{In}$  [32] and the recoil-asymmetry parameter in the decay of  $^{80}\text{Rb}$  [31]. The present analysis now offers for transitions for which one cannot rely on CVC, the value of  $b/Ac = 5.1 \pm 2.4$  obtained as an average over a large number of  $\beta$  transitions for nuclei with masses ranging from  $A = 1$  to 61 (Table XXX).

*b. Reactor neutrino anomaly.* So far, an average value for the weak-magnetism contribution has been used in detailed calculations of the cumulative electron and antineutrino spectra emerging from a nuclear reactor. In one of the original works [49], it was noted that the variation in  $b/Ac$  values for all known transitions causes substantial uncertainty in these spectra. Instead, a subset of all known transitions was used with a fairly constrained average value of [49] ( $M_n$  is the nucleon mass),

$$b/Ac = \frac{3}{4}M_n(0.5 \pm 0.5)\% \text{ MeV}^{-1} = 3.5 \pm 3.5. \quad (63)$$

The downside to this approach is twofold: first, it is not clear whether the chosen subset is a reasonable representation of the behavior of nuclear transitions at fission-fragment masses, while, second, each of those transitions has an unequal weighting. Specifically, transitions with a large  $b/Ac$  value might have a large production rate whereas one with a low  $b/Ac$  value might only be barely populated, or vice

TABLE XXIX. Overview of the values for  $(b/Ac)^{\text{exp}}$  for all ground-state to ground-state and ground-state to first-excited  $2^+$ - or  $4^+$ -state transitions with  $A < 39$  discussed here (“mir” = mirror  $\beta$  transition). Values of  $(b/Ac)^{\text{exp}}$  for  $\beta$  transitions from  $T = 1$  and  $3/2$  states are in italics. The last column lists the average values for all transitions in a subshell. Because of widely differing error bars unweighted averages were calculated. When for a given mass value the  $(b/Ac)^{\text{exp}}$  value is available for both the  $\beta^-$  and  $\beta^+$  transitions in a  $T = 1$  multiplet, sharing the same analog  $\gamma$  transition (i.e., for  $A = 18, 20, 24, 24,$  and  $30$ ), the average of both  $(b/Ac)^{\text{exp}}$  values is used to calculate the unweighted average for the respective subshell. Averages in square brackets indicate averages for the mirror transitions separately (from Table XVI). Note that the  $f_{7/2}$  subshell is not shown here, but that the value  $(b/Ac)^{\text{exp}} = 6.2(14)$  for the  $^{42}\text{Ti} \rightarrow ^{42}\text{Sc}^1$  transition from a  $T = 1$  state (see Table XXVI) agrees with the  $f_{7/2}$  subshell average of  $8.05(97)$  for the mirror transitions (Table XVI).

$\beta$ transition	$A$	$J_i^\pi \rightarrow J_f^\pi$	Subshell	$j$	Type	$\log ft$	$(b/Ac)^{\text{exp}}$	$(b/Ac)^{\text{exp}}$ subshell avg.
$n \xrightarrow{\beta^-} p$	1	$1/2^+ \rightarrow 1/2^+$	$s_{1/2}$	$l + 1/2$	mir	3.01853(28)	3.6867(20)	3.99(27)
$\text{H} \xrightarrow{\beta^-} \text{He}$	3	$1/2^+ \rightarrow 1/2^+$			mir	3.0532(38)	4.2012(28)	[3.94(36)]
$\text{He} \xrightarrow{\beta^-} \text{Li}$	6	$0^+ \rightarrow 1^+$			$T = 1$	2.905753(61)	4.088(42)	
$\text{Li} \xrightarrow{\beta^-} \text{Be}^a$	8	$2^+ \rightarrow 2^+$	$p_{3/2}$	$l + 1/2$	$T = 1$	5.72	7.5(2) <sup>a</sup>	7.04(23)
$\text{B} \xrightarrow{\beta^+} \text{Be}^a$	8	$2^+ \rightarrow 2^+$			$T = 1$	5.77	7.5(2) <sup>a</sup>	[6.2506(67)]
$\text{Li} \xrightarrow{\beta^-} \text{Be}$	9	$3/2^- \rightarrow 3/2^-$			$T = 3/2$	5.3246(80)	7.31(23)	
$\text{C} \xrightarrow{\beta^+} \text{B}$	9	$3/2^- \rightarrow 3/2^-$			$T = 3/2$	5.320(12)	7.42(25)	
$\text{C} \xrightarrow{\beta^+} \text{B}$	11	$3/2^+ \rightarrow 3/2^+$			mir	3.59294(21)	6.2506(68)	
$\text{N} \xrightarrow{\beta^+} \text{C}$	13	$1/2^+ \rightarrow 1/2^+$	$p_{1/2}$	$l - 1/2$	mir	3.67037(45)	3.1712(80)	[2.94(21)]
$\text{O} \xrightarrow{\beta^+} \text{N}$	15	$1/2^+ \rightarrow 1/2^+$			mir	3.64368(58)	2.7557(70)	
$\text{F} \xrightarrow{\beta^+} \text{O}$	17	$5/2^+ \rightarrow 5/2^+$	$d_{5/2}$	$l + 1/2$	mir	3.36006(36)	6.0416(51)	6.5(15) <sup>b</sup>
$\text{Ne} \xrightarrow{\beta^+} \text{F}$	18	$0^+ \rightarrow 1^+$			$T = 1$	3.0955(11)	5.72(55)	[5.39(34)]
$\text{F} \xrightarrow{\beta^+} \text{O}$	18	$1^+ \rightarrow 0^+$			$T = 1$	3.5783(23)	5.77(55)	
$\text{Ne} \xrightarrow{\beta^+} \text{F}$	19	$1/2^+ \rightarrow 1/2^+$			mir	3.23591(25)	4.8807(27)	
$\text{F} \xrightarrow{\beta^-} \text{Ne}^1$	20	$2^+ \rightarrow 2^+$			$T = 1$	4.98364(31)	8.28(41)	
$\text{Na} \xrightarrow{\beta^+} \text{Ne}^1$	20	$2^+ \rightarrow 2^+$			$T = 1$	4.9972(64)	8.40(42)	
$\text{Na} \xrightarrow{\beta^+} \text{Ne}$	21	$3/2^+ \rightarrow 3/2^+$			mir	3.60991(40)	5.5233(93)	
$\text{Mg} \xrightarrow{\beta^+} \text{Na}$	23	$3/2^+ \rightarrow 3/2^+$			mir	3.67225(70)	6.416(23)	
$\text{Ne} \xrightarrow{\beta^-} \text{Na}$	23	$5/2^+ \rightarrow 3/2^+$			$T = 3/2$	5.2810(86)	9.38(37)	
$\text{Na} \xrightarrow{\beta^-} \text{Mg}^2$	24	$4^+ \rightarrow 4^+$			$T = 1$	6.12609(46)	4.8(12)	
$\text{Al} \xrightarrow{\beta^+} \text{Mg}^2$	24	$4^+ \rightarrow 4^+$			$T = 1$	6.129(57)	4.8(13)	
$\text{Na(m)} \xrightarrow{\beta^-} \text{Mg}$	24	$1^+ \rightarrow 0^+$			$T = 1$	5.936(88)	20.7(30)	
$\text{Al(m)} \xrightarrow{\beta^+} \text{Mg}$	24	$1^+ \rightarrow 0^+$			$T = 1$	5.79(13)	17.5(32)	
$\text{Al(m)} \xrightarrow{\beta^+} \text{Mg}^1$	24	$1^+ \rightarrow 2^+$			$T = 1$	5.921(50)	15.8(21)	
$\text{Al} \xrightarrow{\beta^+} \text{Mg}$	25	$5/2^+ \rightarrow 5/2^+$			mir	3.56972(37)	6.5875(91)	
$\text{Si} \xrightarrow{\beta^+} \text{Al}$	27	$5/2^+ \rightarrow 5/2^+$			mir	3.61665(28)	7.651(10)	
$\text{P} \xrightarrow{\beta^+} \text{Si}$	29	$1/2^+ \rightarrow 1/2^+$	$s_{1/2}$	$l + 1/2$	mir	3.67802(72)	5.763(23)	5.76(46)
$\text{S} \xrightarrow{\beta^+} \text{P}$	30	$0^+ \rightarrow 1^+$			$T = 1$	4.324(16)	6.08(34)	[5.44(21)]
$\text{P} \xrightarrow{\beta^+} \text{Si}$	30	$1^+ \rightarrow 0^+$			$T = 1$	4.839(12)	6.36(34)	
$\text{S} \xrightarrow{\beta^+} \text{P}$	31	$1/2^+ \rightarrow 1/2^+$			mir	3.68127(48)	5.299(15)	
$\text{Cl} \xrightarrow{\beta^+} \text{S}$	33	$3/2^+ \rightarrow 3/2^+$	$d_{3/2}$	$l - 1/2$	mir	3.74802(74)	-0.4561(51)	0.6(12)
$\text{Ar} \xrightarrow{\beta^+} \text{Cl}$	35	$3/2^+ \rightarrow 3/2^+$			mir	3.75548(46)	-0.8684(71)	[0.64(53)]
$\text{K} \xrightarrow{\beta^+} \text{Ar}^1$	36	$1^+ \rightarrow 2^+$			$T = 1$	4.778(40)	0.189(42)	
$\text{K} \xrightarrow{\beta^+} \text{Ar}^2$	36	$1^+ \rightarrow 0^+$			$T = 1$	4.902(52)	1.37(31)	
$\text{K} \xrightarrow{\beta^+} \text{Ar}$	37	$3/2^+ \rightarrow 3/2^+$			mir	3.66383(52)	2.104(13)	
$\text{Ca} \xrightarrow{\beta^+} \text{K}$	39	$3/2^+ \rightarrow 3/2^+$			mir	3.63180(61)	1.2316(32)	

<sup>a</sup>The  $A = 8$  multiplet was not included in the analysis performed in Sec. III C since error bars on the  $\log ft$  values are difficult to estimate because broad levels of  $^8\text{Be}$  participate in the  $\beta$  decay [116,515]. The value for  $(b/Ac)^{\text{exp}}$  listed here was therefore taken from recent  $\beta$ -ray angular distribution measurements [13]. Earlier experiments yielded  $b/Ac = 6.61(113)$  [516],  $7.0(5)$  [17], and  $6.5(2)$  [517].

<sup>b</sup>The values for the transitions from the  $^{24m}\text{Na}$  and  $^{24m}\text{Al}$  isomeric states were not included in this average.

TABLE XXX. Overview of unweighted averages of  $(b/Ac)^{\text{exp}}$  and of ratios of experimental and shell model calculated values for  $M_{\text{GT}}$ ,  $M_L$  and  $b/Ac$  mentioned in the text (the relevant sections and figures are mentioned in the last column). A few strongly deviating values, which were discussed in the text (i.e.  $^{31}\text{S}$ , the  $^{16}\text{N} \xrightarrow{\beta^-} ^{16}\text{O}^2$  transition, and the cases of  $^{24m}\text{Na}$  and  $^{24m}\text{Al}$ ), were omitted when calculating these averages. Values obtained when not omitting these few cases are given in footnotes. Note, however, that the value for  $^{24m}\text{Al}$  was addressed by the shell model calculations, which were found to agree well with the experimental result (see Table XXVIII).

	Quantity	Mass region or isospin value	Average	Section / Figure
$T = 1/2$	$(b/Ac)^{\text{exp}}$	$A = 1-3, 11-61$ ; 28 transitions	$5.6 \pm 2.7$	Sec. III D / Fig. 6
mirror	$(b/Ac)^{\text{exp}} / (b/Ac)^{\text{theo}}$	$A = 1-3, 11-31, 37-45$ ; 18 transitions	$0.96(11)^{\text{a}}$	Sec. III B 3 b / Fig. 8
transitions	$M_{\text{GT}}^{\text{exp}} / M_{\text{GT}}^{\text{theo}}$	$A = 1-3, 11-45$ ; 20 transitions	$0.97(8)$	Sec. III B 4 / Fig. 9
	$M_L^{\text{exp}} / M_L^{\text{theo}}$	$A = 11-45$ ; 18 transitions	$0.99(35)^{\text{b}}$	Sec. III B 4 / Fig. 10
$T = 1, 3/2, 2$	$(b/Ac)^{\text{exp}}, T = 1$	$T = 1$ ; $A = 6-42$ ; 39 transitions	$4.2 \pm 2.0^{\text{c}}$	Sec. III C 1 / Fig. 12
	$(b/Ac)^{\text{exp}}, T = 3/2$	$T = 3/2$ ; $A = 9-53$ ; 15 transitions	$6.3 \pm 2.4$	Sec. III C 1 / Fig. 12
	$(b/Ac)^{\text{exp}}, T = 1, 3/2, 2$	$T = 1, 3/2, 2$ ; $A = 6-53$ ; 55 transitions	$4.8 \pm 2.3^{\text{d}}$	Sec. III D / Fig. 12
	$(b/Ac)^{\text{exp}} / (b/Ac)^{\text{theo}}$	$T = 1$ ; $A = 6-30$ ; 14 transitions	$1.01(15)$	Sec. III C 2 / Fig. 14
	$M_{\text{GT}}^{\text{exp}} / M_{\text{GT}}^{\text{theo}}$	$T = 1$ ; $A = 6-30$ ; 13 transitions	$1.04(11)^{\text{e}}$	Sec. III C 2 / Fig. 13
all	$(b/Ac)^{\text{exp}}$	$T = 1/2, 1, 3/2, \text{ and } 2$ ; $A = 1-61$ ; 83 transitions	$5.1 \pm 2.4^{\text{f}}$	Sec. III D / Fig. 15

<sup>a</sup>The values for  $^{33}\text{Cl}$  and  $^{35}\text{Ar}$  (i.e., resp. 2.22 and  $-5.63$ ), which deviate significantly from all other values (see Table XVIII and Sec. III B 4), were not included.

<sup>b</sup>When not omitting the strongly deviating value for  $^{31}\text{S}$  (see Table XIX) the average changes to  $1.04(34)$ .

<sup>c</sup>When not omitting the large values for  $^{24m}\text{Na}$  and  $^{24m}\text{Al}$  (see Table XXV and Fig. 15) the average becomes  $4.9 \pm 3.5$ .

<sup>d</sup>When not omitting the large values for  $^{24m}\text{Na}$  and  $^{24m}\text{Al}$  (see Table XXV and Fig. 15) the average becomes  $5.3 \pm 3.2$ .

<sup>e</sup>When not omitting the large value of 2.76 for the  $2^- \rightarrow 1^-$  transition  $^{16}\text{N} \xrightarrow{\beta^-} ^{16}\text{O}^2$  (see Table XXVIII), the average is  $1.16(47)$ .

<sup>f</sup>When not omitting the very large values for  $^{24m}\text{Na}$  and  $^{24m}\text{Al}$  (see Table XXV and Fig. 15) the average becomes  $5.4 \pm 3.1$ .

versa, thereby invalidating a straight average. Finally, it has been noted that the inclusion of recoil-order corrections to the allowed  $\beta$  spectrum shape has been oversimplified [53,54] (see also [104]), with the traditional calculations lacking additional energy-dependent terms related to weak magnetism and an absence of induced tensor currents. As these transitions are nonanalog, the latter is nonzero also in the standard model without second-class currents. Our results presented here serve both as a demonstration of the spread in  $b/Ac$  values for nuclei much higher in mass than previously available and as a motivation for experimental measurement of its value in the fission-fragment mass region.

### 3. Higher-order form factors $d, f, g, \text{ etc.}$

In contrast to the transitions between analog states discussed in the previous two paragraphs, for hindered Gamow-Teller transitions (i.e., with  $\log ft$  values of about 6.7 and larger) between nonanalog states, matrix elements of rank-1 spherical tensor operators with an  $M1$  character [1,3], i.e., the  $b, c$ , and  $d$  form factors, are usually suppressed, whereas matrix elements of rank-2 spherical tensor operators with  $E2$  character [3] [as in, e.g., the  $f$  and  $g$  form factors (see Tables X and XI)] are not. As a consequence, the  $f/Ac$  and  $g/A^2c$  recoil term contributions [1] to  $\beta$ -decay observables can become typically of size similar to or even larger than the  $b/Ac$  contribution from the weak-magnetism term (see, e.g., the cases of  $^{60}\text{Co}$  [33] and  $^{67}\text{Cu}$  [34]). It was shown in Ref. [33] that whereas for such hindered  $\beta$  transitions theoretical calculations often have difficulties to reproduce the experimental value for the Gamow-Teller matrix element, satisfactory results can nevertheless be obtained by combining the value for this matrix element (and so the  $c$  form factor) deduced

from the experimental  $ft$  value [Eq. (62)] with theoretically calculated matrix elements for the other form factors, and then using the thus obtained ratios for, e.g.,  $f/Ac$  and  $g/A^2c$ .

Given the reasonably good performance of the shell model calculations for the  $b$  form factor (i.e., the  $M_{\text{GT}}$  and  $M_L$  matrix elements) for the 14  $\beta$  transitions from  $T = 1$  states discussed here in some detail, it may be of interest for experiments involving these ground-state to ground-state transitions to also know the values calculated for the other form factors. These are therefore listed in Table XXXI.

*a. Induced tensor form factor.* Of special interest is the tensor form factor ratio  $d/Ac = d_I/Ac$  [assuming no second-class currents, i.e.,  $d_{II} = 0$  (see Table X)], as this is nonzero for Gamow-Teller transitions and is second in line, after the weak magnetism form factor, regarding its effect in  $\beta$  spectrum shape measurements and angular correlation measurements. Our calculated values for  $d/Ac$  (listed in column 7 of Table XXXI) turn out to be a factor of about 2 or more smaller than the corresponding values of  $b/Ac$ , except for the already mentioned transition  $^{16}\text{N} (2^-) \rightarrow ^{16}\text{O} (1^-)$  for which the calculated Gamow-Teller matrix element is about a factor of 3 lower than experiment (see Sec. III C 2 c and Table XXVIII).

Figure 16 shows the shell model values for the  $d/Ac$  form factor for the  $T = 1$  transitions listed in Table XXXI as obtained with the respective interaction (indicated in boldface in the table) that performed best in reproducing the Gamow-Teller matrix element. Of course the value for  $d/Ac$  should ideally be calculated on a case-by-case basis as it depends on nuclear structure (see, e.g., Ref. [516]). Nevertheless, the unweighted average of these ten values, i.e.,  $d/Ac = 0.8 \pm 3.7$ , could be used as an estimate in the analysis of experimental data when no other information is available.

TABLE XXXI. Form factors calculated in the shell model for the 14  $T = 1$   $\beta$  transitions in Table XXVIII. The shell model interactions that performed best in reproducing the experimentally obtained Gamow-Teller matrix elements (see Table XXVIII) are indicated in boldface. Note that the shell model sign for the individual form factors is arbitrary but that this arbitrariness disappears in the form factor ratios.

$\beta$ decay	$J_i(T_i) \rightarrow J_f(T_f)$	Shell model										
		interaction	$c = c_1$	$c_2$ (fm <sup>2</sup> )	$b/Ac$	$d/Ac$	$f/Ac$	$g/A^2c$	$j_1/A^2c$	$j_2/A^2c$	$j_3/A^2c$	$h/A^2c$
${}^6\text{He} \xrightarrow{\beta^-} {}^6\text{Li}$	$0^+(1) \rightarrow 1^+(0)$	<b>CK6162BME</b>	-2.348	-2.241	4.777	-0.028 <sup>a</sup>	0.0	0.0	14.43	0.0	0.0	195.2
		PWBT	-1.819	-1.482	4.710	0.330	0.0	0.0	54.52	0.0	0.0	232.1
${}^{10}\text{C} \xrightarrow{\beta^+} {}^{10}\text{B}^1$	$0^+(1) \rightarrow 1^+(0)$	CK6162BME	+2.210	+2.346	4.643	-0.498	0.0	0.0	15.29	0.0	0.0	195.5
		CK8162BME	+2.141	+2.191	4.573	-0.444	0.0	0.0	26.30	0.0	0.0	206.0
		CK816POT	+2.213	+2.306	4.596	-0.443	0.0	0.0	20.74	0.0	0.0	200.6
		PWBT	+2.208	+2.322	4.814	-0.385	0.0	0.0	18.16	0.0	0.0	198.4
${}^{12}\text{B} \xrightarrow{\beta^-} {}^{12}\text{C}$	$1^+(1) \rightarrow 0^+(0)$	CK6162BME	-0.558	-0.569	4.689	3.554	0.0	0.0	40.07	0.0	0.0	219.0
		CK8162BME	+0.573	+0.589	4.625	3.549	0.0	0.0	38.42	0.0	0.0	218.1
		CK816POT	-0.554	-0.574	4.588	3.715	0.0	0.0	35.73	0.0	0.0	215.6
		<b>PWBT</b>	+0.699	+0.704	4.530	2.861	0.0	0.0	43.81	0.0	0.0	222.5
${}^{12}\text{N} \xrightarrow{\beta^+} {}^{12}\text{C}$	$1^+(1) \rightarrow 0^+(0)$	CK6162BME	+0.558	+0.569	4.689	3.554	0.0	0.0	40.07	0.0	0.0	219.0
		CK8162BME	-0.573	-0.589	4.625	3.549	0.0	0.0	38.42	0.0	0.0	218.2
		CK816POT	+0.554	+0.574	4.588	3.715	0.0	0.0	35.73	0.0	0.0	215.6
		<b>PWBT</b>	-0.699	-0.704	4.530	2.861	0.0	0.0	43.81	0.0	0.0	222.5
${}^{16}\text{N} \xrightarrow{\beta^-} {}^{16}\text{O}^1$	$2^-(1) \rightarrow 3^-(0)$	<b>MK</b>	-0.338	-0.904	4.253	1.313	-0.617	196.5	-317.8	47.62	257.7	-120.2
${}^{16}\text{N} \xrightarrow{\beta^-} {}^{16}\text{O}^2$	$2^-(1) \rightarrow 1^-(0)$	<b>MK</b>	-0.079	-0.251	4.193	-6.013	-0.142	57.36	100.9	-204.2	786.2	275.9
${}^{16}\text{N} \xrightarrow{\beta^-} {}^{16}\text{O}^3$	$2^-(1) \rightarrow 2^-(0)$	<b>MK</b>	-0.595	-1.464	6.691	0.063	-0.193	143.8	-160.2	-14.18	188.4	29.08
${}^{18}\text{Ne} \xrightarrow{\beta^+} {}^{18}\text{F}$	$0^+(1) \rightarrow 1^+(0)$	<b>MK</b>	-2.252	-3.941	5.176	-0.521	0.0	0.0	11.44	0.0	0.0	191.9
		USD	-2.250	-3.952	5.207	-0.509	0.0	0.0	9.026	0.0	0.0	189.3
${}^{18}\text{F} \xrightarrow{\beta^+} {}^{18}\text{O}$	$1^+(0) \rightarrow 0^+(1)$	<b>MK</b>	-1.300	-2.276	5.179	0.521	0.0	0.0	11.44	0.0	0.0	191.8
		USD	-1.299	-2.282	5.209	0.509	0.0	0.0	9.029	0.0	0.0	189.6
${}^{20}\text{F} \xrightarrow{\beta^-} {}^{20}\text{Ne}^1$	$2^+(1) \rightarrow 2^+(0)$	USD	+0.246	+0.602	8.171	3.211	0.035	-9.187	-174.8	310.0	-605.7	15.35
		<b>USD-A</b>	-0.251	-0.607	8.008	3.068	0.124	-32.07	-166.3	296.8	-603.6	23.51
		USD-B	-0.244	-0.595	8.258	3.238	0.091	-23.67	-174.2	302.3	-616.8	15.98
${}^{20}\text{Na} \xrightarrow{\beta^+} {}^{20}\text{Ne}^1$	$2^+(1) \rightarrow 2^+(0)$	USD	-0.246	-0.602	8.171	3.211	0.070	-9.187	-174.8	310.0	-605.7	15.34
		<b>USD-A</b>	+0.251	+0.607	8.008	3.068	0.246	-32.07	-166.3	296.8	-603.6	23.51
		USD-B	+0.244	+0.595	8.258	3.238	0.181	-23.67	-174.2	302.3	-616.8	15.98
${}^{24m}\text{Al} \xrightarrow{\beta^+} {}^{24}\text{Mg}$	$1^+(1) \rightarrow 0^+(0)$	USD	+0.139	+0.401	12.05	6.385	0.0	0.0	-276.0	0.0	0.0	-81.31
		<b>USD-A</b>	-0.100	-0.332	13.42	8.500	0.0	0.0	-401.0	0.0	0.0	-199.7
		USD-B	+0.199	+0.504	9.778	5.465	0.0	0.0	-175.4	0.0	0.0	14.57
${}^{30}\text{S} \xrightarrow{\beta^+} {}^{30}\text{P}$	$0^+(1) \rightarrow 1^+(0)$	<b>USD</b>	+0.532	+0.919	5.821	-1.065	0.0	0.0	87.72	0.0	0.0	263.2
		USD-A	-0.354	-0.580	6.497	-1.243	0.0	0.0	113.0	0.0	0.0	287.8
		USD-B	-0.473	-0.768	5.983	-1.029	0.0	0.0	117.7	0.0	0.0	293.6
${}^{30}\text{P} \xrightarrow{\beta^+} {}^{30}\text{Si}$	$1^+(0) \rightarrow 0^+(1)$	<b>USD</b>	+0.307	+0.530	5.820	1.064	0.0	0.0	87.59	0.0	0.0	264.2
		USD-A	-0.204	-0.335	6.520	1.242	0.0	0.0	113.3	0.0	0.0	288.7
		USD-B	-0.273	-0.443	5.983	1.038	0.0	0.0	117.6	0.0	0.0	292.6

<sup>a</sup>Note that experimentally the value  $d/Ac = 0.2(11)$  was obtained in Ref. [367].

It is of interest to note here the renewed interest in precision  $\beta$ -spectrum shape measurements for nuclear decays, using a variety of techniques [107–109,111–114,518–523], including two of the cases considered here, i.e.,  ${}^6\text{He} \rightarrow {}^6\text{Li}$  [108,109] and  ${}^{20}\text{F} \rightarrow {}^{20}\text{Ne}^1$  (see Fig. 18 in Appendix B) [111]. Such measurements could possibly contribute to extending the experimental knowledge on the  $d$  form factor as well.

*b. Overview and comparison with theoretical calculations.* Table XXXII gives an overview of  $T = 1$   $\beta$  transitions (with

$A = 6, 8, 12,$  and  $20$ ) for which, apart from  $b/Ac$ , also experimental values for higher-order form factors are available, and compares these with the shell model calculations presented here (Table XXXI) and from the literature. While the shell model calculations presented here were already found to reproduce very well the experimental values for the  $b$  and  $b/Ac$  form factors (see Table XXXI and Sec. III C 2 c), it is seen in Table XXXII that they also reproduce within a factor of 2 to 3 the available experimental values for the higher-order form factors  $d/Ac, f/Ac, g/A^2c, j_2/A^2c,$  and  $j_3/A^2c$ . The same

TABLE XXXII. Overview of experimental values and theoretical calculations for the higher-order form factors (for definitions see Tables X and XI) for  $T = 1$   $\beta$  transitions (with  $A = 6, 8, 12$ , and  $20$ ). Experimental values were obtained from  $\beta$ -ray angular distribution measurements,  $\beta$ -spectrum shape measurements, and measurements of the width of the analog  $\gamma$  transition. Experimental values for  $b/Ac$  are only listed when they were obtained in the experiment described in the given reference, and so were not deduced from the width of the analog  $\gamma$  transition available in the literature. Theoretical values listed are both from this work (Table XXXI) and from the literature. Note that notwithstanding several attempts (e.g., [143,511,524,525]) it appears notoriously difficult to experimentally address the recoil form factors for the transition from  $^{22}\text{Na}(3^+, T = 0)$  to  $^{22}\text{Ne}^1(2^+, T = 1)$ , which is therefore not included here.

$\beta$ decay	Expt. value or shell model calculation	Ref.	$b/Ac$	$d/Ac$	$f/Ac$	$g/A^2c$	$j_2/A^2c$	$j_3/A^2c$
$^6\text{He}(0^+) \rightarrow ^6\text{Li}(1^+)$	expt.	[18] <sup>a</sup>		+2.0(15)				
	expt.	[527] <sup>a</sup>		-1.2 to +2.0				
	expt.	[367] <sup>a</sup>		+0.2(11)				
	theor.	[18]		+0.12				
	CK6162BME	This work		-0.028				
$^8\text{Li}/\text{B}(2^+) \rightarrow ^8\text{Be}(2^+)$	PWBT	This work		+0.33				
	expt.	[13]	7.5(2)	5.5(17)	1.0(3)		-490(70)	-980(280)
$^{12}\text{B}/\text{N}(1^+) \rightarrow ^{12}\text{C}(0^+)$	expt.	[25,26]		+4.96(10)				
	CK816POT	This work		3.72				
	PWBT	This work		2.86				
$^{20}\text{F}/\text{Na}(2^+) \rightarrow ^{20}\text{Ne}^1(2^+)$	expt.	[29] <sup>b</sup>	8.41(39)	8.00(73)			-21(130)	-1273(211)
	expt.	[528] in [9]			+0.31(14)	-54(25)		
	expt.	[19]	8.3(4)			$-53_{-24}^{+46}$ <sup>c</sup>		
	USD-A	This work	8.01	3.07	+0.124 ( $^{20}\text{F}$ ) +0.246 ( $^{20}\text{Na}$ )	-32.1	296.8	-603.6
	USD-B	This work	8.26	3.24	+0.091 ( $^{20}\text{F}$ ) +0.181 ( $^{20}\text{Na}$ )	-23.7	302.3	-616.8
	CCW	[3]	6.70	3.51	-0.080 ( $^{20}\text{F}$ ) +0.160 ( $^{20}\text{Na}$ )	-20.6	333.0	-663.5
	PW	[529] in [9]	6.78	3.93	0.183	-32		
Kuo	[530] in [9]	7.28	5.33	0.245	-43			

<sup>a</sup>Analysis of the data from [526].

<sup>b</sup>Including also the results from [20–23].

<sup>c</sup>Value mentioned in [29].

is found to be true for other theoretical calculations, where available.

#### IV. CONCLUSION

In the first section of this paper the input data for the corrected  $\mathcal{F}t$  values of the isospin  $T = 1/2$  mirror  $\beta$  transitions from the neutron up to  $A = 75$  were analyzed and combined with new and/or extended calculations of the transition-dependent radiative and nuclear structure correction factors, finally leading to new and, in all but a few cases, also more precise  $\mathcal{F}t^{\text{mirror}}$  values. These will lead to improved sensitivity in searches for new physics (e.g. scalar, tensor, or right-handed weak currents) in correlation measurements with mirror nuclei.

For six mirror  $\beta$  transitions, including the neutron, the new  $\mathcal{F}t$  values could be combined with existing results from  $\beta$ -correlation measurements to obtain nine  $\mathcal{F}t_0$  values [Eq. (14) and Table VIII] leading to a 0.11% test of CVC. From the weighted average of these  $\mathcal{F}t_0$  values and Eq. (14) a value for  $|V_{\text{ud}}|^2$  was obtained with an uncertainty that is within a factor of 2 from the value deduced for the pure Fermi transitions [55]

(see also [88]). It was shown that the neutron and the mirror nuclei  $\beta$  transitions now, for the first time, clearly contribute to the value of  $V_{\text{ud}}$ , but also that the current efforts to further advance towards a more precise and reliable value for the  $\Delta_R^V$  radiative correction are more than ever of crucial importance for addressing  $V_{\text{ud}}$  and testing the unitarity of the CKM quark-mixing matrix.

The  $\mathcal{F}t^{\text{mirror}}$  values also provide the Gamow-Teller weak form factor,  $c$ , via the GT/F mixing ratio,  $\rho$ , that is obtained from it, with the sign of  $c$  being determined by shell model calculations. Combining these  $c$  form factors with an analysis of the nuclear magnetic moments of the  $T = 1/2$  mirror nuclei, thus providing the weak-magnetism form factors,  $b$ , allowed determination of the “normalized” weak-magnetism form factor ratio,  $b/Ac$ , for mirror  $\beta$  transitions up to  $A = 75$ . A clear shell model dependence could be observed with large (small) values being observed in subshells with spin  $j = l + 1/2$  ( $j = l - 1/2$ ) due to the rather strong single-particle configuration of the mirror nuclei.

Shell model calculations of the matrix elements were performed for the mirror  $\beta$  decays up to  $A = 45$ . The calculated Gamow-Teller and orbital current matrix elements,  $M_{\text{GT}}$  and

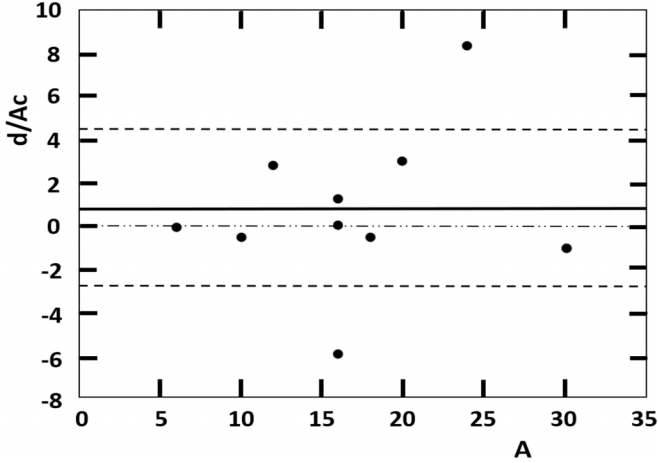


FIG. 16. Values for  $d/Ac$  for 10  $T = 1$  to  $T = 0$  transitions obtained from the shell model using the interaction that is in each case performing best in reproducing the experimental Gamow-Teller matrix element (see Table XXXI). When two transitions within the same multiplet were evaluated, i.e., for  $A = 12$  and  $A = 20$  (yielding the same values for  $d/Ac$ ), only one is included in the figure. Note also that for the “special” multiplets with  $A = 18$  and  $A = 30$  (Figs. 18 and 20 in Appendix B, respectively), i.e., with only  $\beta^+$  transitions, the value for the  $T = 1$  to  $T = 0$  transition is plotted here, with the value for the  $T = 0$  to  $T = 1$  transition having the opposite sign (see Table XXXI). Finally, as no error bars are available and the individual values vary a lot, an unweighted average was calculated, leading to  $0.8 \pm 3.7$ . This is indicated by the bold and dashed horizontal lines.

$M_L$  respectively, were compared with the ones deduced from the experimental Gamow-Teller and weak magnetism form factors,  $c$  and  $b$  respectively, using the impulse approximation. Good agreement between theory and experiment was found for  $M_{GT}$  and reasonably good agreement for  $M_L$ . Also for the ratio  $b/Ac$  good overall correspondence between theory and experiment was found. For the more difficult cases of  $^{33}\text{Cl}$  and  $^{35}\text{Ar}$ , with a strong oblate deformation, good correspondence between experiment and theory was obtained with single-particle calculations using a deformed Woods-Saxon potential.

In order to get a broader picture on the size of the weak magnetism form factor, e.g., in view of correlation measurements with  $\beta$  transitions between nonanalog states or calculations related to the reactor neutrino anomaly, a much broader survey was performed as well. This considered existing experimental data for analog  $\beta$  and  $\gamma$  transitions from common isobaric multiplets and resulted in values for the Gamow-Teller and weak magnetism form factors for 57  $\beta$  transitions from states with isospin  $T = 1, 3/2, \text{ and } 2$ , and for masses up to  $A = 53$ . Whereas the  $b/Ac$  values for these  $\beta$  transitions do not exhibit the clear subshell-related systematic that is obeyed by the  $T = 1/2$  mirror transitions because many of them involve excited states with strongly mixed configurations, transitions to ground states or first-excited  $2^+$  or  $4^+$  states (with usually a rather clean configuration) are found to exhibit the same subshell dependence as the mirror  $\beta$  transitions. Shell model calculations performed for 14  $\beta$  decays from  $T = 1$  states with  $A = 6$  to 30 again showed

good agreement between theoretical and experimental values for  $M_{GT}$  and  $M_L$  as well as for the  $b$  and  $b/Ac$  values deduced from these.

Taking into account the effect of weak magnetism in correlation measurements with mirror nuclei will definitely enhance the sensitivity of such measurements for determining  $V_{ud}$  or probing possible new physics phenomena, such as scalar or tensor type weak currents or tests of parity or time-reversal violation. The overall good agreement that was found between theory and experiment gives some confidence in the theoretical calculations so that the weak magnetism recoil correction can also reliably be addressed theoretically for other allowed  $\beta$  transitions in light nuclei. Note, however, that for nuclei heavier than the ones dealt with here the shell model calculations necessarily have to be performed in a truncated model space leading to uncertainties in the calculated matrix elements and form factors. More extended calculations then have to be performed or other theoretical approaches used. Clearly, the recent advances in *ab initio* calculations can be of great value to this.

Should detailed theoretical calculations not be available for the interpretation in terms of new physics of  $\beta$ -correlation measurements with a specific isotope in the mass range  $A = 3$  to 61, one could for transitions between states with a near-single particle character use the average values for the specific subshells that are listed in the last columns of Tables XVI and XXIX. For transitions between states without a clear single-particle character one could use the overall average value  $b/Ac = 5.1 \pm 2.4$  (Table XXX) that was obtained for the set of 83  $\beta$  transitions considered here.

Of course direct measurements of the weak magnetism term,  $b$ , would be even more beneficial and could also help to further improve theory. At present, a series of dedicated  $\beta$ -spectrum shape measurements are ongoing and planned, using a wide variety of detection systems. All focus on extracting the weak-magnetism term and/or the so-called Fierz interference term (the latter being sensitive to the presence of possible scalar or tensor type contributions to the weak interaction [531]), to which the  $\beta$  spectrum shape is primarily sensitive. Indeed, the shape of the  $\beta$  spectrum depends on the weak-magnetism form factor ratio,  $b/Ac$ , via a term that is linear in the  $\beta$ -particle energy, and on the Fierz interference term via a term that is inversely proportional to the energy [532].

Recently, the electron-spectrum shape in the decay of unpolarized neutrons was investigated to produce the first results for the Fierz interference term in free neutron decay [533]. Later, more precise results were obtained from the energy dependence of the asymmetry parameter in free neutron decay, with  $\Delta b = 0.048$  [78] and  $\Delta b = 0.021$  [79]. The Nab experiment aims at determining the Fierz interference term with precision  $\Delta b \approx 0.003$  using an unpolarized cold neutron beam at the Spallation Neutron Source at Oak Ridge National Laboratory [534]. Similar plans exist for the PERC-NOMOS neutron beam station that will be set up at the beam facility MEPHISTO of the FRM II research reactor in Munich, Germany [535,536].

At the nuclear side, large-volume NaI and CsI scintillators stopping all radiation to minimize systematic errors have been used for the transitions  $^6\text{He} \rightarrow ^6\text{Li}$  [107–109] and

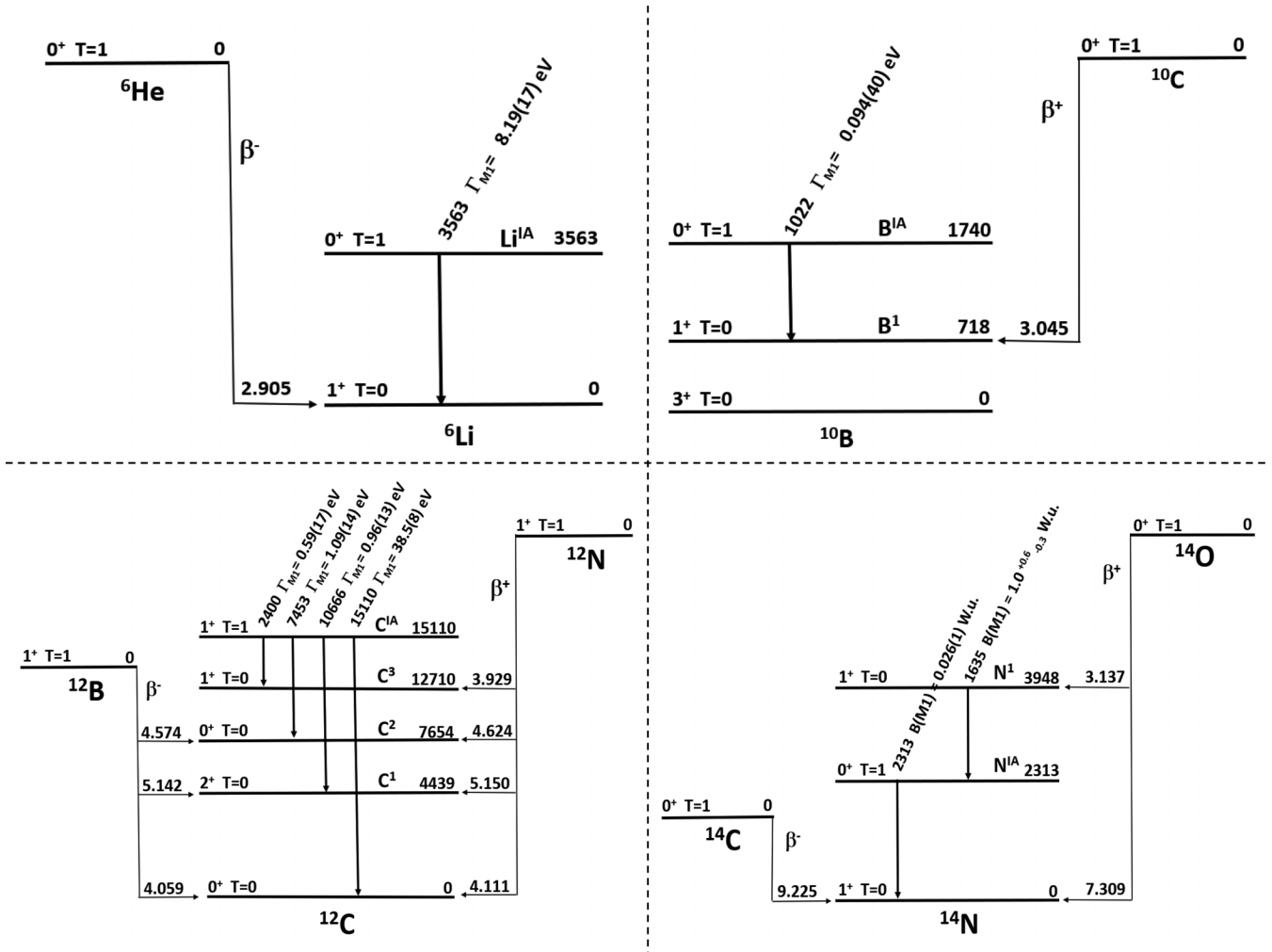


FIG. 17. Partial decay schemes (not to scale) showing the  $\beta$  transitions and their analog  $\gamma$  transitions in  $T = 1$  multiplets with  $A = 6$  to 14 for which the weak-magnetism form factor is determined here, with their respective  $\log ft$  value (for  $\beta$  transitions), or the transition energy and  $\Gamma_{M1}$  or  $B(M1)$  value (for  $\gamma$  transitions). For each ground state and excited state the spin-parity, isospin, and energy (in keV) is given. The excited state labels (e.g.,  $Li^{1A}$  or  $C^3$ ) are also used in the first column of Tables XXII to XXVIII for easy reference.

$^{20}\text{F} \rightarrow ^{20}\text{Ne}^1$  (Fig. 18 in Appendix B) [111] (using the setup described in [112]). Other authors used a superconducting spectrometer [518] to observe the  $\beta$  spectra of  $^{14}\text{O}$  [537] and  $^{66}\text{Ga}$  [538], or metallic magnetic calorimeters to study the  $\beta$  spectra of  $^{63}\text{Ni}$  and  $^{241}\text{Po}$  [519]. More recently, the  $\beta$  spectrum of  $^{45}\text{Ca}$  was measured using the UCNA spectrometer [539] with the Nab/UCNB prototype detection system (consisting of 1.5 mm thick, highly segmented silicon detectors, with an active area diameter of 11.5 cm, and a thin front end dead layer) [522].

Further, at the LIRAT facility at GANIL (Caen) a  $^6\text{He}$  source was sandwiched between two yttrium aluminum perovskite (YAP:Ce) scintillators providing a  $4\pi$  geometry (b-STILED experiment) [111]. A  $4\pi$  solid angle was also achieved by installing two plastic scintillators in a strong magnetic field for measuring the  $\beta$ -spectrum shape of the pure Gamow-Teller decay of  $^{114}\text{In}$  (InESS experiment at WISArD-ISOLDE) [114]. The same  $\beta$  decay is presently also being investigated by a combination of a plastic scintillator, serving

as a trigger device, and a hexagonally structured multiwire drift chamber filled with a mixture of helium and isobutane gas (miniBETA experiment) [113,520,521]. The determination of the weak magnetism form factor for the  $1^+ \rightarrow 0^+$  pure Gamow-Teller  $\beta$  decay of  $^{114}\text{In}$  in these two experiments would be the first direct determination of weak magnetism in the mass range of fission fragments and would be of special interest for further theoretical work on the reactor neutrino problem.

Concluding, the newly updated  $\mathcal{F}_T^{\text{mirror}}$  values for the mirror  $\beta$  transitions allow for more sensitive tests of non-standard-model scalar, tensor, or right-handed weak currents. Further, the better control of the induced form factors that is provided by this work allows future correlation coefficients measurements in nuclear  $\beta$  decay to better take into account the recoil correction when interpreting results in terms of new physics or when determining the  $V_{ud}$  quark-mixing matrix element. When a precision of the order of 1% or better is obtained in such measurements, radiative correc-

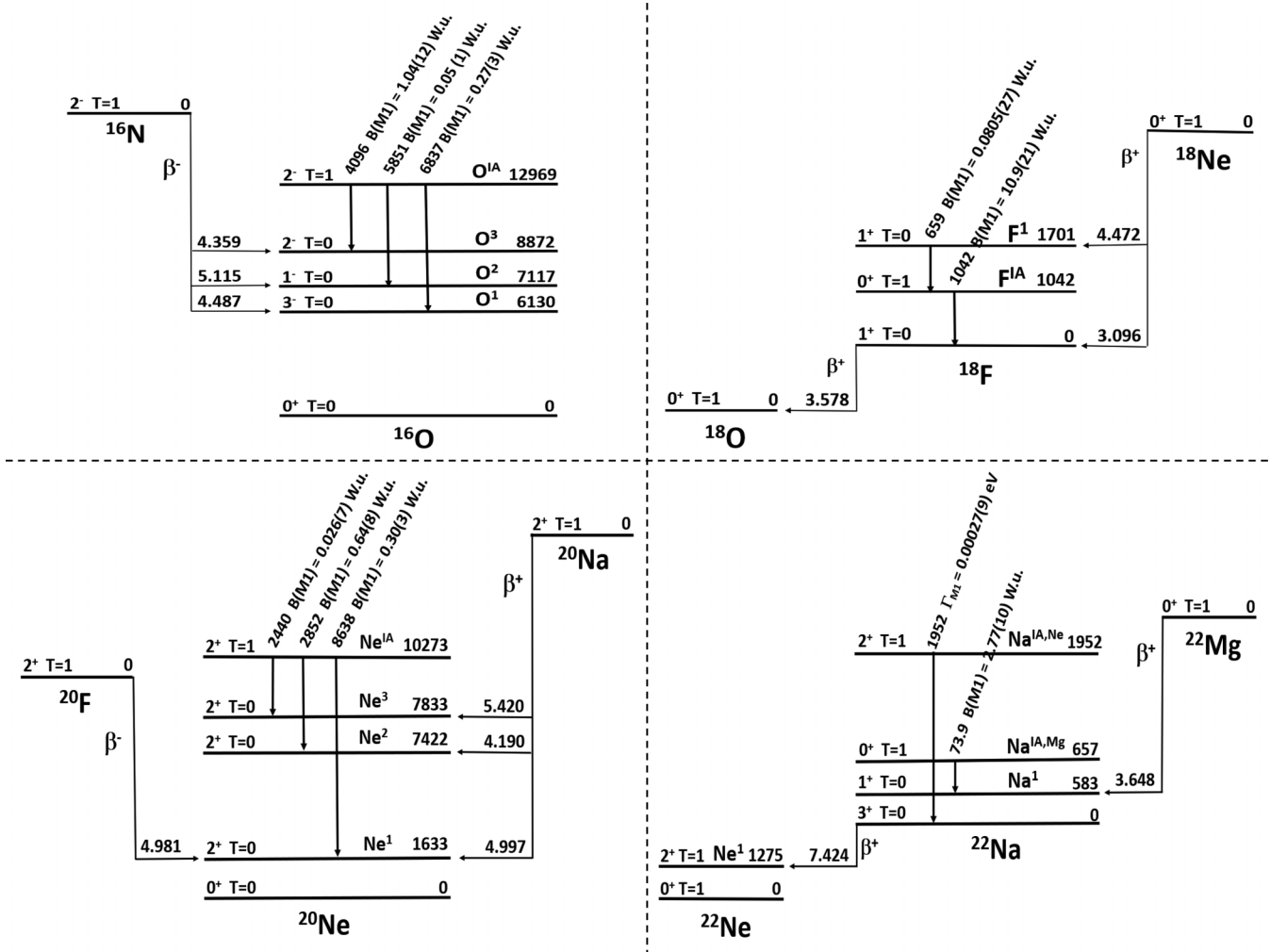


FIG. 18. Partial decay schemes (not to scale) showing the  $\beta$  transitions and their analog  $\gamma$  transitions in  $T = 1$  multiplets with  $A = 16$  to  $22$  for which the weak-magnetism form factor is determined here, with their respective  $\log ft$  value (for  $\beta$  transitions), or the transition energy and  $\Gamma_{M1}$  or  $B(M1)$  value (for  $\gamma$  transitions). For each ground state and excited state the spin-parity, isospin, and energy (in keV) is given. The excited state labels (e.g.,  $O^{IA}$  or  $O^3$ ) are also used in the first column of Tables XXII to XXVIII for easy reference.

tions have to be considered as well. For the neutron these were addressed in, e.g., Refs. [86,141,540–546]. For measurements of the  $\beta\nu$  correlation and the  $\beta$ -asymmetry parameter with the mirror nuclei these are discussed in detail in, e.g., Refs. [84,85,543].

#### ACKNOWLEDGMENT

This work was supported by the Research Foundation-Flanders (BE) under Grant No. G.0812.18N. L.H. is supported through the U.S. Department of Energy, Low Energy Physics Grant No. DE-FG02-ER41042 and NSF Grant No. PHY-1914133.

### APPENDIX A: SINGLE-PARTICLE EVALUATION OF WEAK MAGNETISM

#### 1. Overview

The evaluation of the weak magnetism form factor using the impulse approximation [Eq. (44)] requires the evaluation

of both the  $M_{GT}$  and  $M_L$  matrix elements. Expressed in the usual way, we find

$$\frac{b}{Ac} = \frac{1}{g_A} \left( g_M + g_V \frac{M_L}{M_{GT}} \right). \quad (A1)$$

For a general operator  $\mathcal{O}_i$  we can project onto a basis state in second quantization to find

$$\langle f | \mathcal{O}_i \tau^\pm | i \rangle = \sum_{\alpha, \beta} \langle \alpha | \mathcal{O}_i | \beta \rangle \langle f | a_\alpha^\dagger a_\beta | i \rangle, \quad (A2)$$

where  $\alpha$  and  $\beta$  are single-particle proton (neutron) and neutron (proton) states for  $\beta^-$  ( $\beta^+$ ) decay. The quantities  $\langle f | a_\alpha^\dagger a_\beta | i \rangle$  are called one-body transition densities, and can be calculated using both the shell model and mean field techniques.

The simplest way of evaluating Eq. (A2) assumes a single particle in a spherical harmonic oscillator potential, thereby reducing the sum to a single element,  $\gamma$ , with a trivial  $\langle f | a_\alpha^\dagger a_\beta | i \rangle = \delta_{\alpha\beta} \delta_{\alpha\gamma}$ . The single-particle state is chosen based

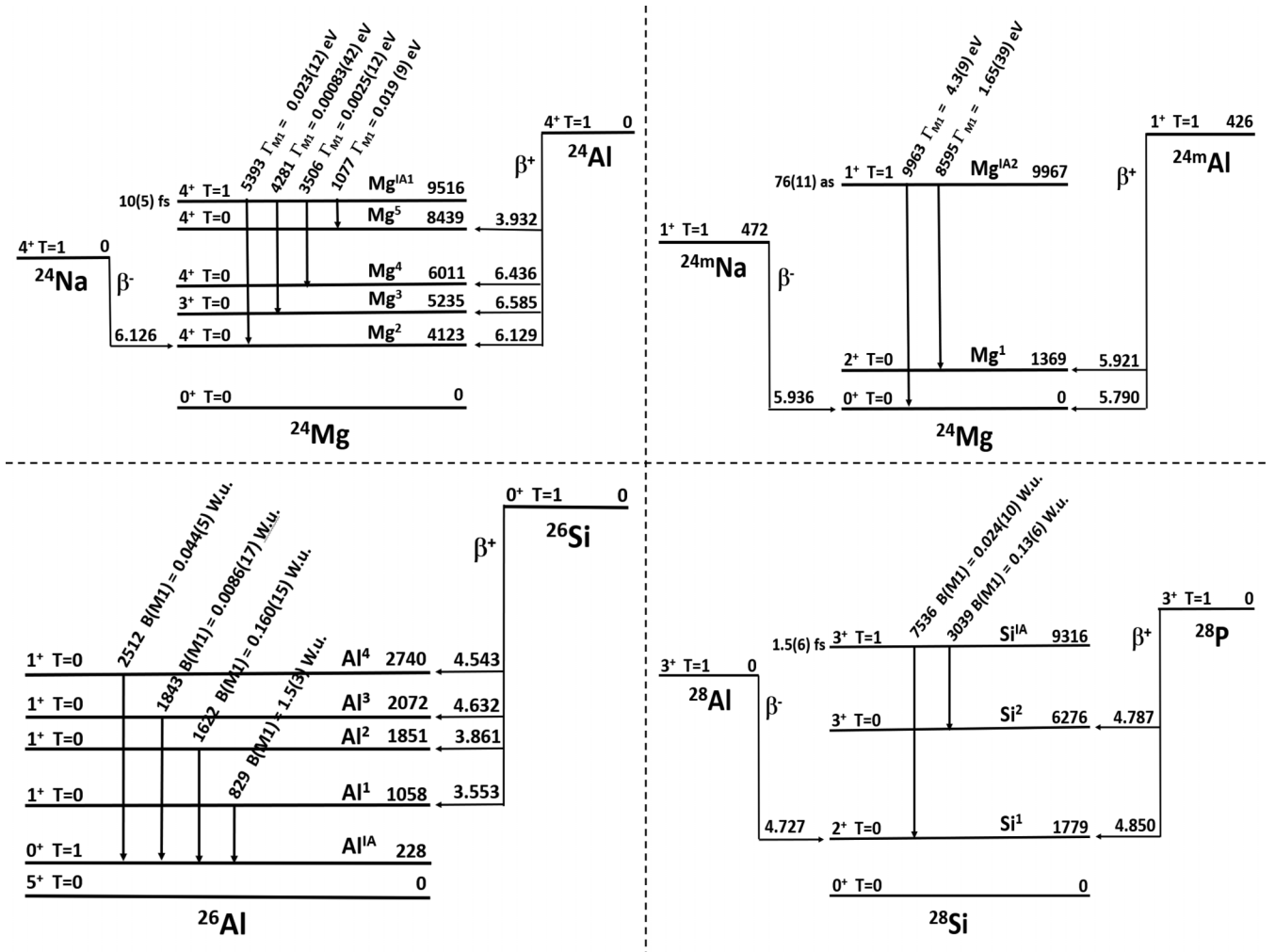


FIG. 19. Partial decay schemes (not to scale) showing the  $\beta$  transitions and their analog  $\gamma$  transitions in  $T = 1$  multiplets with  $A = 24$  to 28 for which the weak-magnetism form factor is determined here, with their respective  $\log ft$  value (for  $\beta$  transitions), or the transition energy and  $\Gamma_{M1}$  or  $B(M1)$  value (for  $\gamma$  transitions). For each ground state and excited state the spin-parity, isospin, and energy (in keV) is given. The excited state labels (e.g.,  $Mg^{A1}$  or  $Mg^5$ ) are also used in the first column of Tables XXII to XXVIII for easy reference.

on regular  $jj$  coupling, assuming the same radial functions for  $j = l \pm 1/2$ . In this case the ratio trivially reduces to

$$\frac{M_L}{M_{GT}} = \frac{\langle n_f l_f j_f | l | n_i l_i j_i \rangle}{\langle n_f l_f j_f | \sigma | n_i l_i j_i \rangle} = (-1)^{j_i - j_f} \frac{\begin{Bmatrix} 1/2 & l & j_i \\ 1 & j_f & l \end{Bmatrix}}{\begin{Bmatrix} l & 1/2 & j_i \\ 1 & j_f & 1/2 \end{Bmatrix}} \frac{\sqrt{l(l+1)(2l+1)}}{\sqrt{6}}, \quad (\text{A3})$$

where  $J_i$  and  $J_f$  are initial and final nuclear spins. In the case  $j_i = j_f = l + 1/2$ , Eq. (A3) reduces to  $l$ , while for  $j_i = j_f = l - 1/2$  it reduces to  $-(l + 1)$ , and  $-1/2$  otherwise. For transitions where  $j_i = j_f$ , the orbital component can constitute a large part of the total  $b/Ac$  value. This scenario is typically limited to lower nuclear masses, in particular mirror nuclei and transitions from isospin multiplets, precisely the two cases we discussed in Sec. III A 2.

The simple spherical harmonic oscillator potential, while clearly of use, paints an overly simplified picture of the nuclear environment. We can then move forwards to a more realistic potential, such as a Woods-Saxon form. In this case we construct the Hamiltonian as

$$\mathcal{H} = -\frac{\hbar^2}{2m} \nabla^2 - V_0 f(r) - V_s \left( \frac{\hbar}{m_\pi c} \right)^2 \frac{1}{r} \frac{df}{dr} l \cdot s, \quad (\text{A4})$$

where  $f(r)$  has the typical Woods-Saxon form

$$f(r) = \frac{1}{1 + \exp((r - R)/a_0)}, \quad (\text{A5})$$

with  $R$  the nuclear radius, and

$$V_0 = V \left( 1 \pm \chi \frac{N - Z}{N + Z} \right). \quad (\text{A6})$$

Here  $V$  and  $\chi$  are free parameters based on the approach by Refs. [547,548]. These are typically put to 49.6 MeV and 0.86, respectively. As the spherical harmonic oscillator states form a good basis for our improved wave functions and analytical

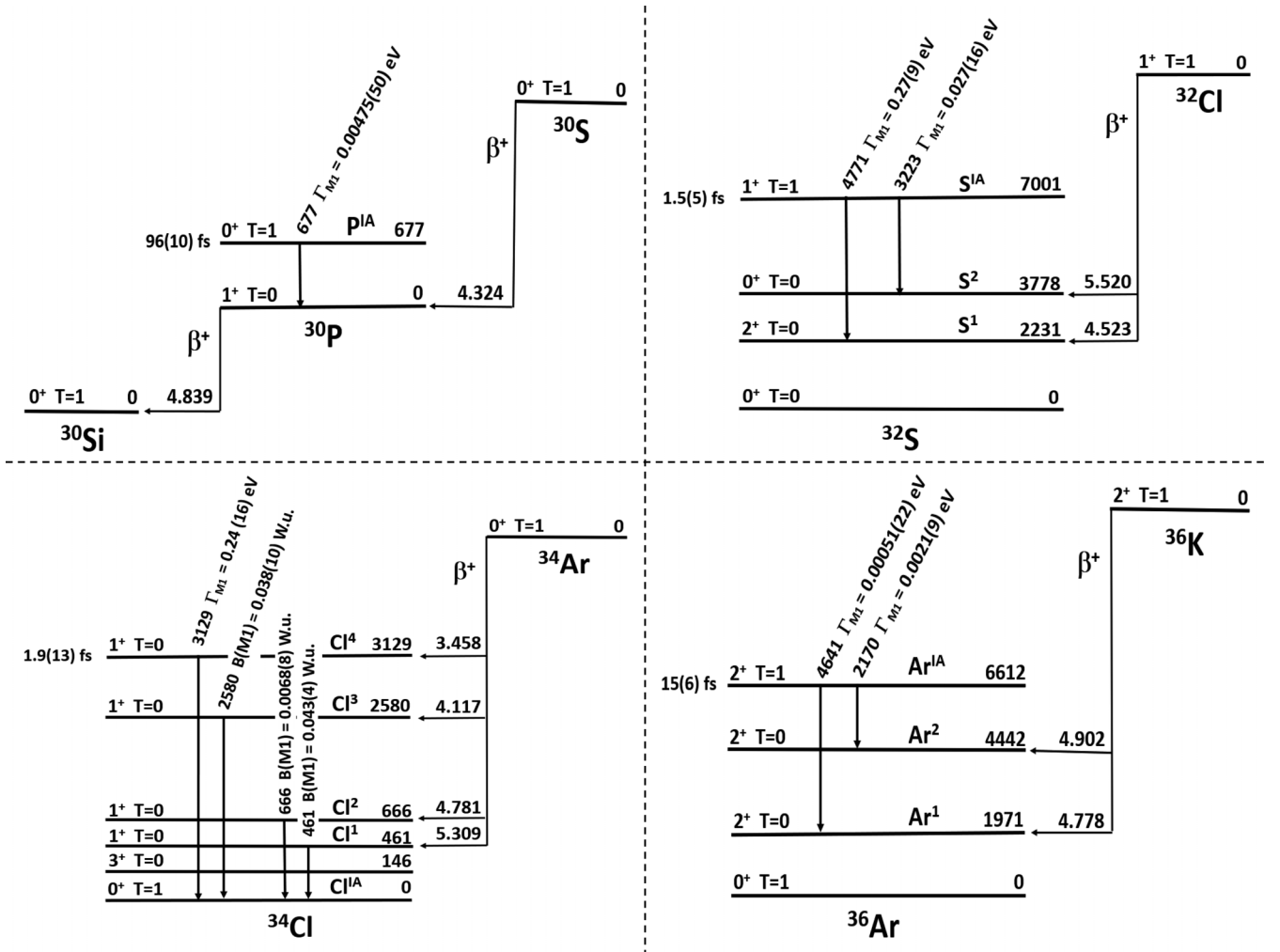


FIG. 20. Partial decay schemes (not to scale) showing the  $\beta$  transitions and their analog  $\gamma$  transitions in  $T = 1$  multiplets with  $A = 30$  and  $36$  for which the weak-magnetism form factor is determined here, with their respective  $\log ft$  value (for  $\beta$  transitions), or the transition energy and  $\Gamma_{M1}$  or  $B(M1)$  value (for  $\gamma$  transitions). For each ground state and excited state the spin-parity, isospin, and energy (in keV) is given. The excited state labels (e.g.,  $P^{IA}$  or  $Cl^4$ ) are also used in the first column of Tables XXII to XXVIII for easy reference.

results are available, we write the new nuclear state as

$$|v j\rangle = \sum_{nl} C_{nlj}^v |nl j\rangle, \quad (\text{A7})$$

where  $|nl j\rangle$  are the spherical harmonic oscillator basis states as before. As  $j$  remains a good quantum number in a spherical potential, the Hamiltonian of Eq. (A4) serves to mix different radial quantum numbers. In keeping with the extreme single particle approximation, the result of Eq. (A3) is then trivially extended to

$$\frac{M_L}{M_{GT}} = \frac{\sum_{kl} C_{nk,ljk}^{v_k*} C_{nl,lji}^{v_l} \langle n_k l_k j_k | \mathbf{L} | n_l l_l j_l \rangle}{\sum_{kl} C_{nk,ljk}^{v_k*} C_{nl,lji}^{v_l} \langle n_k l_k j_k | \boldsymbol{\sigma} | n_l l_l j_l \rangle}. \quad (\text{A8})$$

This result is strictly only valid for a state with only one single particle in the final state responsible for the nuclear spin, i.e., odd- $A$  nuclei. In even- $A$  nuclei, even though we only consider one active nucleon in the decay process, we have to consider at least two nucleons coupling to the correct total spin. It is shown [127] that this can be established by multiplying our

previous result with a factor  $C(K)$  which depends only on the spherical tensor operator rank,  $K$ , i.e.,  $\langle f | a_{\alpha}^{\dagger} a_{\beta} | i \rangle = C(K)$ . As both the Gamow-Teller and orbital matrix element are rank 1 operators, this factor drops out in the simple approximation we have made here. As this is in general not true for states described by multiple nucleon configurations—as is done for instance in the shell model—we consider here the simple case of an even-even to odd-odd transition with two valence nucleons in initial and final states. In this case valence particle 1 transforms into particle 2 and we write for  $\beta^{\pm}$  decay

$$C(K) = \sqrt{\frac{\hat{J}_i \hat{J}_f \hat{T}_i \hat{T}_f}{1 + \delta_{j_i j_2}}} (-1)^{T_f - T_{3f}} \begin{pmatrix} T_f & 1 & T_i \\ -T_{3f} & \pm 1 & T_{3i} \end{pmatrix} \\ \times \begin{Bmatrix} \frac{1}{2} & T_f & \frac{1}{2}(T_f + T_i) \\ T_i & \frac{1}{2} & 1 \end{Bmatrix} \sqrt{\frac{3}{2}} (-1)^K \\ \times 2[\delta_{j_i j_1} - (-1)^{j_1 + j_2}] \begin{Bmatrix} j_2 & J_f & j_1 \\ J_i & j_1 & K \end{Bmatrix}, \quad (\text{A9})$$

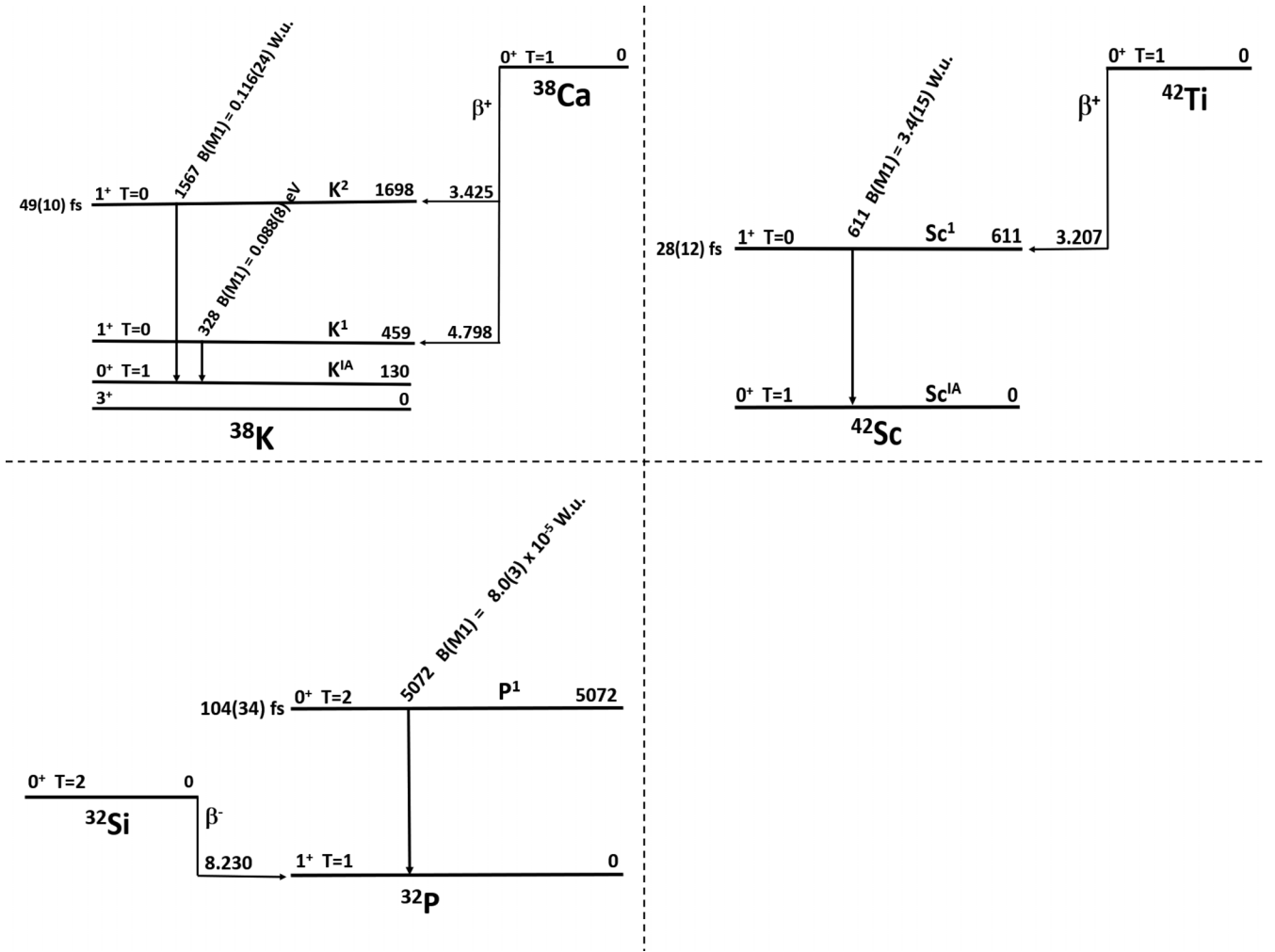


FIG. 21. Partial decay schemes (not to scale) showing the  $\beta$  transitions and their analog  $\gamma$  transitions in  $T = 1$  multiplets with  $A = 38$  and  $42$ , and a single  $T = 2$  multiplet with  $A = 32$  for which the weak-magnetism form factor is determined here, with their respective  $\log ft$  value (for  $\beta$  transitions), or the transition energy and  $\Gamma_{M1}$  or  $B(M1)$  value (for  $\gamma$  transitions). For each ground state and excited state the spin-parity, isospin, and energy (in keV) is given. The excited state labels (e.g.,  $K^{IA}$  or  $K^2$ ) are also used in the first column of Tables XXII to XXVIII for easy reference.

where we introduced the hat notation  $\hat{j} = 2j + 1$ . An equivalent formula can be written down for odd-odd to even-even decays using the results from Ref. [549].

## 2. Axially deformed potentials

While the generalization to a Woods-Saxon potential described in the previous section most certainly helps in the correct determination of the valence particle, its corresponding state is typically still dominated by a single harmonic oscillator component. The reason for this is the large distance between nuclear levels with equal  $j$  and parity, particularly visible in the lower- $Z$  nuclei. As many of the cases studied in this work lie close to the  $N = Z$  line, large (mainly quadrupole) deformations are found even for light nuclei, with also higher-order deformations being non-negligible in the low- to medium- $Z$  region of interest here [495].

It is of interest then to extend the potential of Eq. (A4) to include axial deformations,

$$\mathcal{H}' = \mathcal{H} + V_0 R \frac{df}{dr} \sum_{n=1} \beta_{2n} Y_{2n}^0, \quad (\text{A10})$$

with  $Y_l^m$  the standard spherical harmonic function. In this case  $j$  is no longer a good quantum number, and we must instead resort to the projection of  $\mathbf{j}$  along the symmetry axis of the nucleus written as  $\Omega$ . Writing the angular momentum of a rotating deformed core as  $\mathbf{R}$ , we denote by  $K$  the projection along the symmetry axis of the sum  $\mathbf{j} + \mathbf{R}$ . It follows then directly that in the rotational ground state, we have  $K = \Omega$  for odd- $A$  nuclei. In even-even nuclei the valence particles couple to  $K = 0$ , while in odd-odd nuclei  $K$  can be  $|\Omega_p \pm \Omega_n|$ . The new single-particle wave function will be of the Nilsson type and be a combination of wave functions of the type of Eq. (A7) with the appropriate spin projections such that

$$|\mu\Omega\rangle = \sum_{nl} \sum_{vj} C_{v\Omega}^\mu C_{nlj}^v |nlj\rangle \equiv \sum_j C_{j\Omega} |Nlj\Omega\rangle, \quad (\text{A11})$$

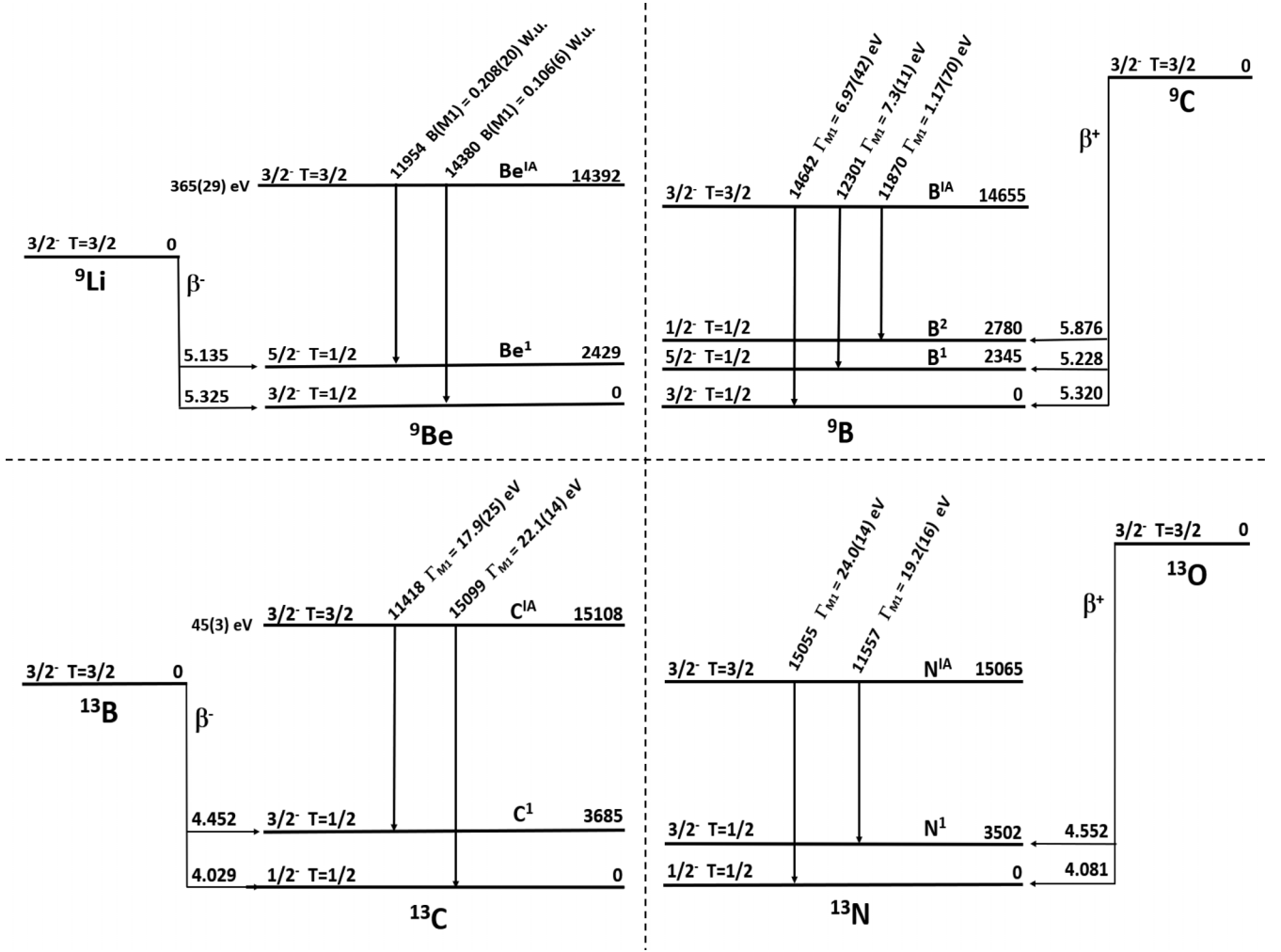


FIG. 22. Partial decay schemes (not to scale) showing the  $\beta$  transitions and their analog  $\gamma$  transitions in  $T = 3/2$  multiplets with  $A = 9$  to 13 for which the weak-magnetism form factor is determined here, with their respective  $\log ft$  value (for  $\beta$  transitions), or the transition energy and  $\Gamma_{M1}$  or  $B(M1)$  value (for  $\gamma$  transitions). For each ground state and excited state the spin-parity, isospin, and energy (in keV) is given. The excited state labels (e.g.,  $\text{Be}^{IA}$  or  $\text{Be}^I$ ) are also used in the first column of Tables XXII to XXVIII for easy reference.

where in the last term we have written our solution using the notation by Davidson<sup>2</sup> [550]. The matrix element for odd- $A$  decays is then written as [127]

$$\begin{aligned}
 & \langle \phi(J_f K_f; \Omega_f) | | O_{KLs} \tau^\pm | | \phi(J_i K_i; \Omega_i) \rangle \\
 &= \sqrt{\frac{\hat{J}_i \hat{J}_f}{(1 + \delta_{K_f 0})(1 + \delta_{K_i 0})}} \sum_{j_2 j_1} C_{j_2 \Omega_2} C_{j_1 \Omega_1} \left\{ (-1)^{J_2 - K_2 + j_2 - \Omega_2} \begin{pmatrix} J_f & K & J_i \\ -K_f & \Omega_2 - \Omega_1 & K_i \end{pmatrix} \begin{pmatrix} j_2 & K & j_1 \\ -\Omega_2 & \Omega_2 - \Omega_1 & \Omega_1 \end{pmatrix} \right. \\
 & \left. + \begin{pmatrix} J_f & K & J_i \\ K_f & -\Omega_2 - \Omega_1 & K_i \end{pmatrix} \begin{pmatrix} j_2 & K & j_1 \\ \Omega_2 & -\Omega_2 - \Omega_1 & \Omega_1 \end{pmatrix} \right\} \langle j_2 || O_{KLs} || j_1 \rangle. \tag{A12}
 \end{aligned}$$

<sup>2</sup>The difference with the treatment of Davidson lies in the spherical potential used. Unless this is exactly a modified spherical oscillator wave function as per Nilsson [496], more than one  $C_{Nj}$  will be non-zero. In the limit of zero deformation, Eq. (A7) will generally contain more than one term.

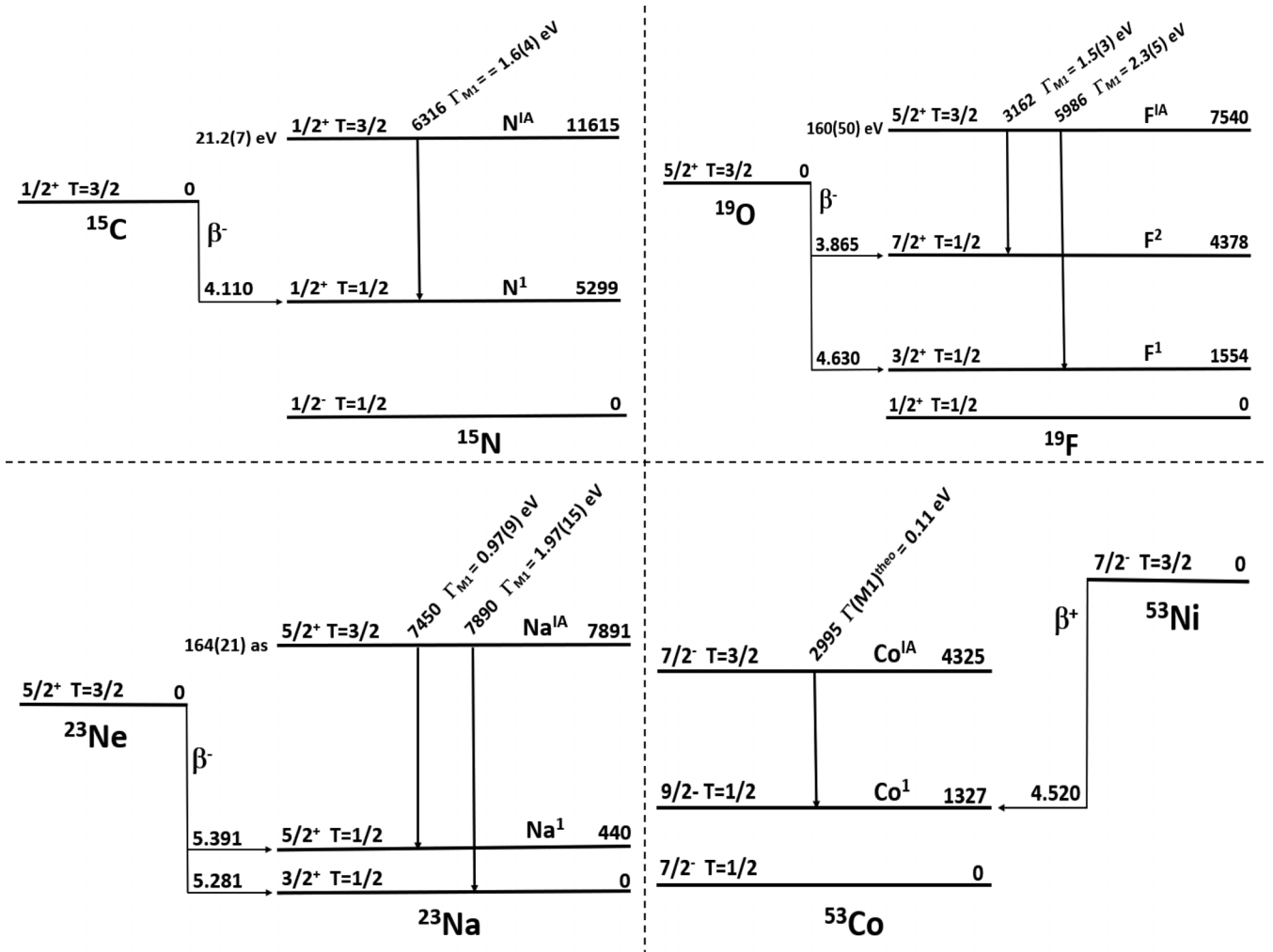


FIG. 23. Partial decay schemes (not to scale) showing the  $\beta$  transitions and their analog  $\gamma$  transitions in  $T = 3/2$  multiplets with  $A = 15$  to  $53$  for which the weak-magnetism form factor is determined here, with their respective  $\log ft$  value (for  $\beta$  transitions), or the transition energy and  $\Gamma_{M1}$  or  $B(M1)$  value (for  $\gamma$  transitions). For each ground state and excited state the spin-parity, isospin, and energy (in keV) is given. The excited state labels (e.g.,  $N^{IA}$  or  $N^1$ ) are also used in the first column of Tables XXII to XXVIII for easy reference.

In the case of even- $A$  decays initial and final states are approximated by a coupling of two valence particles to the correct total angular momentum. Using the results of Ref. [551], the spin-reduced matrix element for even-even to odd-odd decays is found to be

$$\begin{aligned}
 & \langle \phi(J_f K_f; \Omega_f) | \sum_{n=1,2} \{ O_{KLS} \tau_n^\pm \} | \phi(J_i K_i = 0; \Omega_i = 0) \rangle \\
 &= \sqrt{\frac{\hat{J}_i \hat{J}_f}{2(1 + \delta_{K_f 0})}} \begin{pmatrix} J_f & K & J_i \\ -K_f & K_f & 0 \end{pmatrix} [1 + (-1)^{J_i}] \\
 & \times \sum_{j_2 j_1} C_{j_2 - \Omega_2} C_{j_1 \Omega_1} (-1)^{j_2 - \Omega_2} \begin{pmatrix} j_2 & K & j_1 \\ -\Omega_2 & K_f & -\Omega_1 \end{pmatrix} \\
 & \times \langle j_2 || O_{KLS} || j_1 \rangle, \tag{A13}
 \end{aligned}$$

while the reverse case can be found in several publications [127,551]. Here  $\langle j_2 || O_{KLS} || j_1 \rangle$  are simple spin-reduced single-particle matrix elements for the harmonic oscillator wave functions.

The final task is then to calculate the different  $C_{\Omega_j}$ , which is performed by the code described in Ref. [339]. This automatically uses these results to calculate the relevant factors such as  $b/Ac$  and  $d/Ac$ . It enables coupling to results from more advanced calculations through the single-particle density matrix elements  $\rho_{\alpha\beta} = \langle f | a_\alpha^\dagger a_\beta | i \rangle$ . Further, it calculates the spectrum shape and integrated  $f$  value using these nuclear structure inputs based on the spectral shape description from Ref. [119].

## APPENDIX B: PARTIAL DECAY SCHEMES

Figures 17–21 show the partial decay schemes for all pairs of analog  $\beta$  and  $\gamma$  transitions from states in the  $T = 1$  triplets with  $A = 6$  to  $42$  and the  $T = 2$  multiplet with  $A = 32$ , indicating the  $\log ft$  value for the  $\beta$  transitions and the energy and the  $\Gamma_{M1}$  or  $B(M1)$  value [Eq. (60)] for the  $\gamma$  transitions. Figures 22 and 23 provide the same information for the pairs of analog  $\beta$  and  $\gamma$  transitions from states in the  $T = 3/2$  multiplets with mass  $A = 9$  to  $53$ .

- [1] B. R. Holstein, *Rev. Mod. Phys.* **46**, 789 (1974); **48**, 673(E) (1976).
- [2] F. P. Calaprice and B. R. Holstein, *Nucl. Phys. A* **273**, 301 (1976).
- [3] F. P. Calaprice, W. Chung, and B. H. Wildenthal, *Phys. Rev. C* **15**, 2178 (1977).
- [4] H. Behrens, H. Genz, M. Conze, F. Feldmeier, W. Stock, and A. Richter, *Ann. Phys. (NY)* **115**, 276 (1978).
- [5] R. P. Feynman and M. Gell-Mann, *Phys. Rev.* **109**, 193 (1958).
- [6] R. E. Tribble and G. T. Garvey, *Phys. Rev. Lett.* **32**, 314 (1974).
- [7] W. Kaina, V. Soergel, H. Thies, and W. Trost, *Phys. Lett. B* **70**, 411 (1977).
- [8] C. S. Wu, Y. K. Lee, and L. W. Mo, *Phys. Rev. Lett.* **39**, 72 (1977).
- [9] L. V. Elmbt, J. Deutsch, and R. Prieels, *Nucl. Phys. A* **469**, 531 (1987).
- [10] F. P. Calaprice and D. E. Alburger, *Phys. Rev. C* **17**, 730 (1978).
- [11] J. B. Camp, *Phys. Rev. C* **41**, 1719 (1990).
- [12] L. Grenacs, *Annu. Rev. Nucl. Part. Sci.* **35**, 455 (1985).
- [13] T. Sumikama, K. Matsuta, T. Nagatomo, M. Ogura, T. Iwakoshi, Y. Nakashima, H. Fujiwara, M. Fukuda, M. Mihara, K. Minamisono, T. Yamaguchi, and T. Minamisono, *Phys. Rev. C* **83**, 065501 (2011).
- [14] D. Wilkinson, *Phys. Lett. B* **31**, 447 (1970).
- [15] B. R. Holstein and S. B. Treiman, *Phys. Rev. C* **3**, 1921 (1971).
- [16] B. R. Holstein and S. B. Treiman, *Phys. Rev. D* **13**, 3059 (1976).
- [17] R. E. Tribble and G. T. Garvey, *Phys. Rev. C* **12**, 967 (1975).
- [18] F. P. Calaprice, *Phys. Rev. C* **12**, 2016 (1975).
- [19] L. Fifield, F. Calaprice, C. Zimmerman, M. Hurst, A. Pakkanen, T. Symons, F. Watt, and K. Allen, *Nucl. Phys. A* **288**, 57 (1977).
- [20] N. Dupuis-Rolin, J. Deutsch, D. Favart, and R. Prieels, *Phys. Lett. B* **79**, 359 (1978).
- [21] R. E. Tribble and D. P. May, *Phys. Rev. C* **18**, 2704 (1978).
- [22] R. E. Tribble, D. P. May, and D. M. Tanner, *Phys. Rev. C* **23**, 2245 (1981).
- [23] R. D. Rosa, W. W. Daehnick, S. K. Saha, and P. C. Li, *Phys. Rev. C* **37**, 2722 (1988).
- [24] D. Wilkinson, *Eur. Phys. J. A* **7**, 307 (2000).
- [25] T. Minamisono, K. Matsuta, T. Yamaguchi, K. Minamisono, T. Ikeda, Y. Muramoto, M. Fukuda, Y. Nojiri, A. Kitagawa, K. Koshigiri, and M. Morita, *Phys. Rev. Lett.* **80**, 4132 (1998).
- [26] K. Minamisono, K. Matsuta, T. Minamisono, T. Yamaguchi, T. Sumikama, T. Nagatomo, M. Ogura, T. Iwakoshi, M. Fukuda, M. Mihara, K. Koshigiri, and M. Morita, *Phys. Rev. C* **65**, 015501 (2001).
- [27] N. Smirnova and C. Volpe, *Nucl. Phys. A* **714**, 441 (2003).
- [28] T. Sumikama, K. Matsuta, T. Nagatomo, M. Ogura, T. Iwakoshi, Y. Nakashima, H. Fujiwara, M. Fukuda, M. Mihara, K. Minamisono, T. Yamaguchi, and T. Minamisono, *Phys. Lett. B* **664**, 235 (2008).
- [29] K. Minamisono, T. Nagatomo, K. Matsuta, C. D. P. Levy, Y. Tagishi, M. Ogura, M. Yamaguchi, H. Ota, J. A. Behr, K. P. Jackson, A. Ozawa, M. Fukuda, T. Sumikama, H. Fujiwara, T. Iwakoshi, R. Matsumiya, M. Mihara, A. Chiba, Y. Hashizume, T. Yasuno *et al.*, *Phys. Rev. C* **84**, 055501 (2011).
- [30] J. Jackson, S. Treiman, and H. Wyld, Jr., *Nucl. Phys.* **4**, 206 (1957).
- [31] J. R. A. Pitcairn, D. Roberge, A. Gorelov, D. Ashery, O. Aviv, J. A. Behr, P. G. Bricault, M. Dombisky, J. D. Holt, K. P. Jackson, B. Lee, M. R. Pearson, A. Gaudin, B. Dej, C. Höhr, G. Gwinner, and D. Melconian, *Phys. Rev. C* **79**, 015501 (2009).
- [32] F. Wauters, V. De Leebeeck, I. Kraev, M. Tandecki, E. Traykov, S. Van Gorp, N. Severijns, and D. Zákoucký, *Phys. Rev. C* **80**, 062501(R) (2009).
- [33] F. Wauters, I. Kraev, D. Zákoucký, M. Beck, M. Breitenfeldt, V. De Leebeeck, V. V. Golovko, V. Y. Kozlov, T. Phalet, S. Rocchia, G. Soti, M. Tandecki, I. S. Towner, E. Traykov, S. Van Gorp, and N. Severijns, *Phys. Rev. C* **82**, 055502 (2010).
- [34] G. Soti, F. Wauters, M. Breitenfeldt, P. Finlay, P. Herzog, A. Knecht, U. Köster, I. S. Kraev, T. Porobic, P. N. Prashanth, I. S. Towner, C. Tramm, D. Zákoucký, and N. Severijns, *Phys. Rev. C* **90**, 035502 (2014).
- [35] B. Fenker, A. Gorelov, D. Melconian, J. A. Behr, M. Anholm, D. Ashery, R. S. Behling, I. Cohen, I. Craiciu, G. Gwinner, J. McNeil, M. Mehlman, K. Olchanski, P. D. Shidling, S. Smale, and C. L. Warner, *Phys. Rev. Lett.* **120**, 062502 (2018).
- [36] B. Märkisch, H. Mest, H. Saul, X. Wang, H. Abele, D. Dubbers, M. Klopff, A. Petoukhov, C. Roick, T. Soldner, and D. Werder, *Phys. Rev. Lett.* **122**, 242501 (2019).
- [37] N. Severijns and O. Naviliat-Cuncic, *Annu. Rev. Nucl. Part. Sci.* **61**, 23 (2011).
- [38] O. Naviliat-Cuncic and M. González-Alonso, *Ann. Phys. (Berlin)* **525**, 600 (2013).
- [39] B. R. Holstein, *J. Phys. G: Nucl. Part. Phys.* **41**, 114001 (2014).
- [40] K. K. Vos, H. W. Wilschut, and R. G. E. Timmermans, *Rev. Mod. Phys.* **87**, 1483 (2015).
- [41] M. Gonzalez-Alonso, O. Naviliat-Cuncic, and N. Severijns, *Prog. Part. Nucl. Phys.* **104**, 165 (2019).
- [42] A. Falkowski, M. González-Alonso, and O. Naviliat-Cuncic, *J. High Energ. Phys.* **2021**, 126.
- [43] O. Naviliat-Cuncic and N. Severijns, *Phys. Rev. Lett.* **102**, 142302 (2009).
- [44] E. Liénard, G. Ban, C. Couratin, P. Delahaye, D. Durand, X. Fabian, B. Fabre, X. Fléchar, P. Finlay, F. Mauger, A. Méry, O. Naviliat-Cuncic, B. Pons, T. Porobic, G. Quémener, N. Severijns, J. C. Thomas, and P. Velten, *Hyperfine Interact.* **236**, 1 (2015).
- [45] M. Brodeur, J. Kelly, J. Long, C. Nicoloff, and B. Schultz, *Nucl. Instrum. Methods Phys. Res., Sect. B* **376**, 281 (2016).
- [46] M. Beck, F. Ayala Guardia, M. Borg, J. Kahlenberg, R. Muñoz Horta, C. Schmidt, A. Wunderle, W. Heil, R. Maisonnobe, M. Simson, T. Soldner, R. Viro, O. Zimmer, M. Klopff, G. Konrad, S. Baeßler, F. Glück, and U. Schmidt, *Phys. Rev. C* **101**, 055506 (2020).
- [47] G. Mention, M. Fechner, T. Lasserre, T. A. Mueller, D. Lhuillier, M. Cribier, and A. Letourneau, *Phys. Rev. D* **83**, 073006 (2011).
- [48] T. A. Mueller, D. Lhuillier, M. Fallot, A. Letourneau, S. Cormon, M. Fechner, L. Giot, T. Lasserre, J. Martino, G. Mention, A. Porta, and F. Yermia, *Phys. Rev. C* **83**, 054615 (2011).
- [49] P. Huber, *Phys. Rev. C* **84**, 024617 (2011).
- [50] A. C. Hayes and P. Vogel, *Annu. Rev. Nucl. Part. Sci.* **66**, 219 (2016).
- [51] X. B. Wang and A. C. Hayes, *Phys. Rev. C* **95**, 064313 (2017).

- [52] A. C. Hayes, G. Jungman, E. A. McCutchan, A. A. Sonzogni, G. T. Garvey, and X. B. Wang, *Phys. Rev. Lett.* **120**, 022503 (2018).
- [53] L. Hayen, J. Kostensalo, N. Severijns, and J. Suhonen, *Phys. Rev. C* **99**, 031301(R) (2019).
- [54] L. Hayen, J. Kostensalo, N. Severijns, and J. Suhonen, *Phys. Rev. C* **100**, 054323 (2019).
- [55] J. C. Hardy and I. S. Towner, *Phys. Rev. C* **102**, 045501 (2020).
- [56] D. Dubbers and B. Märkisch, *Annu. Rev. Nucl. Part. Sci.* **71**, 139 (2021).
- [57] O. Naviliat-Cuncic, T. A. Girard, J. Deutsch, and N. Severijns, *J. Phys. G: Nucl. Part. Phys.* **17**, 919 (1991).
- [58] N. Severijns, M. Beck, and O. Naviliat-Cuncic, *Rev. Mod. Phys.* **78**, 991 (2006).
- [59] V. Egorov, C. Brianc¸on, V. Brudanin, J. Dionisio, J. Deutsch, V. Gorozhankin, Y. Gurov, R. Prieels, V. Sandukovsky, N. Severijns, M. Simoes, Y. Shitov, C. Vieu, V. Vorobel, T. Vylov, I. Yutlandov, and S. Zapparov, *Nucl. Phys. A* **621**, 745 (1997).
- [60] E. G. Adelberger, C. Ortiz, A. Garcia, H. E. Swanson, M. Beck, O. Tengblad, M. J. G. Borge, I. Martel, H. Bichsel, and the ISOLDE Collaboration, *Phys. Rev. Lett.* **83**, 1299 (1999).
- [61] A. Gorelov, D. Melconian, W. P. Alford, D. Ashery, G. Ball, J. A. Behr, P. G. Bricault, J. M. D’Auria, J. Deutsch, J. Dilling, M. Domsbky, P. Dubé, J. Fingler, U. Giesen, F. Glück, S. Gu, O. Häusser, K. P. Jackson, B. K. Jennings, M. R. Pearson *et al.*, *Phys. Rev. Lett.* **94**, 142501 (2005).
- [62] P. A. Vetter, J. R. Abo-Shaeer, S. J. Freedman, and R. Maruyama, *Phys. Rev. C* **77**, 035502 (2008).
- [63] X. Flé¸hard, P. Velten, E. Liénard, A. Méry, D. Rodríguez, G. Ban, D. Durand, F. Mauger, O. Naviliat-Cuncic, and J. C. Thomas, *J. Phys. G: Nucl. Part. Phys.* **38**, 055101 (2011).
- [64] M. G. Sternberg, R. Segel, N. D. Scielzo, G. Savard, J. A. Clark, P. F. Bertone, F. Buchinger, M. Burkey, S. Caldwell, A. Chaudhuri, J. E. Crawford, C. M. Deibel, J. Greene, S. Gulick, D. Lascar, A. F. Levand, G. Li, A. Pérez Galván, K. S. Sharma, J. Van Schelt *et al.*, *Phys. Rev. Lett.* **115**, 182501 (2015).
- [65] V. Araujo-Escalona, D. Atanasov, X. Flé¸hard, P. Alfaurt, P. Ascher, B. Blank, L. Daudin, M. Gerbaux, J. Giovinazzo, S. Grévy, T. Kurtukian-Nieto, E. Liénard, G. Quéméner, N. Severijns, S. Vanlangendonck, M. Versteegen, and D. Zákoucký, *Phys. Rev. C* **101**, 055501 (2020).
- [66] M. T. Hassan, W. A. Byron, G. Darius, C. DeAngelis, F. E. Wietfeldt, B. Collett, G. L. Jones, A. Komives, G. Noid, E. J. Stephenson, F. Bateman, M. S. Dewey, T. R. Gentile, M. P. Mendenhall, and J. S. Nico, *Phys. Rev. C* **103**, 045502 (2021).
- [67] M. T. Burkey, G. Savard, A. T. Gallant, N. D. Scielzo, J. A. Clark, T. Y. Hirsh, L. Varriano, G. H. Sargsyan, K. D. Launey, M. Brodeur, D. P. Burdette, E. Heckmaier, K. Joerres, J. W. Klimes, K. Kolos, A. Laminack, K. G. Leach, A. F. Levand, B. Longfellow, B. Maaß *et al.*, *Phys. Rev. Lett.* **128**, 202502 (2022).
- [68] M. A.-P. Brown *et al.* (UCNA Collaboration), *Phys. Rev. C* **97**, 035505 (2018).
- [69] D. Combs, G. Jones, W. Anderson, F. Calaprice, L. Hayen, and A. Young, *arXiv:2009.13700*.
- [70] N. Severijns, J. Deutsch, F. Gimeno-Nogues, B. H. King, I. Pepe, R. Prieels, P. A. Quin, J. Camps, P. De Moor, P. Schuurmans, W. Vanderpoorten, L. Vanneste, J. Wouters, M. Allet, O. Naviliat-Cuncic, and B. R. Holstein, *Phys. Rev. Lett.* **70**, 4047 (1993).
- [71] N. Severijns, J. Deutsch, F. Gimeno-Nogues, B. H. King, I. Pepe, R. Prieels, P. A. Quin, J. Camps, P. De Moor, P. Schuurmans, W. Vanderpoorten, L. Vanneste, J. Wouters, M. Allet, O. Naviliat-Cuncic, and B. R. Holstein, *Phys. Rev. Lett.* **73**, 611(E) (1994).
- [72] M. Allet, K. Bodek, J. Camps, J. Deutsch, M. Ferro-Luzzi, F. Gimeno-Nogues, J. Govaerts, J. Lang, R. Müller, S. Navert, O. Naviliat-Cuncic, I. Pepe, R. Prieels, P. Quin, N. Severijns, J. Sromicki, E. Stephan, E. Thomas, and J. Zejma, *Phys. Lett. B* **383**, 139 (1996).
- [73] E. Thomas, R. Prieels, M. Allet, K. Bodek, J. Camps, J. Deutsch, F. Gimeno-Nogues, J. Govaerts, J. Lang, O. Naviliat-Cuncic, I. Pepe, P. Quin, N. Severijns, and J. Sromicki, *Nucl. Phys. A* **694**, 559 (2001).
- [74] D. Melconian, J. Behr, D. Ashery, O. Aviv, P. Bricault, M. Domsbky, S. Fostner, A. Gorelov, S. Gu, V. Hanemaayer, K. Jackson, M. Pearson, and I. Vollrath, *Phys. Lett. B* **649**, 370 (2007).
- [75] V. Kozlov, M. Beck, S. Coeck, P. Delahaye, P. Friedag, M. Herbane, A. Herlert, I. Kraev, M. Tandecki, S. V. Gorp, F. Wauters, C. Weinheimer, F. Wenander, D. Zákoucký, and N. Severijns, *Nucl. Instrum. Methods Phys. Res., Sect. B* **266**, 4515 (2008).
- [76] A. Kozela, G. Ban, A. Bia¸lek, K. Bodek, P. Gorel, K. Kirch, S. Kistryn, O. Naviliat-Cuncic, N. Severijns, E. Stephan, and J. Zejma, *Phys. Rev. C* **85**, 045501 (2012).
- [77] T. E. Chupp, R. L. Cooper, K. P. Coulter, S. J. Freedman, B. K. Fujikawa, A. García, G. L. Jones, H. P. Mumm, J. S. Nico, A. K. Thompson, C. A. Trull, F. E. Wietfeldt, and J. F. Wilkerson, *Phys. Rev. C* **86**, 035505 (2012).
- [78] X. Sun *et al.* (UCNA Collaboration), *Phys. Rev. C* **101**, 035503 (2020).
- [79] H. Saul, C. Roick, H. Abele, H. Mest, M. Klopff, A. K. Petukhov, T. Soldner, X. Wang, D. Werder, and B. Märkisch, *Phys. Rev. Lett.* **125**, 112501 (2020).
- [80] V. Cirigliano, A. Garcia, D. Gazit, O. Naviliat-Cuncic, G. Savard, and A. Young, Precision beta decay as a probe of new physics, *arXiv:1907.02164*.
- [81] T. Bhattacharya, V. Cirigliano, S. D. Cohen, A. Filipuzzi, M. González-Alonso, M. L. Graesser, R. Gupta, and H.-W. Lin, *Phys. Rev. D* **85**, 054512 (2012).
- [82] V. Cirigliano, S. Gardner, and B. R. Holstein, *Prog. Part. Nucl. Phys.* **71**, 93 (2013).
- [83] V. Cirigliano, M. González-Alonso, and M. L. Graesser, *J. High Energ. Phys.* **02** (2013) 046.
- [84] L. Hayen and A. R. Young, Consistent description of angular correlations in  $\beta$  decay for Beyond Standard Model physics searches, *arXiv:2009.11364*.
- [85] S. Vanlangendonck, N. Severijns, L. Hayen, and F. Glück, *Phys. Rev. C* **106**, 015506 (2022).
- [86] I. S. Towner and J. C. Hardy, *Rep. Prog. Phys.* **73**, 046301 (2010).
- [87] J. C. Hardy and I. S. Towner, *Phys. Rev. C* **91**, 025501 (2015).
- [88] L. Hayen, *Phys. Rev. D* **103**, 113001 (2021).
- [89] N. Severijns, M. Tandecki, T. Phalet, and I. S. Towner, *Phys. Rev. C* **78**, 055501 (2008).
- [90] L. Hayen and N. Severijns, *arXiv:1906.09870*.
- [91] O. Naviliat-Cuncic and N. Severijns, *Eur. Phys. J. A* **42**, 327 (2009).

- [92] N. Severijns and O. Naviliat-Cuncic, *Phys. Scr.* **T152**, 014018 (2013).
- [93] X. Fabian, G. Ban, R. Boussaïd, M. Breitenfeldt, C. Couratin, P. Delahaye, D. Durand, P. Finlay, X. Fléchar, B. Guillon, Y. Lemièr, A. Leredde, E. Liénard, A. Méry, O. Naviliat-Cuncic, E. Pierre, T. Porobic, G. Quéméner, D. Rodríguez, N. Severijns, J.C. Thomas, and S. Van Gorp, *EPJ Web Conf.* **66**, 08002 (2014).
- [94] X. Fabian, X. Fléchar, B. Pons, E. Liénard, G. Ban, M. Breitenfeldt, C. Couratin, P. Delahaye, D. Durand, P. Finlay, B. Guillon, Y. Lemièr, F. Mauger, A. Méry, O. Naviliat-Cuncic, T. Porobic, G. Quéméner, N. Severijns, and J.-C. Thomas, *Phys. Rev. A* **97**, 023402 (2018).
- [95] E. Liénard, invited talk at Solvay Workshop on Beta Decay Weak Interaction Studies in the Era of the LHC, Brussels, 2014 (unpublished), [https://fys.kuleuven.be/iks/wi/solvay\\_workshop\\_2014](https://fys.kuleuven.be/iks/wi/solvay_workshop_2014).
- [96] G. Ron *et al.*, invited talk at Solvay Workshop on Beta Decay Weak Interaction Studies in the Era of the LHC, Brussels, 2014 (unpublished), [https://fys.kuleuven.be/iks/wi/solvay\\_workshop\\_2014/](https://fys.kuleuven.be/iks/wi/solvay_workshop_2014/).
- [97] M. Brodeur, C. Nicoloff, T. Ahn, J. Allen, D. W. Bardayan, F. D. Becchetti, Y. K. Gupta, M. R. Hall, O. Hall, J. Hu, J. M. Kelly, J. J. Kolata, J. Long, P. O'Malley, and B. E. Schultz, *Phys. Rev. C* **93**, 025503 (2016).
- [98] P. Velten, M. L. Bissell, G. Neyens, and N. Severijns, Measurement of the  $\beta$ -asymmetry parameter in  $^{35}\text{Ar}$  decay with a laser polarized beam, CERN document CERN-INTC-2014-062; INTC-P-426; <https://cds.cern.ch/record/001953732>.
- [99] W. Gins, R. Harding, M. Baranowski, M. Bissell, R. G. Ruiz, M. Kowalska, G. Neyens, S. Pallada, N. Severijns, P. Velten, F. Wienholtz, Z. Xu, X. Yang, and D. Zakoucky, *Nucl. Instrum. Methods Phys. Res., Sect. A* **925**, 24 (2019).
- [100] W. Gins, Development of a dedicated laser-polarization beamline for ISOLDE-CERN, Ph.D. thesis, Katholieke Universiteit Leuven, 2019 (unpublished), <https://fys.kuleuven.be/iks/nm/phd-master-theses>.
- [101] J. Kopp, M. Maltoni, and T. Schwetz, *Phys. Rev. Lett.* **107**, 091801 (2011).
- [102] B. Dasgupta and J. Kopp, *Phys. Rep.* **928**, 1 (2021).
- [103] D. A. Dwyer and T. J. Langford, *Phys. Rev. Lett.* **114**, 012502 (2015).
- [104] A. C. Hayes, J. L. Friar, G. T. Garvey, G. Jungman, and G. Jonkmans, *Phys. Rev. Lett.* **112**, 202501 (2014).
- [105] J. Petković, T. Marketin, G. Martínez-Pinedo, and N. Paar, *J. Phys. G: Nucl. Part. Phys.* **46**, 085103 (2019).
- [106] M. Estienne, M. Fallot, A. Algora, J. Briz-Monago, V. M. Bui, S. Cormon, W. Gelletly, L. Giot, V. Guadilla, D. Jordan, L. Le Meur, A. Porta, S. Rice, B. Rubio, J. L. Taín, E. Valencia, and A.-A. Zakari-Issoufou, *Phys. Rev. Lett.* **123**, 022502 (2019).
- [107] X. Huyan, O. Naviliat-Cuncic, D. Bazin, A. Gade, M. Hughes, S. Liddick, K. Minamisono, S. Noji, S. V. Paulauskas, A. Simon, P. Voytas, and D. Weisshaar, *Hyperfine Interact.* **237**, 93 (2016).
- [108] X. Huyan, O. Naviliat-Cuncic, P. Voytas, S. Chandavar, M. Hughes, K. Minamisono, and S. Paulauskas, *Nucl. Instrum. Methods Phys. Res., Sect. A* **879**, 134 (2018).
- [109] X. Huyan, M. Hughes, and Naviliat-Cuncic, *Acta Phys. Pol. B* **49**, 249 (2018).
- [110] I. Mukul, M. Hass, O. Heber, T. Hirsh, Y. Mishnayot, M. Rappaport, G. Ron, Y. Shachar, and S. Vaintraub, *Acta Phys. Pol. B* **49**, 269 (2018).
- [111] O. Naviliat-Cuncic and X. Fléchar (private communication).
- [112] M. Hughes, E. A. George, O. Naviliat-Cuncic, P. A. Voytas, S. Chandavar, A. Gade, X. Huyan, S. N. Liddick, K. Minamisono, S. V. Paulauskas, and D. Weisshaar, *Phys. Rev. C* **97**, 054328 (2018).
- [113] L. DeKeukeleere, D. Rozpedzik, K. Bodek, L. Hayen, L. Lojek, M. Perkowski, N. Severijns, and S. Vanlangendonck, Beta spectrum shape measurements using a multi-wire drift chamber and a plastic scintillator, (2022), poS PANIC2021 450, Proc. Particles and Nuclei International Conference, 5-10 September 2021(online), <https://doi.org/10.22323/1.380.0450>.
- [114] S. Vanlangendonck and N. Severijns (private communication).
- [115] G. Azuelos, J. E. Kitching, and K. Ramavataram, *Phys. Rev. C* **15**, 1847 (1977).
- [116] ENSDF, <http://www.nndc.bnl.gov/ensdf/>, 2022.
- [117] V. Tishchenko *et al.* (MuLan Collaboration), *Phys. Rev. D* **87**, 052003 (2013).
- [118] P. A. Zyla *et al.* (Particle Data Group), *Progr. Theor. Exp. Phys.* **2020**, 083C01.
- [119] L. Hayen, N. Severijns, K. Bodek, D. Rozpedzik, and X. Mougeot, *Rev. Mod. Phys.* **90**, 015008 (2018).
- [120] S. Pastore, A. Baroni, J. Carlson, S. Gandolfi, S. C. Pieper, R. Schiavilla, and R. B. Wiringa, *Phys. Rev. C* **97**, 022501(R) (2018).
- [121] A. Sirlin, *Phys. Rev.* **164**, 1767 (1967).
- [122] I. Towner, *Nucl. Phys. A* **540**, 478 (1992).
- [123] C.-Y. Seng, M. Gorchtein, H. H. Patel, and M. J. Ramsey-Musolf, *Phys. Rev. Lett.* **121**, 241804 (2018).
- [124] C.-Y. Seng, M. Gorchtein, and M. J. Ramsey-Musolf, *Phys. Rev. D* **100**, 013001 (2019).
- [125] A. Czarnecki, W. J. Marciano, and A. Sirlin, *Phys. Rev. D* **100**, 073008 (2019).
- [126] K. Shiells, P. G. Blunden, and W. Melnitchouk, *Phys. Rev. D* **104**, 033003 (2021).
- [127] H. Behrens and W. Bühring, *Electron Radial Wave Functions and Nuclear Beta-Decay* (Clarendon, Oxford, 1982).
- [128] M. Gorchtein and C.-Y. Seng, *J. High Energy Phys.* **10** (2021) 053.
- [129] W. Huang, M. Wang, F. Kondev, G. Audi, and S. Naimi, Atomic mass adjustment, 2021, <https://www.anl.gov/sites/www/files/2021-03/mass.mas20.txt>.
- [130] W. Huang, M. Wang, F. Kondev, G. Audi, and S. Naimi, *Chin. Phys. C* **45**, 030002 (2021).
- [131] M. Wang, W. Huang, F. Kondev, G. Audi, and S. Naimi, *Chin. Phys. C* **45**, 030003 (2021).
- [132] G. Audi, A. Wapstra, and C. Thibault, *Nucl. Phys. A* **729**, 337 (2003), special issue, 2003 NUBASE and Atomic Mass Evaluations.
- [133] K. Olive, *Chin. Phys. C* **38**, 090001 (2014).
- [134] J. C. Hardy and I. S. Towner, *Phys. Rev. C* **71**, 055501 (2005).
- [135] F. M. Gonzalez *et al.* (UCN $\tau$  Collaboration), *Phys. Rev. Lett.* **127**, 162501 (2021).
- [136] B. Rubio (private communication).
- [137] E. G. Myers, A. Wagner, H. Kracke, and B. A. Wesson, *Phys. Rev. Lett.* **114**, 013003 (2015).

- [138] S. Nagy, T. Fritioff, M. Björkhage, I. Bergström, and R. Schuch, *Europhys. Lett.* **74**, 404 (2006).
- [139] R. S. Van Dyck, D. L. Farnham, and P. B. Schwinberg, *Phys. Rev. Lett.* **70**, 2888 (1993).
- [140] A. Czarnecki, W. J. Marciano, and A. Sirlin, *Phys. Rev. D* **70**, 093006 (2004).
- [141] D. Wilkinson, *Nucl. Phys. A* **377**, 474 (1982).
- [142] W. Bambynek, H. Behrens, M. H. Chen, B. Crasemann, M. L. Fitzpatrick, K. W. D. Ledingham, H. Genz, M. Mutterer, and R. L. Intemann, *Rev. Mod. Phys.* **49**, 77 (1977).
- [143] R. B. Firestone, *Table of Isotopes*, 8th ed. (John Wiley and Sons, New York, 1996).
- [144] I. S. Towner and J. C. Hardy, *Phys. Rev. C* **66**, 035501 (2002).
- [145] W. Satuła, P. Baczyk, J. Dobaczewski, and M. Konieczka, *Phys. Rev. C* **94**, 024306 (2016).
- [146] L. Xayavong and N. A. Smirnova, *Phys. Rev. C* **97**, 024324 (2018).
- [147] M. Gorchtein, *Phys. Rev. Lett.* **123**, 042503 (2019).
- [148] S. Raman, C. Houser, T. Walkiewicz, and I. Towner, *At. Data Nucl. Data Tables* **21**, 567 (1978).
- [149] K. Abusaleem and B. Singh, *Nucl. Data Sheets* **112**, 133 (2011).
- [150] N. Achouri and O. Naviliat-Cuncic (private communication).
- [151] N. L. Achouri, J. C. Angélique, G. Ban, B. Bastin, B. Blank, S. Dean, P. Dendooven, J. Giovinnazzo, S. Grévy, K. Jungmann, B. Laurent, E. Liénard, O. Naviliat-Cuncic, N. A. Orr, A. Rogachevskiy, M. Sohani, E. Traykov, and H. Wilschut, *J. Phys. G: Nucl. Part. Phys.* **37**, 045103 (2010).
- [152] E. G. Adelberger, M. M. Hindi, C. D. Hoyle, H. E. Swanson, and R. D. Von Lintig, *Phys. Rev. C* **24**, 313 (1981).
- [153] E. G. Adelberger, M. M. Hindi, C. D. Hoyle, H. E. Swanson, R. D. Von Lintig, and W. C. Haxton, *Phys. Rev. C* **27**, 2833 (1983).
- [154] E. Adelberger, J. Osborne, H. Swanson, and B. Brown, *Nucl. Phys. A* **417**, 269 (1984).
- [155] F. Ajzenberg-Selove, *Nucl. Phys. A* **152**, 1 (1970).
- [156] F. Ajzenberg-Selove, *Nucl. Phys. A* **248**, 1 (1975).
- [157] F. Ajzenberg-Selove, *Nucl. Phys. A* **375**, 1 (1982).
- [158] Y. Akulov and B. Mamyryn, *Phys. Lett. B* **600**, 41 (2004).
- [159] Yu. A. Akulov, B. A. Mamyryn, and L. V. Khabarin, *Pis'ma Zh. Tekh. Fiz.* **14**, 940 (1988) [*Sov. Tech. Phys. Lett.* **14**, 416 (1988)].
- [160] A. M. Aldridge, H. Plendl, and J. Aldridge, *Nucl. Phys. A* **98**, 323 (1967).
- [161] D. E. Alburger and D. H. Wilkinson, *Phys. Rev. C* **6**, 2019 (1972).
- [162] D. E. Alburger and D. H. Wilkinson, *Phys. Rev. C* **8**, 657 (1973).
- [163] D. E. Alburger, *Phys. Rev. C* **9**, 991 (1974).
- [164] D. E. Alburger, *Phys. Rev. C* **13**, 2593 (1976).
- [165] D. E. Alburger, *Phys. Rev. C* **16**, 889 (1977).
- [166] S. Arzumanov, L. Bondarenko, S. Chernyavsky, P. Geltenbort, V. Morozov, V. Nesvizhevsky, Y. Panin, and A. Strepetov, *Phys. Lett. B* **745**, 79 (2015).
- [167] S. Arnell, J. Dubois, and O. Almén, *Nucl. Phys.* **6**, 196 (1958).
- [168] Y. Arai, E. Tanaka, H. Miyatake, M. Yoshii, T. Ishimatsu, T. Shinozuka, and M. Fujioka, *Nucl. Phys. A* **420**, 193 (1984).
- [169] M. Awschalom, F. Larsen, and W. Schimmerling, *Nucl. Instrum. Methods* **75**, 93 (1969).
- [170] J. Äystö, J. Ärje, V. Koponen, P. Taskinen, H. Hyvönen, A. Hautojärvi, and K. Vierinen, *Phys. Lett. B* **138**, 369 (1984).
- [171] G. Azuelos, J. Crawford, and J. Kitching, *Nucl. Instrum. Methods* **117**, 233 (1974).
- [172] G. Azuelos and J. E. Kitching, *Phys. Rev. C* **12**, 563 (1975).
- [173] A. Bacquias, T. Kurtukian-Nieto, P. Ascher, L. Audirac, J. Äystö, B. Blank, V. V. Elomaa, T. Eronen, J. Giovinnazzo, J. Hakala, A. Jokinen, A. Kankainen, P. Karvonen, V. S. Kolhinen, I. D. Moore, S. Rahaman, M. Reponen, J. Rissanen, A. Saastamoinen, and J. Souin, *Eur. Phys. J. A* **48**, 155 (2012).
- [174] S. Bashkin, R. R. Carlson, and E. B. Nelson, *Phys. Rev.* **99**, 107 (1955).
- [175] T. T. Bardin, J. A. Becker, R. E. McDonald, and A. D. W. Jones, *Phys. Rev. C* **2**, 2283 (1970).
- [176] P. Barker, C. Sofield, R. Petty, J. Freeman, S. Hoath, W. Burcham, and G. Squier, *Nucl. Phys. A* **275**, 37 (1977).
- [177] P. Baumann, M. Bounajma, A. Huck, G. Klotz, A. Knipper, G. Walter, G. Marguier, C. Richard-Serre, H. Ravn, E. Hagebø, P. Hoff, and K. Steffensen, *Phys. Rev. C* **50**, 1180 (1994).
- [178] D. Behrens *et al.*, *Nucl. Phys. A* **178**, 76 (1971).
- [179] H. Behrens, M. Kobelt, L. Szybisz, and W.-G. Thies, *Nucl. Phys. A* **246**, 317 (1975).
- [180] B. Blank, *Eur. Phys. J. A* **15**, 121 (2002).
- [181] B. Blank *et al.*, *Eur. Phys. J. A* **44**, 363 (2010).
- [182] J. Black and J. Mahieux, *Nucl. Instrum. Methods* **58**, 93 (1968).
- [183] B. Blank, S. Andriamonje, S. Czajkowski, F. Davi, R. Del Moral, C. Donzaud, J. Dufour, A. Fleury, A. Grewe, R. Grzywacz, A. Heinz, Z. Hanas, A. Junghans, M. Lewitowicz, A. Musquère, M. Pravikoff, M. Pfützner, and J.-E. Sauvestre, *Phys. Lett. B* **364**, 8 (1995).
- [184] B. Blank, *J. Phys. G: Nucl. Part. Phys.* **25**, 629 (1999).
- [185] M. Bormann, E. Fretwurst, P. Schehka, G. Wrege, H. Büttner, A. Lindner, and H. Meldner, *Nucl. Phys.* **63**, 438 (1965).
- [186] L. J. Broussard, H. O. Back, M. S. Boswell, A. S. Crowell, P. Dendooven, G. S. Giri, C. R. Howell, M. F. Kidd, K. Jungmann, W. L. Kruithof, A. Mol, C. J. G. Onderwater, R. W. Pattie, P. D. Shidling, M. Sohani, D. J. van der Hoek, A. Rogachevskiy, E. Traykov, O. O. Versolato, L. Willmann *et al.*, *Phys. Rev. Lett.* **112**, 212301 (2014).
- [187] T. Burrows, *Nucl. Data Sheets* **108**, 923 (2007).
- [188] T. Burrows, *Nucl. Data Sheets* **109**, 171 (2008).
- [189] D. P. Burdette, M. Brodeur, D. W. Bardayan, F. D. Becchetti, D. Blankstein, C. Boomershine, L. Caves, S. L. Henderson, J. J. Kolata, B. Liu, J. Long, P. D. O'Malley, and S. Y. Strauss, *Phys. Rev. C* **101**, 055504 (2020).
- [190] T. W. Burrows, J. W. Olness, and D. E. Alburger, *Phys. Rev. C* **31**, 1490 (1985).
- [191] B. Budick, J. Chen, and H. Lin, *Phys. Rev. Lett.* **67**, 2630 (1991).
- [192] J. Byrne, P. G. Dawber, C. G. Habeck, S. J. Smidt, J. A. Spain, and A. P. Williams, *Europhys. Lett.* **33**, 187 (1996).
- [193] I. Čeliković, M. Lewitowicz, R. Gernhäuser, R. Krücken, S. Nishimura, H. Sakurai, D. Ahn, H. Baba, B. Blank, A. Blazhev, P. Boutachkov, F. Browne, G. de France, P. Doornenbal, T. Faestermann, Y. Fang, N. Fukuda, J. Giovinnazzo, N. Goel, M. Górka *et al.*, *Phys. Rev. Lett.* **116**, 162501 (2016).
- [194] J. E. Cline and P. R. Chagnon, *Bull. Amer. Phys. Soc.* **3**, 206 (1958).
- [195] P. Davies, H. Grawe, K. Moschner, A. Blazhev, R. Wadsworth, P. Boutachkov, F. Ameil, A. Yagi, H. Baba, T. Bäck, M. Dewald, P. Doornenbal, T. Faestermann, A. Gengelbach, J.

- Gerl, R. Gernhaeuser, S. Go, M. Gorska, E. Gregor, T. Isobe *et al.*, *Phys. Lett. B* **767**, 474 (2017).
- [196] W. W. Daehnick and R. D. Rosa, *Phys. Rev. C* **31**, 1499 (1985).
- [197] C. Detrax, C. Moss, and C. Zaidins, *Phys. Lett. B* **34**, 128 (1971).
- [198] J. M. Dickson and T. C. Randle, *Proc. Phys. Soc., London, Sect. A* **64**, 902 (1951).
- [199] L. G. Earwaker, J. G. Jenkin, and E. W. Titterton, *Nature (London)* **195**, 271 (1962).
- [200] T. G. Ebrey and P. R. Gray, *Nucl. Phys.* **61**, 479 (1965).
- [201] M. Edmiston, R. Warner, W. McHarris, and W. Kelly, *Nucl. Instrum. Methods* **141**, 315 (1977).
- [202] G. Ewan, E. Hagberg, P. Hansen, B. Jonson, S. Mattsson, H. Ravn, and P. Tidemand-Petersson, *Nucl. Phys. A* **352**, 13 (1981).
- [203] V. F. Ezhov, A. Z. Andreev, G. Ban, B. A. Bazarov, P. Geltenbort, A. G. Glushkov, V. A. Knyazkov, N. A. Kovrizhnykh, G. B. Krygin, O. Naviliat-Cuncic, and V. L. Ryabov, *JETP Lett.* **107**, 671 (2018).
- [204] T. Faestermann, R. Schneider, A. Stolz, K. Summerer, E. Wefers, J. Friese, H. Geissel, M. Hellstrom, P. Kienle, H.-J. Korner, M. Mineva, M. Munch, G. Munzenberg, C. Schlegel, K. Schmidt, P. Thirof, H. Weick, and K. Zeitelhack, *Eur. Phys. J. A* **15**, 185 (2002).
- [205] S. M. Fischer, T. Anderson, P. Kerns, G. Mesoloras, D. Svelnys, C. J. Lister, D. P. Balamuth, P. A. Hausladen, and D. G. Sarantites, *Phys. Rev. C* **72**, 024321 (2005).
- [206] P. Finlay, A. T. Laffoley, G. C. Ball, P. C. Bender, M. R. Dunlop, R. Dunlop, G. Hackman, J. R. Leslie, A. D. MacLean, D. Miller, M. Moukaddam, B. Olaizola, N. Severijns, J. K. Smith, D. Southall, and C. E. Svensson, *Phys. Rev. C* **96**, 025501 (2017).
- [207] C. Fontbonne, P. Ujic, F. de Oliveira Santos, X. Flechard, F. Rotaru, N. L. Achouri, V. G. Alcindor, B. Bastin, F. Boulay, J. B. Briand, A. M. Sanchez-Benitez, H. Bouzomita, C. Borcea, R. Borcea, B. Blank, B. Carniol, I. Celikovic, P. Delahaye, F. Delaunay, D. Etasse *et al.*, *Phys. Rev. C* **96**, 065501 (2017).
- [208] J. S. Geiger and B. W. Hooton, *Can. J. Phys.* **49**, 663 (1971).
- [209] H. Genz, J. Reisberg, A. Richter, B. Schmitz, G. Schrieder, K. Werner, and H. Behrens, *Nucl. Instrum. Methods* **134**, 309 (1976).
- [210] J. Giovinazzo *et al.*, *Acta Phys. Pol. B* **51**, 577 (2020).
- [211] S. Gorodetzky, A. Gallmann, G. Frick, J. Coffin, and F. Jundt, in *Comptes Rendus du Congrès International de Physique Nucléaire*, ditions du Centre National de la Recherche Scientifique, Paris (1964), Vol. II, p. 408.
- [212] J. Goss, F. Riffle, D. Parsignault, and J. Harris, *Nucl. Phys. A* **115**, 113 (1968).
- [213] S. Gorodetzky, E. Aslanides, A. Gallmann, and G. Frick, *Nucl. Phys. A* **109**, 417 (1968).
- [214] J. Grinyer, G. F. Grinyer, M. Babo, H. Bouzomita, P. Chauveau, P. Delahaye, M. Dubois, R. Frigot, P. Jardin, C. Leboucher, L. Maunoury, C. Seiffert, J. C. Thomas, and E. Traykov, *Phys. Rev. C* **91**, 032501(R) (2015).
- [215] J. Grinyer, G. F. Grinyer, M. Babo, H. Bouzomita, P. Chauveau, P. Delahaye, M. Dubois, R. Frigot, P. Jardin, C. Leboucher, L. Maunoury, C. Seiffert, J. C. Thomas, and E. Traykov, *Phys. Rev. C* **92**, 045503 (2015).
- [216] D. Grober and W. Gruhle, Institut fuer Anorganische Chemie und Kernchemie, Mainz University, Report No. BMBW-FBK-71-09, 1971 (unpublished), p. 90.
- [217] R. N. H. Haslam *et al.*, *Can. J. Phys.* **30**, 257 (1952).
- [218] E. Hagberg, J. Hardy, B. Jonson, S. Mattsson, and P. Tidemand-Petersson, *Nucl. Phys. A* **313**, 276 (1979).
- [219] J. Hardy, H. Schmeing, E. Hagberg, W. Perry, J. Wills, E. Clifford, V. Koslowsky, I. Towner, J. Camplan, B. Rosenbaum, R. Kirchner, and H. Evans, *Phys. Lett. B* **91**, 207 (1980).
- [220] H. Hama, M. Yoshii, K. Taguchi, T. Ishimatsu, T. Shinozuka, and M. Fujioka, in *Nuclei Far From Stability: 5th International Conference*, September 1987, Rosseau Lake, ON, Canada, edited by I. S. Towner, AIP Conf. Proc. No. 164 (AIP, New York, 1987), p. 650.
- [221] E. Hagberg, T. Alexander, I. Neeson, V. Koslowsky, G. Ball, G. Dyck, J. Forster, J. Hardy, J. Leslie, H. Mak, H. Schmeing, and I. Towner, *Nucl. Phys. A* **571**, 555 (1994).
- [222] E. Hagberg, I. S. Towner, T. K. Alexander, G. C. Ball, J. S. Forster, J. C. Hardy, J. G. Hykawy, V. T. Koslowsky, J. R. Leslie, H.-B. Mak, I. Neeson, and G. Savard, *Phys. Rev. C* **56**, 135 (1997).
- [223] P. Hornshoj, L. Hojsholt-Poulsen, and N. Rud, *Nucl. Phys. A* **288**, 429 (1977).
- [224] J. Honkanen, M. Kortelahti, K. Eskola, and K. Vierinen, *Nucl. Phys. A* **366**, 109 (1981).
- [225] P. Hornshoj, J. Kolind, and N. Rud, *Phys. Lett. B* **116**, 4 (1982).
- [226] J. Honkanen, V. Koponen, H. Hyvonen, P. Taskinen, J. ysto, and K. Ogawa, *Nucl. Phys. A* **471**, 489 (1987).
- [227] J. Honkanen, V. Koponen, P. Taskinen, K. Eskola, J. ysto, S. Messelt, and K. Ogawa, *Nucl. Phys. A* **496**, 462 (1989).
- [228] J. Huikari, M. Oinonen, A. Algora, J. Cederkall, S. Courtin, P. Dessagne, L. Fraile, S. Franchoo, H. Fynbo, W. Huang, A. Jokinen, A. Knipper, F. Marechal, C. Miehe, E. Nacher, K. Perajarvi, E. Poirier, L. Weissman, J. ysto, and the ISOLDE Collaboration, *Eur. Phys. J. A* **16**, 359 (2003).
- [229] S. E. Hunt, R. Kline, and D. Zaffarano, *Phys. Rev.* **95**, 611A (1954).
- [230] V. E. Jacob, J. C. Hardy, J. F. Brinkley, C. A. Gagliardi, V. E. Mayes, N. Nica, M. Sanchez-Vega, G. Tabacaru, L. Trache, and R. E. Tribble, *Phys. Rev. C* **74**, 055502 (2006).
- [231] J. Janecke, *Z. Naturforsch. A* **15**, 593 (1960).
- [232] J. Jonecke and H. Hung, *Z. Phys.* **165**, 94 (1961).
- [233] Z. Janas, C. Chandler, B. Blank, P. H. Regan, A. M. Bruce, W. N. Catford, N. Curtis, S. Czajkowski, P. Dessagne, A. Fleury, W. Gelletly, J. Giovinazzo, R. Grzywacz, M. Lewitowicz, C. Longour, C. Marchand, C. Miehe, N. A. Orr, R. D. Page, C. J. Pearson *et al.*, *Phys. Rev. Lett.* **82**, 295 (1999).
- [234] G. H. Jenks, F. H. Sweeton, and J. A. Ghormley, *Phys. Rev.* **80**, 990 (1950).
- [235] W. M. Jones, *Phys. Rev.* **83**, 537 (1951).
- [236] W. M. Jones, *Phys. Rev.* **100**, 124 (1955).
- [237] P. Jones, *J. Nucl. Mater.* **21**, 239 (1967).
- [238] H. Junde, H. Xiaolong, and J. Tuli, *Nucl. Data Sheets* **106**, 159 (2005).
- [239] H. Junde, *Nucl. Data Sheets* **109**, 787 (2008).
- [240] F. Jundt, E. Aslanides, B. Fride, and A. Gallmann, *Nucl. Phys. A* **170**, 12 (1971).

- [241] A. Kankainen, T. Eronen, D. Gorelov, J. Hakala, A. Jokinen, V. S. Kolhinen, M. Reponen, J. Rissanen, A. Saastamoinen, V. Sonnenschein, and J. Äystö, *Phys. Rev. C* **89**, 051302(R) (2014).
- [242] R. W. Kavanagh and D. R. Goosman, *Phys. Lett.* **12**, 229 (1964); Erratum: **13**, 358 (1964).
- [243] T. M. Kavanagh, K. P. Lee, and W. T. Link, *Can. J. Phys.* **42**, 1429 (1964).
- [244] J. A. Kadlecěk, *Bull. Amer. Phys. Soc.* **13**, 676 (1968).
- [245] P. Kienle, T. Faestermann, J. Friese, H.-J. Körner, M. Münch, R. Schneider, A. Stolz, E. Wefers, H. Geissel, G. Münzenberg, C. Schlegel, K. Sümmerer, H. Weick, M. Hellström, and P. Thirolf, *Prog. Part. Nucl. Phys.* **46**, 73 (2001).
- [246] O. C. Kistner and B. M. Rustad, *Phys. Rev.* **114**, 1329 (1959).
- [247] J. D. King, R. N. H. Haslam, and R. W. Parsons, *Can. J. Phys.* **38**, 231 (1960).
- [248] R. M. Kline and D. J. Zaffarano, *Phys. Rev.* **96**, 1620 (1954).
- [249] S. Kochan, B. Rosner, I. Tserruya, and R. Kalish, *Nucl. Phys. A* **204**, 185 (1973).
- [250] D. N. Kundu, T. W. Donaven, M. L. Pool, and J. K. Long, *Phys. Rev.* **89**, 1200 (1953).
- [251] T. Kurtukian-Nieto, B. Blank, P. Ascher, M. Gerbaux, J. Giovinazzo, S. Grévy, and M. Versteegen, Centre d'Études Nucléaires de Bordeaux Gradignan, Rapport d'Activité 2015–2019, 2017 (unpublished), p. 71.
- [252] L. Kucuk, S. E. A. Orrigo, A. Montaner-Pizá, B. Rubio, Y. Fujita, W. Gelletly, B. Blank, Y. Oktem, T. Adachi, A. Algora, P. Ascher, R. B. Cakirli, G. de France, H. Fujita, E. Ganioglu, J. Giovinazzo, S. Grévy, F. M. Marqués, F. Molina, F. de Oliveira Santos, L. Perrot, R. Raabe, P. C. Srivastava, G. Susoy, A. Tamii, and J. C. Thomas, *Eur. Phys. J. A* **53**, 134 (2017).
- [253] K. H. Lindenberger and J. A. Scheer, *Z. Phys.* **158**, 111 (1960).
- [254] M. J. López Jiménez, B. Blank, M. Chartier, S. Czajkowski, P. Dessagne, G. de France, J. Giovinazzo, D. Karamanis, M. Lewitowicz, V. Maslov, C. Miché, P. H. Regan, M. Stanoiu, and M. Wiescher, *Phys. Rev. C* **66**, 025803 (2002).
- [255] J. Long, T. Ahn, J. Allen, D. W. Bardayan, F. D. Becchetti, D. Blankstein, M. Brodeur, D. Burdette, B. Frenzt, M. R. Hall, J. M. Kelly, J. J. Kolata, P. D. O'Malley, B. E. Schultz, S. Y. Strauss, and A. A. Valverde, *Phys. Rev. C* **96**, 015502 (2017).
- [256] J. Long, M. Brodeur, M. Baines, D. W. Bardayan, F. D. Becchetti, D. Blankstein, C. Boomershine, D. P. Burdette, A. M. Clark, B. Frenzt, S. L. Henderson, J. M. Kelly, J. J. Kolata, B. Liu, K. T. Macon, P. D. O'Malley, A. Pardo, C. Seymour, S. Y. Strauss, and B. Vande Kolk, *Phys. Rev. C* **101**, 015501 (2020).
- [257] O. Lönsjö, *Physica Norvegica* **1**, 41 (1962).
- [258] L. L. Lucas and M. P. Unterwieser, *J. Res. Natl. Inst. Stand. Technol.* **105**, 541 (2000).
- [259] D. MacMahon, *Appl. Radiat. Isot.* **64**, 1417 (2006).
- [260] C. Magron, P. Alfaut, B. Blank, L. Daudin, T. Eronen, M. Gerbaux, J. Giovinazzo, D. Gorelov, S. Grévy, H. Guérin, J. Hakala, V. S. Kolhinen, J. Koponen, T. Kurtukian Nieto, I. D. Moore, H. Penttilä, I. Pohjalainen, J. Reinikainen, M. Reponen, S. Rinta-Antila *et al.*, *Eur. Phys. J. A* **53**, 77 (2017).
- [261] L. Makela, P. B. Dworkin, and A. E. Litherla, *Bull. Am. Phys. Soc.* **14**, 550 (1969).
- [262] F. M. Mann and R. W. Kavanagh, *Nucl. Phys. A* **235**, 299 (1974).
- [263] F. Mann, H. Wilson, and R. Kavanagh, *Nucl. Phys. A* **258**, 341 (1976).
- [264] W. Mampe, L. N. Bondarenko, V. I. Morozov, Y. N. Panin, and A. I. Fomin, *Pis'ma Zh. Eksp. Teor. Fiz.* **57**, 77 (1993) [*JETP Lett.* **57**, 82 (1993)].
- [265] J. S. Merritt and J. G. V. Taylor, Atomic Energy of Canada Ltd., Chalk River Laboratory, Chalk River, Ontario, Report No. AECL-2510, 1966 (unpublished).
- [266] M. V. Mihailović and B. Povh, *Nucl. Phys.* **7**, 296 (1958).
- [267] C. Moss, C. Détraz, and C. Zaidins, *Nucl. Phys. A* **170**, 111 (1971).
- [268] D. Morrissey and the A1200 Group, in *Proceedings of the Fifth International Symposium on Physics of Unstable Nuclei* [*Nucl. Phys. A* **588**, c203 (1995)].
- [269] T. Muller, E. Gelsema, and P. Endt, *Physica* **24**, 577 (1958).
- [270] A. Negret and B. Singh, *Nucl. Data Sheets* **114**, 841 (2013).
- [271] J. W. Nelson, E. B. Carter, G. E. Mitchell, and R. H. Davis, *Phys. Rev.* **129**, 1723 (1963).
- [272] A. Novick, *Phys. Rev.* **72**, 972 (1947).
- [273] M. Oinonen, A. Jokinen, J. Äystö, P. Baumann, F. Didierjean, A. Honkanen, A. Huck, M. Huysse, A. Knipper, G. Marguier, Y. Novikov, A. Popov, M. Ramdhane, D. M. Seliverstov, P. Van Duppen, G. Walter, *Phys. Rev. C* **56**, 745 (1997).
- [274] M. Oinonen, P. Baumann, P. Dendooven, Y. Fujita, M. Górška, H. Grawe, Z. Hu, Z. Janas, A. Jokinen, R. Kirchner, O. Klepper, A. Knipper, W. Liu, H. Penttilä, A. Plochocki, M. Ramdhane, E. Roeckl, G. Walter, and J. Äystö, *Eur. Phys. J. A* **5**, 151 (1999).
- [275] B. M. Oliver, H. Farrar, and M. Bretscher, *Intern. J. Radiat. Applic. Instrum. Part A, Appl. Radiat. Isot.* **38**, 959 (1987).
- [276] S. E. A. Orrigo, B. Rubio, W. Gelletly, P. Aguilera, A. Algora, A. I. Morales, J. Agramunt, D. S. Ahn, P. Ascher, B. Blank, C. Borcea, A. Boso, R. B. Cakirli, J. Chiba, G. de Angelis, G. de France, F. Diel, P. Doornenbal, Y. Fujita, N. Fukuda *et al.*, *Phys. Rev. C* **103**, 014324 (2021).
- [277] R. W. Pattie, N. B. Callahan, C. Cude-Woods, E. R. Adamek, L. J. Broussard, S. M. Clayton, S. A. Currie, E. B. Dees, X. Ding, E. M. Engel, D. E. Fellers, W. Fox, P. Geltenbort, K. P. Hickerson, M. A. Hoffbauer, A. T. Holley, A. Komives, C.-Y. Liu, S. W. T. MacDonald, M. Makela *et al.*, *Science* **360**, 627 (2018).
- [278] J. Park, R. Krücken, D. Lubos, R. Gernhäuser, M. Lewitowicz, S. Nishimura, D. S. Ahn, H. Baba, B. Blank, A. Blazhev, P. Boutachkov, F. Browne, I. Čeliković, G. de France, P. Doornenbal, T. Faestermann, Y. Fang, N. Fukuda, J. Giovinazzo, N. Goel *et al.*, *Phys. Rev. C* **97**, 051301 (2018).
- [279] J. R. Penning and F. H. Schmidt, *Phys. Rev.* **105**, 647 (1957).
- [280] R. Pfaff, D. J. Morrissey, W. Benenson, M. Fauerbach, M. Hellström, C. F. Powell, B. M. Sherrill, M. Steiner, and J. A. Winger, *Phys. Rev. C* **53**, 1753 (1996).
- [281] A. Pichlmaier, V. Varlamov, K. Schreckenbach, and P. Geltenbort, *Phys. Lett. B* **693**, 221 (2010).
- [282] L. E. Piilonen, Ph.D. thesis, Princeton University, 1985 (unpublished).
- [283] H. S. Plendl *et al.*, in *Conference on Low Energy Nuclear Physics, Harwell, September 1962*, AERA-R-4131 (unpublished), p. 22, abstract 7a8.
- [284] M. M. Povov, Y. Gagarinskii, M. Senin, T. Mikhalenko, and Y. Morozov, *Sov. J. At. Energy* **4**, 393 (1958).
- [285] I. D. Prokoshkin and A. A. Tiapkin, *J. Exptl. Theoret. Phys.* **32**, 177 (1957) [*Sov. Phys. JETP* **5**, 148 (1957)].
- [286] B. M. Rebeiro, S. Triambak, P. Z. Mabika, P. Finlay, C. S. Sumithrarachchi, G. Hackman, G. C. Ball, P. E. Garrett, C. E.

- Svensson, D. S. Cross, R. Dunlop, A. B. Garnsworthy, R. Kshetri, J. N. Orce, M. R. Pearson, E. R. Tardiff, H. Al-Falou, R. A. E. Austin, R. Churchman, M. K. Djongolov *et al.*, *Phys. Rev. C* **99**, 065502 (2019).
- [287] I. Reusen, A. Andreyev, J. Andrzejewski, N. Bijmens, S. Franchoo, M. Huyse, Y. Kudryavtsev, K. Kruglov, W. F. Mueller, A. Piechaczek, R. Raabe, K. Rykaczewski, J. Szerypo, P. Van Duppen, L. Vermeeren, J. Wauters, and A. Wöhr, *Phys. Rev. C* **59**, 2416 (1999).
- [288] A. Ritchie, *Nucl. Instrum. Methods* **64**, 181 (1968).
- [289] A. Rogers, J. Giovinazzo, C. Lister, B. Blank, G. Canchel, J. Clark, G. de France, S. Grévy, S. Gros, E. McCutchan, F. de Oliveira Santos, G. Savard, D. Seweryniak, I. Stefan, and J.-C. Thomas, *Nucl. Data Sheets* **120**, 41 (2014).
- [290] H. Roderick, O. Lönsjö, and W. E. Meyerhof, *Phys. Rev.* **97**, 97 (1955).
- [291] B. Rubio, S. Orrigo, L. Kucuk, A. Montaner-Pizá, Y. Fujita, H. Fujita, B. Blank, W. Gelletly, T. Adachi, J. Agramunt, A. Algora, P. Ascher, B. Bilgier, L. Cáceres, R. Cakirli, G. de France, E. Ganioglu, M. Gerbaux, J. Giovinazzo, S. Grevy *et al.*, *Nucl. Data Sheets* **120**, 37 (2014).
- [292] C. R. Rudy and K. C. Jordan, U.s. Depratment of Energy, Mound Lab, Miamisburg, OH, Report No. MLM-2458, 1977 (unpublished).
- [293] K. Rykaczewski, R. Anne, G. Auger, D. Bazin, C. Borcea, V. Borrel, J. M. Corre, T. Dörfler, A. Fomichov, R. Grzywacz, D. Guillemaud-Mueller, R. Hue, M. Huyse, Z. Janas, H. Keller, M. Lewitowicz, S. Lukyanov, A. C. Mueller, Y. Penionzhkevich, M. Pfützner *et al.*, *Phys. Rev. C* **52**, R2310 (1995).
- [294] E. R. J. Saettler, F. P. Calaprice, A. L. Hallin, and M. M. Lowry, *Phys. Rev. C* **48**, 3069 (1993).
- [295] A. D. Schelberg, M. B. Sampson, and A. C. G. Mitchell, *Rev. Sci. Instrum.* **19**, 458 (1948).
- [296] F. Schweizer, *Phys. Rev.* **110**, 1414 (1958).
- [297] P. J. Scanlon and D. Crabtree, *Can. J. Phys.* **48**, 1578 (1970).
- [298] A. Serebrov, V. Varlamov, A. Kharitonov, A. Fomin, Y. Pokotilovski, P. Geltenbort, J. Butterworth, I. Krasnoschekova, M. Lasakov, R. Tal'daev, A. Vassiljev, and O. Zhrebetsov, *Phys. Lett. B* **605**, 72 (2005).
- [299] N. Severijns and B. Blank, *J. Phys. G: Nucl. Part. Phys.* **44**, 074002 (2017).
- [300] A. P. Serebrov, E. A. Kolomensky, A. K. Fomin, I. A. Krasnoschekova, A. V. Vassiljev, D. M. Prudnikov, I. V. Shoka, A. V. Chechkin, M. E. Chaikovskiy, V. E. Varlamov, S. N. Ivanov, A. N. Pirozhkov, P. Geltenbort, O. Zimmer, T. Jenke, M. Van der Grinten, and M. Tucker, *Phys. Rev. C* **97**, 055503 (2018).
- [301] D. R. Semon, M. C. Allen, H. Dejbakhsh, C. A. Gagliardi, S. E. Hale, J. Jiang, L. Trache, R. E. Tribble, S. J. Yennello, H. M. Xu, X. G. Zhou, and B. A. Brown, *Phys. Rev. C* **53**, 96 (1996).
- [302] P. D. Shidling *et al.*, *Phys. Rev. C* **90**, 032501(R) (2014).
- [303] Y. P. Shen, W. P. Liu, J. Su, N. T. Zhang, L. Jing, Z. H. Li, Y. B. Wang, B. Guo, S. Q. Yan, Y. J. Li, S. Zeng, G. Lian, X. C. Du, L. Gan, X. X. Bai, J. S. Wang, Y. H. Zhang, X. H. Zhou, X. D. Tang, J. J. He *et al.*, *Phys. Rev. C* **91**, 047304 (2015).
- [304] P. D. Shidling, R. S. Behling, B. Fenker, J. C. Hardy, V. E. Iacob, M. Mehlman, H. I. Park, B. T. Roeder, and D. Melconian, *Phys. Rev. C* **98**, 015502 (2018).
- [305] T. Shinozuka, M. Fujioka, H. Miyatake, M. Yoshii, H. Hama, and T. Kamiya, *Phys. Rev. C* **30**, 2111 (1984).
- [306] T. Shinozuka *et al.*, *Proceeding of the XXIII Yamada Conference: Nuclear Weak Processes and Nuclear Structure, Osaka, 1989*, edited by M. Morita, H. Ejiri, H. Ohtsubo and T. Sato (World Sci., Singapore, 1989), p. 108.
- [307] B. M. Sherrill *et al.*, *Proceedings of the 6th International Conference on Atomic Masses and Fundamental Constants, Germany, 1992*, edited by R. Neugart and A. Wöhr (1993), p. 891.
- [308] B. Singh, *Nucl. Data Sheets* **106**, 601 (2005).
- [309] L. Sinclair, R. Wadsworth, J. Dobaczewski, A. Pastore, G. Lorusso, H. Suzuki, D. S. Ahn, H. Baba, F. Browne, P. J. Davies, P. Doornenbal, A. Estrade, Y. Fang, N. Fukuda, J. Henderson, T. Isobe, D. G. Jenkins, S. Kubono, Z. Li, D. Lubos *et al.*, *Phys. Rev. C* **100**, 044311 (2019).
- [310] J. J. Simpson, *Phys. Rev. C* **35**, 752 (1987).
- [311] J. H. C. Smith and D. B. Cowie, *J. Appl. Phys.* **12**, 78 (1941).
- [312] K. Straub, *Zerfallseigenschaften von Nukliden in der Umgebung von  $^{100}\text{Sn}$* , Ph.D. thesis, Technische Universität Munchen, 2011 (unpublished), <https://d-nb.info/1010249754/34>.
- [313] A. Steyerl, J. M. Pendlebury, C. Kaufman, S. S. Malik, and A. M. Desai, *Phys. Rev. C* **85**, 065503 (2012).
- [314] J. Su, W. P. Liu, N. C. Shu, S. Q. Yan, Z. H. Li, B. Guo, W. Z. Huang, S. Zeng, E. T. Li, S. J. Jin, X. Liu, Y. B. Wang, G. Lian, Y. J. Li, Y. S. Chen, X. X. Bai, J. S. Wang, Y. Y. Yang, R. F. Chen, S. W. Xu *et al.*, *Phys. Rev. C* **87**, 024312 (2013).
- [315] H. Suzuki, T. Kubo, N. Fukuda, N. Inabe, D. Kameda, H. Takeda, K. Yoshida, K. Kusaka, Y. Yanagisawa, M. Ohtake, H. Sato, Y. Shimizu, H. Baba, M. Kurokawa, T. Ohnishi, K. Tanaka, O. Tarasov, D. Bazin, D. Morrissey, B. Sherrill *et al.*, in *XVth International Conference on ElectroMagnetic Isotope Separators and Techniques Related to their Applications*, December 2–7, 2012 at Matsue, Japan [*Nucl. Instrum. Methods Phys. Res., Sect. B* **317**, 756 (2013)].
- [316] H. Suzuki, T. Kubo, N. Fukuda, N. Inabe, D. Kameda, H. Takeda, K. Yoshida, K. Kusaka, Y. Yanagisawa, M. Ohtake, H. Sato, Y. Shimizu, H. Baba, M. Kurokawa, K. Tanaka, O. B. Tarasov, D. Bazin, D. J. Morrissey, B. M. Sherrill, K. Ieki *et al.*, *Phys. Rev. C* **96**, 034604 (2017).
- [317] D. C. Sutton, Ph.D. thesis, Princeton University, 1962 (unpublished).
- [318] W. L. Talbert and M. G. Stewart, *Phys. Rev.* **119**, 272 (1960).
- [319] I. Tanihata, T. Minamisono, A. Mizobuchi, and K. Sugimoto, *J. Phys. Soc. Jpn.* **34**, 848 (1973).
- [320] D. Tilley, H. Weller, and H. Hasan, *Nucl. Phys. A* **474**, 1 (1987).
- [321] S. Triambak, P. Finlay, C. S. Sumithrarachchi, G. Hackman, G. C. Ball, P. E. Garrett, C. E. Svensson, D. S. Cross, A. B. Garnsworthy, R. Kshetri, J. N. Orce, M. R. Pearson, E. R. Tardiff, H. Al-Falou, R. A. E. Austin, R. Churchman, M. K. Djongolov, R. D'Entremont, C. Kierans, L. Milovanovic *et al.*, *Phys. Rev. Lett.* **109**, 042301 (2012).
- [322] P. Ujjic, F. de Oliveira Santos, M. Lewitowicz, N. L. Achouri, M. Assié, B. Bastin, C. Borcea, R. Borcea, A. Buta, A. Coc, G. de France, O. Kamalou, J. Kiener, A. Lepailleur, V. Meot, A. Pautrat, M. G. Saint Laurent, O. Sorlin, M. Stanoiu, and V. Tatischeff, *Phys. Rev. Lett.* **110**, 032501 (2013).
- [323] M. Unterweger and L. Lucas, *Appl. Radiat. Isot.* **52**, 527 (2000).

- [324] A. A. Valverde, M. Brodeur, T. Ahn, J. Allen, D. W. Bardayan, F. D. Becchetti, D. Blankstein, G. Brown, D. P. Burdette, B. Frentz, G. Gilardy, M. R. Hall, S. King, J. J. Kolata, J. Long, K. T. Macon, A. Nelson, P. D. O'Malley, M. Skulski, S. Y. Strauss *et al.*, *Phys. Rev. C* **97**, 035503 (2018).
- [325] S. S. Vasil'ev and L. Ya. Shavtvalov, *J. Exptl. Theoret. Phys.* **45**, 1385 (1963) [*Sov. Phys. JETP* **18**, 995 (1963)].
- [326] S. S. Vasilev, N. N. Kolesnikov, and L. Y. Shavtvalov, *Vestn. Mosk. Univ. Fiz. Astron.* **5**, 3 (1969).
- [327] R. Wallace and J. A. Welch, *Phys. Rev.* **117**, 1297 (1960).
- [328] L. Weissman, J. Cederkall, J. Äystö, H. Fynbo, L. Fraile, V. Fedosseyev, S. Franchoo, A. Jokinen, U. Köster, G. Martínez-Pinedo, T. Nilsson, M. Oinonen, K. Peräjärvi, M. D. Seliverstov, and the ISOLDE Collaboration, *Phys. Rev. C* **65**, 044321 (2002).
- [329] G. Wick, D. Robinson, and J. Freeman, *Nucl. Phys. A* **138**, 209 (1969).
- [330] D. H. Wilkinson and D. E. Alburger, *Phys. Rev. C* **10**, 1993 (1974).
- [331] H. S. Wilson, R. W. Kavanagh, and F. M. Mann, *Phys. Rev. C* **22**, 1696 (1980).
- [332] J. A. Winger, D. P. Bazin, W. Benenson, G. M. Crawley, D. J. Morrissey, N. A. Orr, R. Pfaff, B. M. Sherrill, M. Thoennessen, S. J. Yennello, and B. M. Young, *Phys. Rev. C* **48**, 3097 (1993).
- [333] D. Woods, M. Baker, J. Keightley, L. Keightley, J. Makepeace, A. Pearce, A. Woodman, M. Woods, S. Woods, and S. Waters, *Appl. Radiat. Isot.* **56**, 327 (2002).
- [334] V. K. Wohlleben and E. Schuster, *Radiochimica Acta* **12**, 75 (1969).
- [335] D.H. Youngblood, J. Aldridge, and C. Class, *Nucl. Phys.* **65**, 602 (1965).
- [336] A. T. Yue, M. S. Dewey, D. M. Gilliam, G. L. Greene, A. B. Laptev, J. S. Nico, W. M. Snow, and F. E. Wietfeldt, *Phys. Rev. Lett.* **111**, 222501 (2013).
- [337] K. Zuber and B. Singh, *Nucl. Data Sheets* **125**, 1 (2015).
- [338] B. R. Holstein, *Phys. Rev. C* **10**, 1215 (1974).
- [339] L. Hayen and N. Severijns, *Comput. Phys. Commun.* **240**, 152 (2019).
- [340] E. C. G. Sudarshan and R. E. Marshak, *Phys. Rev.* **109**, 1860 (1958).
- [341] F. P. Calaprice, S. J. Freedman, W. C. Mead, and H. C. Vantine, *Phys. Rev. Lett.* **35**, 1566 (1975).
- [342] G. Jones, A Measurement of the Beta Decay Asymmetry of  $^{19}\text{Ne}$  as a Test of the Standard Model, Ph.D. thesis, Princeton University, 1996 (unpublished), <https://ui.adsabs.harvard.edu/abs/1996PhDT.....10J/abstract>.
- [343] G. S. Masson and P. A. Quin, *Phys. Rev. C* **42**, 1110 (1990).
- [344] J. D. Garnett, E. D. Commins, K. T. Lesko, and E. B. Norman, *Phys. Rev. Lett.* **60**, 499 (1988).
- [345] A. Converse, M. Allet, W. Haeberli, W. Hajdas, J. Lang, J. Liechti, H. Lüscher, M. Miller, R. Müller, O. Naviliat-Cuncic, P. Quin, and J. Sromicki, *Phys. Lett. B* **304**, 60 (1993).
- [346] N. Severijns, J. Wouters, J. Vanhaverbeke, and L. Vanneste, *Phys. Rev. Lett.* **63**, 1050 (1989).
- [347] J. S. Allen, R. L. Burman, W. B. Herrmannsfeldt, P. Stähelin, and T. H. Braid, *Phys. Rev.* **116**, 134 (1959).
- [348] N. D. Scielzo, S. J. Freedman, B. K. Fujikawa, and P. A. Vetter, *Phys. Rev. Lett.* **93**, 102501 (2004).
- [349] C.-Y. Seng, X. Feng, M. Gorchtein, and L.-C. Jin, *Phys. Rev. D* **101**, 111301(R) (2020).
- [350] W. J. Marciano and A. Sirlin, *Phys. Rev. Lett.* **96**, 032002 (2006).
- [351] C. Chang, A. Nicholson, E. Rinaldi, E. Berkowitz, N. Garron, D. A. Brantley, H. Monge-Camacho, C. J. Monahan, C. Bouchard, M. A. Clark, B. Joó, T. Kurth, K. Orginos, P. Vranas, and A. Walker-Loud, *Nature (London)* **558**, 91 (2018).
- [352] R. Gupta, Y.-C. Jang, B. Yoon, H.-W. Lin, V. Cirigliano, and T. Bhattacharya (Precision Neutron Decay Matrix Elements (PNDME) Collaboration), *Phys. Rev. D* **98**, 034503 (2018).
- [353] Y. Aoki, T. Blum, G. Colangelo, S. Collins, M. Della Morte, P. Dimopoulos, S. Dürr, X. Feng, H. Fukaya, M. Golterman, S. Gottlieb, R. Gupta, S. Hashimoto, U. M. Heller, G. Herdoiza, P. Hernandez, R. Horsley, A. Jüttner, T. Kaneko, E. Lunghi *et al.*, *Eur. Phys. J. C* **82**, 869 (2022).
- [354] M. Ademollo and R. Gatto, *Phys. Rev. Lett.* **13**, 264 (1964).
- [355] L. Armstrong and C. W. Kim, *Phys. Rev. C* **5**, 672 (1972).
- [356] S. Weinberg, *Phys. Rev.* **112**, 1375 (1958).
- [357] G. Morpurgo, *Phys. Rev.* **114**, 1075 (1959).
- [358] R. J. Blin-Stoyle, *Fundamental Interactions and the Nucleus* (North-Holland, New York, 1973), p. 345.
- [359] D. H. Wilkinson, *Isospin in Nuclear Physics* (North-Holland, Amsterdam, 1969), p. 751.
- [360] M. MacCormick and G. Audi, *Nucl. Phys. A* **925**, 61 (2014).
- [361] M. Gell-Mann, *Phys. Rev.* **111**, 362 (1958).
- [362] W. Y. P. Hwang, *Phys. Rev. C* **21**, 1086 (1980).
- [363] L. L. Foldy and S. A. Wouthuysen, *Phys. Rev.* **78**, 29 (1950).
- [364] A. Falkowski, M. González-Alonso, A. Palavrić, and A. Rodríguez-Sánchez, [arXiv:2112.07688](https://arxiv.org/abs/2112.07688).
- [365] L. De Braeckeleer, E. G. Adelberger, J. H. Gundlach, M. Kaplan, D. Markoff, A. M. Nathan, W. Schieff, K. A. Snover, D. W. Storm, K. B. Swartz, D. Wright, and B. A. Brown, *Phys. Rev. C* **51**, 2778 (1995).
- [366] I. S. Towner, *Phys. Rep.* **155**, 263 (1987).
- [367] W. Kleppinger, F. Calaprice, and B. R. Holstein, *Nucl. Phys. A* **293**, 46 (1977).
- [368] M. González-Alonso and J. Martin Camalich, *Phys. Rev. Lett.* **112**, 042501 (2014).
- [369] W. M. MacDonald, *Phys. Rev.* **100**, 51 (1955).
- [370] M. Gell-Mann and V. L. Telegdi, *Phys. Rev.* **91**, 169 (1953).
- [371] G. Morpurgo, *Phys. Rev.* **110**, 721 (1958).
- [372] S. Raman, T. Walkiewicz, and H. Behrens, *At. Data Nucl. Data Tables* **16**, 451 (1975).
- [373] A. De-Shalit and H. Feshbach, *Theoretical Nuclear Physics: Nuclear Structure* (John Wiley and Sons, New York, 1990).
- [374] N. M. Parzuchowski, T. D. Morris, and S. K. Bogner, *Phys. Rev. C* **95**, 044304 (2017).
- [375] D. H. Wilkinson, *Phys. Rev. C* **7**, 930 (1973).
- [376] D. H. Wilkinson, *Nucl. Phys. A* **209**, 470 (1973).
- [377] D. Wilkinson, *Nucl. Phys. A* **225**, 365 (1974).
- [378] M. Ericson, A. Figureau, and C. Thévenet, *Phys. Lett. B* **45**, 19 (1973).
- [379] J. Delorme, M. Ericson, A. Figureau, and C. Thévenet, *Ann. Phys.* **102**, 273 (1976).
- [380] I. S. Towner and F. C. Khanna, *Phys. Rev. Lett.* **42**, 51 (1979).
- [381] J. Kostensalo, M. Haaranen, and J. Suhonen, *Phys. Rev. C* **95**, 044313 (2017).
- [382] F. F. Deppisch and J. Suhonen, *Phys. Rev. C* **94**, 055501 (2016).

- [383] J. Suhonen, *Phys. Rev. C* **96**, 055501 (2017).
- [384] J. T. Suhonen, *Frontiers in Physics* **5**, 55 (2017).
- [385] J.-I. Fujita, S. Fujii, and K. Ikeda, *Phys. Rev.* **133**, B549 (1964).
- [386] K. Koshigiri, H. Ohtsubo, and M. Morita, *Prog. Theor. Phys.* **66**, 358 (1981).
- [387] A. Barroso and R. J. Blin-Stoyle, *Nucl. Phys. A* **251**, 446 (1975).
- [388] M. Rho, *Prog. Part. Nucl. Phys.* **1**, 105 (1978).
- [389] T. Siiskonen, M. Hjorth-Jensen, and J. Suhonen, *Phys. Rev. C* **63**, 055501 (2001).
- [390] B. A. Brown and B. H. Wildenthal, *Annu. Rev. Nucl. Part. Sci.* **38**, 29 (1988).
- [391] G. Martínez-Pinedo, A. Poves, E. Caurier, and A. P. Zuker, *Phys. Rev. C* **53**, R2602 (1996).
- [392] N. J. Stone, Table of nuclear magnetic dipole and electric quadrupole moments, IAEA-INDC International Nuclear Data Committee, Report No. INDC(NDS)-0658, 2014, <http://www-nds.iaea.org/publications>.
- [393] T. Mertzimekis, K. Stamou, and A. Psaltis, *Nucl. Instrum. Methods Phys. Res., Sect. A* **807**, 56 (2016).
- [394] S. M. Perez, W. A. Richter, B. A. Brown, and M. Horoi, *Phys. Rev. C* **77**, 064311 (2008).
- [395] C. Clement and S. Perez, *Phys. Lett. B* **81**, 269 (1979).
- [396] S. Cohen and D. Kurath, *Nucl. Phys.* **73**, 1 (1965).
- [397] B. A. Brown and W. A. Richter, *Phys. Rev. C* **74**, 034315 (2006).
- [398] M. Honma, T. Otsuka, B. A. Brown, and T. Mizusaki, *Phys. Rev. C* **65**, 061301(R) (2002).
- [399] B. Buck, A. C. Merchant, and S. M. Perez, *Phys. Rev. C* **63**, 037301 (2001).
- [400] J. S. Berryman, K. Minamisono, W. F. Rogers, B. A. Brown, H. L. Crawford, G. F. Grinyer, P. F. Mantica, J. B. Stoker, and I. S. Towner, *Phys. Rev. C* **79**, 064305 (2009).
- [401] V. V. Golovko, I. Kraev, T. Phalet, N. Severijns, B. Delauré, M. Beck, V. Kozlov, A. Lindroth, S. Versyck, D. Zákoucký, D. Vénos, D. Srnka, M. Honusek, P. Herzog, C. Tramm, U. Köster, and I. S. Towner, *Phys. Rev. C* **70**, 014312 (2004).
- [402] M. Honma, T. Otsuka, B. A. Brown, and T. Mizusaki, *Phys. Rev. C* **69**, 034335 (2004).
- [403] F. Alder and F. C. Yu, *Phys. Rev.* **81**, 1067 (1951).
- [404] F. Alder and F. C. Yu, *Phys. Rev.* **82**, 105 (1951).
- [405] O. Ames, E. A. Phillips, and S. S. Glickstein, *Phys. Rev.* **137**, B1157 (1965).
- [406] A. Andl, K. Bekk, S. Göring, A. Hanser, G. Nowicki, H. Rebel, G. Schatz, and R. C. Thompson, *Phys. Rev. C* **26**, 2194 (1982).
- [407] M. Arnold, J. Kowalski, T. Stehlin, F. Trager, and G. zu Putlitz, *Z. Phys. A* **314**, 303 (1983).
- [408] M. Avgoulea, Y. P. Gangrsky, K. P. Marinova, S. G. Zemlyanoi, S. Fritzsche, D. Iablonskyi, C. Barbieri, E. C. Simpson, P. D. Stevenson, J. Billowes, P. Campbell, B. Cheal, B. Tordoff, M. L. Bissell, D. H. Forest, M. D. Gardner, G. Tungate, J. Huikari, A. Nieminen, H. Penttila *et al.*, *J. Phys. G: Nucl. Part. Phys.* **38**, 025104 (2011).
- [409] C. Babcock, H. Heylen, J. Billowes, M. Bissell, K. Blaum, P. Campbell, B. Cheal, R. G. Ruiz, C. Geppert, W. Gins, M. Kowalska, K. Kreim, S. Lenzi, I. Moore, R. Neugart, G. Neyens, W. Nörtershäuser, J. Papuga, and D. Yordanov, *Phys. Lett. B* **750**, 176 (2015).
- [410] J. D. Baldeschweiler, *J. Chem. Phys.* **36**, 152 (1962).
- [411] M. R. Baker, C. H. Anderson, and N. F. Ramsey, *Phys. Rev.* **133**, A1533 (1964).
- [412] A. M. Bernstein, R. A. Haberstroh, D. R. Hamilton, M. Posner, and J. L. Snider, *Phys. Rev.* **136**, B27 (1964).
- [413] A. Beckmann, K. D. Böklen, and D. Elke, *Z. Phys.* **270**, 173 (1974).
- [414] J. Bleck, D. Haag, W. Leitz, and W. Ribbe, *Phys. Lett. B* **26**, 134 (1968).
- [415] J. Blaser, O. Lutz, and W. Steinkilberg, *Z. Naturforsch. A* **27**, 72 (1972).
- [416] E. Bodenstedt, G. Strube, W. Engels, H. Blumberg, R.-M. Lieder, and E. Gerdau, *Phys. Lett.* **6**, 290 (1963).
- [417] E. Brun, J. J. Kraushaar, W. L. Pierce, and W. J. Veigele, *Phys. Rev. Lett.* **9**, 166 (1962).
- [418] F. Buchinger, E. B. Ramsay, E. Arnold, W. Neu, R. Neugart, K. Wendt, R. E. Silverans, P. Lievens, L. Vermeeren, D. Berdichevsky, R. Fleming, D. W. L. Sprung, and G. Ulm, *Phys. Rev. C* **41**, 2883 (1990); **42**, 2754(E) (1990).
- [419] F. P. Calaprice, E. D. Commins, and D. A. Dobson, *Phys. Rev.* **137**, B1453 (1965).
- [420] P. Callaghan, M. Kaplan, and N. Stone, *Nucl. Phys. A* **201**, 561 (1973).
- [421] B. Cheal, E. Mané, J. Billowes, M. L. Bissell, K. Blaum, B. A. Brown, F. C. Charlwood, K. T. Flanagan, D. H. Forest, C. Geppert, M. Honma, A. Jokinen, M. Kowalska, A. Krieger, J. Krämer, I. D. Moore, R. Neugart, G. Neyens, W. Nörtershäuser, M. Schug *et al.*, *Phys. Rev. Lett.* **104**, 252502 (2010).
- [422] T. E. Cocolios, A. N. Andreyev, B. Bastin, N. Bree, J. Büscher, J. Elseviers, J. Gentens, M. Huyse, Y. Kudryavtsev, D. Pauwels, T. Sonoda, P. V. d. Bergh, and P. Van Duppen, *Phys. Rev. C* **81**, 014314 (2010).
- [423] E. D. Commins and H. R. Feldman, *Phys. Rev.* **131**, 700 (1963).
- [424] R. G. Cornwell, W. Happer, and J. D. McCullen, *Phys. Rev.* **141**, 1106 (1966).
- [425] R. G. Cornwell and J. D. McCullen, *Phys. Rev.* **148**, 1157 (1966).
- [426] S. S. Dharmatti and H. E. Weaver, *Phys. Rev.* **83**, 845 (1951).
- [427] H. T. Duong, S. Liberman, J. Pinard, A. Coc, C. Thibault, F. Touchard, M. Carré, J. Lermé, J. Vialle, L. Juncar, S. Büttgenbach, A. Pesnelle, and the Isolde Collaboration, *J. Phys. (Paris)* **47**, 1903 (1986).
- [428] H. Duong, C. Ekström, M. Gustafsson, T. Inamura, P. Juncar, P. Lievens, I. Lindgren, S. Matsuki, T. Murayama, R. Neugart, T. Nilsson, T. Nomura, M. Pellarin, S. Penselin, J. Persson, J. Pinard, I. Ragnarsson, O. Redi, H. Stroke, and J. Vialle, *Nucl. Instrum. Methods Phys. Res., Sect. A* **325**, 465 (1993).
- [429] B. W. Epperlein and O. Lutz, *Z. Naturforsch. A* **23**, 1413 (1968).
- [430] B. W. Epperlein, O. Lutz, and A. Schwenk, *Z. Naturforsch. A* **30**, 955 (1975).
- [431] G. H. Fuller, *J. Phys. Chem. Ref. Data* **5**, 835 (1976).
- [432] M. Fukuda, T. Izumikawa, T. Ohtsubo, M. Tanigaki, S. Fukuda, Y. Nakayama, K. Matsuta, Y. Nojiri, and T. Minamisono, *Phys. Lett. B* **307**, 278 (1993).
- [433] W. Geithner, B. A. Brown, K. M. Hilligsøe, S. Kappertz, M. Keim, G. Kotrotsios, P. Lievens, K. Marinova, R. Neugart, H. Simon, and S. Wilbert, *Phys. Rev. C* **71**, 064319 (2005).
- [434] V. V. Golovko, I. S. Kraev, T. Phalet, N. Severijns, D. Zákoucký, D. Vénos, P. Herzog, C. Tramm, D. Srnka, M.

- Honusek, U. Köster, B. Delauré, M. Beck, V. Y. Kozlov, A. Lindroth, and S. Coeck, *Phys. Rev. C* **72**, 064316 (2005).
- [435] P. Herzog, N. J. Stone, and P. D. Johnston, *Hyperfine Interact.* **2**, 294 (1976).
- [436] P. Herzog, N. Stone, and P. Johnston, *Nucl. Phys. A* **259**, 378 (1976).
- [437] J. W. Hugg, *Phys. Rev. C* **30**, 1328 (1984).
- [438] G. Jakob, K.-H. Speidel, S. Kremeyer, H. Busch, U. Grabow, A. Gohla, J. Cub, J. Gerber, A.-M. Oros, K. Heyde, and J. Rikovska, *Nucl. Phys. A* **601**, 117 (1996).
- [439] J. O. Jönsson, L. Sanner, and B. Wannberg, *Phys. Scr.* **2**, 16 (1970).
- [440] J. O. Jönsson, M. Olsmats, L. Sanner, and B. Wannberg, *Nucl. Phys. A* **166**, 306 (1971).
- [441] A. Klein, B. Brown, U. Georg, M. Keim, P. Lievens, R. Neugart, M. Neuroth, R. Silverans, L. Vermeeren, and ISOLDE Collaboration, *Nucl. Phys. A* **607**, 1 (1996).
- [442] J. T. LaTourrette, W. E. Quinn, and N. F. Ramsey, *Phys. Rev.* **107**, 1202 (1957).
- [443] N. S. Laulainen and M. N. McDermott, *Phys. Rev.* **177**, 1606 (1969).
- [444] G. Lindstrom, *Arkiv Fysik* **4**, 1 (1952).
- [445] P. Lievens, L. Vermeeren, R. E. Silverans, E. Arnold, R. Neugart, K. Wendt, and F. Buchinger, *Phys. Rev. C* **46**, 797 (1992).
- [446] O. Lutz, A. Nolle, and A. Schwenk, *Z. Naturforsch. A* **28**, 1370 (1973).
- [447] K. Matsuta, T. Tsubota, C. Ha, T. Miyake, M. Sasaki, K. Sato, K. Minamisono, K. Tanaka, S. Kaminaka, A. Takemura, T. Sumikama, T. Nagatomo, K. Hashimoto, M. Mihara, M. Fukuda, T. Minamisono, T. Ohtsubo, Y. Nojiri, S. Momota, A. Kitagawa *et al.*, *Nucl. Phys. A* **701**, 383 (2002).
- [448] K. Matsuta, K. Arimura, T. Nagatomo, K. Akutsu, T. Iwakoshi, S. Kudo, M. Ogura, M. Takechi, K. Tanaka, T. Sumikama, K. Minamisono, T. Miyake, T. Minamisono, M. Fukuda, M. Mihara, A. Kitagawa, M. Sasaki, M. Kanazawa, M. Torikoshi, M. Suda *et al.*, *Nucl. Phys. A* **746**, 493 (2004).
- [449] D. W. MacArthur, F. P. Calaprice, A. L. Hallin, M. B. Schneider, and D. F. Schreiber, *Phys. Rev. C* **26**, 1753 (1982).
- [450] K. Matsuta, A. Ozawa, Y. Nojiri, T. Minamisono, M. Fukuda, S. Momota, T. Ohtsubo, S. Fukuda, K. Sugimoto, I. Tanihata, K. Yoshida, K. Omata, J. R. Alonso, G. F. Krebs, and T. J. M. Symons, *Hyperfine Interact.* **78**, 123 (1993).
- [451] K. Matsuta, T. Onishi, C. Ha, K. Sato, H. Akai, M. Sasaki, T. Yamaguchi, T. Miyake, K. Minamisono, K. Tanaka, K. Kidera, A. Morishita, M. Fukuda, M. Mihara, T. Minamisono, A. Kitagawa, M. Torikoshi, M. Kanazawa, T. Nishio, S. Koda *et al.*, Electromagnetic Moments of Short-Lived  $\beta$ -Emitter  $^{27}\text{Si}$ , in Osaka University Laboratory for Nuclear Studies Annual Report 1997 (unpublished), p. 49.
- [452] K. Matsuta, T. Minamisono, M. Fukuda, M. Mihara, T. Onishi, K. Sato, M. Sasaki, K. Minamisono, C. Ha, T. Miyake, H. Akai, T. Ohtsubo, S. Momota, Y. Nojiri, S. Fukuda, K. Yoshida, A. Ozawa, T. Suzuki, I. Tanihata, G. F. Krebs *et al.*, Quadrupole Moment of  $^{39}\text{Ca}$ , Report No. RIKEN-98, 1999 (unpublished), p. 79.
- [453] K. Minamisono, P. F. Mantica, T. J. Mertzimekis, A. D. Davies, M. Hass, J. Pereira, J. S. Pinter, W. F. Rogers, J. B. Stoker, B. E. Tomlin, and R. R. Weerasiri, *Phys. Rev. Lett.* **96**, 102501 (2006).
- [454] A. J. Miller, K. Minamisono, D. M. Rossi, R. Beerwerth, B. A. Brown, S. Fritzsche, D. Garand, A. Klose, Y. Liu, B. Maaß, P. F. Mantica, P. Müller, W. Nörtershäuser, M. R. Pearson, and C. Sumithrarachchi, *Phys. Rev. C* **96**, 054314 (2017).
- [455] S. Millman, P. Kusch, and I. I. Rabi, *Phys. Rev.* **56**, 165 (1939).
- [456] T. Minamisono, J. W. Hugg, J. R. Hall, D. G. Mavis, H. F. Glavish, and S. S. Hanna, *Phys. Rev. C* **14**, 376 (1976).
- [457] T. Minamisono, J. W. Hugg, J. R. Hall, D. G. Mavis, D. L. Clark, and S. S. Hanna, *Phys. Rev. C* **14**, 2335 (1976).
- [458] T. Minamisono, J. Hugg, D. Mavis, T. Saylor, H. Glavish, and S. Hanna, *Phys. Lett. B* **61**, 155 (1976).
- [459] T. Minamisono, Y. Nojiri, K. Matsuta, K. Takeyama, A. Kitagawa, T. Ohtsubo, O. A., and M. Izumi, *Nucl. Phys. A* **516**, 365 (1990).
- [460] T. Minamisono, T. Ohtsubo, S. Fukuda, Y. Nakayama, T. Araki, K. Mashitani, K. Matsuda, E. Takahashi, M. Tanigaki, M. Tanaka, H. Shiohara, Y. Someda, Y. Aoki, A. Kitagawa, M. Fukuda, K. Matsuta, and Y. Nojiri, *Hyperfine Interact.* **78**, 111 (1993).
- [461] P. J. Mohr, D. B. Newell, and B. N. Taylor, *Rev. Mod. Phys.* **88**, 035009 (2016).
- [462] J. Morgenstern, J. Schmidt, G. Flügge, and H. Schmidt, *Phys. Lett. B* **27**, 370 (1968).
- [463] Y. I. Neronov and V. S. Aleksandrov, *JETP Lett.* **94**, 418 (2011).
- [464] Y. Neronov and N. Seregin, *J. Exp. Theor. Phys.* **115**, 777 (2012).
- [465] Y. I. Neronov and A. E. Barzakh, *Zh. Eksp. Teor. Fiz.* **72**, 1659 (1977) [*Sov. Phys. JETP* **45**, 871 (1977)].
- [466] T. Ohtsubo, D. J. Cho, Y. Yanagihashi, S. Ohya, and S. Muto, *Phys. Rev. C* **54**, 554 (1996).
- [467] A. F. Oluwole, S. G. Schmelling, and H. A. Shugart, *Phys. Rev. C* **2**, 228 (1970).
- [468] M. L. Pitt, M. Jozoff, F. P. Calaprice, G. Wang, and E. K. Warburton, *Bull. Am. Phys. Soc.* **33**(8) 1564, AD9 (1988).
- [469] T. J. Procter, J. Billowes, M. L. Bissell, K. Blaum, F. C. Charlwood, B. Cheal, K. T. Flanagan, D. H. Forest, S. Fritzsche, C. Geppert, H. Heylen, M. Kowalska, K. Kreim, A. Krieger, J. Krämer, K. M. Lynch, E. Mané, I. D. Moore, R. Neugart, G. Neyens *et al.*, *Phys. Rev. C* **86**, 034329 (2012).
- [470] M. Puchalski, J. Komasa, and K. Pachucki, *Phys. Rev. A* **92**, 020501(R) (2015).
- [471] V. Royden, *Phys. Rev.* **96**, 543 (1954).
- [472] M. M. Robertson, J. E. Mack, and V. W. Cohen, *Phys. Rev.* **140**, B820 (1965).
- [473] S. Rosenblum and W. Steyert, *Phys. Lett. B* **55**, 450 (1975).
- [474] W. Rogers, D. Clark, S. Dutta, and A. Martin, *Phys. Lett. B* **177**, 293 (1986).
- [475] W. Sahm and A. Schwenk, *Z. Naturforsch. A* **29**, 1754 (1974).
- [476] W. Sahm and A. Schwenk, *Z. Naturforsch. A* **29**, 1763 (1974).
- [477] K.-H. Speidel, G. Jakob, J. Cub, S. Kremeyer, H. Busch, U. Grabow, J. Gerber, J. Rikovska, and K. Heyde, *Nucl. Phys. A* **578**, 300 (1994).
- [478] N. J. Stone, U. Köster, J. R. Stone, D. V. Fedorov, V. N. Fedoseyev, K. T. Flanagan, M. Hass, and S. Lakshmi, *Phys. Rev. C* **77**, 067302 (2008).
- [479] K. Sugimoto, A. Mizobuchi, K. Nakai, and K. Matuda, *J. Phys. Soc. Jpn.* **21**, 213 (1966).
- [480] K. Sugimoto, A. Mizobuchi, and T. Minamisono in *Proceedings of the International Conference on Hyperfine Interactions*

- in Excited Nuclei*, Rehovot and Jerusalem, 1970, edited by G. Goldring and R. Kalish (Gordon and Breach, London, 1971), Vol. 1, p. 325.
- [481] M. Tanigaki, M. Matsui, M. Mihara, M. Mori, M. Tanaka, T. Yanagisawa, T. Ohtsubo, T. Izumikawa, A. Kitagawa, M. Fukuda, K. Matsuta, Y. Nojiri, and T. Minamisono, *Hyperfine Interact.* **78**, 105 (1993).
- [482] E. Tiesinga, P. J. Mohr, D. B. Newell, and B. N. Taylor, *Rev. Mod. Phys.* **93**, 025010 (2021).
- [483] C. Thibault, F. Touchard, S. Büttgenbach, R. Klapisch, M. de Saint Simon, H. T. Duong, P. Jacquinet, P. Juncar, S. Liberman, P. Pillet, J. Pinard, J. L. Vialle, A. Pesnelle, and G. Huber, *Phys. Rev. C* **23**, 2720 (1981).
- [484] G. Schneider, A. Mooser, M. Bohman, N. Schön, J. Harrington, T. Higuchi, H. Nagahama, S. Sellner, C. Smorra, K. Blaum, Y. Matsuda, W. Quint, J. Walz, and S. Ulmer, *Science* **358**, 1081 (2017).
- [485] P. Vingerhoets, K. T. Flanagan, M. Avgoulea, J. Billowes, M. L. Bissell, K. Blaum, B. A. Brown, B. Cheal, M. De Rydt, D. H. Forest, C. Geppert, M. Honma, M. Kowalska, J. Krämer, A. Krieger, E. Mané, R. Neugart, G. Neyens, W. Nörtershäuser, T. Otsuka *et al.*, *Phys. Rev. C* **82**, 064311 (2010).
- [486] P. Vingerhoets, K. Flanagan, J. Billowes, M. Bissell, K. Blaum, B. Cheal, M. De Rydt, D. Forest, C. Geppert, M. Honma, M. Kowalska, J. Krämer, K. Kreim, A. Krieger, R. Neugart, G. Neyens, W. Nörtershäuser, J. Papuga, T. Procter, M. Rajabali *et al.*, *Phys. Lett. B* **703**, 34 (2011).
- [487] C. Von Platen, J. Bonn, U. Kopf, R. Neugart, and E.-W. Otten, *Z. Phys. A* **244**, 44 (1971).
- [488] H. E. Walchli, Some Improved Measurements of Nuclear Magnetic Dipole Moments by Means of Nuclear Magnetic Resonance, Oak Ridge National Laboratory Technical Report No. ORNL-1775, 1954 (unpublished), <https://www.osti.gov/servlets/purl/4360222>.
- [489] H. E. Weaver, *Phys. Rev.* **89**, 923 (1953).
- [490] S. Wender and J. Cameron, *Nucl. Phys. A* **241**, 332 (1975).
- [491] G. Wolber, H. Figger, R. A. Haberstroh, and S. Penselin, *Z. Phys. A: Hadrons Nucl.* **236**, 337 (1970).
- [492] D. T. Yordanov, M. L. Bissell, K. Blaum, M. D. Rydt, C. Geppert, J. Krämer, K. Kreim, M. Kowalska, A. Krieger, P. Lievens, R. Neugart, G. Neyens, W. Nörtershäuser, L. V. Rodríguez, R. Sánchez, and P. Vingerhoets, *J. Phys. G: Nucl. Part. Phys.* **44**, 075104 (2017).
- [493] C. B. Zamboni and R. N. Saxena, *J. Phys. G* **10**, 1571 (1984).
- [494] Z. Dong-Mei, Z. Yong-Nan, Z. Xi-Zhen, Y. Da-Qing, Z. Yi, F. Ping, W. Zhi-Qiang, L. Hai-Long, X. Guo-Ji, and Z. Sheng-Yun, *Chin. Phys. C* **33**, 218 (2009).
- [495] P. Möller, A. J. Sierk, T. Ichikawa, and H. Sagawa, *At. Data Nucl. Data Tables* **109-110**, 1 (2016).
- [496] S. G. Nilsson, *Dan. Mat. Fys. Medd.* **29**, 1 (1955).
- [497] B. Wildenthal, *Prog. Part. Nucl. Phys.* **11**, 5 (1984).
- [498] T. Kuo and G. Brown, *Nucl. Phys.* **85**, 40 (1966).
- [499] A. Poves and A. Zuker, *Phys. Rep.* **70**, 235 (1981).
- [500] D. Millener and D. Kurath, *Nucl. Phys. A* **255**, 315 (1975).
- [501] B. R. Barrett, P. Navrátil, and J. P. Vary, *Prog. Part. Nucl. Phys.* **69**, 131 (2013).
- [502] H. Hergert, S. Bogner, T. Morris, A. Schwenk, and K. Tsukiyama, *Phys. Rep.* **621**, 165 (2016), Memorial Volume in Honor of Gerald E. Brown.
- [503] S. R. Stroberg, A. Calci, H. Hergert, J. D. Holt, S. K. Bogner, R. Roth, and A. Schwenk, *Phys. Rev. Lett.* **118**, 032502 (2017).
- [504] P. Gysbers, G. Hagen, J. Holt, G. Jansen, T. Morris, P. Navrátil, T. Papenbrock, S. Quaglioni, A. Schwenk, S. Stroberg, and K. Wendt, *Nat. Phys.* **15**, 428 (2019).
- [505] H. Hergert, *Front. Phys.* **8**, 379 (2020).
- [506] J. Blatt and V. Weisskopf, *Theoretical Nuclear Physics* (John Wiley and Sons, New York, 1952), p. 627.
- [507] P. Schuurmans, J. Camps, T. Phalet, N. Severijns, B. Vereecke, and S. Vrsyck, *Nucl. Phys. A* **672**, 89 (2000).
- [508] N. Severijns, D. Vénos, P. Schuurmans, T. Phalet, M. Honusek, D. Srnka, B. Vereecke, S. Vrsyck, D. Zákoucký, U. Köster, M. Beck, B. Delauré, V. Golovko, and I. Kraev, *Phys. Rev. C* **71**, 064310 (2005).
- [509] C. Dossat, N. Adimi, F. Aksouh, F. Becker, A. Bey, B. Blank, C. Borcea, R. Borcea, A. Boston, M. Caamano, G. Canchel, M. Chartier, D. Cortina, S. Czajkowski, G. de France, F. de Oliveira Santos, A. Fleury, G. Georgiev, J. Giovinazzo, S. Grévy *et al.*, *Nucl. Phys. A* **792**, 18 (2007).
- [510] J. Su, W. Liu, N. Zhang, Y. Shen, Y. Lam, N. Smirnova, M. MacCormick, J. Wang, L. Jing, Z. Li, Y. Wang, B. Guo, S. Yan, Y. Li, S. Zeng, G. Lian, X. Du, L. Gan, X. Bai, Z. Gao *et al.*, *Phys. Lett. B* **756**, 323 (2016).
- [511] S. Triambak, L. Phuthu, A. García, G. C. Harper, J. N. Orce, D. A. Short, S. P. R. Steininger, A. Diaz Varela, R. Dunlop, D. S. Jamieson, W. A. Richter, G. C. Ball, P. E. Garrett, C. E. Svensson, and C. Wrede, *Phys. Rev. C* **95**, 035501 (2017).
- [512] S. Triambak, L. Phuthu, A. García, G. C. Harper, J. N. Orce, D. A. Short, S. P. R. Steininger, A. Diaz Varela, R. Dunlop, D. S. Jamieson, W. A. Richter, G. C. Ball, P. E. Garrett, C. E. Svensson, and C. Wrede, *Phys. Rev. C* **95**, 049901(E) (2017).
- [513] N. A. Smirnova (private communication).
- [514] E. K. Warburton and B. A. Brown, *Phys. Rev. C* **46**, 923 (1992).
- [515] F. C. Barker, *Aust. J. Phys.* **42**, 25 (1989).
- [516] B. R. Holstein, *Phys. Rev. C* **4**, 740 (1971).
- [517] R. D. McKeown, G. T. Garvey, and C. A. Gagliardi, *Phys. Rev. C* **22**, 738 (1980).
- [518] L. D. Knutson, G. W. Severin, S. L. Cotter, L. Zhan, P. A. Voytas, and E. A. George, *Rev. Sci. Instrum.* **82**, 073302 (2011).
- [519] X. Mougeot, M.-M. Bé, C. Bisch, and M. Loidl, *Phys. Rev. A* **86**, 042506 (2012).
- [520] K. Łojek, K. Bodek, and M. Kuzniak, *Nucl. Instrum. Methods Phys. Res., Sect. A* **611**, 284 (2009).
- [521] K. Łojek, D. Rozpedzik, K. Bodek, M. Perkowski, and N. Severijns, *Nucl. Instrum. Methods Phys. Res., Sect. A* **802**, 38 (2015).
- [522] L. J. Broussard *et al.*, *Hyperfine Interact.* **240**, 1 (2019).
- [523] M. Perkowski, K. Bodek, L. De Keukeleere, L. Hayen, A. Kozela, K. Łojek, D. Rozpedzik, and N. Severijns, *Acta Phys. Pol. B* **49**, 261 (2018).
- [524] M. Skalsey, T. A. Girard, and A. Rich, *Phys. Rev. C* **32**, 1014 (1985).
- [525] C. J. Bowers, S. J. Freedman, B. Fujikawa, A. O. Macchiavelli, R. W. MacLeod, J. Reich, S. Q. Shang, P. A. Vetter, and E. Wasserman, *Phys. Rev. C* **59**, 1113 (1999).

- [526] C. H. Johnson, F. Pleasonton, and T. A. Carlson, *Phys. Rev.* **132**, 1149 (1963).
- [527] T. Sato, J. Yamane, and M. Morita, *Prog. Theor. Phys.* **58**, 1218 (1977).
- [528] J. Pearson and R. Spear, *Nucl. Phys.* **54**, 434 (1964).
- [529] B. M. Freedom and B. H. Wildenthal, *Phys. Rev. C* **6**, 1633 (1972).
- [530] T. Kuo, *Nucl. Phys. A* **103**, 71 (1967).
- [531] J. Jackson, S. Treiman, and H. W. J. Wyld, *Phys. Rev.* **106**, 517 (1957).
- [532] M. González-Alonso and O. Naviliat-Cuncic, *Phys. Rev. C* **94**, 035503 (2016).
- [533] K. P. Hickerson *et al.* (UCNA Collaboration), *Phys. Rev. C* **96**, 042501(R) (2017).
- [534] L. J. Broussard, B. Zeck, E. Adamek, S. Baeßler, N. Birge, M. Blatnik, J. Bowman, A. Brandt, M. Brown, J. Burkhart, N. Callahan, S. Clayton, C. Crawford, C. Cude-Woods, S. Currie, E. Dees, X. Ding, N. Fomin, E. Frlez, J. Fry *et al.*, *Nucl. Instrum. Methods Phys. Res., Sect. A* **849**, 83 (2017).
- [535] D. Dubbers, H. Abele, S. Baeßler, B. Märkisch, M. Schumann, T. Soldner, and O. Zimmer, *Nucl. Instrum. Methods Phys. Res., Sect. A* **596**, 238 (2008).
- [536] X. Wang, G. Konrad, and H. Abele, *Nucl. Instrum. Methods Phys. Res., Sect. A* **701**, 254 (2013).
- [537] E. A. George, P. A. Voytas, G. W. Severin, and L. D. Knutson, *Phys. Rev. C* **90**, 065501 (2014).
- [538] G. W. Severin, L. D. Knutson, P. A. Voytas, and E. A. George, *Phys. Rev. C* **89**, 057302 (2014).
- [539] B. Plaster, R. Rios, H. O. Back, T. J. Bowles, L. J. Broussard, R. Carr, S. Clayton, S. Currie, B. W. Filippone, A. García, P. Geltenbort, K. P. Hickerson, J. Hoagland, G. E. Hogan, B. Hona, A. T. Holley, T. M. Ito, C.-Y. Liu, J. Liu, M. Makela *et al.*, J. Yuan (UCNA Collaboration), *Phys. Rev. C* **86**, 055501 (2012).
- [540] F. Glück and K. Tóth, *Phys. Rev. D* **41**, 2160 (1990).
- [541] F. Glück and K. Tóth, *Phys. Rev. D* **46**, 2090 (1992).
- [542] F. Glück, *Phys. Rev. D* **47**, 2840 (1993).
- [543] F. Glück, *Phys. Lett. B* **436**, 25 (1998).
- [544] A. N. Ivanov, M. Pitschmann, and N. I. Troitskaya, *Phys. Rev. D* **88**, 073002 (2013).
- [545] A. N. Ivanov, R. Höllwieser, N. I. Troitskaya, M. Wellenzohn, and Y. A. Berdnikov, *Phys. Rev. C* **95**, 055502 (2017).
- [546] A. N. Ivanov, R. Höllwieser, N. I. Troitskaya, M. Wellenzohn, and Y. A. Berdnikov, *Phys. Rev. D* **99**, 053004 (2019).
- [547] B. Hird, *Comput. Phys. Commun.* **6**, 30 (1973).
- [548] J. Dudek, W. Nazarewicz, and T. Werner, *Nucl. Phys. A* **341**, 253 (1980).
- [549] M. E. Rose and R. K. Osborn, *Phys. Rev.* **93**, 1326 (1954).
- [550] J. P. Davidson, *Collective Models of the Nucleus* (Academic, New York, 1968).
- [551] J. Berthier and P. Lipnik, *Nucl. Phys.* **78**, 448 (1966).